Macroscopic amplification of nanoscopic motions induced by molecular machines

Antoine Goujon

UNIVERSITÉ DE STRASBOURG

ÉCOLE DOCTORALE DES SCIENCES CHIMIQUES

Institut Charles Sadron

THÈSE présentée par :

Antoine GOUJON

soutenue le : **20 Septembre 2016**

pour obtenir le grade de : **Docteur de l'université de Strasbourg**

Discipline/ Spécialité : Chimie Organique et Supramoléculaire

Macroscopic Amplification of Nanoscopic Motions Induced by Molecular Machines

THÈSE dirigée par :

Dr. GIUSEPPONE Nicolas Professeur, Université de Strasbourg

RAPPORTEURS :

Dr. HASENKNOPF Bernold Professeur, Université Pierre et Marie Curie – Paris 6

Dr. BOUTEILLER Laurent Directeur de Recherche, Université Pierre et Marie Curie – Paris 6

Dr. DE COLA Luisa Professeur, Université de Strasbourg – Présidente du Jury

Table of content

Abstract

The last twenty years have seen tremendous progresses in the design and synthesis of complex molecular machines, often inspired by the beauty of the machinery found in biological systems. However, amplification of the molecular machines motion over several orders of magnitude above their typical length scale is still an ambitious challenge. This work describes how self-organization of molecular machines or motors allows for the synthesis of materials translating the motions of their components into a macroscopic response.

The three first chapters describe the use of a [c2]daisy chains architecture, a molecule able to perform contraction/extension motions similarly to the sarcomere units of muscles, into systems such as supramolecular polymers and covalent networks. Their inclusion into hydrogen bonding supramolecular polymers based on the uracil:2,6-diacetylaminopyridine recognition motifs combined with lateral interactions such as π-stacking provided micrometric muscle-like fibers contracting and extending upon deprotonation and protonation. The incorporation of ureidopyrimidone moieties as supramolecular connectors yielded highly organized gels, which evolved to a liquid state upon contraction of the polymer chains. Finally, covalent poly[c2]daisy chains were synthesized and investigated, notably the formation of a 3D network swelling into a gel. This material could contract and extend at the macroscopic scale upon contraction and extension of the molecular machines used as monomers.

Finally, a fourth chapter is dedicated to the improvement of contractile chemical gels made by using a molecular motor as reticulating nodes. A modulating unit, able to be switched between a “closed” and an “opened” state, was introduced into the polymer network along with the motor. The locked structure in the “closed” state allowed contraction of the gel upon rotation of the molecular motors, while the “opened” state allowed unwinding of the entangled polymer chains and extension of the gel when the motor is off.

Overall, the work presented in this manuscript demonstrates that carefully designed molecular machines can be incorporated into large supramolecular or covalent assemblies, providing materials which collective motions alter their macroscopic properties. These results provide valuable insights for the elaboration of a new class of muscle-like materials based on molecular machines.

J'aimerais dédier ce travail à la mémoire de ma grand-mère, Yvonne.

Remerciements

Avant tout, mes remerciements vont au Professeur Nicolas Giuseppone. Je lui suis infiniment reconnaissant de m'avoir accepté au sein de l'équipe et de m'avoir confié un projet ambitieux et fascinant. J'ai beaucoup apprécié nos discussions et réflexions, ces quatre années scientifiquement riches. J'ai appris que si la recherche est parfois très exigeante et ingrate, c'est aussi une des aventures les plus enrichissantes à laquelle j'ai eu la chance de participer, et j'espère bien ne pas m'arrêter ici !

En seconde position, mais pas de loin, je remercie chaleureusement le Docteur Emilie Moulin, qui m'a appris rigueur et persévérance. Merci pour m'avoir intégré dans l'équipe, pour l'aide au quotidien et tout un tas de choses trop longues à énumérer ici…

J'aimerais ensuite remercier le Docteur Gad Fuks. Son éternel optimisme, (quasi) inaltérable, a été d'une grande aide à de nombreuses occasions. Merci pour les belles discussions scientifiques tout comme celles qui l'étaient moins, sans doute celles dont je me souviendrai le plus !

Je remercie le Dr. Guangyan Du qui a initié le travail sur les rotaxanes. Merci au Dr. Thomas Lang de m'avoir épaulé sur ce projet vers la fin de ma thèse. Concernant le travail sur les moteurs, merci au Dr. Quan Li et surtout au Dr. Justin T. Foy, pour ces beaux moments partagés en dehors du laboratoire et notre victoire en championnat de beer-pong. Merci à Jean-Remy « ce sont » Collard-Itté à qui je souhaite bon courage pour la suite de son doctorat ! Au cours de ces années, j'ai également eu l'occasion de superviser des stagiaires qui se sont tous révélés très talentueux ; merci à Cristian Rete, Joachim Heiser, et Damien Dattler. Félicitations surtout pour m'avoir supporté en tant que « chef ». Merci à Artem Osypenko et Susanne Schneider, mes compagnons de thèse, nous avons commencé ensemble il y a quatre ans, et en l'espace d'une semaine, tout sera fini. Bonne continuation à tous les deux ! Merci aux compagnons de soirée ; Dr. Yves Ruff pour tous ses bon conseils, Simon McKie pour les discussions toujours animées, Dr. Eric Lutz pour son éternelle bonne humeur. Et, évidemment, tous les autres membres actuels et passés de l'équipe, Dr. Daniel Funeriu pour nos intenses débats, Prof. Mounir Maaloum, Dr. Thomas Ellis, Dr. Joseph J. Armao, Dr. Valentina Garavini, Dr. Adrian Wolf, Dr. Eric Busseron, Dr. Cristina Misuraca, Dr. Yuya Domoto, Dr. Yunjie Xiang, Quing Cao, Ting Liang, Dr. Manickasundaram Samiappan et Dr Junjun Tan. Merci tout particulièrement à Julie Lemoine (même si elle m'ennuie tout le temps) et Odile Gavat sans qui

le laboratoire ne pourrait pas tourner. Merci aussi à Mélodie Archimbaud pour son bref mais sympathique séjour dans l'équipe.

Merci beaucoup au Dr. Giacomo Mariani et au Prof. Eric Buhler pour les expériences de diffusion de la lumière et des neutrons, cruciales dans mon projet. Merci également au Dr. Michel Rawiso pour la diffusion des rayons X. Merci au Professeur Patrice Woisel pour sa collaboration.

Merci à la plateforme de caractérisation de l'Institut Charles Sadron et à tout son personnel, notamment pour les expériences de GPC, Dr. Mélanie Legros, Catherine Foussat, et Catherine Saettel. Merci à Yves Gilbert pour l'entretien de la RMN, et à Laurence Oswald pour toutes les tâches qu'elle accomplit à l'institut. Merci au service de RMN de la Faculté de Chimie, notamment Maurice Coppe et Bruno Vincent.

Merci au personnel administratif pour sa gentillesse et disponibilité : Virginie Oberlé, Lea Koch, Magali Meyer, Paule Vannson, Odile Lemblé, ainsi que Jean Marc.

Merci à l'actuel directeur de l'Institut Charles Sadron, Dr. Christian Gauthier, ainsi qu'au Dr. Jean-Michel Guenet qui l'était au début de ma thèse.

La place me manque mais j'aimerais remercier tous mes amis, pour tout un tas de raisons trop longues à mentionner ici : Maxime P, Quentin, William, Jules, Thomas, Maya, Alex, Maxime H., Michelle, Paul, Léa, Aliette, Laurent, Jean-Vivien, Cécile, Elise, Margrethe, Perrine, Guillaume, Arthur, Julien E, Joy, Laura, Nicolas, Mathilde, Lumo, et j'en oublie sans doute un paquet qui m'en voudront…

Un énorme merci à mon frère et mes parents. Je ne serai pas là aujourd'hui sans leur support sans faille. Les mots me manquent pour décrire tout ce que je ressens pour eux, mais ils le savent très bien.

Florence, tu as été bien courageuse de me supporter durant ces quatre années ! Tu as été de loin celle qui croyait le plus en moi, et un soutien indéfectible en toutes circonstances. Je parlais d'aventure plus haut : sache que j'espère que celle que nous partageons, la plus importante pour moi, nous la partagerons encore un bon moment…

Finalement, merci beaucoup au Docteur Laurent Bouteiller, au Professeur Bernold Hasenknopf et au Professeur Luisa de Cola d'avoir accepté d'examiner ce travail.

Abbreviations and symbols

Å	ångström
Ac	acetyl
AcOH	acetic acid
ADA	acceptor-donor-acceptor
AFM	atomic force microscopy
Bn	benzyl
Boc	tert-butoxycarbonyl
°C	celsius degree
CDI	carbonyldiimidazol
CuAAC	copper-catalyzed 1,3-dipolar azide-alkyne cycloaddition
δ	chemical shift
DAD	donor-acceptor-donor
DABCO	1,4-diazabicyclo[2.2.2]octane
DB24C8	dibenzo-24-crown-8
DBU	1,8-diazabicyclo[5.4.0]undec-7-ene
DCM	dichloromethane
DFT	density functional theory
DIAD	diisopropyl azodicarboxylate
DMAP	4-dimethylaminopyridine
DMF	dimethylformamide
DMSO	dimethylsulfoxide
DSC	differential scanning calorimetry
DLS	dynamic light scattering
Equiv.	equivalent
ESI-MS	mass spectrometry with electrospray ionization
EtOAc	ethyl acetate
GPC	gel permeation chromatography
h	hour
HPLC	high performance liquid chromatography
HRMS	high resolution mass spectrometry
ITC	isothermal titration calorimetry
J	coupling constant
K	kelvin
K_d	dissociation constant
LC/MS	liquid chromatography coupled to mass spectrometry
LDA	lithium diisopropylamide
MALDI-TOF	matrix-assisted laser desorption/ionization – time of
µL	microliter

µm	micrometer
mL	milliliter
µmol	micromole
mmol	millimole
MS	mass spectrometry
Ms	mesityl
MW	microwave
nm	nanometer
NMR	nuclear magnetic resonance
OTs	tosylate
ppm	parts per million
PEG	poly(ethylene glycol)
PMDETA	N,N,N′,N″,N″-Pentamethyldiethylenetriamine
PPA	polyphosphoric acid
PPh_3	triphenylphosphine
RALS	right angle light scattering
R_f	retardation factor
R_g	gyration radius
R_H	hydrodynamic radius
r.t.	room temperature
SANS	small angle neutron scattering
SAXS	small angle x-ray scattering
SLS	static light scattering
T	temperature
TBAF	tetrabutylammonium fluoride
TBDPS	*tert*-butyldiphenylsilyl
TBS	*tert*-butyldimethylsilyl
TEM	transmission electron microscopy
TFA	trifluoroacetic acid
THF	tetrahydrofuran
TGA	thermogravimetric analysis
TMEDA	tetramethylenediamine
TMSA	trimethylsilylacetylene
TLC	thin layer chromatography
Ts	tosyl
TfO	triflate
UPLC	ultra performance liquid chromatography
Upy	ureidopyrimidinone
UV	ultra-violet
Vis	visible

Résumé en français

Les cinquante dernières années ont vu les scientifiques partir à la découverte et la conquête du monde nanométrique. D'énormes progrès en chimie et en physique ont fourni les outils nécessaires pour surpasser les défis technologiques et fondamentaux inhérents à cette échelle de taille, tels que le mouvements Brownien ou la difficulté à visualiser et manipuler des objets de cette dimension. Lors d'un désormais classique discours intitulé « There's plenty of room at the bottom : an invitation to enter a new field of physics », Richard Feynman, lauréat du prix Nobel de physique, insiste sur la nécessité de se tourner vers les opportunités et les défis offerts par les nanotechnologies. Avec en tête la stimulante perspective que représente la construction de molécules-machines capable d'opérer à l'échelle nanométrique, les chimistes ont exploité les outils issus de la chimie organique de synthèse et de la chimie supramoléculaire afin d'élaborer les premiers prototypes de machines moléculaires, en adoptant une approche de type « bottom-up ».

Les systèmes biologiques disposent d'une machinerie moléculaire reposant sur une collection d'assemblages de protéines aux fonctions variées. Ces machines biologiques remplissent des fonctions cruciales, allant de la synthèse de protéines (ribosome), le transport (kinésine), la synthèse de notre principale source d'énergie l'ATP (l'ATP synthase) jusqu'à l'amplification de leurs mouvements à l'échelle macroscopique, dans le cas des muscles. Dans ce dernier exemple, l'organisation hiérarchique de chaque composant est cruciale pour l'obtention d'une réponse macroscopique (**Figure 1**). La sous-unité la plus petite du muscle est appelée le sarcomère. Elle est constituée de myofilaments présentant des myosines, des moteurs biologiques alimentés par l'ATP, qui peuvent « marcher » le long de filaments d'actine, ce qui a pour résultat de réduire la taille globale du sarcomère. Ces unités sont organisées en fibres appelés myofibrilles, qui elles même s'agrègent en de plus grosses fibres musculaires. Cette organisation compacte et précise est à l'origine de l'amplification des mouvements collectifs de ces machines à l'échelle macroscopique. Les têtes de myosines fonctionnent hors-équilibre, consommant de l'énergie sous forme d'ATP afin d'assurer un travail et un mouvement d'extension ou de contraction continue.

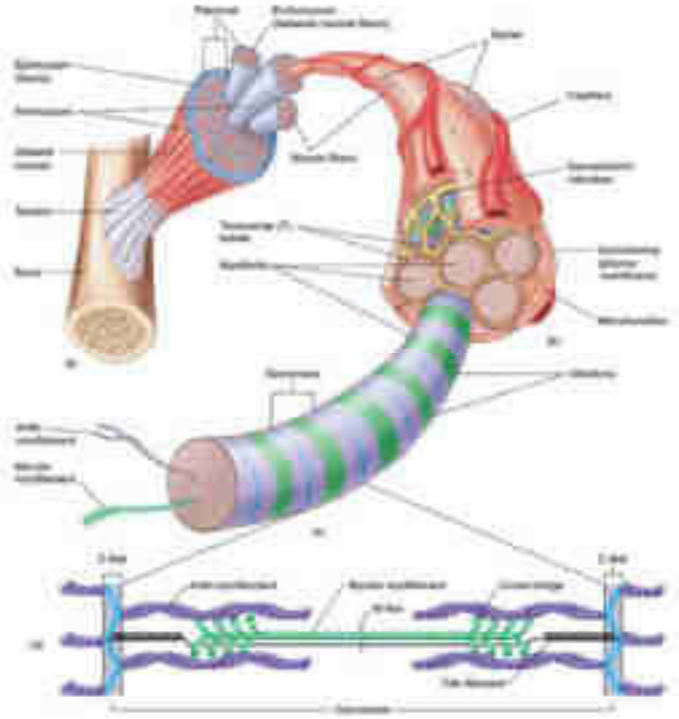

Figure 1 | Organisation hiérarchique des composants des muscles.

La première architecture artificielle capable d'effectuer un tel mouvement a été décrite par le groupe du Professeur Jean Pierre Sauvage en l'an 2000 (**Figure 2a**). Ils décrivirent la synthèse et l'utilisation de rotaxanes interpénétrés de type [c2]daisy chains, présentant différents sites de coordination afin de fixer des cations métalliques. En jouant sur la nature du métal et sa géométrie de coordination, ils ont été capables de commuter cette molécule entre un état contracté et étendu de façon réversible. Ce mouvement, conduisant à une variation de taille d'environ 1 nm, est reminiscent des contractions/extensions du sarcomère dans les muscles. Cependant, afin d'amplifier ce mouvement à des échelles de tailles supérieures, il est nécessaire de l'organiser dans de plus grandes structures tels que des assemblages polymériques. Cette approche sera expérimentée par les groupes de Stoddart et Grubbs (**Figure 2b,c**) qui ont décrit en 2009 la synthèse de polymères covalents de [c2]daisy chains. Dans cet exemple, les machines moléculaires peuvent être commutées entre leur état étendu et contracté par action d'une base ou d'un acide. Ces mouvements, répétés dans tout le polymère, permettent à l'architecture entière de se contracter ou s'étendre. Cependant, le faible degré de polymérisation (11 et 22 respectivement) ainsi que d'autres problèmes synthétiques et de caractérisations empêchèrent ces polymères de devenir de potentiels prototypes de muscles moléculaires.

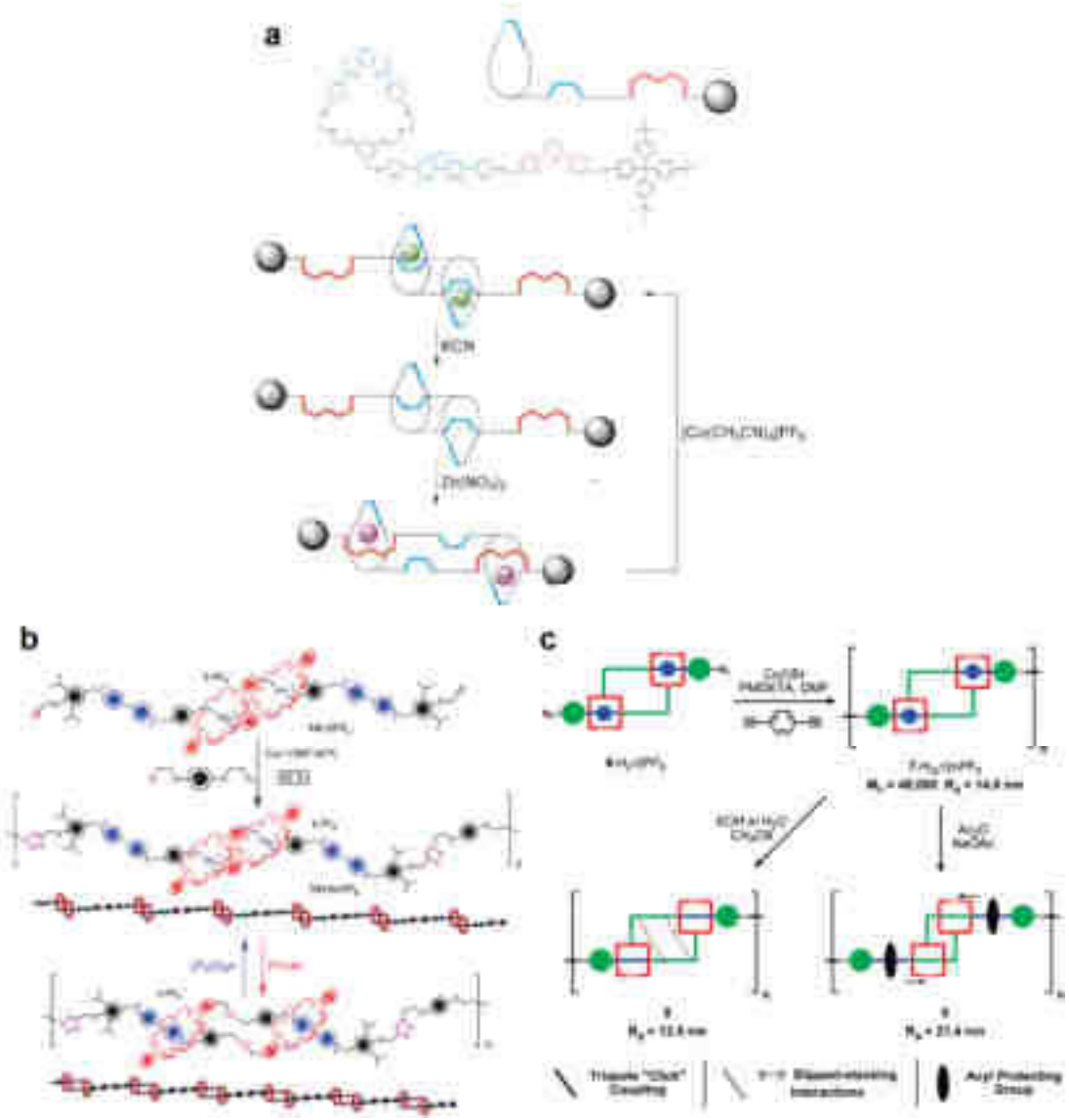

Figure 2 | a) [c2]daisy chains de Sauvage et polymères covalents de [c2]daisy chains de b) Stoddart et c) Grubbs.

Ces problèmes furent surmontés par notre équipe en 2012, avec la synthèse de [c2]daisy chains fonctionnalisées par des ligands terpyridine. L'addition d'ions métalliques tels que le fer (II) a permis de former de longues chaines uniques de polymère supramoléculaire de coordination, pouvant être contracté par l'ajout de base puis ré-étendu par réaction avec un acide. La combinaison d'expérience de diffusion des neutrons et de la lumière a permis d'observer une augmentation de la densité de masse linéaire des chaines polymères lors de la réaction avec une base, confirmant leur contraction. Ces longues chaines, associées à un degré de polymérisation aux alentours de 3000, se contractent de 16 à 9 µm, ce qui en fit le premier exemple d'amplification macroscopique de mouvements nanométriques collectifs de machines moléculaires dans une chaine polymère.

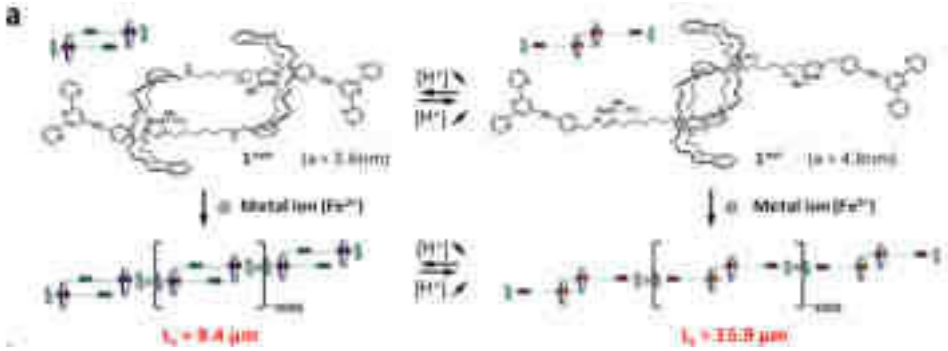

Figure 3 | [c2]daisy chains fonctionnalisés par des terpyridines polymérisés par l'ajout de Fer (II). Les chaines en résultant peuvent être commuté entre un état étendu et contracté par réaction acido/basiques.

Dans les précédents exemples, les machines moléculaires utilisées opèrent à l'équilibre thermodynamique : elles peuvent être commutées entre deux états qui représentent des minimas thermodynamiques. Cependant, la plupart des machines moléculaires biologiques décrites plus haut effectuent des mouvements continus, fonctionnent hors-équilibre, consommant de l'énergie sous forme d'ATP. En 1999, le groupe du Professeur Ben Feringa a décrit la synthèse d'un moteur moléculaire capable de décrire une rotation unidirectionnelle quand il est alimenté par de l'énergie sous forme de lumière : ces composés peuvent effectuer un mouvement continu lors d'un apport d'énergie constant.

Figure 4 | Un moteur moléculaire synthétisé par notre groupe, inspire par les travaux de Feringa.

Ces moteurs sont basés sur un alcène encombré qui subit une isomérisation par exposition à la lumière UV. Il en résulte un intermédiaire instable, qui va se relaxer en effectuant une inversion d'hélice, processus thermique, afin d'achever une rotation à 180°C. La répétition de ces deux étapes permet d'effectuer une rotation complète autour de la double liaison centrale (**Figure 4**).

En 2015, notre groupe reporta l'utilisation de moteurs moléculaires inspirés des travaux de Feringa en tant que nœuds de réticulation de réseaux polymères, résultant en un gel chimique. Lorsqu'irradié dans l'UV, le gel a pu être contracté jusqu'à atteindre 20% de sa taille initiale après 2 heures (**Figure 5**). Cette contraction résulte de la rotation des moteurs qui progressivement emmêlent les chaines polymères, réduisant la taille du réseau et donc du gel. Cet exemple est le premier cas d'amplification à l'échelle macroscopique de la rotation continue de moteurs moléculaires.

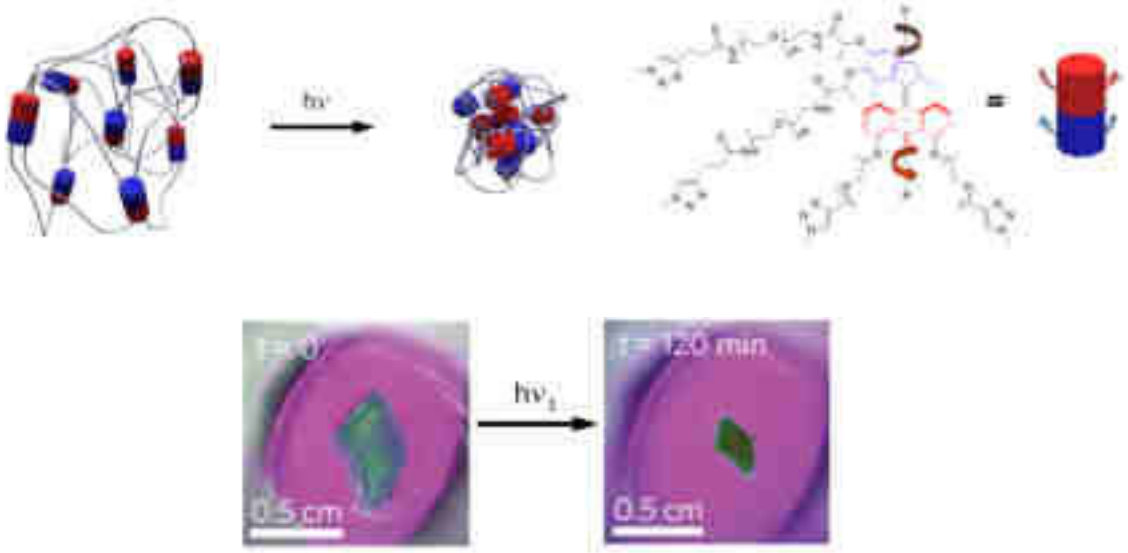

Figure 5 | Un réseau polymérique 3D se contractant sous l'action de moteurs moléculaires, resultant en la reduction de la taille d'une morceau de gel de 100% à 20% de son volume initial en deux heures, sous exposition à la lumière UV.

L'objectif de cette thèse est double : 1/ organiser des polymères de [c2]daisy chains au-delà de la chaine unique, dans des fibres ou réseaux, de façon à obtenir des matériaux capables de traduire à l'échelle macroscopique les mouvements collectifs de nanomachines le constituant, et 2/ introduire un composant appelé modulateur dans les gel moteur/polymères, afin de rendre leur contraction réversible, une fonction naturellement impossible due à la nature unidirectionnelle des moteurs moléculaires utilisés (**Scheme 1**).

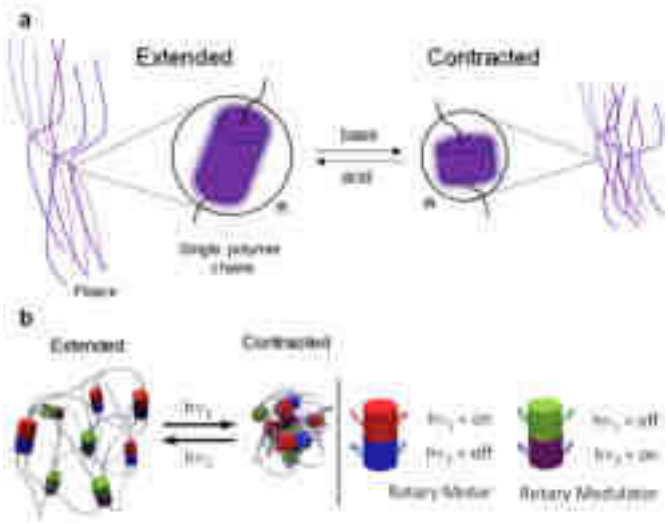

Scheme 1 | a) Organisation de polymères de [c2]daisy chains en des fibres contractiles, b) introduction d'un modulateur dans les systèmes moteurs/polymères afin d'inverser la contraction.

Le premier chapitre de ce manuscrit décrit la synthèse de polymères supramoléculaires à liaisons hydrogène basés sur l'association de [c2]daisy chains $\mathbf{2}^{\mathbf{Ext}}$ fonctionnalisés par un motif 2,6-diacetylaminopyridine et d'un connecteur bis-uracil **3**. Le connecteur devrait assurer l'agrégation des chaines grâce à une combinaison d'interactions π et de Van der Waals. Le caractère amphiphile de l'unité de répétition, constituée d'un rotaxane polaire chargé et d'un connecteur apolaire présentant des chaines alkyl, devrait induire davantage d'interaction latérales inter chaines (**Scheme 2**).

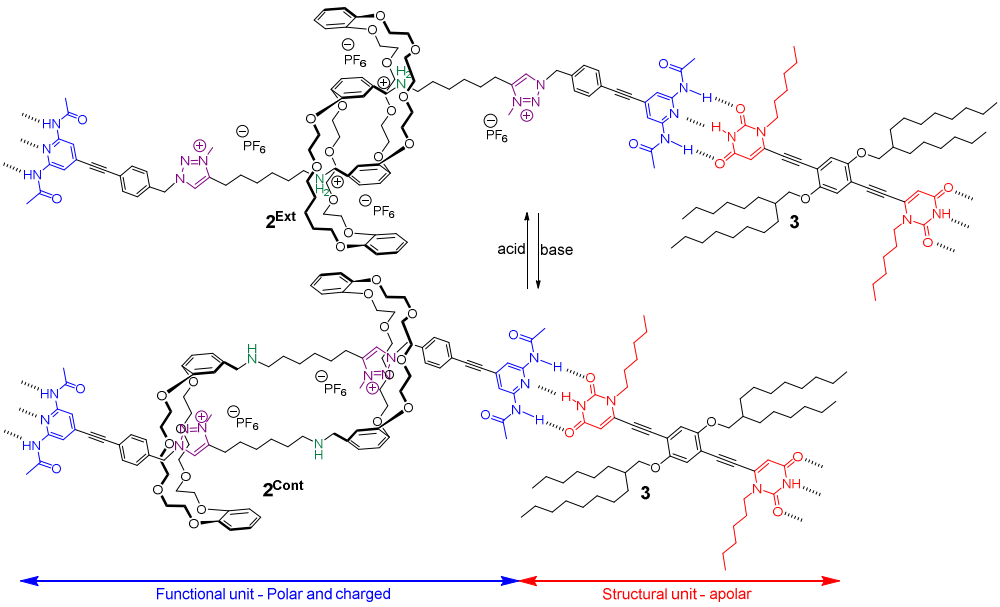

Scheme 2 | Un co-polymère supramoléculaire basés sur un connecteur uracil et des [c2]daisy chains 2,6diacetylaminopyridine complémentaires.

L'unité rotaxane a pu être contractée et étendue de façon réversible en déprotonnant/protonant l'ammonium, ce qui a pu être suivi par spectroscopie RMN ^{1}H. L'association des deux composés en proportion 1 :1 induit la formation d'un polymère à liaisons hydrogène, comme en témoignèrent les déplacements chimiques caractéristiques observés pour les signaux des protons N-H, dans l'état contracté et étendu. Nous avons pu observer qu'au-delà d'une certaine concentration, un élargissement notable des pics en RMN apparaissait : signe d'une probable agrégation des chaines polymères en de plus grosses architectures. Des expériences de diffusions des neutrons et de la lumière ont montré qu'en effet à ces concentrations des structures de grandes dimensions, avec une organisation au-delà de la chaine polymère unique, sont présentes, et différentes dans l'état contracté ou étendu. Ces structures ont ensuite été étudiées par TEM et AFM. Dans l'état étendu, l'échantillon analysé par TEM révèle de longues fibres longues de plusieurs micromètres (**Figure 6a,b,c,d**). Des zooms effectués par AFM permettent de déterminer que ces fibres sont le résultat de l'agrégation latérale de chaines uniques de polymère supramoléculaire. La structure contractée a par contre révélé des objets discrets et réguliers d'une taille comprise entre 400 et 600 nm. Les expériences d'AFM ont démontré que ces structures émergent d'une organisation similaire à celle de l'échantillon étendu (**Figure 6e,f,g,h**). Les contractions/extensions ont également pu être effectuées *in situ*. L'analyse d'un échantillon étendu traité avec une base produit de petits objets similaires à l'échantillon contracté, et le traitement de l'échantillon contracté avec un acide révèlent de longues fibres qui rappellent l'échantillon étendu.

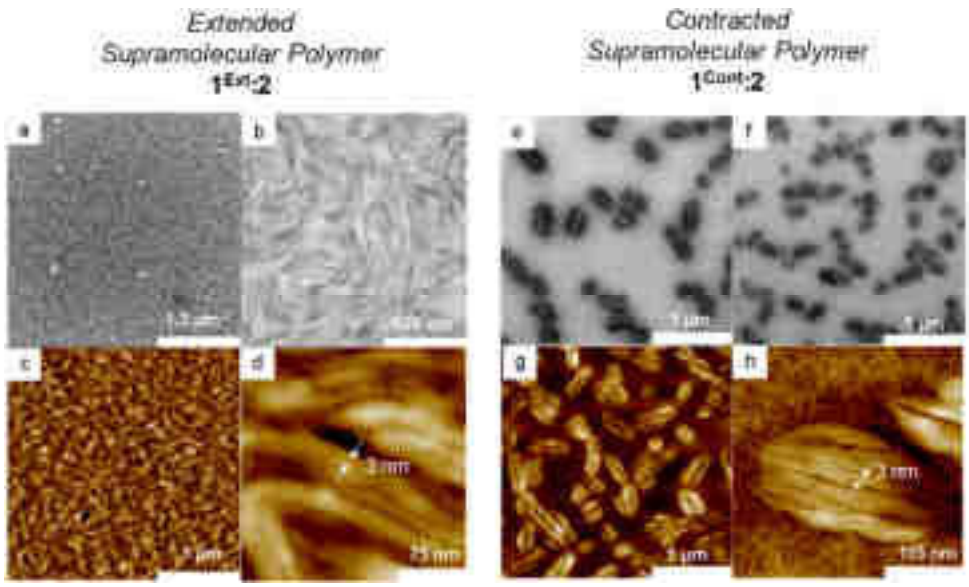

Figure 6 | Images TEM et AFM de **2^{Ext}:3** (a,b,c,d) et **2^{Cont}:3** (e,f,g,h).

Cet exemple représente le premier polymère supramoléculaire à liaisons hydrogène basé sur des rotaxanes de type [c2]daisy chains. Les architectures qu'ils décrivent, des fibres émergentes de l'agrégation latérale de chaines simples, sont capables d'être commutées entre deux états, ce qui est le résultat de l'amplification des mouvements nanoscopiques de leurs constituants à l'échelle microscopique.

Le deuxième chapitre décrit la synthèse et l'étude de [c2]daisy chains fonctionnalisés par des dérivés uréidopyrimidinones protégés par un groupement photolabile. Leur irradiation à 365 nm a permis de retirer le groupement protecteur et de révéler le groupement ureidopyrimidinone, déclenchant la polymérisation du système par liaisons hydrogène. La déprotection du composé étendu a produit un gel, tandis que la déprotection de l'espèce contractée nous a fourni une solution (**Figure 7**). Le gel peut être converti en solution par déprotonation/contraction des sous unités [c2]daisy chains et reconverti en gel par l'addition d'un acide, déclenchant la ré extension des chaines polymère. Les polymères supramoléculaires ont été étudiés par ITC, DSC, RMN, ainsi que des expériences de diffusion du rayonnement.

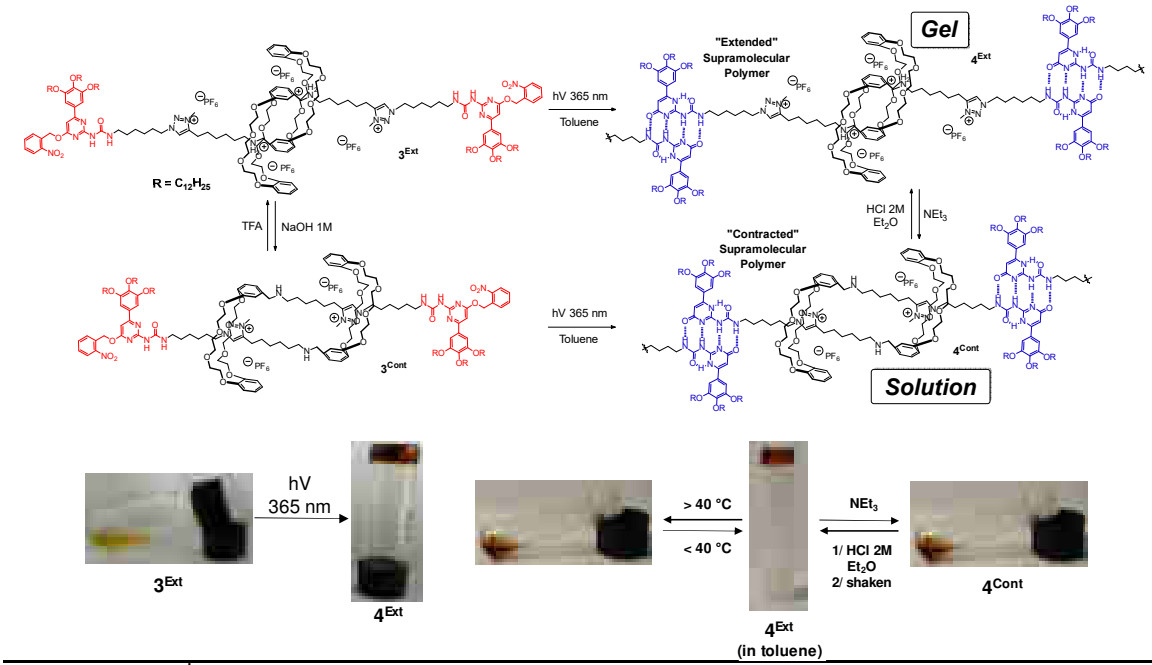

Figure 7 | Polymérisation des rotaxane $\mathbf{3^{Ext}}$ et $\mathbf{3^{Cont}}$ et caractère stimulable des polymères obtenus.

Ces expériences de diffusion des neutrons et de la lumière ont révélé des structures drastiquement différentes dans le gel (polymère étendu) et la solution (polymère contracté) (**Figure 8**). Dans le cas du système contracté, la solution, des chaines polymère sans organisation particulière ont été observé et associé avec un faible degré de polymérisation de 22, ce qui est en accord avec les expériences d'ITC. La proximité des éthers couronnes par

rapport au site d'association peut expliquer ce résultat. La diffusion des neutrons sur le gel, le polymère étendu, laisse imaginer une structure bien plus complexe, notamment à travers la présence de pics de structure. Un traitement original des données a permis de soustraire la contribution du monomère à ces données, afin d'obtenir de nouvelles données associées à la structure du gel uniquement. Ce traitement nous a permis de proposer que dans le polymère contracté, la gélification est dûe à la formation de colonnes de dimer ureidopyrimidinones, servant de nœuds de réticulation et formant un réseau. La formation de ces colonnes est défavorisée pour des raisons stériques dans l'état contracté, ce qui empêche la formation d'un réseau dans ce cas et donc la gélification du système.

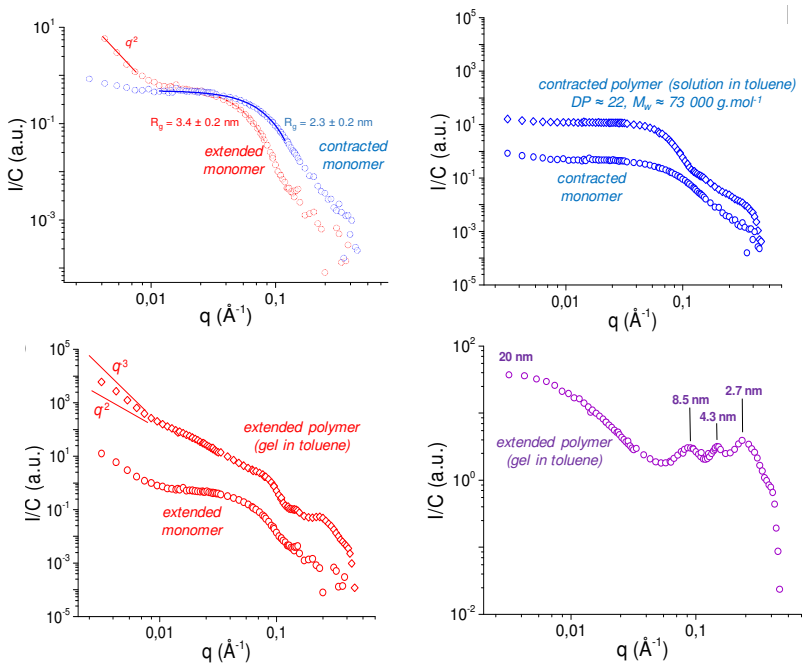

Figure 8 | Expériences de diffusion des neutrons menées sur les polymère $\mathbf{4}^{\text{Ext-G}}$ et $\mathbf{4}^{\text{Cont-S}}$.

Dans ce système, les mouvements collectifs des machines moléculaires sont traduits par des transitions d'états physiques à l'échelle macroscopique, résultat d'une réorganisation complète du système à plusieurs échelles. Cependant, la dépendance du degré de polymérisation à l'état étendu/contracté des [c2]daisy chains limite cette approche supramoléculaire.

Le troisième chapitre décrit la synthèse de réseaux covalents à base de [c2]daisy chains. La synthèse de tels réseaux devrait produire des gels chimiques capables de modifier leur taille en fonction de l'état étendu/contracté des [c2]daisy chains le constituant. Ces réseaux ont été synthétisé en combinant le pseudo rotaxane **16** à deux connecteurs **30** et **32** dans des proportions

variées dans des moules métalliques (**Figure 9**). Les matériaux obtenus gonflent dans la plupart des solvants organiques pour donner un gel chimique qui sera ensuite méthylé.

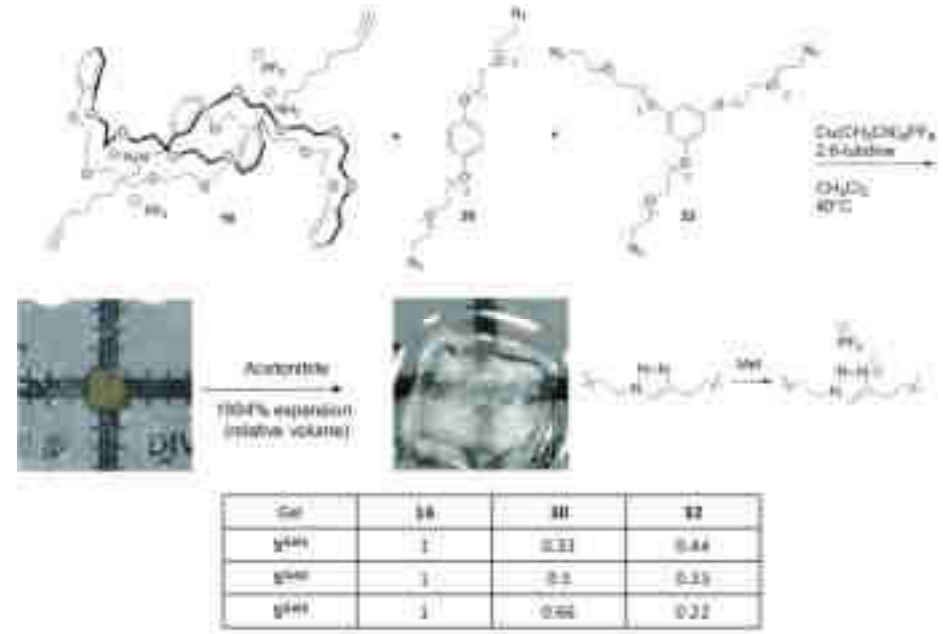

Figure 9 | Synthèse de réseaux covalents à base de [c2]daisy chains.

Ce gel peut être contracté par immersion dans une solution basique, puis ré étendu par immersion dans une solution acide (**Figure 10**). Ces contractions/extensions ont pu être répétées plusieurs fois sans dégradation du matériau, et les gels non méthylés ne se contractant pas, il semblait que la contraction/extension observée découle directement du mouvement des [c2]daisy chains constituant le réseau.

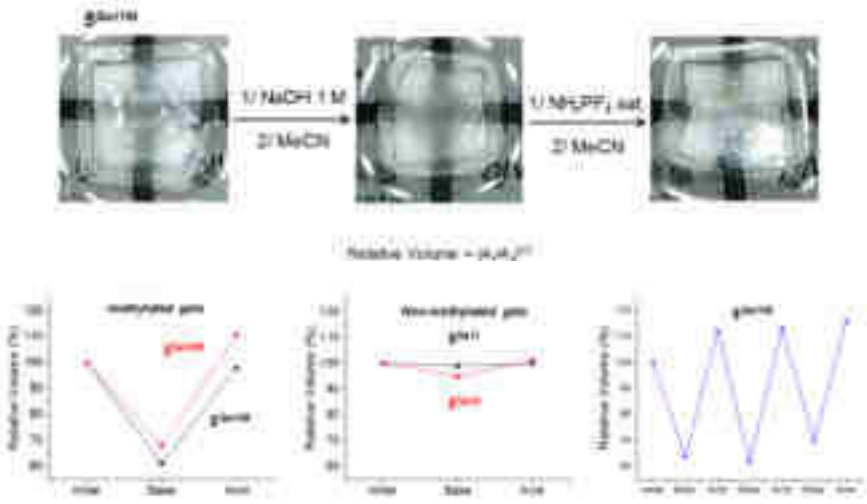

Figure 10 | Variation de volume des gels après traitement avec une solution basique ou une solution acide.

Des expériences de diffusion des neutrons furent effectuées sur des échantillons contractés et étendus de ces gels. Il fut observé que lors de la contraction, la densité de masse linéaire augmente, confirmant une contraction des chaines polymère (**Figure 11**). Cette expérience confirme que les variations macroscopiques de volumes observées viennent directement de la contraction/extension des chaines de polymères constituant le matériau.

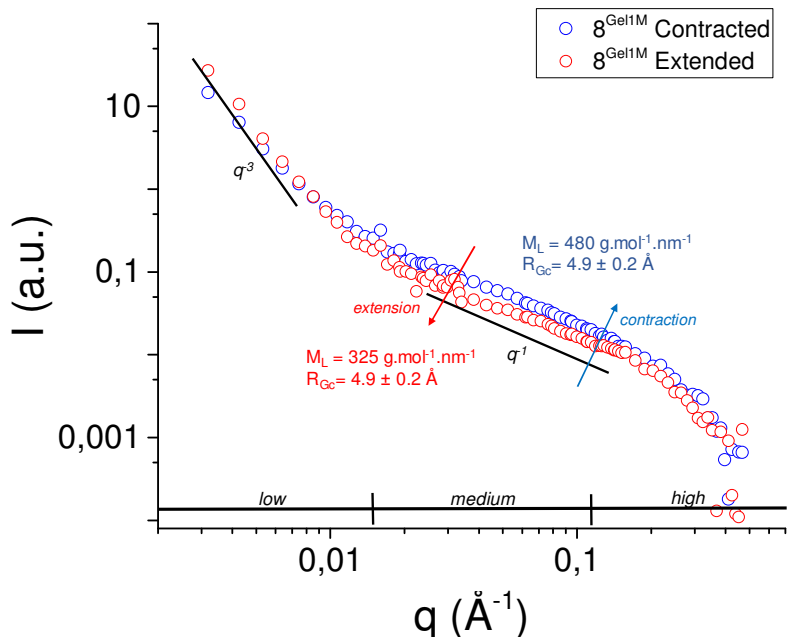

Figure 11 | Diffusion des neutrons d'un échantillon étendu (en rouge) et contracté (en bleu).

Le quatrième chapitre décrit l'addition d'une unité modulatrice aux gels contractiles basés sur l'action de moteurs moléculaires rotatifs emmêlant des chaines polymère et réduisant la taille du réseau. Le caractère unidirectionnel de ces moteurs, qui ne peut pas être inversé sans modification chimique, rend la contraction irréversible. Dans ces travaux, nous avons introduit une unité capable de relâcher la tension accumulée lors de la contraction, autorisant les chaines polymère à se dérouler (**Figure 12**). Ce modulateur devrait fonctionner à une longueur d'onde orthogonale au moteur, ce qui fait des composés de type diarylethene des bons candidats. Ces composés peuvent être commutés entre une forme « ouverte » (lumière visible) et une forme fermée (lumière UV). Lors de l'irradiation par des UV, les moteurs tournent et contractent le gel, le modulateur fermé soutenant le travail des moteurs. Lors de l'exposition à la lumière visible, le moteur est inactif et la libre rotation permise entre les liaisons centrales permet aux chaines de se dérouler, restaurant la taille initiale du réseau et donc du gel.

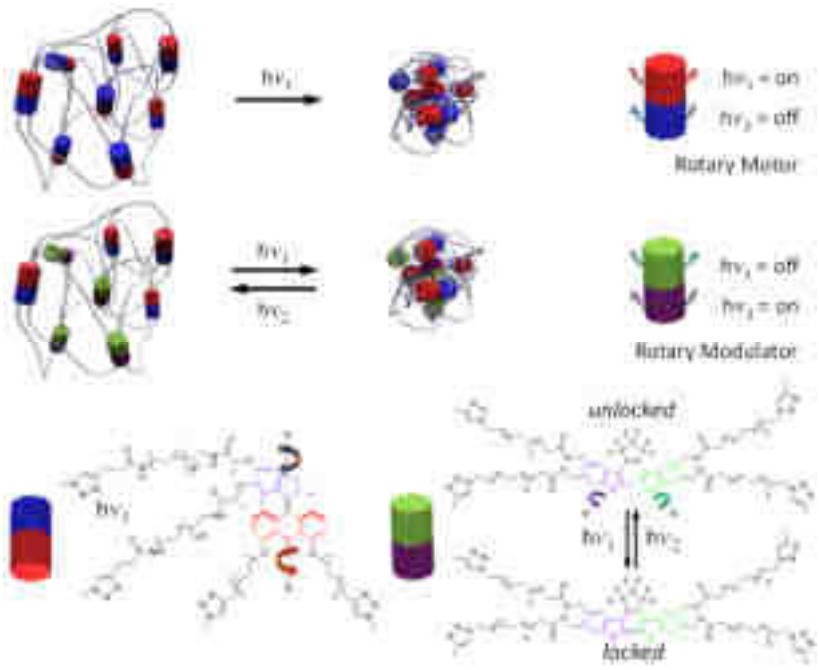

Figure 12 | Principe de fonctionnement d'un réseaux polymère intégrant des unité moteur moléculaire et modulateur comme point de réticulation.

Deux moteurs **M-9** et **M-10** et une unité modulatrice **R-11** ont été synthétisés. Des expériences de modélisation ont montré que la libre rotation est bien possible autour des liaisons simples de l'unité modulatrice. De plus, son photochromisme a été démontré par des expériences d'irradiations suivies en RMN et spectroscopie UV Visible. A partir de ces composés, différents gels avec différentes proportions de modulateurs ont été synthétisés (**Figure 13**).

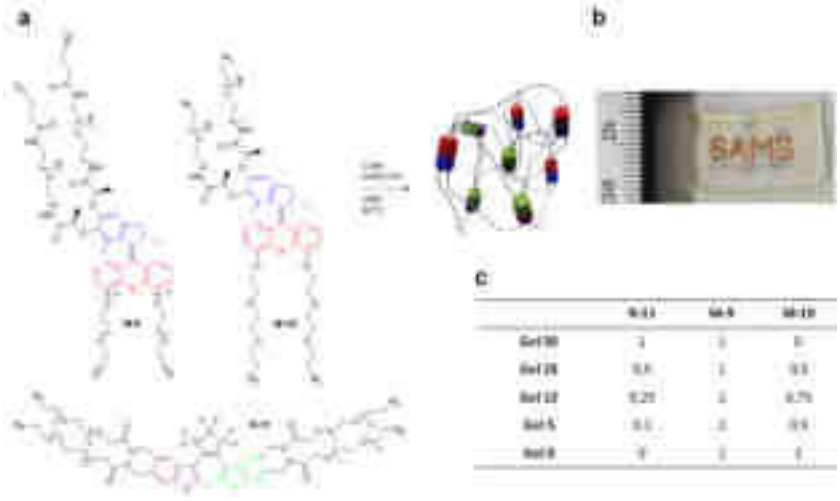

Figure 13 | Synthèse de réseaux polymères intégrant différentes proportions de moteur/modulateur.

Lors de l'exposition à la lumière UV, les gels ont pris une couleur pourpre liée à la forme fermée du modulateur, et ont vu leur taille réduire d'environ 30-40% au bout de deux heures. Comme anticipé par des études théoriques et un modèle mathématique, tous les gels, même ceux disposant d'une faible quantité d'unité modulatrice, sont retournés à leur volume initial après exposition à la lumière visible (**Figure 14**).

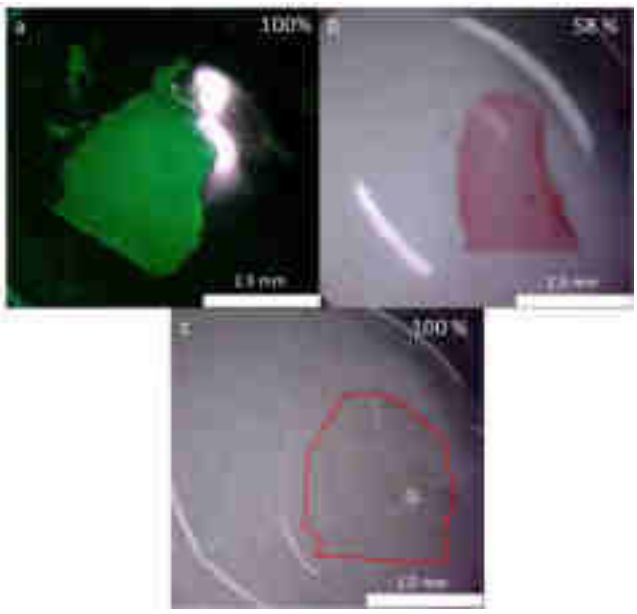

Figure 14 | Photographie d'un morceau de gel 50 a) avant irradiation, b) après trois heures d'irradiation UV, c) après exposition à la lumière visible.

De plus, un gel sans modulateur n'a pas montré d'augmentation de son volume dans les mêmes conditions, prouvant la nécessité d'introduire une unité modulatrice. La vitesse initiale de contraction dépend de la proportion de modulateur, et le gel n'en disposant que d'une faible quantité (5% par rapport aux moteurs) présente une vitesse initiale similaire au gel sans modulateur (**Figure 15a**). De plus, les gels ont été soumis à la fois à la lumière UV et visible. En fixant la distance échantillon-UV, varier la distance visible-échantillon a pour conséquence de fixer le gel dans des volumes précis, résultat d'un contrôle sur la proportion de modulateur ouvert/fermé. Chaque volume observé est le résultat d'un état stationnaire hors-équilibre, et dépend du ratio des fréquences effectives de rotation du moteur et du modulateur dans des directions opposées (**Figure 15b**). Cette propriété est réminiscente des systèmes hors-équilibre biologiques qui modulent souvent des flux allant dans des sens inverses (réactions chimiques, auto-assemblages/désassemblages…) afin de contrôler leurs activités et propriétés. L'approche décrite ici a été le premier exemple d'une approche systémique pour introduire des fonctions réversibles dans des matériaux exploitant des composés agissant de façon irréversible.

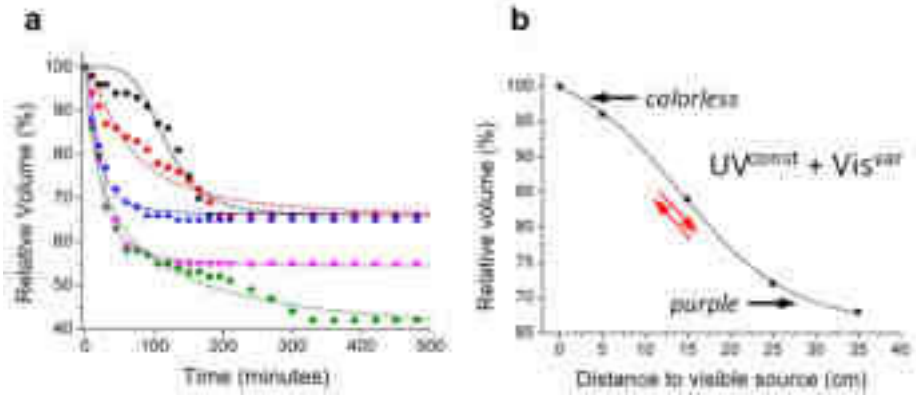

Figure 15 | a) Cinétique de contraction des gel moteur/modulateur, b) expérience d'exposition à plusieurs sources de lumières

Les travaux décris dans cette thèse montrent que la conception de machines moléculaires originales et leur intégration dans des systèmes complexes permet l'amplification de mouvements nanométriques à plusieurs échelles. Le dernier système, un système hors-équilibre capable de moduler son activité et sa taille, présente beaucoup de points communs avec les systèmes biologiques, et l'intégration de ces fonctions dans un matériau macroscopique sont tout à fait originales. Dans l'ensemble, les résultats obtenus ici devraient servir de de base à l'élaboration de matériaux encore plus complexes et efficaces dont l'activité et les propriétés sont modulées par le mouvement de machines moléculaires.

General introduction and Objectives

The past fifty years have witnessed the conquest of the nanoscopic world. Tremendous progresses in chemistry and physics provided tools to overcome issues associated with the nanoscopic scale such as Brownian motion and difficulties to visualize the structures of interest. In a now classic lecture entitled "*There's Plenty of Room at the Bottom: an Invitation to Enter a New Field of Physics*", Physics Nobel prize laureate Richard Feynman urged the necessity to turn ourselves to possibilities and challenges offered by nanotechnologies.[1]

With the exciting perspective of building small machines operating at the nanoscale, chemists exploited the tools provided by supramolecular chemistry and mechanical bonds to elaborate prototype of molecular machinery,[2] using a "bottom-up" approach.

Nanoscopic motions are used by biomolecular machines in various ways, from the synthesis of ATP by rotary motor ATP synthase to the amplification of myosin/actin gliding motions in muscles.[3]

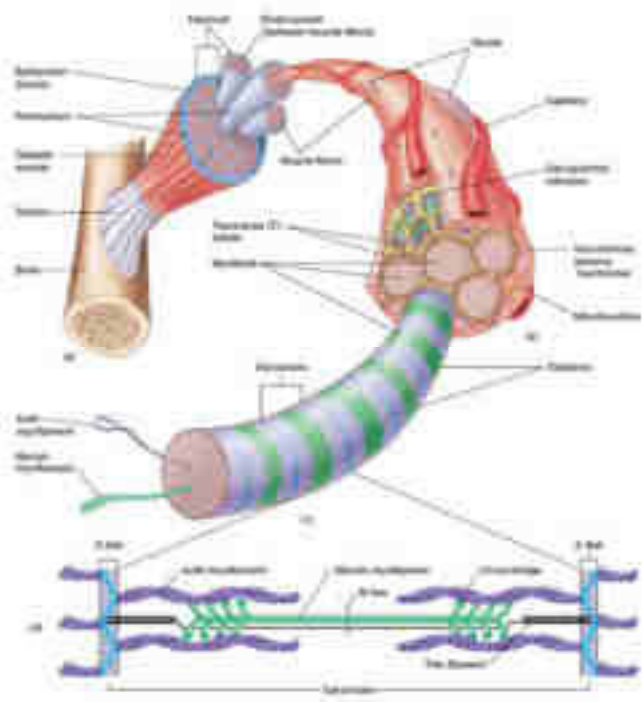

Figure 16 | Hierarchical organization of muscles.[1]

[1] Feynman, R. P. *Engineering and Science*.
[2] Kay, E. R. & Leigh, D. A. Rise of the molecular machines. *Angew. Chem. Int. Ed.* **54**, 10080-10088 (2015).
[3] Kinbara, K. & Aida, T. Toward intelligent molecular machines: Directed motions of biological and artificial molecules and assemblies. *Chem. Rev.* **105**, 1377-1400 (2005).

Regarding this last example, hierarchical and perfect organization of contractile units is responsible for the macroscopic actuation of these complex structures (**Figure 16**).[4]

The smallest subunit of a muscle is the sarcomere. Within this unit, myofilaments are composed of myosin, an ATP-fueled biomolecular motor, which "walks" along actin myofilaments, thus bringing the z-disk closer and then reducing the size of the sarcomere. Sarcomeres are organized into fibers called myofibrils, which themselves aggregate into wider muscle fibers. This compact hierarchical organization is responsible for the amplification of the collective motions of biomolecular machines up to the macroscopic scale.

Inspired by this elegant combination of molecular machines and self-assembly, the result of thousands years of evolution, several groups engaged in the challenge to synthesize an artificial molecular muscle operating thousands of molecular machines at the same time.[5] The first system fitting this description was reported by our group in 2012, taking advantage of pH switchable interpenetrated rotaxanes called [c2]daisy chains functionalized with terpyridine units (**Figure 17a**).[6]

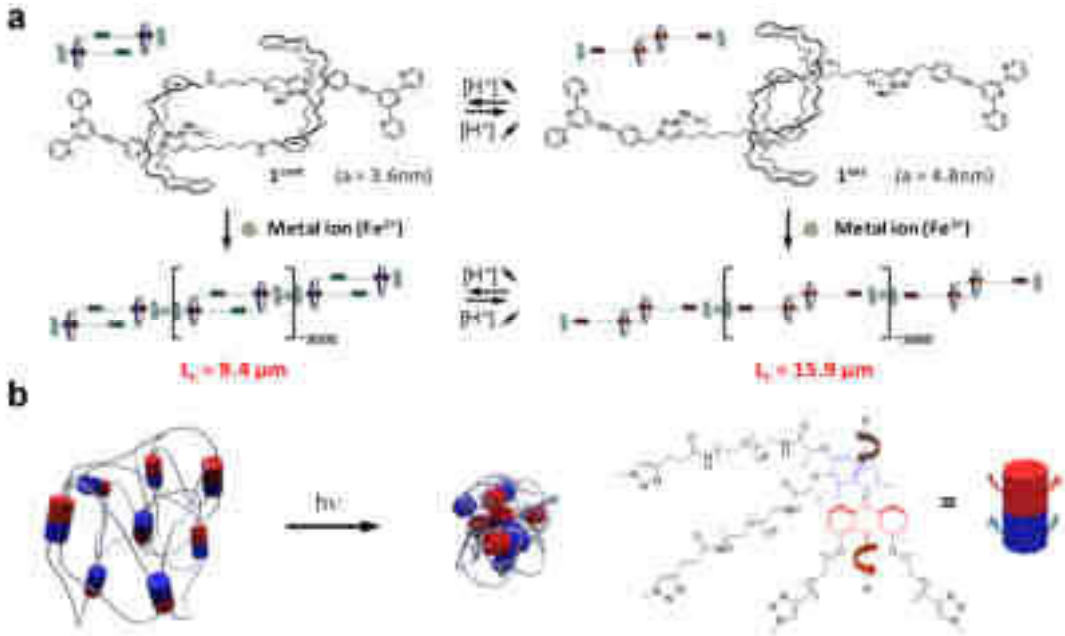

Figure 17 | a) Coordination supramolecular polymer made of contractile [c2]daisy chains units. Their collective contraction/extension changes the average size of the polymer chains.[2] b) A polymer network including light-driven molecular motors as reticulating nodes and contracting upon irradiation at 365 nm.[3]

[4] Krans, J. L. The sliding filament theory of muscle contraction. *Nat. Educ.* **3**, 66-69 (2010).
[5] Coskun, A., Banaszak, M., Astumian, R. D., Stoddart, J. F. & Grzybowski, B. A. Great expectations: can artificial molecular machines deliver on their promise? *Chem. Soc. Rev.* **41**, 19-30 (2012).
[6] Du, G., Moulin, E., Jouault, N., Buhler, E. & Giuseppone, N. Muscle-like supramolecular polymers: Integrated motion from thousands of molecular machines. *Angew. Chem. Int. Ed.* **51**, 12504-12508 (2012).

The addition of iron (II) triggered the formation of long supramolecular single polymer chains (degree of polymerization around 3000), which were fully characterized by a series of light and neutron scattering experiments. These investigations revealed that deprotonation, *i.e.* contraction, of a single [c2]daisy chain was translated into a response at the microscopic scale, namely a contraction of the polymer chains from 15.9 µm to 9.4 µm, and with a collective motion that can be reversed upon addition of acid.

More recently, our group has also demonstrated that light-driven molecular motors can be used as cross-linking nodes into a polymer network thus allowing for the formation of gels that contract upon light irradiation (**Figure 17b**).[7] Rotation of the motors induced entanglement of the polymer chains, leading to the reduction of the overall size of the network, and thus the size of the gel from 100% to 20%. This system was the first example of molecular machine-based soft material displaying macroscopic contraction induced by the collective motions of motors, *i.e.* working out of equilibrium.

Following up to these results, the general goal of the work presented in this manuscript was twofold: first, to amplify the concerted motions of nanomachines up to the macroscopic scale, by taking advantage of [c2]daisy chains based materials, and second to develop reversible version of the contractile gels using light-driven molecular motors.

On the one hand, the [c2]daisy chains needed to be organized into fibers and networks to observe their motions efficiently amplified at the macroscopic scale such as in muscles (**Figure 18a**).[5] The ultimate goal was the synthesis of stimuli-responsive muscle-like gels or films, operating like artificial molecular muscles. This work required careful design of rotaxanes and their supramolecular connector to induce inter-chains aggregation or reticulation of the single-chains into a 3D network.

[7] Li, Q. *et al.* Macroscopic contraction of a gel induced by the integrated motion of light-driven molecular motors. *Nat. Nanotech.* **10**, 161-165 (2015).

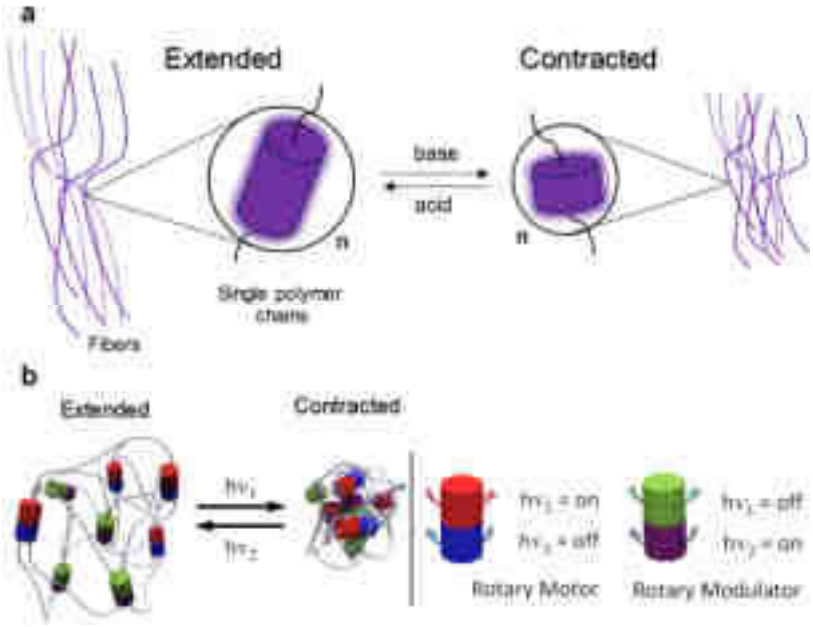

Figure 18 | a) [c2]daisy chains subunits organized in polymer chains and then into fibers which size can be controlled by the extended/contracted state of the rotaxane units. b) A two-component contractile chemical network responding to orthogonal stimuli.

On another hand, light-driven molecular motor based materials needed to be improved. Indeed, as light-driven molecular motors operate through a ratchet-like mechanism, the reversibility of the contraction was not possible. Reversible functions are essential for the design of useful materials based on molecular machines. Herein, we have investigated the addition of another component to the gel: a modulating unit able to unwind the polymer chains, thus leading to its extension (**Figure 18b**).

Our expectations on the elaboration of such systems was to give valuable insights on how nanoscopic motions of responsive units involved in the formation of a material can affect its properties at the macroscopic scale, thus representing a stepping stone towards the elaboration of a new class of muscle-like materials.

Bibliography

Chapter I: Supramolecular Chemistry: from early concepts to supramolecular polymers

I. Supramolecular Chemistry

From the synthesis of urea in 1828 by Wöhler[8] to the one of the Vitamin B12 by Woodward in 1973,[9] chemical synthesis continuously improved its ability to synthesize complex targets, to the point it is seen as an art by majors contributors to the field.[10] The growth of this area of research has been mainly driven by the formation of covalent bonds and the study of the properties associated to individual molecules. In the late 80's, the work related to the field of supramolecular chemistry has been described as "chemistry beyond the molecule",[11] focusing not anymore only on the geometric and electronic structures of individual molecules, but on how they interact with each other to create larger and complex supramolecular structures, from which might emerge new properties that are more than the addition of those of the components.

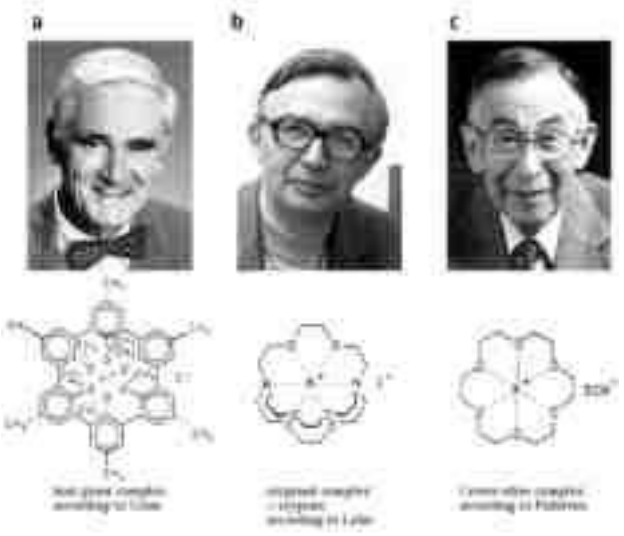

Figure 19 | 1987 Chemistry Nobel Prize winners a) Donald J. Cram and a lithium receptor, b) Jean-Marie Lehn and a cryptate, c) Charles J. Pedersen and a potassium-crown ether complex.[12]

Donald J. Cram, Jean-Marie Lehn and Charles J. Pedersen were awarded the Chemistry Nobel Prize in 1987 "for their development and use of molecules with structure-specific

[8] Friedrich, W. Ueber künstliche bildung des harnstoffs. *Ann. Phys.* **12**, 253-256 (1828).
[9] Woodward, R. B. The total synthesis of vitamin B12. *Pure Appl. Chem.* **33**, 145-178 (1973).
[10] Nicolaou, K. C., Sorensen, E. J. & Winssinger, N. The art and science of organic and natural products synthesis. *J. Chem. Educ.* **75**, 1225-1258 (1998).
[11] Lehn, J.-M. Supramolecular chemistry - scope and perspectives molecules, supermolecules, and molecular devices (Nobel Lecture). *Angew. Chem. Int. Ed. Engl.* **27**, 89-112 (1988).
[12] Cram, D. J., Lehn, J.-M., Pedersen, J. P. The Nobel Prize in Chemistry (1987), Retrieved June 28, 2016, from http://www.nobelprize.org/nobel_prizes/chemistry/laureates/1987/.

interactions of high selectivity" (**Figure 19**), this work being the first step towards many new areas of research.[13]

The synthesis of efficient host-guest systems, *i.e.* an entity made of a receptor and an associated substrate like a key and a lock,[14] could be seen as the first milestone of this new chemical adventure.[15] In **Figure 19**, each laureate is represented along with its emblematic host-guest system. Cation recognitions by macrocycle like cryptands[16] and crown ethers[17] have been achieved with high substrate specificity and applied to fields such as transport[18] and catalysis.[19] All these macrocycles hold their properties from non-covalent interactions. Supramolecular chemistry revolves around the synthesis of molecules able to associate *via* a variety of non-covalent interactions, which are forming the toolbox of the supramolecular chemist (**Figure 20**).

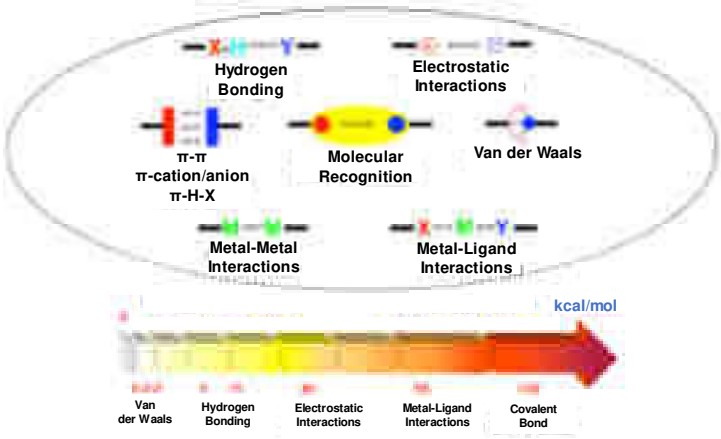

Figure 20 | "The toolbox of a supramolecular chemist" reproduced from Prof. Mir Wais Hosseini lecture: "Introduction to supramolecular chemistry".

Molecular design allows to "program" the ability of individual molecules to associate into much complex entities *via* supramolecular interactions. The main advantage of building around these interactions is their reversibility: compared to covalent bonds, electrostatic interactions,

[13] Busseron, E., Ruff, Y., Moulin, E. & Giuseppone, N. Supramolecular self-assemblies as functional nanomaterials. *Nanoscale* **5**, 7098-7140 (2013).
[14] Lichtenthaler, F. W. 100 years'schlüssel-schloss-prinzip': What made Emil Fischer use this analogy? *Angew. Chem. Int. Ed. Engl.* **33**, 2364-2374 (1995).
[15] Cram, D. J. The design of molecular hosts, guests, and their complexes (Nobel Lecture). *Angew. Chem. Int. Ed. Engl.* **27**, 1009-1020 (1988).
[16] Dietrich, B., Lehn, J. M. & Sauvage, J. P. Diaza-polyoxa-macrocycles et macrobicycles. *Tetrahedron Lett.* **10**, 2885-2888 (1969).
[17] Pedersen, C. J. Cyclic polyethers and their complexes with metal salts. *J. Am. Chem. Soc.* **89**, 2495-2496 (1967).
[18] Kirch, M. & Lehn, J.-M. Selective Transport of alkali metal cations through a liquid membrane by macrobicyclic carriers. *Angew. Chem. Int. Ed. Engl.* **14**, 555-556 (1975).
[19] Nakamura, K., Nishiyama, S., Tsuruya, S. & Masai, M. Oxidation of catechol with $KMnO_4$ by using crown ethers as phase transfer catalysts. *J. Mol. Catal.* **93**, 195-210 (1994).

hydrogen bonding, π-π stacking and to some extent, metal-ligand interactions can be broken and can repair themselves without external intervention.

Nature, unsurprisingly, is a great source of inspiration for supramolecular chemists. Indeed, biological systems often combine various non-covalent interactions in order to create complex functional systems. From the structure of DNA to the folding of proteins, non-covalent interactions rule the organization of highly relevant biological entities. From precise structures and dynamics imposed by supramolecular interactions emerge complex functions which characterize living systems.[20,21]

Inspired by biological functions, supramolecular chemists synthesized models which structures and functions mimic those of proteins.[22]

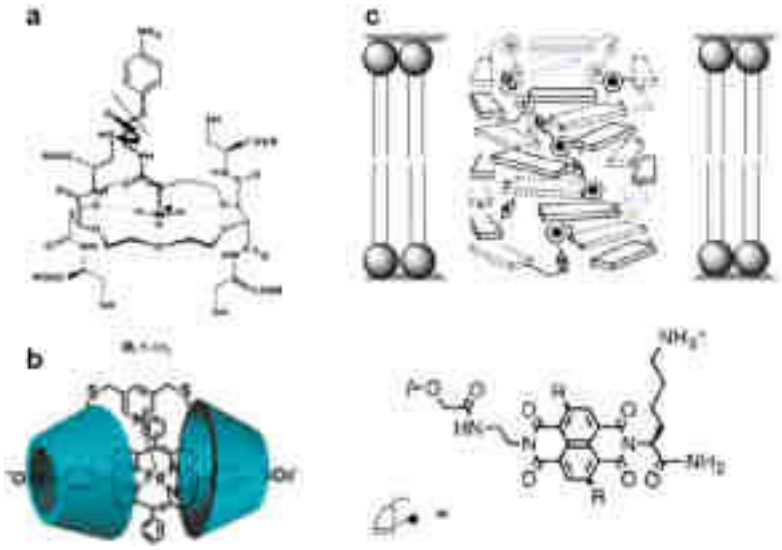

Figure 21 | a) A synthetic esterase model,[26] b) a myoglobin model,[23,24] c) Self-assembly of an artificial ion channel within a lipid bilayer.[25]

For instance, the functionalization of a crown ether with cysteine derivatives offered an effective esterase artificial model (**Figure 21a**).[26] Recognition of an ammonium ion by the

[20] Mann, S. Life as a nanoscale phenomenon. *Angew. Chem. Int. Ed.* **47**, 5306-5320 (2008).
[21] Gautam R. Desiraju. Chemistry - the middle kingdom. *Curr. Sci.* **88**, 374-380 (2005).
[22] Tu, Y. *et al.* Mimicking the cell: bio-inspired functions of supramolecular assemblies. *Chem. Rev.* **116**, 2023-2078 (2016).
[23] Kano, K., Kitagishi, H., Kodera, M. & Hirota, S. Dioxygen binding to a simple myoglobin model in aqueous solution. *Angew. Chem. Int. Ed.* **44**, 435-438 (2005).
[24] Watanabe, K., Kitagishi, H. & Kano, K. Supramolecular iron porphyrin/cyclodextrin dimer complex that mimics the functions of hemoglobin and methemoglobin. *Angew. Chem. Int. Ed.* **52**, 6894-6897 (2013).
[25] Bhosale, S. *et al.* Photoproduction of proton gradients with π-dtacked fluorophore scaffolds in Lipid Bilayers. *Science* **313**, 1463-1473 (2006).
[26] Lehn, J.-M. & Sirlin, C. Molecular catalysis: enhanced rates of thiolysis with high structural and chiral recognition in complexes of a reactive macrocyclic receptor molecule. *J. Chem. Soc. Chem. Commun.* **21**, 949-951 (1978).

macrocycle pre-arranged the ester in close proximity to the thiol of the cysteine residues. An accelerated rate of hydrolysis in presence of this host proved that the conception of artificial enzyme is possible by synthesizing structures able to combine recognition properties via non-covalent interactions and catalytically active residues in a similar way than what is found in proteins.

Binding and transport of relevant molecular species has also been explored by supramolecular chemists,[27,28,29] inspired for example by the delivery of oxygen by proteins such as myoglobin. The group of Koji Kano synthesized an hemoprotein model able to effectively bind and release oxygen (**Figure 21b**).[23,24] The 1:1 complex obtained from a bis-β-cyclodextrine pyridine ligand and a bis-phenylsulfonate iron (III) porphyrin displays an hydrophobic pocket and an hydrophilic outside, ensuring solubility in water. This supramolecular complex is able to effectively bind oxygen upon reduction of the metal into iron (II), with spectroscopic signatures very close to what has been measured for myoglobin. The creation of gradients of concentration is another complex function achieved by biological assemblies.[27] The groups of Matile and Würthner reported barrel-like structures self-assembled into lipid membranes of vesicles from photo-active naphthalene diimide and oligophenyl derivatives (**Figure 21c**).[25] Irradiation of these structures induces the formation of a charge-separated state within the barrel, which leads to the simultaneous oxidation of a sacrificial electron donor outside the vesicle and reduction of a quinone acceptor inside the vesicle. Reduction into the corresponding hydroquinone then leads to a rise of the pH into the vesicle. The self-assembly of photo- and electroactive compounds in this case gives an architecture which function is similar to what is observed in photosynthetic systems.

Enthusiasm for the synthesis of structures of increasing complexity grew, and impressive control over the self-assembly of synthetic molecules has been achieved, as illustrated in **Figure 22**. For instance, the group of Prof. Fujita described the stepwise self-assembly of a cuboctahedron by a combination of controled bond angles, metal-ligand interactions, and stoichiometry (**Figure 22a**).[30] The mixing of twenty four tripyridine ligands and twelve palladium (II) cations led to the formation of a cuboctahedron, which faces were then closed by

[27] Vinothkumar, K. R. & Henderson, R. Structures of membrane proteins. *Q. Rev. Biophys.* **43**, 65-158 (2010).
[28] Busschaert, N., Caltagirone, C., Van Rossom, W. & Gale, P. A. Applications of supramolecular anion recognition. *Chem. Rev.* **115**, 8038-8155 (2015).
[29] Santoni, M.-P. *et al.* Palladium(II)-directed self-assembly of a neutral molecular triangle as a heteroditopic receptor for ion pairs. *Inorg. Chem.* **53**, 10039-10041 (2014).
[30] Sun, Q.-F., Sato, S. & Fujita, M. An M18L24 stellated cuboctahedron through post-stellation of an M12L24 core. *Nat. Chem.* **4**, 330-333 (2012).

the subsequent addition of six equivalent of palladium (II). Additionally, this stellated structure can be reversibly opened and closed by adding tetramethylenediamine and additional palladium (II) respectively. This open-close switching is similar to what can be observed in the gate opening-closing at the surface of some viruses.[31]

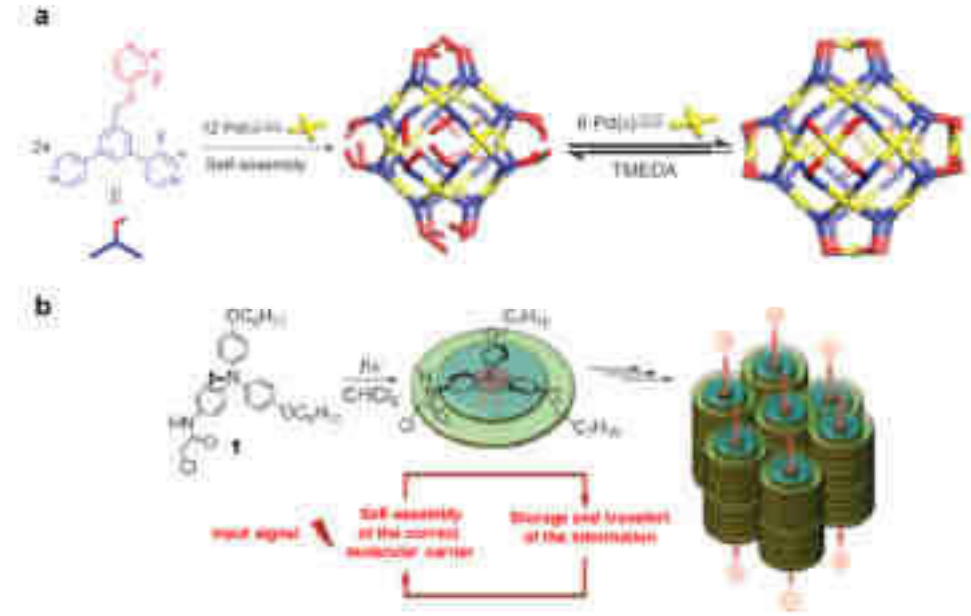

Figure 22 | a) Stepwise assembly of a M18L24 supramolecular cage,[30] b) Light-triggered self-assembly of triarylamines into conductive nanowires.[32]

Figure 22b pictures the light-triggered self-assembly of triarylamine molecules, occurring *via* a combination of radical propagation, π-stacking and hydrogen bonding.[32] The resulting assembly presents interesting hole transporting properties and displays high conductivity analogous to metallic wires.[33] These organic nanowires are good examples of how the properties of a self-assembled system are more than the simple addition of the properties of its sub-components. Moreover, compared to the discrete assembly presented in the previous examples, this kind of self-assembled objects are usually referred as supramolecular polymers.

[31] Hsu, C. H., Sehgal, O. P. & Pickett, E. E. Stabilizing effect of divalent metal ions on virions of southern bean mosaic virus. *Virology* **69**, 587-595 (1976).
[32] Moulin, E. *et al.* The hierarchical self-assembly of charge nanocarriers: A highly cooperative process promoted by visible light. *Angew. Chem. Int. Ed.* **49**, 6974-6978 (2010).
[33] Faramarzi, V. *et al.* Light-triggered self-construction of supramolecular organic nanowires as metallic interconnects. *Nat. Chem.* **4**, 485-490 (2012).

II. Supramolecular Polymers

A. Definition and examples

Supramolecular polymers are polymers in which monomers are held together by reversible interactions instead of covalent bonds, such as hydrogen bondings, electrostatic interactions, metal-ligand complexes, etc…[34] Thus, compared to covalent polymers, they display original properties such as self-healing, better processing, stimuli-responsive/dynamic behavior.[35] Lehn and his collaborators reported the first hydrogen bonding supramolecular polymer in 1990 by using the uracil:diacetylaminopyridine recognition pattern to decorate a tartaric acid derivative (**Figure 23a**).[36,37]

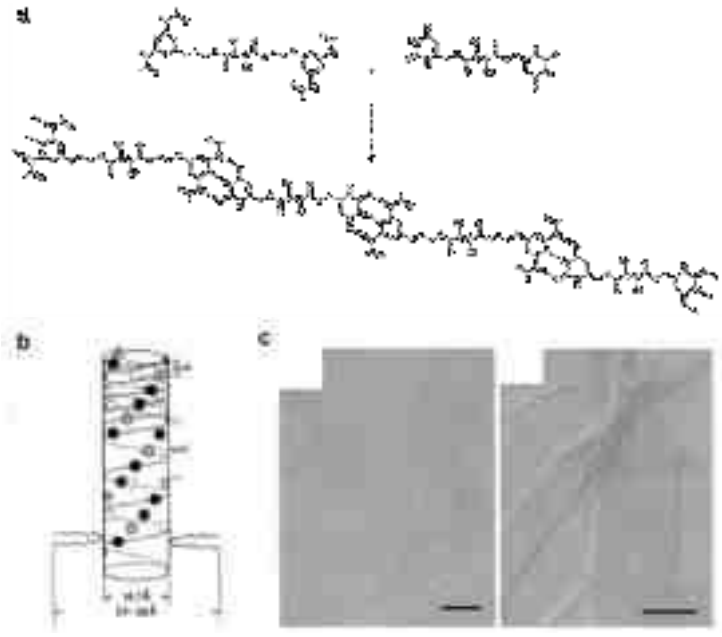

Figure 23 | a) First example of a hydrogen bonding supramolecular polymer by Lehn and coworkers, b) Helical organization of three strands of supramolecular polymers, c) Images of the supramolecular polymer obtained by scanning electron microscopy (scale bar = 200 nm).[36,37]

The resulting supramolecular polymer displayed a liquid crystalline behavior and further investigation by electron microscopy (**Figure 23c**) and neutron scattering revealed a triple helix structure (**Figure 23b**), which further aggregates into large fibers. This secondary self-assembly

[34] Brunsveld, L; Folmer, B. J. B, Meijer, E. W. & Sijbesma, R. P. Supramolecular polymers. *Chem. Rev.* **101**, 4071-4098 (2001).
[35] Yang, L., Tan, X., Wang, Z. & Zhang, X. Supramolecular polymers: historical development, preparation, characterization, and functions. *Chem. Rev.* **115**, 7196-7239 (2015).
[36] Fouquey, C., Lehn, J.-M. & Levelut, A.-M. Molecular recognition directed self-assembly of supramolecular liquid crystalline polymers from complementary chiral components. *Adv. Mater.* **2**, 254-257 (1990).
[37] Gulik-Krzywicki, T., Fouquey, C. & Lehn, J. Electron microscopic study of supramolecular liquid crystalline polymers formed by molecular-recognition-directed self-assembly from complementary chiral components. *Proc. Natl. Acad. Sci. U.S.A.* **90**, 163-167 (1993).

process is believed to be stabilized by lateral Van der Waals interactions due to the long alkyl chains present on tartaric acid.

Supramolecular polymerization occurs *via* different pathways compared to a covalent process. Because each step is reversible, each elongation or reduction of the size of the structure can be associated with an equilibrium as displayed in **Figure 24a**.[38,39] We will distinguish two steps in the supramolecular polymerization phenomenon, the nucleation step characterized by an equilibrium constant called K_1, and an elongation step called K_2. We will also name $\sigma = K_1/K_2$ the cooperativity factor.

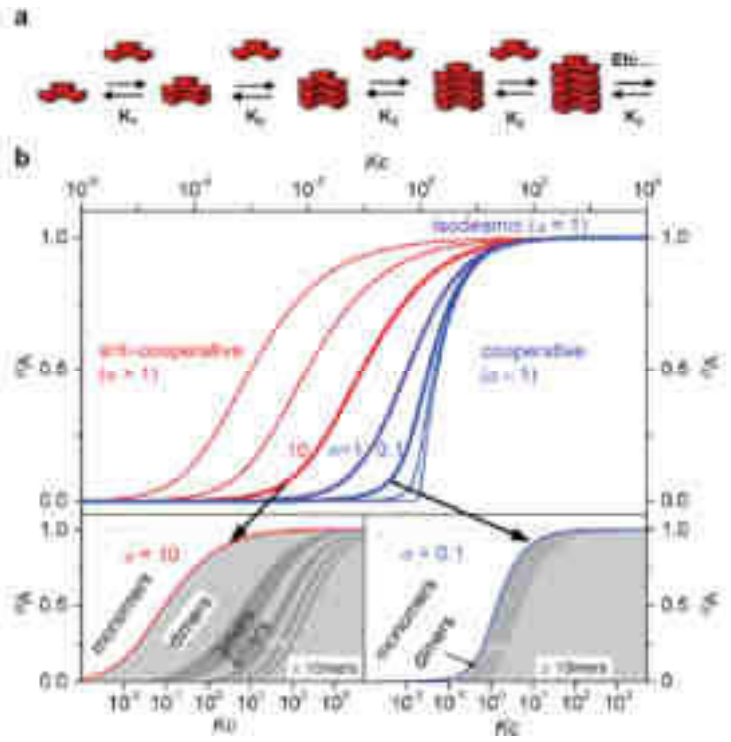

Figure 24 | a) Schematic representation of a supramolecular polymerization process, each step being associated with an equilibrium constant K_x. b) Fraction of aggregated molecules α_a as a function of the normalized concentration Kc.[38]

When $K_1 = K_2$ (and by consequence, $\sigma = 1$), the polymerization mechanism is called isodesmic. In this case, a single equilibrium constant $K = K_1 = K_2$ can be used to describe the system and the degree of polymerization for a fixed concentration can be estimated *via* the following equation:

[38] Gershberg, J. *et al.* Anti-cooperative supramolecular polymerization: a new K $_2$ –K model applied to the self-assembly of perylene bisimide dye proceeding via well-defined hydrogen-bonded dimers. *Chem. Sci.* **7**, 1729-1737 (2016).
[39] De Greef, T. F. A. *et al.* Supramolecular polymerization. *Chem. Rev.* **109**, 5687-5754 (2009).

$$n = (C \times K)^{1/2} \quad (1)$$

With n being the degree of polymerization, C the concentration in mol.L^{-1}, and K the association constant of each step in M^{-1}. In an isodesmic polymerization process, every step is independent from the others.

When $K_2 > K_1$, then $\sigma < 1$, which is characteristic of a cooperative polymerization process. In this case, the association of two monomers is slower than the elongation process. This can happen when the first step requires that the monomers adopt a specific conformation to self-assemble, such as, for example, an amide group which needs to rotate in the good direction.[40] Once this first step has been achieved, the elongation process is facilitated as the nucleus is already pre-organized.

When $K_2 < K_1$, then $\sigma > 1$, which is characteristic of an anti-cooperative polymerization process. In this case, the elongation process is disfavored compared to the nucleation one. This has been observed when the formation of a dimer is very stable and hinders the approach of other monomers.[38]

For supramolecular polymers, controlling the concentration of the components allows for controling the size of the self-assembled objects. For instance, in the case of an anti-cooperative process, the system only yields dimers over a large concentration range as shown in **Figure 24b**. Thus, high concentration is required to obtain supramolecular polymers with a degree of polymerization exceeding those of small oligomers. For a cooperative mechanism, a critical concentration is required for the assembly of the nucleus (**Figure 24b**). Once this is reached, increasing the concentration leads to drastic increase of the degree of polymerization.

One last main example remains, the ring-chain polymerization, which is related to the competition between ring formation and elongation process, but it will not be discussed here. We should also mention that recently the groups of Takeuchi[41] and Aida[424] described systems in which the polymerization process can be described as a living polymerization model similar to what can be observed for the synthesis of covalent polymers. The advantage of a living

[40] Fenske, M. T. *et al.* Cooperative self-assembly of discoid dimers: Hierarchical formation of nanostructures with a pH switch. *J. Am. Chem. Soc.* **135**, 8342-8349 (2013).
[41] Ogi, S., Sugiyasu, K., Manna, S., Samitsu, S. & Takeuchi, M. Living supramolecular polymerization realized through a biomimetic approach. *Nat. Chem.* **6**, 188-195 (2014).
[42] Kang, J. *et al.* Noncovalent assembly. A rational strategy for the realization of chain-growth supramolecular polymerization. *Science* **347**, 646-651 (2015).

supramolecular polymerization process would be a control rate of growth and thus a limited polydispersity of the sample.

Supramolecular polymers have been synthesized by playing with the whole range of non-covalent interactions available to synthetic chemists. Herein, we will describe a few examples of an extensive literature.[35]

Hydrogen bonding is a broadly used interaction for the synthesis of supramolecular polymers[43] and some examples will be more specifically discussed in the next section. Here we will briefly mention the work of Meijer and coworkers on benzene-1,3,5-tricarboxamide[44] (**Figure 25a)** also abbreviated BTA, as an illustration. These discotic monomers can polymerize into columnar assemblies by the combination of hydrogen bonding and π-stacking, in a cooperative fashion. Among many examples, BTAs have been functionalized with fluorinated aromatics and gadolinium complexes in order to produce functional supramolecular polymers tested as Magnetic Resonance Imaging (MRI) contrast agents.[45]

Prof. Takuzo Aida and his collaborators reported the supramolecular polymerization of an amphiphilic hexa-*peri*-hexabenzocoronene into large tubular structures.[46] The amphiphilic character of the compound showed in **Figure 25b** helps stabilizing the main π-stacking driven polymerization process of the hexabenzocoronene core. The obtained supramolecular polymers were analyzed by Transmition Electron Microscopy (TEM) and Scanning Electron Microscopy (SEM), revealing very large molecular ordering of the fibers composed in average of 5 x 10^4 monomers. The conductivity of these structures, emerging from the supramolecular assembly, and for which monomers are reminiscent of graphene, showed promising electrical conductivity and resistivity, being an organic semi-conductor with properties close to inorganic semi-conductor such as gallium nitride.

[43] Bouteiller, L. Assembly via hydrogen bonds of low molar mass compounds into supramolecular polymers. *Adv Polym Sci* **207**, 79-112 (2007).
[44] Cantekin, S., de Greef, T. F. A. & Palmans, A. R. A. Benzene-1,3,5-tricarboxamide: a versatile ordering moiety for supramolecular chemistry. *Chem. Soc. Rev.* **41**, 6125-6137 (2012).
[45] Besenius, P. *et al.* Paramagnetic self-assembled nanoparticles as supramolecular MRI contrast agents. *Contrast Media Mol. Imaging* **7**, 356-361 (2012).
[46] Hill, J. P. *et al.* Self-assembled hexa-peri-hexabenzocoronene graphitic nanotube. *Science* **304**, 1481-1483 (2004).

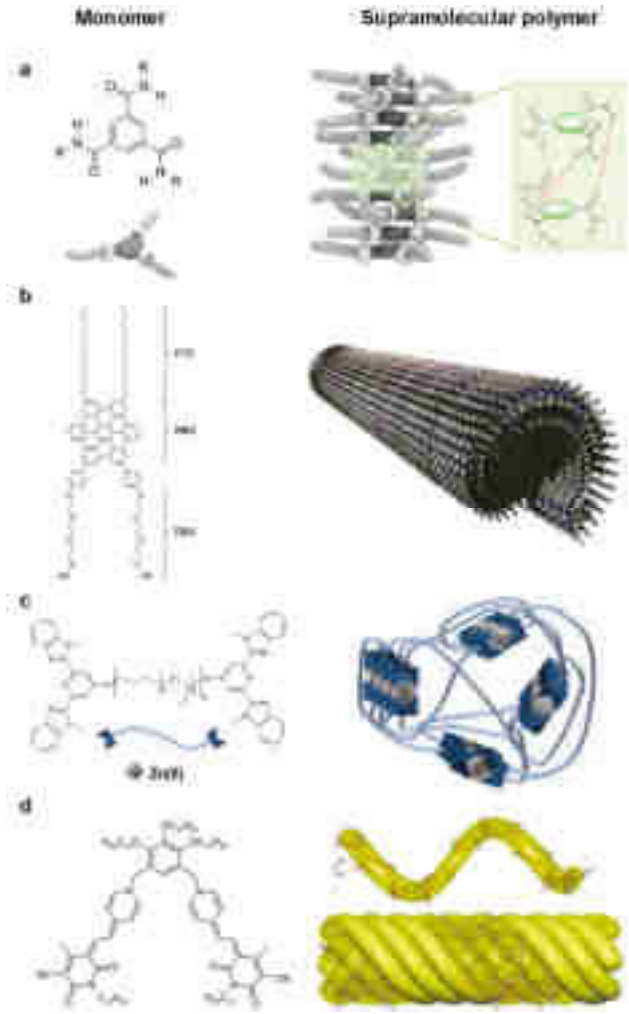

Figure 25 | Short selection of supramolecular polymers and their corresponding monomers based on a) hydrogen bonding and π-stacking[44], b) π-stacking and amphiphilic organisation[46], c) metal-ligand complexes[47] and d) dipole-dipole interactions.[48]

Metal-ligand complexes represent a popular choice of supramolecular connectors. By playing with the nature of the ligand and the metal, the kinetic lability can be tuned, leading to coordination supramolecular polymers ranging from classic reversible supramolecular polymers to strong covalent-like polymer chains.[49] For a ligand such as terpyridine, simply switching the metallic cation for another one can make the polymer displaying an inert (with metals like Ru(II) or Fe(II)) or dynamic (Zn(II)) behavior.[50] An elegant exploitation of this dynamic behavior has been presented by Rowan and coworkers, who studied a bis-

[47] Burnworth, M. *et al.* Optically healable supramolecular polymers. *Nature* **472**, 334-337 (2011).
[48] Würthner, F., Yao, S. & Beginn, U. Highly odered merocyanine dye assemblies by supramolecular polymerization and hierarchical self-organization. *Angew. Chem. Int. Ed.* **42**, 3247-3250 (2003).
[49] Leong, W. L. & Vittal, J. J. One-dimensional coordination polymers: complexity and diversity in structures, properties, and applications. *Chem. Rev.* **111**, 688-764 (2011).
[50] Chiper, M., Hoogenboom, R. & Schubert, U. S. Toward main chain metallo-terpyridyl supramolecular polymers: 'The metal does the trick'. *Macromol. Rapid Commun.* **30**, 565-578 (2009).

methylbenzylimidazole pyridine complex based supramolecular polymer displaying light-induced self-healing properties (**Figure 25c**).[47] The films obtained using Zn(II) or La(III) can be depolymerized and re-associated upon light irradiation, leading to defects repairing in the structure. The films showed similar strain-stress curves before damage and after healing, proving that they fully recovered their mechanical properties.

More exotic supramolecular polymers rely on less commonly used non-covalent interactions, such as halogen bonding[51], d-d interaction in heavy metals such as platinum,[52] or dipole interactions for instance. Würthner and his group described the supramolecular polymerization of merocyanines dyes.[48] Bis-merocyanines represented in **Figure 25d** exhibit two donor-acceptor moieties with a tridodecyloxybenzyl core to favor solubility in apolar solvents, in which dipole-dipole interactions are strong. H-aggregates of merocyanines were observed at concentrations as low as 10^{-7} M in methylcyclohexane, and increasing the concentration led to the formation of a gel. Investigations by molecular modeling and cryo-TEM showed that the monomer polymerizes into helical structures, which then further hierarchically assemble into large and stiff fibers.

Overall, supramolecular polymers are a class of promising materials for many applications, because of the original properties previously mentioned.[53] Careful design of monomers along with the mild conditions required for their assembly allow the inclusion of molecular building blocks with properties interesting in various fields, such as molecular electronics, sensing/imaging, photovoltaics, therapeutic applications and many others.[5]

As they will be of interest later in this manuscript, we will now briefly discuss hydrogen bonding supramolecular polymers and two connectors in particular.

B. Hydrogen bonding supramolecular polymers

Hydrogen-bonding supramolecular polymers are attractive because hydrogen bond recognition patterns are usually easily accessible from a synthetic point of view and their variety allows to tune the strength of the connection (**Figure 26**).[54,55,56] Most of the examples described

[51] Gilday, L. C. *et al.* Halogen bonding in supramolecular chemistry. *Chem. Rev.* **115**, 7118-7195 (2015).
[52] Aliprandi, A., Genovese, D., Mauro, M. & De Cola, L. Recent advances in phosphorescent Pt(II) complexes featuring metallophilic interactions: Properties and applications. *Chem. Lett.* **44**, 1152-1169 (2015).
[53] Aida, T., Meijer, E. W. & Stupp, S. I. Functional supramolecular polymers. *Science* **335**, 813-817 (2012).
[54] González-Rodríguez, D. & Schenning, A. P. H. J. Hydrogen-bonded supramolecular π-functional materials. *Chem. Mater.* **23**, 310-325 (2011).
[55] Armstrong, G. & Buggy, M. Hydrogen-bonded supramolecular polymers: A literature review. *J. Mater. Sci.* **40**, 547-559 (2005).
[56] Shimizu, L. S. Perspectives on main-chain hydrogen bonded supramolecular polymers. *Polym. Int.* **56**, 444-452 (2007).

share common features: good kinetic lability and thermal reversibility. These properties allow for a good error checking capacity: monomers will associate and dissociate until they form the more thermodynamically stable structure (the arrangement which forms the more hydrogen bonds), a characteristic which is of high importance in order to achieve long-range molecular organization. Moreover, good self-healing properties have been shown to emerge from hydrogen-bonding supramolecular polymer networks.[57]

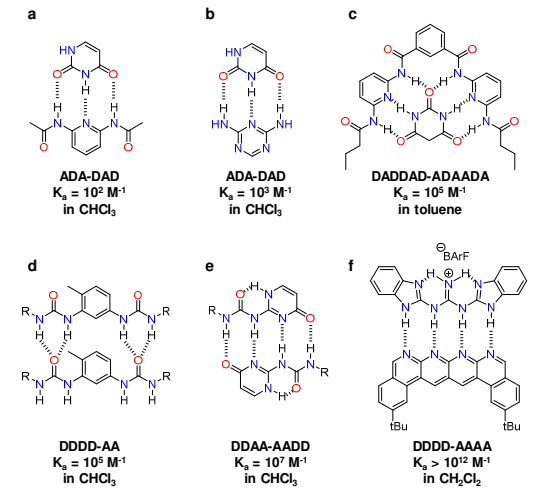

Figure 26 | Selection of hydrogen bonding recognition patterns (A: acceptor of hydrogen bonds, D: donor of hydrogen bonds).[54]

Notable examples of materials based on connectors displayed in **Figure 26** have been reported in the literature. In particular, bis-ureas in **Figure 26d** and ureidopyrimidinones in **Figure 26e** respectively reported by Bouteiller[58] and Meijer[59], have been successfully integrated into materials displaying rheological properties and viscosity close to those of regular polymers. The four-fold hydrogen bonding motif displayed in **Figure 26f** is the strongest hydrogen bonding pattern known to date.[60]

We will focus our following discussion on ADA-DAD systems such as the uracil:diacetylaminopyridine couple (**Figure 26a**) and the self-complementary ureidopyrimidinone (**Figure 26b**), a AADD system.

[57] Cordier, P., Tournilhac, F., Soulié-Ziakovic, C. & Leibler, L. Self-healing and thermoreversible rubber from supramolecular assembly. *Nature* **451**, 977-980 (2008).
[58] Isare, B., Pensec, S., Raynal, M. & Bouteiller, L. Bisurea-based supramolecular polymers: From structure to properties. *C. R. Chim.* **19**, 148-156 (2016).
[59] Sijbesma, R. P. *et al.* Reversible polymers formed from self-complementary monomers using quadruple hydrogen bonding. *Science* **278**, 1601-1604 (1997).
[60] Blight, B. A., Hunter, C. A., Leigh, D. A., McNab, H. & Thomson, P. I. T. An AAAA–DDDD quadruple hydrogen-bond array. *Nat. Chem.* **3**, 246-250 (2011).

i. URACIL:DIACETYLAMINOPYRIDINE RECOGNITION PATTERN

After the report of Lehn on the first supramolecular polymer based on the uracil:diacetylaminopyridine motif,[36] a growing interest was observed for the elaboration of supramolecular structures using this recognition pattern. The group of Meijer measured an association constant for this couple of $K_a = 920\ M^{-1}$ in chloroform.[61] It should be noted that the use of 2,6-diaminopyridine instead of 2,6-diacetylaminopyridine drastically reduces the association constant down to $K_a = 84\ M^{-1}$. Uracil derivatives can self-associate[62] and compete with the association of the ADA:DAD dimer, but the labile character of this interaction allows reorganisation of the system until the most thermodynamically stable species is formed. This property and the ease of synthesis of these derivatives made it a popular recognition pattern for the synthesis of hydrogen bonding supramolecular polymers.[63] For instance, ditopic ADA and DAD linear aromatic linkers were synthesized and associated in 1:1 proportion to yield micrometric sized fibres imaged by AFM (**Figure 27a**).[64] The aggregation of these linear chains into wider fibres has been attributed to lateral π-stacking originating from the aromatic core, which was functionalized with alkyl chains to avoid solubility issues. The use of two different blocks and their accurate alternation in the polymer allowed tuning of the hierarchical supramolecular structure: for example, replacing one linear linker by a curved one led to helically organized fibers. While these architectures were synthesized in solution, patterning of HOPG surfaces was achieved associating a ditopic DAD linear linker with a tetra-uracil pyrene compound (**Figure 27b**).[65] Imaging of the surface after deposition of the supramolecular complex by Scanning Tunnelling Microscopy (STM) allowed the observation of rhombohedral structures, which arrangement could be were predicted by molecular modelling.

Overall, these two examples highlight the advantages of the uracil:diacetylaminopyridine couple. The possibility to use two different blocks with different functional or structuring properties is of great interest in the synthesis for original supramolecular assemblies.

---

[61] Beijer, F. H. *et al.* Hydrogen-bonded complexes of diaminopyridines and diaminotriazines: Opposite effect of acylation on complex stabilities. *J. Org. Chem.* **61**, 6371-6380 (1996).
[62] Szekrenyes, Z. *et al.* Melting of hydrogen bonds in uracil derivatives probed by infrared spectroscopy and ab Initio molecular mynamics. *J. Phys. Chem. B* **116**, 4626-4633 (2012).
[63] Marangoni, T. & Bonifazi, D. Nano- and microstructuration of supramolecular materials driven by H-bonded uracil·2,6-diamidopyridine complexes. *Nanoscale* **5**, 8837-8851 (2013).
[64] Yoosaf, K. *et al.* From molecular to macroscopic engineering: Shaping hydrogen-bonded organic nanomaterials. *Chem. Eur. J.* **17**, 3262-3273 (2011).
[65] Lianes-Pallas, A. *et al.* Engineering of supramolecular H-bonded nanopolygons via self-assembly of programmed molecular molecular modules. *J. Am. Chem. Soc.* **131**, 509-520 (2009).

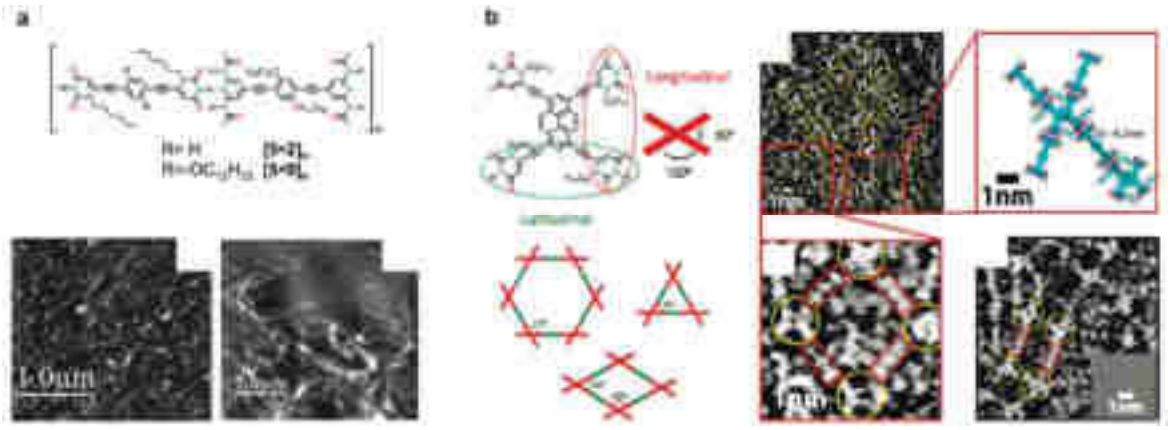

Figure 27 | a) A supramolecular copolymer exploiting the ADA:DAD association, imaged by AFM after evaporation of a drop of a toluene solution.[64] b) Patterning of a surface associating a tetra-uracil compound with a ditopic 2,6-diacetylaminopyridine linker imaged by STM.[65]

ii. UREIDOPYRIMIDINONE

The synthesis and use of ureidopyrimidinones (Upy) as connectors in supramolecular polymers has been explored mainly by the group of Prof. E. W. Meijer. They reported the synthesis of Upy, *i.e.* isocytosine with an urea bridge, as a self-complementary hydrogen bonding group,[66] associating with a very high association constant, for example in chloroform (K_a = 5.7 x 10^7 M^{-1}) and toluene (K_a = 5.9 x 10^8 M^{-1}).[67] Small bis-Upy entities were shown to behave like a polymer even in dilute solution thanks to the strong dimerization properties (**Figure 28a**).[59] The introduction of UPy functional units at the extremities of poly(ethylene butylene) polymers, in addition to urea or urethane functions present within the backbone, gave access to supramolecular thermoplastic elastomers, displaying enhanced mechanical properties compared to the non-functionalized polymer.[68] Imaging of these supramolecular structures by AFM revealed long polymer chains aggregated by additional lateral hydrogen bonding from the urea fragments (**Figure 28b**). The integration of supramolecular interactions into covalent polymers can improve their mechanical properties, but also facilitate their manipulation and processability as illustrated in **Figure 28c**.[69] For instance, increasing the temperature greatly reduced the viscosity of the solution, as the liftetime of the association is reduced by thermal agitation

[66] Beijer, F. H., Sijbesma, R. P., Kooijman, H., Spek, A. L. & Meijer, E. W. Strong dimerization of ureidopyrimidones via quadruple hydrogen bonding. *J. Am. Chem. Soc.* **120**, 6761-6769 (1998).
[67] Söntjens, S. H. M., Sijbesma, R. P., van Genderen, M. H. P. & Meijer, E. W. Stability and lifetime of quadruply hydrogen bonded 2-ureido-4[1 H]-pyrimidinone dimers. *J. Am. Chem. Soc.* **122**, 7487-7493 (2000).
[68] Kautz, H., van Beek, D. J. M., Sijbesma, R. P. & Meijer, E. W. Cooperative End-to-End and Lateral Hydrogen-Bonding Motifs in Supramolecular Thermoplastic Elastomers. *Macromolecules* **39**, 4265-4267 (2006).
[69] Bosman, A. W., Sijbesma, R. P. & Meijer, E. W. Supramolecular polymers at work. *Mater. Today* **7**, 34-39 (2004).

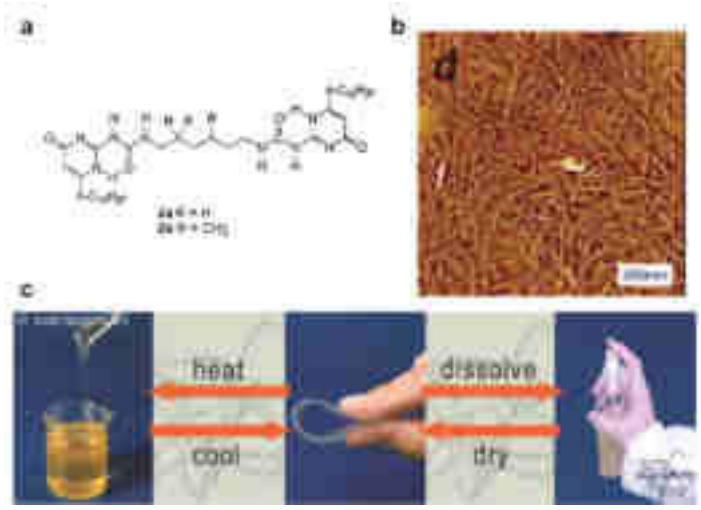

Figure 28 | a) A small ditopic Upy monomer.[59] b) AFM imaging of a supramolecular thermoplastic elastomer.[68] c) Illustration of the improved processability of Upy-functionalized covalent polymers.[69]

Interestingly, Upy dimers can also stack on top of each other, opening new possibilities for producing functional materials. Such stacks of dimers were first observed for analogous 4-fold hydrogen bonding groups called ureido-s-triazine (**Figure 29a**). Small bis-ureido-s-triazine have been proved to self-assemble into a helical arrangement after formation of polymer chains in water, this structure being the results of hydrophobic behaviour, hydrogen-bonding and π-stacking.[70,71] Later on, a similar observation was made for Upy-based compounds (**Figure 29b**). This compound polymerizes into randomly folded single chain supramolecular polymers in chloroform, but in apolar solvent like dodecane, folds into a helical structure.[73] Such behavior is probably the consequence of several phenomena,[70,71,73] namely: 1) solvophobic repulsion between the relatively polar Upy moieties and the apolar solvent, 2) the presence of long alkyl chains on the 3,4,5-trihydroxybenzene derivative which shields Upy dimers from the solvent, increasing compartmentalisation of the Upy core within the helix, 3) apolar solvents do not compete with the formation of hydrogen bonding, making them stronger, 4) hydrogen bonding of delocalized molecules increases their aromatic character, thus favoring π-π interactions, as predicted by theoretical studies,[72] and 5) additional π-stacking and Van der Waals interactions from the 3,4,5-trihydroxybenzene unit functionalized with large alkyl chains stabilizes the main columnar structure.

[70] Brunsveld, L., Vekemans, J. A. J. M., Hirschberg, J. H. K. K., Sijbesma, R. P. & Meijer, E. W. Hierarchical formation of helical supramolecular polymers via stacking of hydrogen-bonded pairs in water. *Proc. Natl. Acad. Sci. U.S.A.* **99**, 4977-4982 (2002).
[71] Hirschberg, J. H. K. K.; Brunsveld, L., Ramzi, Ai., Vekemans, J. A. J. M., Sijbesma, R. P., Meijer, E. W. Helical self-assembled polymers from cooperative stacking of hydrogen-bonded pairs. *Nature* **407**, 167-170 (2000).
[72] Cyranski, M. K., Gilski, M., Jaskolski, M. & Krygowski, T. M. On the aromatic character of the heterocyclic bases of DNA and RNA. *J. Org. Chem.* **68**, 8607-8613 (2003).

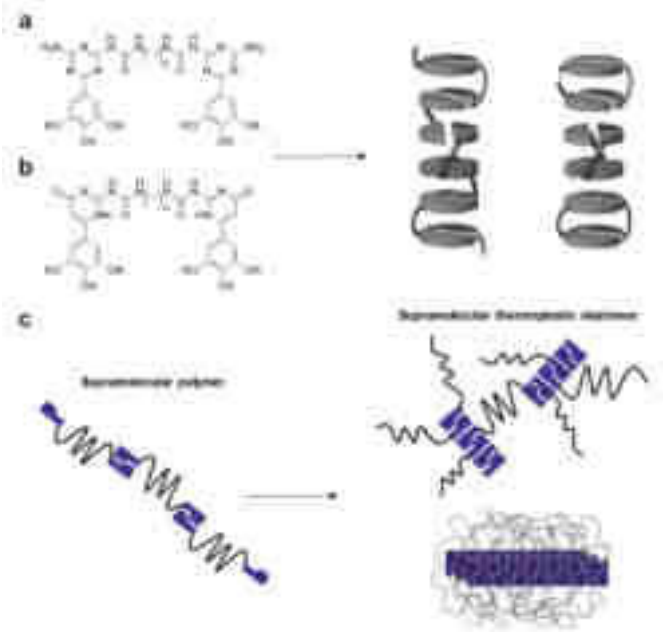

Figure 29 | a) Bis-ureido--triazine compound arranged into helices after supramolecular polymerization.[70,71] b) Bis-Upy compound arranged into helices after supramolecular polymerization.[73] c) Physical cross linking of a single-chain supramolecular polymer *via* interactions between Upy dimers.[74]

For instance, a few years later, Sijbesma and his collaborators reported that the integration of Upy derivatives at the extremity of PDMS polymer chains induced the formation of physical cross-linking nodes made of Upy dimers stacks, which was confirmed by rheology experiments as the behaviour of the material was typical of a critical gel (**Figure 29c**).[74] Such stacking of Upy dimers has been shown to be responsible for new properties in polymers decorated with Upy as end groups. The observed mechanical properties were assessed to the hierarchical organization of the Upy which leads to a phase separation phenomenon.

Ureidopyrimidinones self-associate with a high association constant (up to 10^8 M^{-1}), and have thus been mainly used for the formation of long supramolecular polymers. However, the ability to interact laterally by stacking, and thus adding order to the supramolecular architecture, has not been extensively exploited, and seems interesting for the formation of new self-assembled structures.

[73] Hirschberg, J. H. K. K., Koevoets, R. A., Sijbesma, R. P. & Meijer, E. W. Helical supramolecular aggregates based on ureidopyrimidinone quadruple hydrogen bonding. *Chem. Eur. J.* **9**, 4222-4231 (2003).
[74] Botterhuis, N. E., van Beek, D. J. M., van Gemert, G. M. L., Bosman, A. W. & Sijbesma, R. P. Self-assembly and morphology of polydimethylsiloxane supramolecular thermoplastic elastomers. *J. Polym. Sci. Part A Polym. Chem.* **46**, 3877-3885 (2008).

Chapter II: Interlocked molecules and molecular shuttles

I. Interlocked molecules: synthetic strategies, molecular knots and early prototypes of molecular machines

A. Molecular topology

Knots and interlocked structures are fascinating objects that have always kindle human curiosity and thus are part of the culture and mythology of many civilizations.[75] If nowadays, they can be encountered mainly as decoration on objects and buildings (**Figure 30a**), they used to have a more profound religious and spiritual meaning to many people.[76] The triquetra, a trefoil knot, is an interlaced symbol often met in Celtic art (**Figure 30bi**), and later with the addition of a circle it has been used by Christians communities (**Figure 30bii**).[77] Solomon links can be found as a decoration in many civilizations around the Mediterranean Sea since the Roman era: their meaning is often related to things that never ends, such as immortality, or, on a more poetical note, love (**Figure 30c**).[78] One last example of elegant structure associated to spiritual symbolism are the Borromean rings.[75] If one of these three rings is removed, the two others fall apart, which has been interpreted as a symbol of unity, a way to represent things that cannot be separated from each other's in various cultures (**Figure 30d,e**).

In these examples, the complex topology associated to their sophisticated and elegant symmetry seemed to be at the origin of their use by artists and believers. But scientists were also highly interested by the topological properties of knots, and in 1927, mathematicians Briggs and Alexander suggested a systematic notation method to describe them (**Figure 30f**).[79] Each knot can be associated to a notation:

$$X_z^y$$

where X is the minimum number of nodes, y is the number of components and z is the order of the knot.

[75] Forgan, R. S., Sauvage, J. P. & Stoddart, J. F. Chemical topology: Complex molecular knots, links, and entanglements. *Chem. Rev.* **111**, 5434-5464 (2011).
[76] Siegel, J. S. *et al.* Chemistry. Chemical topology and interlocking molecules. *Science* **304**, 1256-1258 (2004).
[77] Laing, L. R. & Laing, J. *Art of the Celts*. (Thames and Hudson, 1992).
[78] Rose, L. R. *Seeing Solomon's Knot* (Lois Rose, 2005).
[79] Alexander, J. W. & Briggs, G. B. On types of knotted curves. *Ann. Math.* **28**, 562-586 (1926).

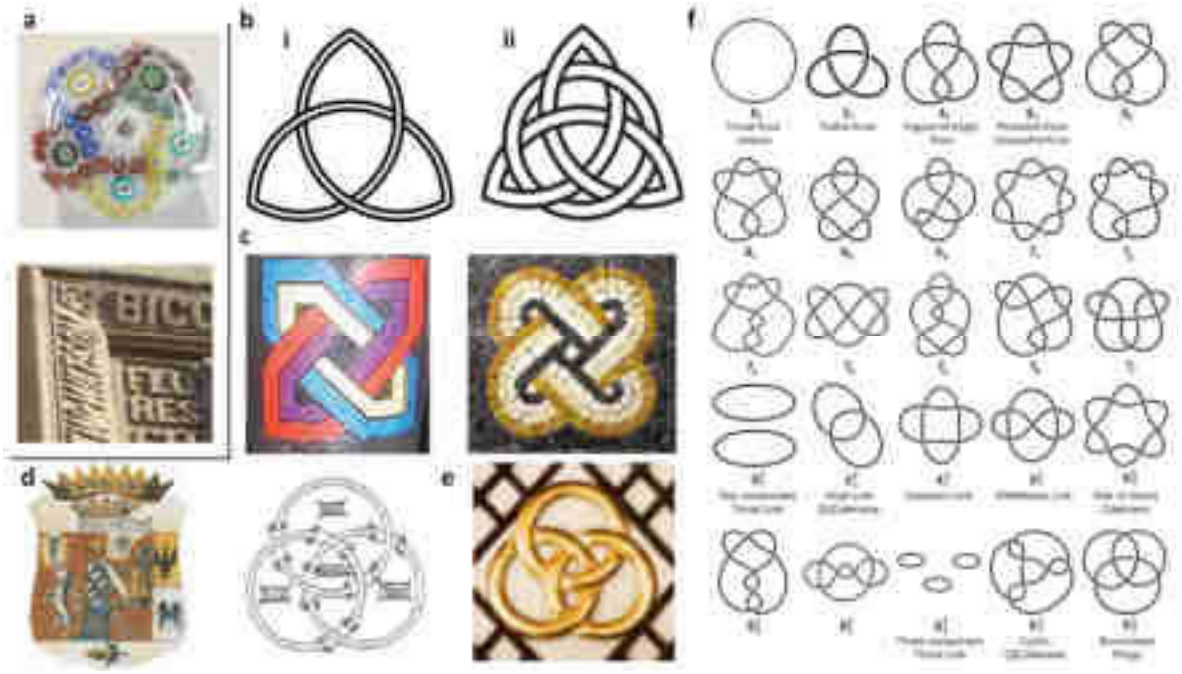

Figure 30 | a) Paperweight displaying a pentafoil knot,[75] b) The Celtic triquetra, a trefoil knot,[75] as pictured by Celt (i) and Christians (ii), c) British glass painting and Italian mosaic displaying a Solomon link,[75] d) Crest showing the Borromean rings and their religious representation,[75] e) Representation of Borromean rings in Buddhism,[75] f) Description of knots and links according to the Alexander-Briggs notation.[79]

Wasserman and Frisch first discussed the possibility to synthesize interwoven molecular systems of complex topology,[80] this kind of object being a great challenge for synthetic chemists and a whole new class of synthetic molecular architecture. The synthesis of the first Hopf link (two interpenetrated rings), a [2]catenane, was described in 1960 by Wasserman (**Figure 31a**).[816] It was the result of the statistical threading of two cyclic components during a macrocyclisation process, and was obtained with a 1% yield. Some years later, Shill published the synthesis of a catenane by direct chemical synthesis, not relying on the statistical method of Wasserman, but the tedious and long synthesis prevented this approach to become popular (**Figure 31b**).[82] These seminal works were followed in 1968 by the synthesis of the first rotaxane by Harrison,[83] which is a macrocycle threaded along an axle (see next section).

[80] Frisch, H. L. & Wasserman, E. Chemical topology. *J. Am. Chem. Soc.* **83**, 3789-3795 (1961).
[81] Wasserman, E. The preparation of interlocking rings: a catenane. *J. Am. Chem. Soc.* **82**, 4433-4434 (1960).
[82] Schill, G. & Lüttringhaus, A. The preparation of catena compounds by directed synthesis. *Angew. Chem. Int. Ed. Engl.* **3**, 546-547 (1964).
[83] Harrison, I. T. & Harrison, S. Synthesis of a stable complex of a macrocycle and a threaded chain. *J. Am. Chem. Soc.* **89**, 5723-5724 (1967).

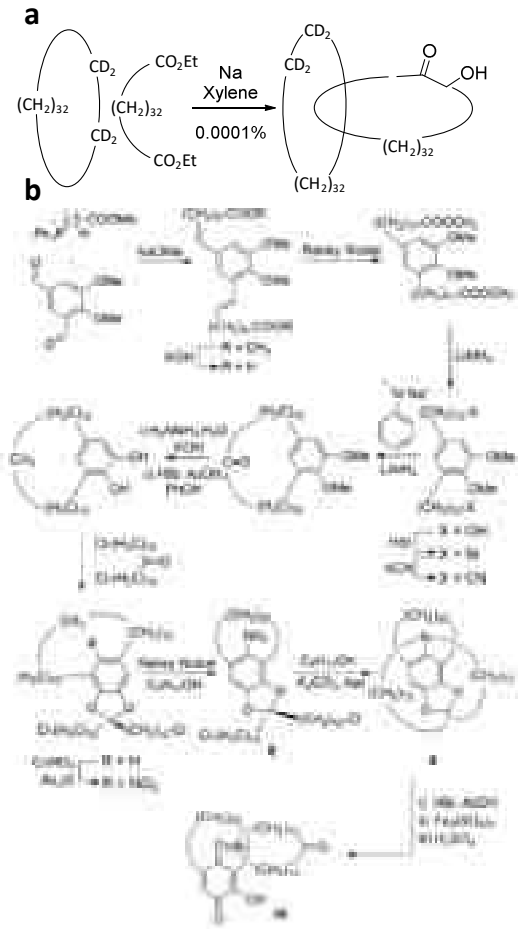

Figure 31 | a) Synthesis of the first [2]catenane by Wasserman.[81] b) Synthetic route described by Schill for the synthesis of [2]catenane.[82]

Despite the exciting perspectives these works opened, the synthesis of molecular knots was somewhat neglected because of the poor efficiency of the synthetic strategies reported at the time. The synthesis of mechanically interlocked molecules did not really become a subject of broad interest before Prof. J.-P. Sauvage made a decisive step towards the efficient synthesis of these molecules.

B. Templated synthesis and increase of complexity

Taking advantage of a template directed synthetic strategy,[84] Sauvage and his collaborators reported in a decisive paper the synthesis of a metallocatenane with a good yield (**Figure 32a**).[85] The reaction of 2,9-bis-(*p*-hydroxyphenyl)-1,10-phenanthroline with a phenanthroline containing macrocycle in the presence of copper(I) provided a pre-organized inclusion complex

[84] Busch, D. H. & Stephenson, N. A. Molecular organization, portal to supramolecular chemistry. Structural analysis of the factors associated with molecular organization in coordination and inclusion chemistry, including the coordination template effect. *Coord. Chem. Rev.* **100**, 119-154 (1990).
[85] Dietrich-Buchecker, C. O., Sauvage, J. P. & Kintzinger, J. Une nouvelle famille de molecules : les metallo-catenanes. *Tetrahedron Lett.* **24**, 5095-5098 (1983).

(a *pseudo*-catenane) which could be closed after reaction with diiodopentaethylene glycol under basic conditions to yield the corresponding metallocatenane with a 42% yield. The synthesis of this simple yet at the time impressive architecture was used as a proven tool for the synthesis of more complex architectures, such as a molecular trefoil knot (**Figure 32b**)[86] or a Solomon link (**Figure 32c**).[87] The same template-based strategy was used in conjunction with poly-phenanthroline ligands, affording the knots with good yields. In both cases, the final complex can be demetallated using potassium cyanide to go from a rigid structure to a loose one, which conformation is different from the rigid metallocatenane.

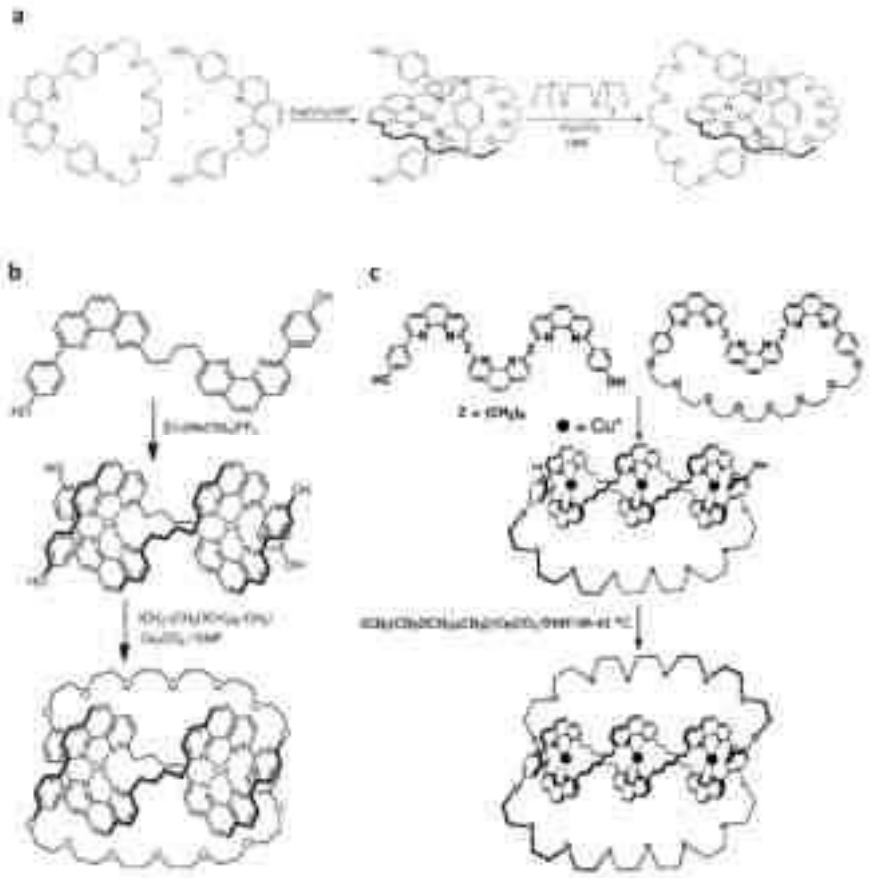

Figure 32 | a) First synthesis of a metallo[2]catenane using a template directed strategy developed by Sauvage.[85] Synthesis of b) a trefoil knot[86] and c) a Solomon link[87] using a similar strategy.

This templated approach inspired many groups who foresaw this methodology as a great tool for the elaboration of complex molecular architectures. Sauvage's work "unlocked" the

[86] Dietrich-Buchecker, C. O. & Sauvage, J.-P. A Synthetic Molecular Trefoil Knot. *Angew. Chem. Int. Ed. Engl.* **28**, 189-192 (1989).
[87] Nierengarten, J. F., Dietrich-Buchecker, C. O. & Sauvage, J. P. Synthesis of a doubly interlocked [2]-catenane. *J. Am. Chem. Soc.* **116**, 375-376 (1994).

field of molecular topology and later of molecular machines. We will, in a non-exhaustive overview, list some of the most noticeable contributions to this field.

Prof. J. F. Stoddart developed a similar yet different strategy to synthesize interlocked systems. His group described the synthesis of a cyclo-bis(paraquat-*p*-phenylene) (also called "blue-box") via a template strategy,[88] a method which was then tweaked to synthesize a [2]catenane exploiting donor-acceptor interactions (**Figure 33a**).[89] The electron-poor bis-pyridinium compound can complex an electron-rich molecule in a pincer-like conformation. Using a bis-hydroquinone macrocycle as the electron-rich component induced the formation of a *pseudo*-catenane (A), in which both pyridines are pre-organized to react further with 1,4-bis(bromomethyl)benzene, leading to the formation of a [2]catenane (B) in a very good yield. This strategy was used to create various interlocked structures, including the "olympiadane", a [5]catenane (**Figure 33b**).[90] The synthesis was achieved by first, synthesizing a [3]catenane using a larger version of the blue box (in black) and two donating macrocycles (in yellow and green). The last step was the introduction of two other blue box (in blue and red). The final [5] catenane was isolated as a purple compound by column chromatography in a 5% yield for the last step. Stoddart's group also described in 2004 the synthesis of molecular Borromean rings,[91] in an elegant one-pot reaction combining coordination chemistry and dynamic covalent chemistry (**Figure 33c**).[92] The simultaneous assembly of 18 components resulted in the formation of the Borromean ring structure, stabilized by π-stacking, after two days of reaction and with a 90%yield, which structure was confirmed by single crystal X-ray diffraction (**Figure 33d**).

[88] Brown, C. L., Philp, D. & Stoddart, J. F. The template-directed synthesis of a rigid tetracationic cyclophane receptor. *Synlett.* **1991**, 462-464 (1991).
[89] Brown, C. L., Philp, D. & Stoddart, J. F. The Self-Assembly of a [2]catenane. *Synlett* **1991**, 459-461 (1991).
[90] Amabilino, D. B., Ashton, P. R., Reder, A. S., Spencer, N. & Stoddart, J. F. Olympiadane. *Angew. Chem. Int. Ed. Engl.* **33**, 1286-1290 (1994).
[91] Chichak, K. S. *et al.* Molecular borromean rings. *Science* **304**, 1308-1312 (2004).
[92] Rowan, S. J., Cantrill, S. J., Cousins, G. R. L., Sanders, J. K. M. & Stoddart, J. F. Dynamic covalent chemistry. *Angew. Chem. Int. Ed.* **41**, 898-952 (2002).

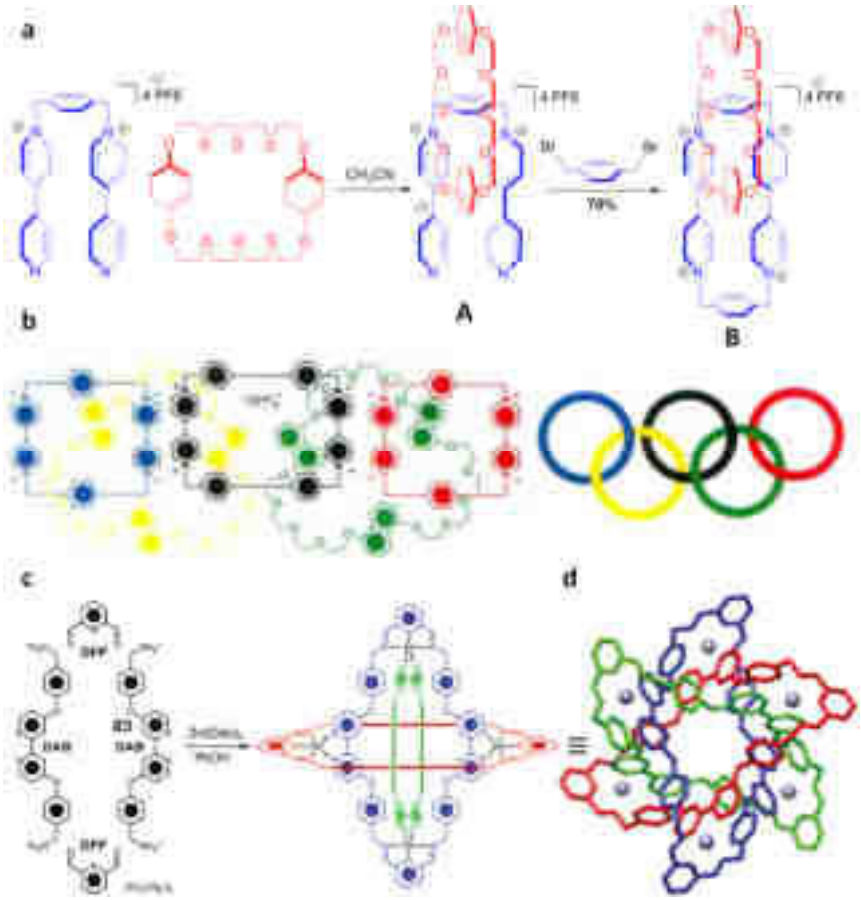

Figure 33 | a) Synthesis of a [2]catenane using donor-acceptor interactions to pre-organize the components.[89] b) This strategy was used to synthezise complex structures like these "olympiadane", a [5]catenane.[90] c) One pot synthesis of Borromean rings.[91]

Although Sauvage's and Stoddart's work provided tools that were used by many other groups in the world, alternative templated syntheses of catenanes were later developed. Prof. Leigh and his group who reported a simple strategy to synthesize [c2]catenane stabilized by hydrogen bonding.[93] The interlocked macrocycles were obtained in a 20% yield after simple reaction between 1,4-bis(aminomethyl)benzene and isophthaloyl chloride (**Figure 34a,b**). The driving force for the formation of the catenated structure is the presence of intermolecular hydrogen bonds between the reaction intermediates. This reaction could also be performed with more complicated sub-components, potentially allowing further functionalization of the [2]catenane. Interestingly, the position of the rings is not static, and exchanges between the two complementary hydrogen bonding pattern happens.[93] The exchange rate can be tuned: for instance, replacement of the benzene group between the two amides by a pyridine unit slow down the process because of additional hydrogen bonds. The more recently discovered halogen

[93] Johnston, A. G., Leigh, D. A., Pritchard, R. J. & Deegan, M. D. Facile synthesis and solid-state structure of a benzylic amide[2]catenane. *Angew. Chem. Int. Ed. Engl.* **34**, 1209-1212 (1995).

bonds were also used to pre-organize components before catenation by the group of Prof. Beer.[94] A combination of first π stacking between an electron poor pyridinium and two electron rich aromatic rings and second an halogen bond between a pyridine unit and iodine favor the formation of a *pseudo*-catenane structure (**Figure 34c**). The two pending alkene can then get engaged in an alkene metathesis reaction using a second generation Grubbs catalyst. This strategy provided the corresponding [2]catenane with a low yield of 6.5%, probably due to the formation of undesired oligomers. Indeed, the complex is efficiently formed at relatively high concentration, thus favoring side reactions such as intermolecular metathesis products during the reaction with Grubbs catalyst.

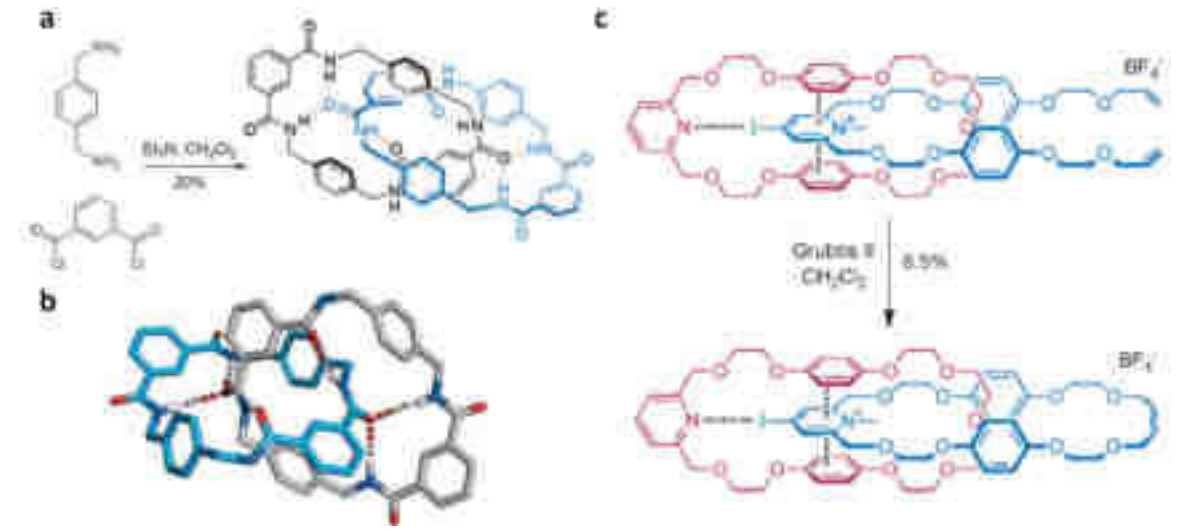

Figure 34 | a) One-pot formation of an hydrogen-bonding stabilized [2]catenane[93] and b) its X-ray structure, c) halogen-bonding templated formation of a [2]catenane.[94]

To date, numerous molecular knots and links have been described in the literature,[95] always pushing through the limit of what can be done in terms of complex topologies and controlled self-assembly. Some years ago, Prof. Leigh and his team developed the one-pot synthesis of a pentafoil knot from fifteen subcomponents with a 44% yield, exploiting dynamic covalent chemistry for the formation of imines and metal-ligand interactions (**Figure 35**).[96] X-ray crystallography revealed the presence of a chloride anion in the center of the star-shaped structure, which can be removed using silver (I) hexafluorophosphate and re-introduced with n-tetrabutylammonium chloride. Recently, by replacing the anion in the cavity with bromide

[94] Gilday, L. C. *et al.* A catenane assembled through a single charge-assisted halogen bond. *Angew. Chem. Int. Ed.* **52**, 4356-4360 (2013).
[95] Gil-Ramírez, G., Leigh, D. A. & Stephens, A. J. Catenanes: Fifty years of molecular links. *Angew. Chem. Int. Ed.* **54**, 6110-6150 (2015).
[96] Ayme, J.-F. *et al.* A synthetic molecular pentafoil knot. *Nat. Chem.* **4**, 15-20 (2012).

and the metals by zinc(II), this knot has been used to catalyze Michael addition and Diels-Alder reaction by promoting the formation of carbocations *via* a heterolytic cleavage reaction.[97] The empty pentafoil knot can bind bromide anions, enhancing the ability of compounds such as bromodiphenylmethane to dissociate into a carbocation and a bromide anion. Additionally, the catalytic properties of the pentafoil knot can be turned off after demetallation with EDTA. In this case, the metal-free pentafoil knot does not present a well-defined cavity necessary for the catalytic activity, as the structure loose the rigidity related to the restricted geometry of the metallic complexes.

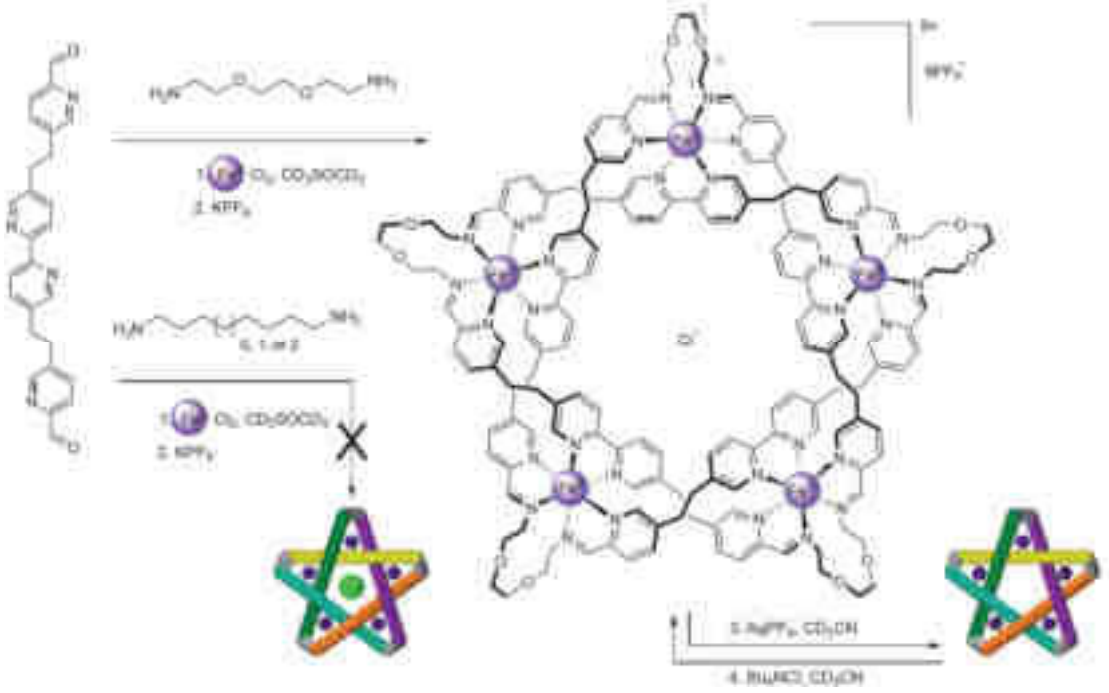

Figure 35 | Synthesis of a pentafoil knot using dynamic covalent chemistry and metal-ligand interactions.[96]

C. Translational isomerism in catenanes: towards molecular shuttles and machines

In the previous section, we focused mostly on the static structure of catenanes, but it did not take long before chemists who were synthesizing this kind of compounds got interested by the dynamics of the relative motions of their components. Sauvage and his collaborators noticed that demetallating their original [2]catenane using potassium cyanide triggered a rearrangement of the system, a motion latter called transitional isomerism (**Figure 36a**).[98] X-ray structures of the metallic complex and the metal-free structure showed different positions for the

[97] Marcos, V. *et al.* Allosteric initiation and regulation of catalysis with a molecular knot. *Science* **352**, 1555-1559 (2016).
[98] Cesario, M., Dietrich-Buchecker, C. O., Guilhem, J., Pascard, C. & Sauvage, J. P. Molecular structure of a catenand and its copper(I) catenate: complete rearrangement of the interlocked macrocyclic ligands by complexation. *J. Chem. Soc. Chem. Commun.* **5**, 244-247 (1985).

phenanthroline ligand before and after demetallation, which can be explained by a "pirouette" motion of a ring around the other. The control of this rotative motion was further achieved by electrochemical switching in a system containing both a terpyridine and a phenanthroline ligands in one of the macrocycle (**Figure 36b**).[99] In its degree of oxidation (I), copper is complexed in a tetrahedral geometry by both phenanthrolines. Upon oxidation into copper (II), the metal can accept more ligands, which make the terpyridine-phenanthroline combination more stable. The macrocycles rotate to allow for the formation of a pentacoordinated complex. Then, reduction of copper (II) into copper (I) allows for the system to go back to its original conformation.

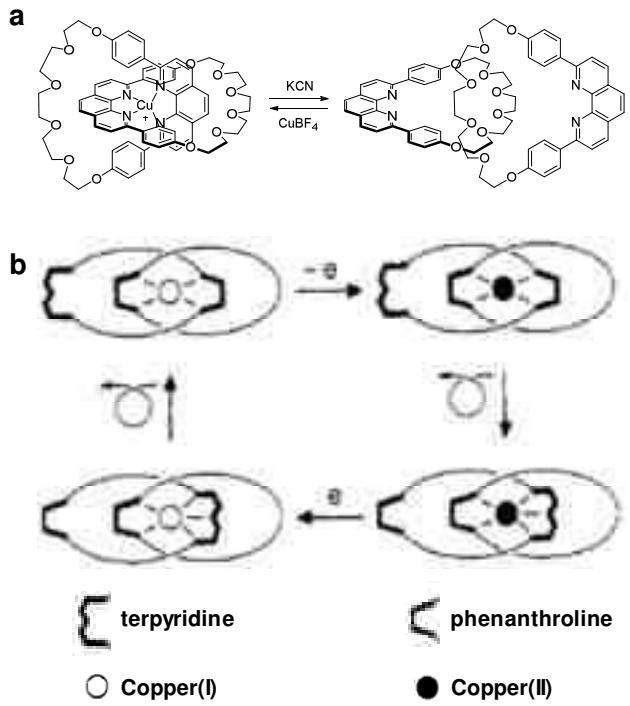

Figure 36 | a) "Pirouetting" induced by the demetallation of a metallo[c2]catenane,[98] b) Electrochemically controlled motions in a metallo[2]catenane.[99]

These results are significant as they demonstrate that control over the molecular topology of supramolecular assemblies can be linked to the control of the motion of their constituents. From this aspect of molecular knots and links emerged the first prototypes of molecular machines.

[99] Livoreil, A., Dietrich-Buchecker, C. O. & Sauvage, J.-P. Electrochemically triggered swinging of a [2]catenate. *J. Am. Chem. Soc.* **116**, 9399-9400 (1994).

II. Molecular shuttles and molecular muscles: molecular machines in action

A. Molecular shuttles and applications

Molecular machines can be described as molecular assemblies in which the motions of their component, relatively to each other, can be controlled.[2,100] These molecules can be divided into two categories: a) bistable systems that operate at thermodynamic equilibrium, which is the case of most molecular shuttles, and b) machines such as molecular motors continuously working out of equilibrium and requiring an energy input. In this section, we will focus on the advances in the field of molecular shuttles, in which a macrocycle can be moved along an axle (such as for instance in a [2]rotaxane) or around another macrocycle (such as for instance in a [2]catenane). Early developments will be discussed and we will then focus on few noticeable examples.

Stoddart and his group described in 1991 a [2]rotaxane, a system composed of a macrocycle threaded around an axle.[101] It is composed of a bluebox macrocycle (the shuttle) threaded along a polyether axle, oscillating between two identical hydroquinone stations, with triisopropylsilyl stoppers to prevent de-threading (**Figure 37a**). In this system, the blue box sits around the hydroquinone station thanks to donor-acceptor interactions. After threading the bluebox around the axle, a splitting of the ^{1}H NMR signals related to the two stations into two sets of signals occurs, indicating the alternated position of the shuttle on both hydroquinone stations. Furthermore, as each peak has the same intensity, the shuttle does not favor one station over the other. Indeed, as pictured on **Figure 37b**, in this completely symmetrical system, the location of the shuttle on one station or the other can be linked to two states of equal energy. The shuttle jumps from one to another thanks to thermal energy, *i.e.* Brownian motion. One could imagine that breaking the symmetry of the assembly could favor the position of the shuttle on a station over the other.

This was achieved by the same team a few years after in 1994, by assembling a similar but unsymmetric system in which the bluebox is complexing a benzidine station known as a better donor than the bisphenol one (**Figure 37c**).[102] In this system, the state in which the shuttle

[100] Kay, E. R., Leigh, D. A. & Zerbetto, F. Synthetic molecular motors and mechanical machines. *Angew. Chem. Int. Ed.* **46**, 72-191 (2007).
[101] Anelli, P. L., Spencer, N. & Stoddart, J. F. A molecular shuttle. *J. Am. Chem. Soc.* **113**, 5131-5133 (1991).
[102] Bissell, R. A., Córdova, E., Kaifer, A. E. & Stoddart, J. F. A chemically and electrochemically switchable molecular shuttle. *Nature* **369**, 133-137 (1994).

complexes the benzidine station is more favored energetically than when it complexes the bisphenol. Upon oxidation or protonation of the benzidine group, the shuttle moves toward the bisphenol unit to minimize electrostatic repulsion. In this case, the energy necessary to occupy the benzidine station becomes much higher, leading to the move of the ring that preferentially settles around the favored bisphenol station.

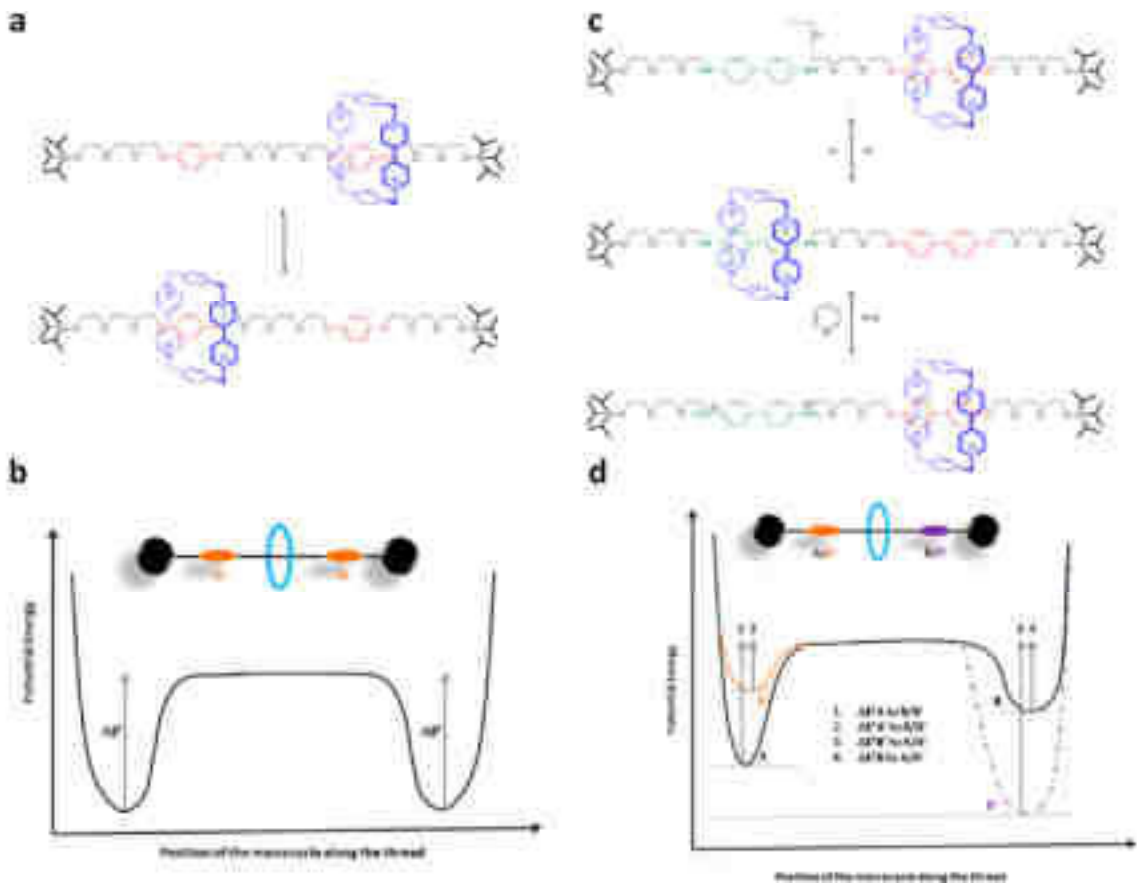

Figure 37 | a) A symmetrical [2]rotaxane[101] and b) its associated energetic profile, c) Corresponding asymmetrical [2]rotaxane[102] and d) its associated energetic profile.

This work illustrates how careful design of the axle and the shuttle can allow efficient control of molecular motions. This was the first step towards a popular area of research, which has seen the elaboration of many stimuli-responsive molecular shuttles[9] and later their implementation in larger functional systems. We will discuss some of the most influential and conceptually original examples.[103]

[103] van Dongen, S. F. M., Cantekin, S., Elemans, J. a a W., Rowan, A. E. & Nolte, R. J. M. Functional interlocked systems. *Chem. Soc. Rev.* **43**, 99-122 (2014).

Crown ether macrocycles have also been used as shuttles thanks to their ability to efficiently complex ammonium groups.[104] Stoddard and his collaborator described a rotaxane in which a dibenzo[24]crown-8 ether complexes an ammonium function close to an anthracene moiety (**Figure 38a**).[105] Upon deprotonation, the ring glides towards the only remaining electron poor group, *i.e.* a bipyridinium group. This motion can be reversed by the addition of acid to re-protonate the amine. Interestingly, for this compound, the position of the macrocycle can also affect the photo- and electrochemical properties of the molecule. In the protonated state, upon irradiation, emission of the anthracene can be quenched by electron transfer toward the bis-pyridinium group. However, in the deprotonated state, when the macrocycle is located around this station, an improvement of the emission is observed. This example highlights how molecular motions can be used to control the electronic properties of molecules. Alternatively, a triazolium unit can act as a second station for a crown ether shuttle (**Figure 38b**).[106] This triazolium approach, first described by Dr. Coutrot and his group, combines the formation of the [2]rotaxane and the second station in one step. The use of a Huisgen 1,3-dipolar cycloaddition under mild conditions allows the introduction of any azide functionalized compound as stopper and thus a variety of function and structure for these interlocked structures.

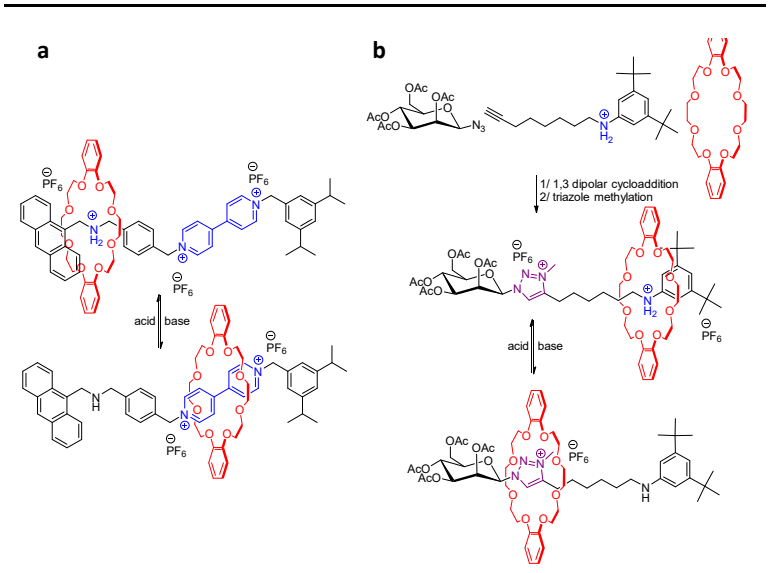

Figure 38 | pH-switchable [2]rotaxane based on a secondary ammonium station and either a) a bipyridinium station or b) a triazolium station.

[104] Glink, P. T., Schiavo, C., Stoddart, J. F. & Williams, D. J. The genesis of a new range of interlocked molecules. *Chem. Commun.* **13**, 1483-1490 (1996).
[105] Ashton, P. R. *et al.* Acid-base controllable molecular shuttles. *J. Am. Chem. Soc.* **120**, 11932-11942 (1998).
[106] Coutrot, F. & Busseron, E. A new glycorotaxane molecular machine based on an anilinium and a triazolium station. *Chem. Eur. J.* **14**, 4784-4787 (2008).

Many examples of similar rotaxanes have been described,[2,100] sometimes using other stimuli such as light irradiation[107] or electrochemistry.[108] In most of these examples however, the system often relies on a back and forth motion between two stations. Unidirectional motion of a molecular shuttle is difficult to achieve and a system able to perform such motion has been described by the group of Prof. Leigh in 2003.[109] In this example, a [3]catenane has been synthesized from a large macrocycle incorporating four stations and two smaller macrocycles threaded around the large one and recognized by hydrogen bonding (**Figure 39**). The use of two shuttles in this example is essential to the unidirectional character of the motion. The two macrocycles influence each other and one is always preventing the other to go in the "wrong" direction. By applying a well-defined sequence of transformations, the motions of the rings can be made, on average, unidirectional.

Figure 39 | Unidirectional motion of a macrocycle along a [3]catenane, (1) 350 nm, CH_2Cl_2, 5 min, 67%; (2) 254 nm, CH_2Cl_2, 20 min, 50%; (3) heat, 100 °C, $C_2H_2Cl_4$, 24 h, 100%; catalytic ethylenediamine, 50 °C, 48 h, 65%; or catalytic Br_2, 400–670 nm, CH_2Cl_2, -78 °C, 10 min, 100%.[109]

Although the field witnessed an increase in the complexity of the synthesized structures and control over the motions, only few examples in the literature report functional rotaxane-based systems and devices.[103] The elaboration of such objects requires either 1) the precise control of individual molecular machines among thousands of them, for example to use a rotaxane to encode values 0 and 1 in a molecular memory-like electronic component,[110] or 2)

[107] Murakami, H., Kawabuchi, A., Matsumoto, R., Ido, T. & Nakashima, N. A multi-mode-driven molecular shuttle: Photochemically and thermally reactive azobenzene rotaxanes. *J. Am. Chem. Soc.* **127**, 15891-15899 (2005).
[108] Armaroli, N. *et al.* Rotaxanes incorporating two different coordinating units in their thread: Synthesis and electrochemically and photochemically induced molecular motions. *J. Am. Chem. Soc.* **121**, 4397-4408 (1999).
[109] Leigh, D. A., Wong, J. K. Y., Dehez, F. & Zerbetto, F. Unidirectional rotation in a mechanically interlocked molecular rotor. *Nature* **424**, 174-179 (2003).
[110] Flood, A. H. *et al.* Chemistry: Whence molecular electronics? *Science* **306**, 2055–2056 (2004).

the collective actions of thousands of molecular machines together to amplify their response at a larger scale.[5] The first approach requires extreme control in terms of precise molecular stimulation, and this kind of material still remains a distant future. This second approach has been exploited several times for rotaxane-based materials, mainly by the group of Stoddart, for example to conceive molecular muscles and molecular nanocarriers.

The design of a [3]rotaxane with pending thiol units on the shuttles allowed grafting molecular machines onto gold cantilevers (**Figure 40a**).[111] In this molecule, the rings can adopt two positions: far (rings around a tetrathiafulvalene (TTF) station, green station in **Figure 40a**) or close (rings around a naphthalene station, red station in **Figure 40a**) from each other's. Upon oxidation of the TTF units, the shuttles switch from their "far" to their "close" state around the naphtalene, thus pulling on the surface. When this force is applied by all rotaxanes at the same time, bending of the gold cantilever occurs, as observed by measuring the variation of deflection of a laser beam aimed at the surface. This process is reversible so that the system can go back to its original state upon reduction of the TTF units. It can be repeated several times, as long as the system is kept in an aqueous solution in which oxidants and reductants are sequentially added. This example proves that the motions of molecular machines can add up to apply force on a larger object.

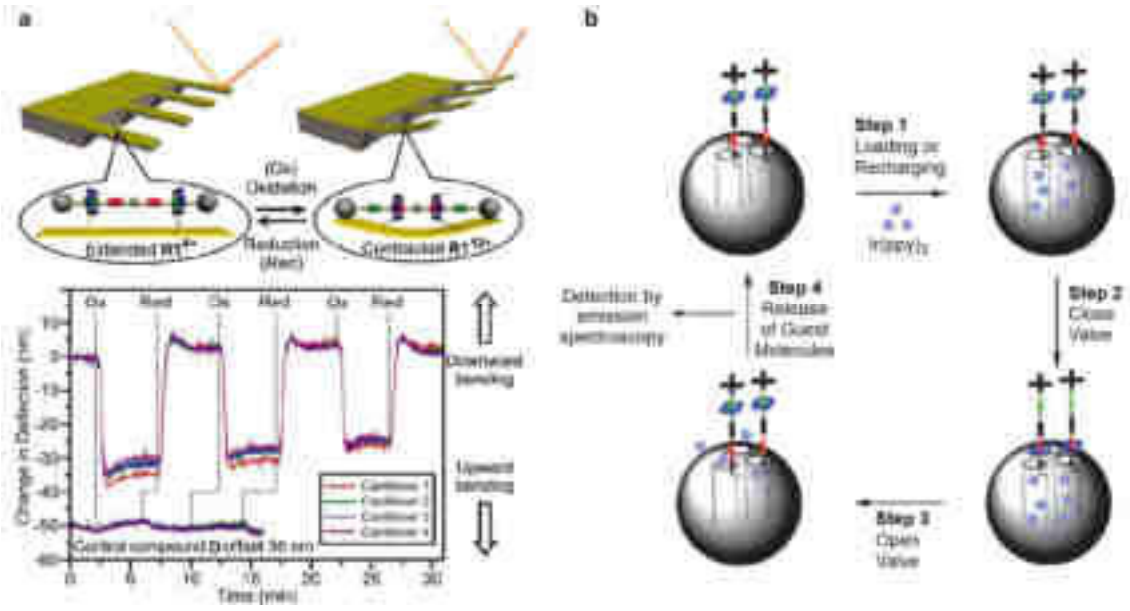

Figure 40 | a) A gold cantilever bent by the collective motions of [3]rotaxanes, as observed by the variation of deflection angle of a laser beam aimed at the gold surface,[111] b) Stepwise loading and release of guest molecules by a mesoporous silica nanoparticle used as a nanocarrier and triggered by a redox stimulus.[112]

[111] Liu, Y. *et al.* Linear artificial molecular muscles. *J. Am. Chem. Soc.* **127**, 9745-9759 (2005).

In another example, mesoporous silica nanoparticles were decorated with [2]rotaxanes presenting a TTF and a naphthalene station that can be used as nanovalves (**Figure 40b**).[112] Similarly to the previous example, the shuttle, a bluebox, initially resides around the TTF station, far from the surface of the nanoparticle, so that the mesoporous particle can be loaded with for instance, a luminescent compound (step 1). Upon oxidation of the TTF units, the bluebox glides around the naphthalene station, thus "closing" the pores (step 2). This process can be reversed at any moment by reduction of the TTF units, leading to the opening of the valve again (step 3) and thus to the release of a loaded compound, i.e. a luminescent iridium complex, as followed by emission spectroscopy (step 4). This example describes a fully functional system using cooperative actions of molecular machines, which applications can be envisioned in the field of drug delivery for example.

Pseudo-collective (*i.e.* concomitant) motions of molecular machines were also exploited to change the macroscopic properties of surfaces, as exemplified by the group of Prof. Leigh.[113] A surface was covered with bistable hydrogen bonding assembled [2]rotaxanes which shuttle can be moved upon light irradiation (**Figure 41a**). Switching from the initial station to the second one "hide" a fluoroalkyne residue, thus increasing the polarity of the surface. This was observed *via* the change of contact angle of liquids drop-casted on the irradiated surface. Most impressively, the rotaxane-based surface was used to control the motion of a drop of diiodomethane. Irradiation of one drop on its side induces its displacement towards the irradiated region (**Figure 41b**), as a consequence of the more polarophilic surface interacting with the liquid. Such surfaces could also be used to move a drop up a twelve-degree incline. It should be mentioned here that, even though the rotaxanes are collectively changing the properties of the surface, the action of the molecular machines on the affected object (here the drop) is indirect, which means that this is not really the collective motions of the molecular machines that are moving the drops.

[112] Nguyen, T. D. *et al.* A reversible molecular valve. *Proc. Natl. Acad. Sci. U S.A.* **102**, 10029-10034 (2005).
[113] Berná, J. *et al.* Macroscopic transport by synthetic molecular machines. *Nat. Mater.* **4**, 704-710 (2005).

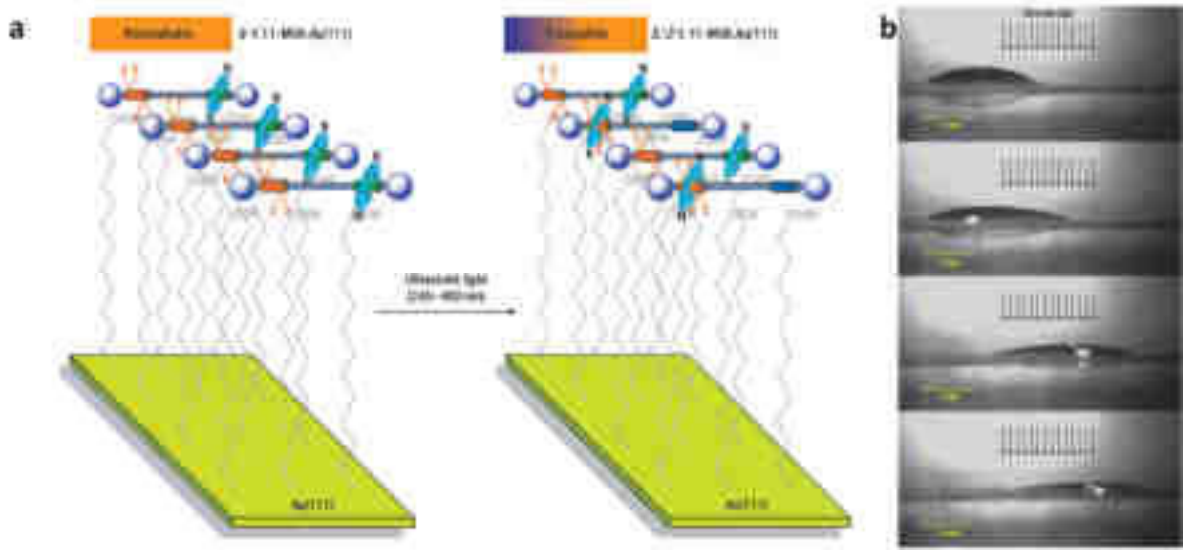

Figure 41 | a) Photoswitchable [2]rotaxane-covered surface,[113] b) motion of a diiodomethane drop upon light irradiation of such a surface.[113]

Another exciting perspective of advanced molecular machines in a far future would be to use them as small chemical plants or self-replicating machines, functions reminiscent of living systems. An elegant step in this direction has been described by the group of Leigh who developed a [2]rotaxane able to iteratively synthesize a small peptide by successive coupling of amino acids taking advantage of the Native Chemical Ligation (NCL)[114,115] reaction (**Figure 42a**).[116] In this [2]rotaxane, the thread is a succession of blocks bearing amino acids in the form of amino esters in a specific sequence, while the shuttle is a macrocycle equipped with an arm presenting a small peptide featuring a cysteine derivative (**Figure 42a(i)**). This cysteine is essential to the NCL reaction,[114,115] as it reacts with amino esters to yield a reactive intermediate. This intermediate then reacts with the N-terminal extremity from the peptide on the arm to add the amino acid to the sequence as shown in **Figure 42a(ii)**. This operation occurs several times until the shuttle reaches the end of the thread and is released in solution. Cleavage of the peptide from the shuttle confirmed that the sequence imposed by the [2]rotaxane was respected as determined by LC/MS. This rotaxane has a function similar to ribosomes, although far from being as efficient and fast.

[114] Muir, T. W., Sondhi, D. & Cole, P. A. Expressed protein ligation: a general method for protein engineering. *Proc. Natl. Acad. Sci. U.S.A.* **95**, 6705-6710 (1998).
[115] Malins, L. R. & Payne, R. J. Recent extensions to native chemical ligation for the chemical synthesis of peptides and proteins. *Curr. Opin. Chem. Biol.* **22**, 70-78 (2014).
[116] Lewandowski, B. *et al.* Sequence-specific peptide synthesis by an artificial small-molecule machine. *Science* **339**, 189-193 (2013).

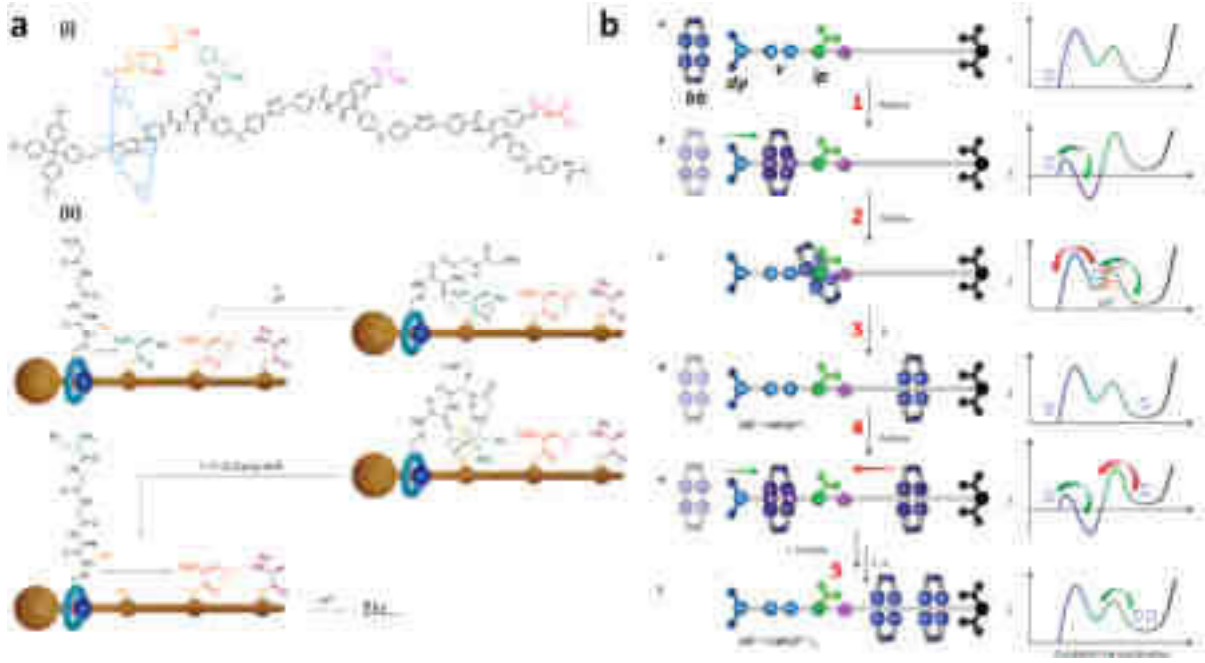

Figure 42 | a) (i) Artificial molecular peptide synthesizer (ii) operating via successive NCL reactions: The shuttle moves along the axle, its arm pickis up the amino acid respecting the sequence imposed by the thread,[116] b) An artificial molecular pump and the energetic profile associated to each step of the pumping process (***bb***: bluebox, ***dp***: dimethylpyridinium, ***v***: viologen, ***ip***: isopropylphenyl).[117]

Molecular pumps are also objects of great interest for synthetic chemists, as they allow the formation of concentration gradients, essential to cellular functions, by pumping ions across membranes for example, consuming chemical fuels in the process. Prof. Stoddart and his collaborators described the synthesis and operation of a molecular thread able to trap macrocycles, by pumping them out of solution following careful molecular design and control of the associated energetic landscape.[117] The concept is pictured on **Figure 42b**. Reduction of the bis-pyridinium moieties from the bluebox ***bb*** and the viologen ***v*** units into their radical leads to the complexation of a bluebox around the axle driven by strong radical-viologen interactions (**1**). The macrocycle thus crosses the dimethylpyridinium stopper ***dp*** and sits around the viologen radical (**2**). Upon oxydation, strong electrostatic repulsion occurs between the four-fold positively charged blue box and the bis-pyridinium station. To minimize this repulsion, the macrocycle has to cross either the dimethylpyridinium stopper or an isopropylphenyl group ***ip***, which is the most kinetically favoured step (**3**). The thread acts as a molecular ratchet that prevents the macrocycle to escape once captured, forcing it to go only in one direction along the axle. This operation can be repeated once as the system can stock up to two macrocycles (**4**). In this example, a ratchet-like system powered by a chemical fuel kinetically traps a

[117] Cheng, C. *et al.* An artificial molecular pump. *Nat. Nanotech.* **10**, 547-553 (2015).

chemical species, which, as the authors claim, locally creates a concentration gradient of bluebox units.

Consumption of a fuel to operate complex functions far from equilibrium is a characteristic property of many complex biological systems.[118] Chemically fuelled biological motors allow the motions of proteins such as myosin or kinesin. Until now, we described bistable systems in which the positions of the ring can be switched between two thermodynamically stable states. The aforementioned artificial molecular pump differs in the way that it kinetically traps the shuttle out of its thermodynamically stable state, but only few examples in the literature describe molecular machines truly operating far from equilibrium.[119] Herein we will discuss two of the most noticeable examples of this kind of systems. In 2006, the synthesis and mechanism of an autonomous piston-like nanomotor was described by the groups of Stoddart and Balzani.[120] In this molecular machine, a bis(bisphenol) macrocycle sits around a bipyridinium station (in blue) thanks to donor-acceptor interactions (**Figure 43a**). The shuttle favors this station over the dimethyl-bipyridinium (in purple) one as it is slightly less electron-rich. Upon reduction of the bipyridinium station into its corresponding cationic radical, thus becoming more electron-rich, the shuttle glides now toward the best accepting dimethyl-bipyridinium station. This process can be reversed by oxidation of the cationic radical, triggering the motion of the shuttle back to the bipyridinium. In this case, no chemical reagents were used to trigger these redox reactions, but a $[Ru(bpy)_3]^{2+}$ complex was grafted as a stopper. When irradiated with visible light, thanks to its long-life excited state, the ruthenium complex transfers an electron to the accepting bipyridinium station. As long as this charged-separated state exists, the macrocycle glides toward the dimethyl-bipyridinium station. However, when charge recombination occurs, the macrocycle goes back to its original position. When continuously irradiated, the macrocycle autonomously oscillates between the two positions like a nanoscopic piston. This artificial molecular machine can operate at a frequency of 10^3 Hz without visible degradation of the compound in solution and requires no additional reactants.

[118] Schliwa, M. & Woehlke, G. Molecular motors. *Nature* **422**, 759-765 (2003).
[119] Li, H. *et al.* Relative unidirectional translation in an artificial molecular assembly fueled by light. *J. Am. Chem. Soc.* **135**, 18609-18620 (2013).
[120] Balzani, V. *et al.* Autonomous artificial nanomotor powered by sunlight. *Proc. Natl. Acad. Sci. U.S.A.* **103**, 1178-1183 (2006).

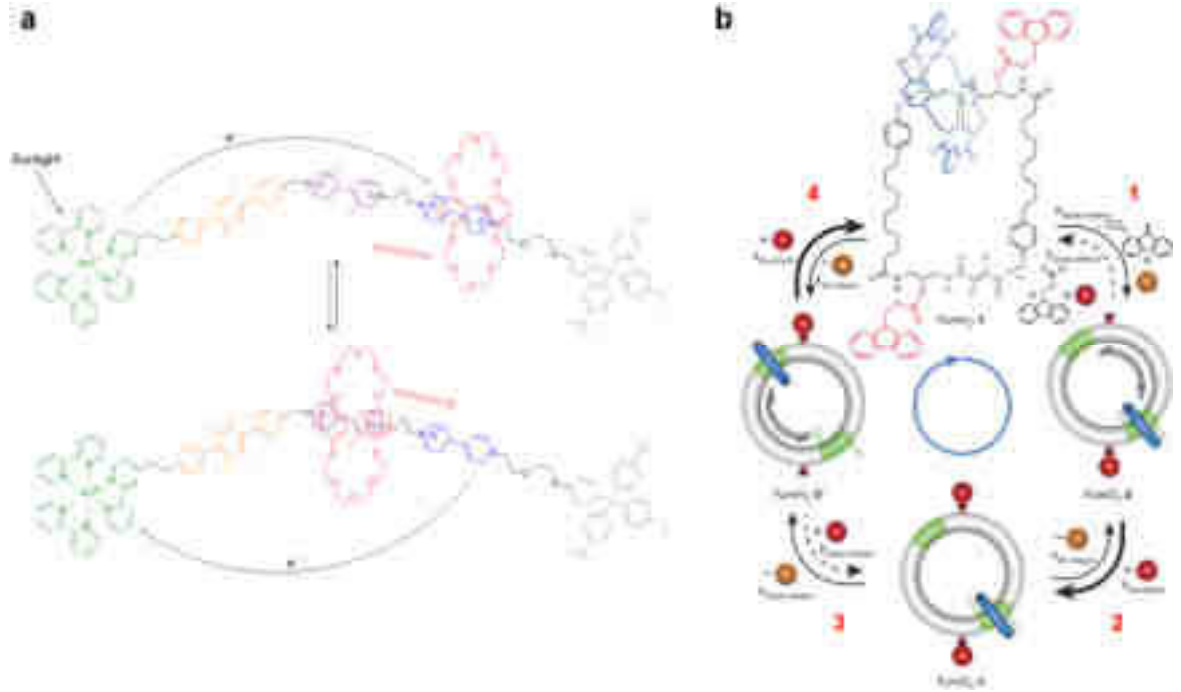

Figure 43 | a) An autonomous nano-piston that operates under visible-light irradiation, changing the affinity of the shuttle for the two stations by repeated charge separation/charge recombination,[120] b) Out of equilibrium unidirectional motion of a macrocycle in a [2]catenane. The random motions of the shuttle are biased by the alternated deprotection/protection of alcohols, acting as ratchets pushing the macrocycle in only one direction.[121]

While in the former example we described a continuously oscillating motion between two stations, continuous unidirectional motion of a shuttle along an axis is also of high interest, as one could imagine synthesizing molecular "trains" transporting chemical species along molecular "rails". The first example of such motion in an artificial interlocked molecular species was recently published by the group of Leigh, in the form of a [2]catenane in which the shuttle can initially oscillate between two identical stations (**Figure 43b**).[121] Two pending alcohols next to each stations are protected with a Fmoc group so that the shuttle is locked onto one of the two stations. Introduction of a chemical fuel, *i.e.* a mixture of potassium bicarbonate, triethylamine and Fmoc-Cl, "turns on" the system and induces a unidirectional rotation of the shuttle along the circular track. To do so, the authors took advantage of the difference of kinetics between the protection and the deprotection of the alcohol units. Indeed, while the speed of deprotection of an alcohol bearing a Fmoc group is always the same, its protection, which is catalyzed by a bulky catalyst, occurs faster in a position next to an unoccupied station, *i.e.* far from the shuttle. After the first deprotection, the macrocycle oscillates between the two available stations *via* Brownian motion (**1**). Presence of the chemical fuels allows the alcohol located far from the shuttle to get re-protected, thus trapping the macrocycle on the second

[121] Wilson, M. R. *et al.* An autonomous chemically fuelled small-molecule motor. *Nature* **534**, 235-240 (2016).

station (**2**). Eventually, the Fmoc group next to the station gets deprotected and the shuttle oscillates between two stations again (**3**). Finally, protection of the free alcohol, when the shuttle is far, complete the rotation (**4**). Overall, the macrocycle can glide in only one direction, thanks to the influence of the shuttle on the reaction kinetics, biasing the Brownian motion.

Examples presented in this section illustrate how molecular shuttles evolved from scientific curiosity to prototype of functional molecular devices and impressive nanomechanical systems. The complex functions they can achieve arise from the combination of covalent and non-covalent interactions in an ambitious molecular design. As seen in the last four examples, molecular machines now present an exciting opportunity to produce artificial systems with structures and properties reminiscent of biological systems.

B. [c2]daisy chains: towards muscle like molecular machines

Some of the most impressive functions performed by biomolecular machines emerge from their cooperative actions and the amplification of their motions. In muscles, the hierarchical arrangement of sarcomeres into myofibrils allows for the efficient amplification of molecular motions up to the macroscopic scale.[4] Several interwoven molecular systems are able to contract/extend upon stimulation,[122] but we will here focus only on the most popular and promising one, namely [c2]daisy chains rotaxanes.

In 2000, the group of Prof. Sauvage described the first interlocked structures behaving like an artificial sarcomere.[123] They synthesized an interpenetrated [2]rotaxane called [c2]daisy chain, as their entanglement is reminiscent of garlands made of daisy flowers usually made by children (**Figure 44**). This rotaxane presents two types of ligands, namely phenanthroline and terpyridine, which can complex different metal cations. In the initial state, copper(I) cations are complexed by the phenanthroline ligand (blue station on **Figure 44**), locking the structure in an "extended" state. After treatment with potassium cyanide, copper(I) is replaced by zinc(II) which can accept up to six ligands, and will thus get complexed by a phenanthroline and a terpyridine ligand. This change of coordination leads to the gliding of the two components of the [c2]daisy chain, thus reducing the size of the molecule to provide the "contracted" state. The zinc(II) can then be replaced by copper(I) to go back to the initial "extended" state. These [c2]daisy chains are effectively able to longitudinally change their size like sarcomeres do, although the switching process by metal exchange is not ideal in terms of reversibility. This

[122] Bruns, C. J. & Stoddart, J. F. Rotaxane-based molecular muscles. *Acc. Chem. Res.* **47**, 2186-2199 (2014).
[123] Jiménez, M., Dietrich-Buchecker, C. & Sauvage, J. Towards synthetic molecular muscles: contraction and stretching of a linear rotaxane dimer. *Angew. Chem. Int. Ed. Engl.* **39**, 3284-3287 (2000).

metal-induced switching was later replaced by an acid/base switching developed by Stoddart and Coutrot, who designed independently [c2]daisy chains based on crown ether/ammonium interactions.[124,125]

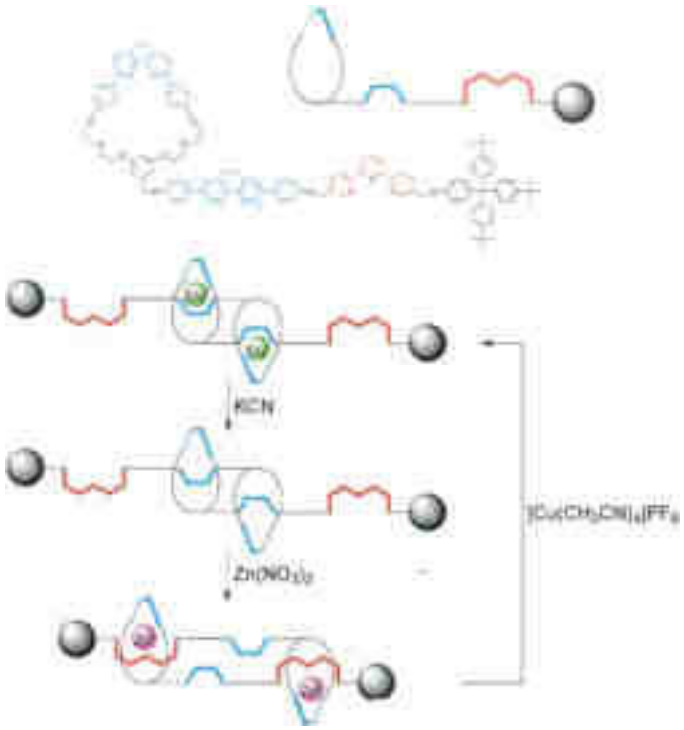

Figure 44 | Metal-switchable [c2]daisy chains behaving like a molecular muscle.

Inspired by the hierarchical organization and multiscale motion observed in muscular tissues, one of the biggest challenge toward the amplification of molecular machines motion is to organize several of them into large assemblies. Over the last ten years, the synthesis of a [c2]daisy chain polymer able to contract and extend upon concerted stimulation of its components was an ambitious goal. The first step in this direction has been presented by the group of Kaneda, who described a photoswitchable [c2]daisy chain oligomer.[126] However, the low polymerization degree and the only partial contraction of the structure demonstrated the limitation of this approach. Noticeable progress was achieved a few years later by the groups of Grubbs and Stoddart, who independently described the synthesis of pH switchable [c2]daisy chains oligomers using a 1,3 dipolar cycloaddition reaction as polymerization method (**Figure**

[124] Cantrill, S. J., Youn, G. J., Stoddart, J. F. & Williams, D. J. Supramolecular daisy chains. *J. Org. Chem.* **66**, 6857-6872 (2001).
[125] Romuald, C., Busseron, E. & Coutrot, F. A new pH-switchable dimannosyl [c2] daisy chain. *Org. Lett.* **10**, 3741-3744 (2008).
[126] Tsuda, S., Aso, Y. & Kaneda, T. Linear oligomers composed of a photochromically contractible and extendable Janus [2]rotaxane. *Chem. Commun.* **29**, 3072-3074 (2006).

45).[127,128] In Stoddart's work, the extended state is obtained when the crown ether rings complex the ammonium cations (**Figure 45a**). Upon deprotonation, the electron rich crown ethers glide toward the next accepting station, in this case a bipyridinium station, yielding the contracted architecture. This process can be reversed by adding acid to retrieve the extended state, as confirmed by typical ^{1}H NMR shifts. Interestingly, kinetics study revealed that, the contraction/extension process seemed to occur faster in the oligomer than in the monomer. In Grubbs' work, deprotonation of the [2]daisy chain polymer did not yield the expected motion. Indeed, in the deprotonated state, the shuttles do not have a well-defined accepting station to complex, and the two biphenyl moieties which were supposed to act as accepting stations stack by π-interactions, locking the structure in its original position. The extension event had to be forced by acylation of the amines. By doing so it was possible to measure an increase of gyration radius (R_g) from 14.8 to 21.4 nm, confirming the change of volume upon motion of the [c2]daisy chains, but the reverse motion could not be achieved without removal of the acyl group. However, in both models, the low polymerization degree (respectively 11 and 22) prevented this kind of material to amplify the motion of individual molecular machines at higher lengths scales.

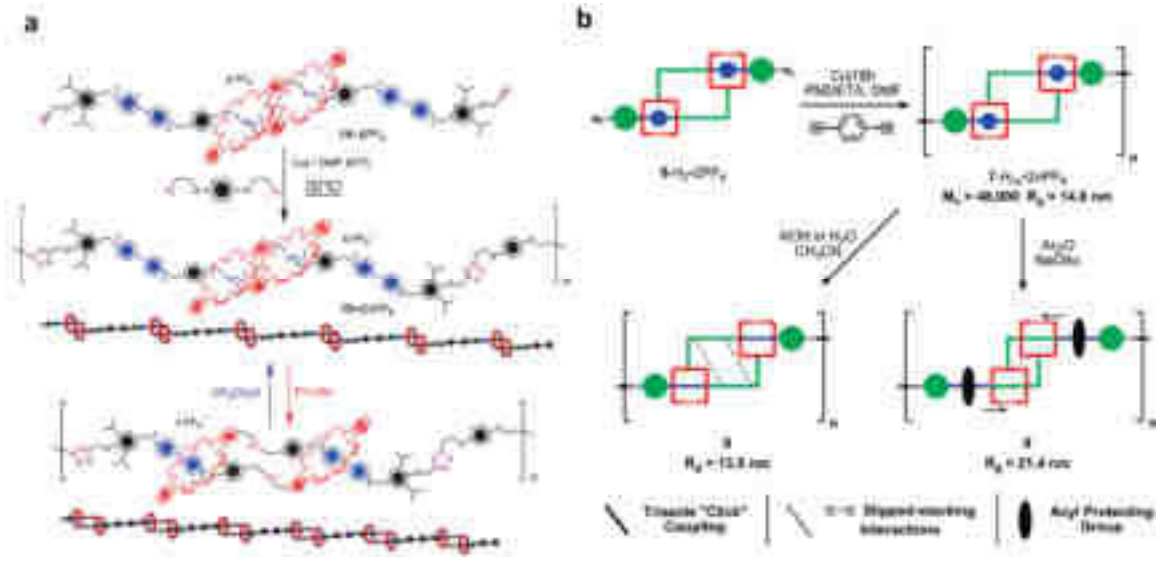

Figure 45 | pH-switchable [c2]daisy chains polymers as described by the group of a) Stoddart, which can be switched between its contracted and extended states by the addition of base and acid respectively,[127] and b) Grubbs, which cannot be extended without chemical modification as the deprotonated structure is locked because of π-π stacking between two biphenyl moieties.[128]

[127] Fang, L. *et al.* Acid-base actuation of [c2]daisy chains. *J. Am. Chem. Soc.* **131**, 7126-7134 (2009).
[128] Clark, P. G., Day, M. W. & Grubbs, R. H. Switching and extension of a [c2]daisy-chain dimer polymer. *J. Am. Chem. Soc.* **131**, 13631-13633 (2009).

To overcome these issues, our group reported on a system in which [c2]daisy chains decorated with terpyridine stoppers were polymerized by the addition of metal cations (**Figure 46**).[6] The terpyridine functionalized [2]daisy chains can reversibly contract and extend upon addition of base or acid, respectively. Addition of a metal inducing the formation of strong bis-terpyridine complex such as iron(II) triggered the formation of long supramolecular polymer chains with a degree of polymerization up to 3000 as determined by scattering experiments. Such a combination of light and neutron scattering experiments were used to determine the structure of the polymer in solution, *i.e.* single wormlike chains which length can be estimated to be around 9.37 µm in the contracted state and 15.86 µm after extension using acid. This global change of the contour length is associated to a local change of linear mass density, confirming the overall contraction/extension of the polymer chains. This work represents the first example where a nanoscopic motion has been amplified by four orders of magnitude above its scale, proving that integration of molecular motion up to the macroscopic scale can be achieved.

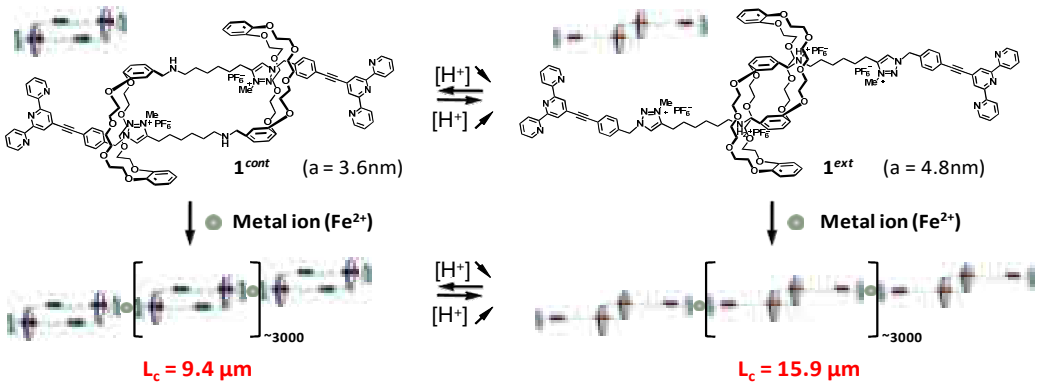

Figure 46 | Muscle-like supramolecular polymer based on [c2]daisy chains associated by coordination chemistry. Deprotonation/protonation of the amine station triggers the collective contraction/extension of the molecular machines, motions that is amplified across several scales in the whole polymer chain.[6]

pH variation is not the ideal stimuli for a prototype of artificial molecular muscle, as it requires constant input of chemicals and the accumulation of waste in the medium or the material is unavoidable. The group of Prof. Huang described a system similar to the one described by our group, also polymerized using terpyridine-metal interactions but based on solvent switchable [c2]daisy chains (**Figure 47**).[129] In this example, the polymer contracts in apolar medium and extends in polar medium. Similar aggregated structures were observed by microscopy in both states. Dynamic Light Scattering (DLS) was used to show a R_g increase

[129] Gao, L., Zhang, Z., Zheng, B. & Huang, F. Construction of muscle-like metallo-supramolecular polymers from a pillar 5 arene-based c2 daisy chain. *Polym. Chem.* **5**, 5734-5739 (2014).

upon extension of the polymer in solution, by measuring chloroform solutions with increasing proportions of DMSO. Solvent-dependent [c2]daisy chains have thus proven to be effective but successive contraction and extension requires progressive dilution of the medium. This is not compatible with the use of supramolecular polymer as the concentration affects the size of the objects.

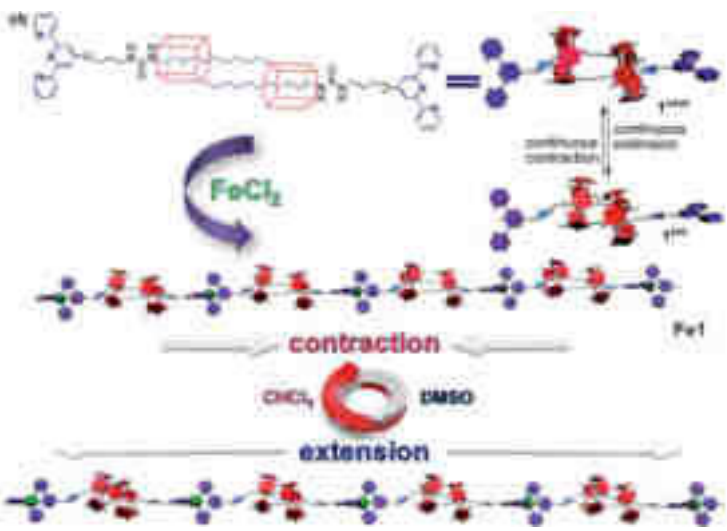

Figure 47 | A solvent-switchable [c2]daisy chains supramolecular polymer.[129]

The most recent example of [c2]daisy chain-based molecular muscle has been reported by Prof. Harada and his group.[130] [c2]daisy chains based on the inclusion of azobenzene in cyclodextrin were incorporated into a polyethylene glycol polymer network. Upon irradiation, the trans-cis isomerization of azobenzene expels it out of the cyclodextrin, reducing the size of the [c2]daisy chain unit and supposedly the overall size of the network. Minor response in the form of bending was observed when the network was swollen in dimethyl sulfoxide, while the dried material displayed impressive but non-reversible bending upon irradiation. This compound could be described as an actuator, but is not able to reversibly contract and extend.

Although tremendous progresses have been achieved in the last few years, the integration of [c2]daisy chains motions in materials such as films or gels able to show a response at the macroscopic scale remains highly challenging, as it requires the precise ordering of functional roxatane units into fibers or network. The work described in this manuscript should provide some answers to these still lasting objectives.

[130] Iwaso, K., Takashima, Y. & Harada, A. Fast response dry-type artificial molecular muscles with [c2]daisy chains. *Nat. Chem.* **8**, 625-632 (2016).

Chapter III: Light-driven rotary molecular motors

I. Rotational molecular motors

Living organisms depend on many biological architectures able to operate out of equilibrium.[27,118] This ability is linked to complex functions such as the formation of concentration gradient, molecular motions or the production of ATP *via* rotation of ATP synthase.[131] The unidirectional rotation of ATP synthase, due a to the existence of a molecular ratchet in the protein, is essential to its biological function, and for elaboration of artificial molecular motors able to reproduce this characteristic is crucial to the elaboration of artificial nanosystems working out of equilibrium and able to produce work.[132]

The synthesis of a molecular ratchet is the first step toward the elaboration of unidirectional rotational molecular rotors. Early prototype of a rotational ratchet was described by Kelly and his group in 1999, when they achieved the unidirectional 120° rotation of a propeller-like motif in a triptycene[4]helicene (**Figure 48**).[133] After conversion of the amine into its corresponding isocyanate (**1**), the triptycene part randomly moves thanks to Brownian motion (**2**), but the energy necessary to slip past the helicene is too high to allow rotation in either direction. However, the isocyanate can eventually react with a pending alcohol located on the helicene (**3**), leading to the formation of a highly strained macrocycle which tension is high enough to overcome the rotational energy barrier preventing to slip past the helicene (**4**). This part of the mechanism corresponds to the ratchet; once the rotation is achieved, a stable confirmation is reached, preventing the system to go back. The direction of the motion is imposed by the helicity of the molecule, forcing the 120° rotation to go only in one direction. Phosgene is a fuel here and is consumed to produce a highly energetic intermediate which enables the rotation.

[131] Yoshida, M., Muneyuki, E. & Hisabori, T. ATP synthase - a marvellous rotary engine of the cell. *Nat. Rev. Mol. Cell Biol.* **2**, 669-677 (2001).
[132] Browne, W. R. & Feringa, B. L. Making molecular machines work. *Nat. Nanotech.* **1**, 25-35 (2006).
[133] Kelly, T. R., Silva, H. De & Silva, R. A. Unidirectional rotary motion in a molecular system. *Nature* **401**, 1995-1997 (1999).

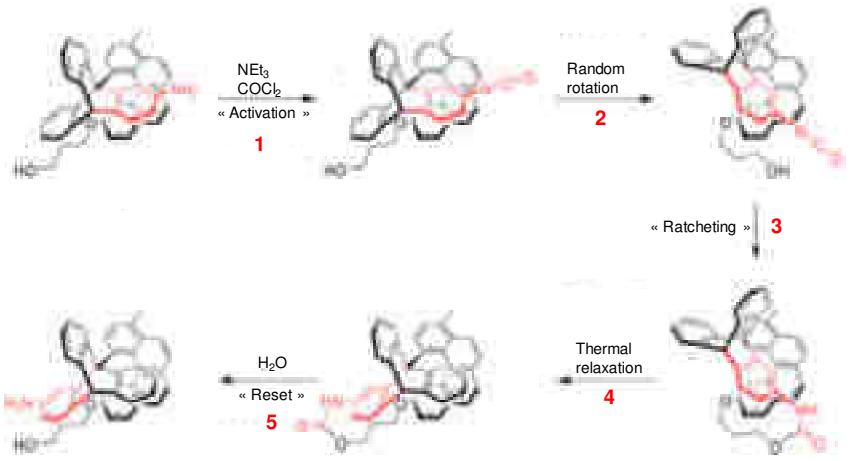

Figure 48 | First chemically fueled molecular ratchet undergoing a 120° unidirectional rotation.[133]

At the very same time, the group of Feringa reported an unidirectional molecular motor able to undergo a 360° rotation, fueled by light (**Figure 49**).[134] Compared to a chemical fuel, simple light irradiation as an energy input avoids the accumulation of chemical waste. This class of motors is based on the light-triggered isomerization of a crowded carbon-carbon double bond. This so called "first generation" of light-driven molecular motors is characterized by its symmetrical structure. The origin of the unidirectional character of the rotation here comes from the presence of stereogenic centers, the Me_{ax} groups, which favor one stable helicity over the other.

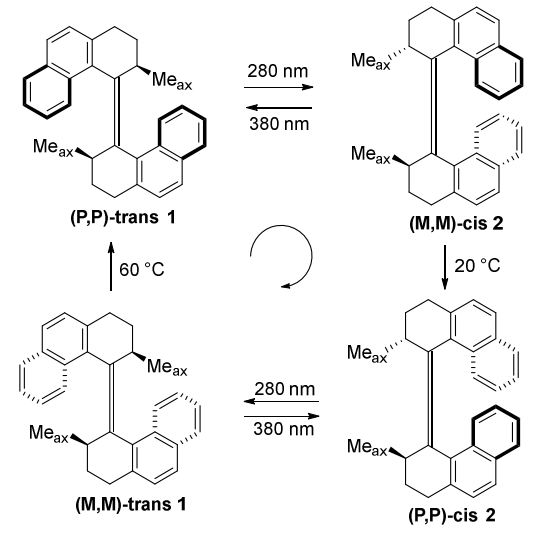

Figure 49 | Feringa's first generation of light-driven molecular motor undergoing a repetitive 360° unidirectional rotation.[134]

[134] Koumura, N., Zijlstra, R. W. J. & Delden, R. A. Van. Light-driven monodirectional molecular rotor. *Nature* **401**, 1997-2000 (1999).

Four steps are required to achieve a 360° rotation of one part relatively to the other. First, isomerization of the central double bond of **(P,P)-trans-1** compound, achieved by UV light irradiation, yields a strained isomer **(M,M)-cis-2**, which helicity is different from the starting material. Thermal helix inversion allows the stabilization of the molecule into the isomer **(P,P)-cis 2**. A similar sequence of light-induced cis-trans isomerization and thermal helix inversion finalize the 360° rotation. Under constant light irradiation and working at a temperature high enough to overcome the energy barrier of the helix inversion, the two parts of the motor constantly rotate in opposite directions relatively to each other.

Whereas the photochemical steps are very fast, the efficiency of the thermal step is limited by the steric hindrance of the intermediates **(M,M)-cis 2** and **(M,M)-trans 2**. Consequently, the speed of these light-activated molecular motors depends mostly on the thermal step, which is the rate determining step. Lowering the energy barrier to perform the helix inversion represents the key to enhance the frequency of rotation. Tuning the chemical structure of the motor in order to improve the rotation speed was the main tool used to design the so-called "second generation" of molecular motors (**Figure 50**).[135,136]

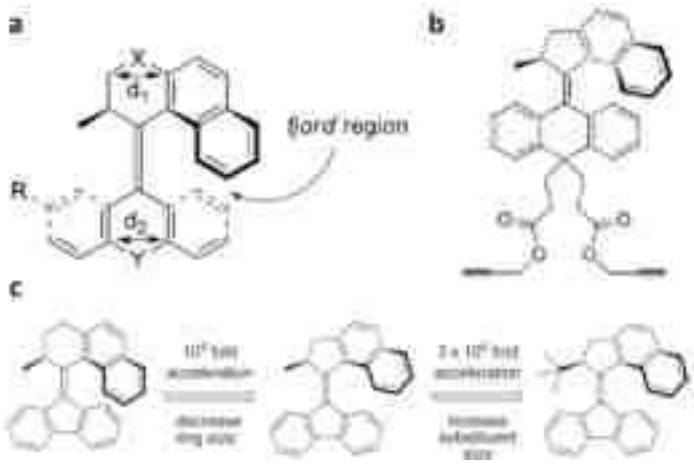

Figure 50 | a) Feringa's second generation of light-driven molecular motor with representation of the fjord region, where the steric hindrance is determining for the rotation speed, and position of the X and Y atoms which nature also influence the rotation frequency.[138] b) Fastest molecular motor to date,[137] c) Influence of the substitution of the motor on the rotation speed.[139]

[135] Pollard, M. M., Klok, M., Pijper, D. & Feringa, B. L. Rate acceleration of light-driven rotary molecular motors. *Adv. Funct. Mater.* **17**, 718-729 (2007).
[136] Klok, M. *et al.* MHz unidirectional rotation of molecular rotary motors. *J. Am. Chem. Soc.* **130**, 10484-10485 (2008).
[137] Brouwer, A. M. & Feringa, B. L. An ultrafast surface-bound photo-active molecular motor. *Photochem. Photobiol. Sci.* **13**, 241-246 (2014)

The design of this second generation of molecular motors is characterized by an asymmetric functionalization around the central carbon double bond (**Figure 50a**).[138] Decreasing the steric hindrance around the fjord region (**Figure 50a**,**c**) drastically reduces the energy barrier associated with the helix inversion, known as the rate determining step, and thus allows to speed up the rotation.[135,136,139] The nature of X and Y bridging atoms is also important as variation from carbon to oxygen or sulfur induces noticeable differences in the rotation frequency, because of the different bond angles imposing different d_1 and d_2 distances. Modification of these distances has therefore a direct influence on the hindrance in the fjord region. Replacing one of the six-member ring across the carbon double bond by a five-member ring also reduces the steric hindrance in the fjord region. This new generation of motor has seen the synthesis of fast rotational machines, with frequencies up to 12 MHz (**Figure 50b**).[137]

From a synthetic point of view, while the synthesis of the first generation of molecular motors could rely on a homocoupling reaction such as the McMurry reaction (a Ti(III) mediated reductive coupling of two ketones),[140] the asymetric synthesis necessary for the second generation of motors required the use of a Barton-Kellogg reaction.[141,142] This reaction allows for the formation of a carbon-carbon double bond between a thioketone and a diazo derivative. The use of this strategy allows for the synthesis of asymmetrically functionalized molecular motors, which opens up many opportunities for the development of applications.

With the perspective of creating nanomechanical devices based on molecular rotary motors, one could foresee that the ability to reverse the direction of rotation would be a great option for this class of compound. Base-catalyzed epimerization of the stereogenic center ruling the direction of the rotation was proposed by Feringa as an answer to this challenge (**Figure 51**).[143] After photoisomerization of a starting motor of configuration (*3'S*)-(*M*)-**1**, the unstable compound of opposite helicity (*3'S*)-(*P*)-**1**, which should undergo a classic thermal inversion, can be epimerized in presence of a base to yield predominantly the stable compound of configuration (*3'R*)-(*P*)-**1**. The helicity of this stable isomer is opposite to the one of the starting

[138] Koumura, N., Geertsema, E. M., Meetsma, A. & Feringa, B. L. Light-driven molecular rotor : unidirectional rotation controlled by a single stereogenic center. *J. Am. Chem. Soc.* **122**, 12005-12006 (2000).
[139] Vicario, J. *et al.* Controlling the speed of rotation in molecular motors. Dramatic acceleration of the rotary motion by structural modification. *Chem. Commun.* **116**, 5910-5912 (2005).
[140] Ephritikhine, M. *et al.* A new look at the McMurry reaction. *Chem. Commun.* **405**, 2549-2554 (1998).
[141] Barton, D. H. R. & Willis, B. J. Olefin synthesis by twofold extrusion processes. *J. Chem. Soc. D Chem. Commun.* **19**, 1225-1226 (1970).
[142] Kellogg, R. M. The molecules R_2CXCR_2 including azomethine, carbonyl and thiocarbonyl ylides. Their syntheses, properties and reactions. *Tetrahedron* **32**, 2165-2184 (1976).
[143] Ruangsupapichat, N., Pollard, M. M., Harutyunyan, S. R. & Feringa, B. L. Reversing the direction in a light-driven rotary molecular motor. *Nat. Chem.* **3**, 53-60 (2011).

motor, which means that it will rotate in the opposite direction under light irradiation. However, to date, this concept has not been applied to any other motor-based chemical systems or devices, probably as the necessity of a base in solution is a potential drawback.

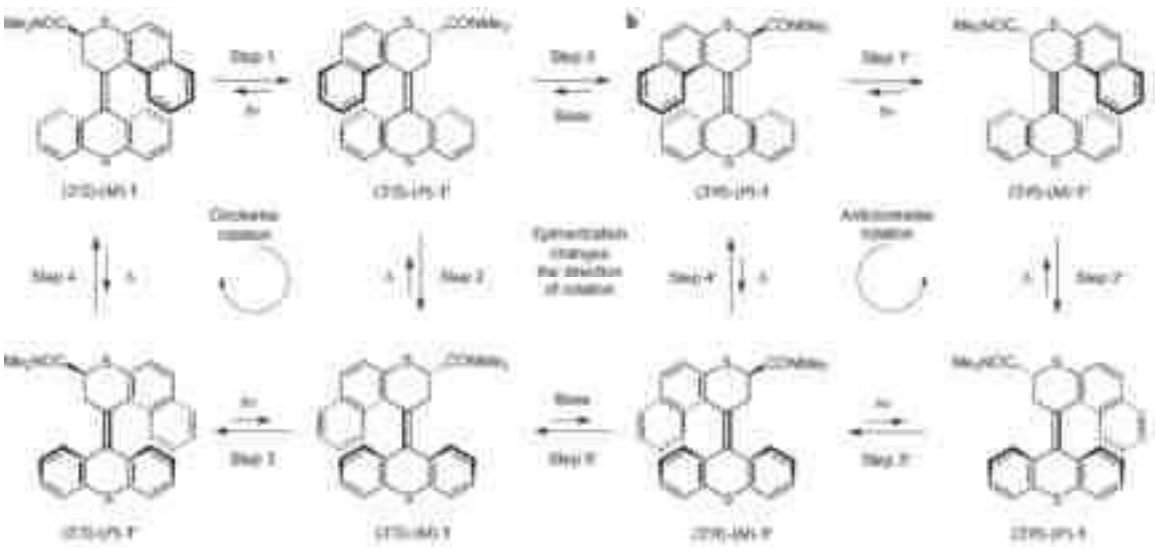

Figure 51 | Inversion of the direction of rotation by a base-catalyzed epimerization.[143]

Recently, Feringa and his group reported the birth of a third generation of molecular motor, which originality lies in its achiral nature (**Figure 52**).[144] In this meso compound, two fluorene derivatives rotate in the same direction, thanks to the presence of a pseudo-asymmetric center, which is enough to discriminate both directions of rotation.

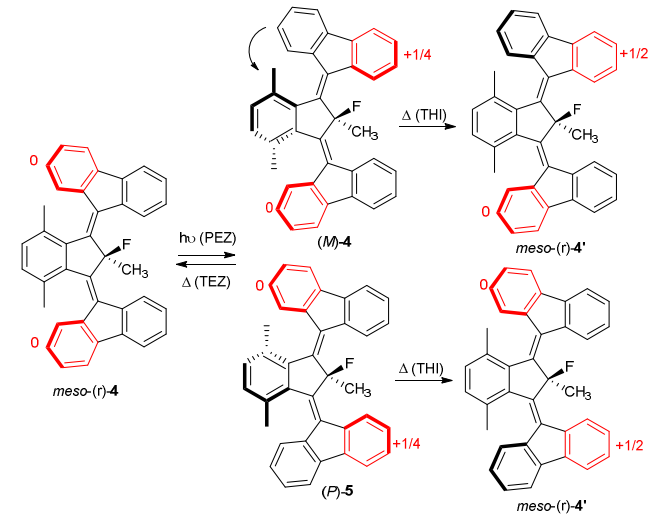

Figure 52 | Third generation of light-driven molecular motor, which operates an unidirectional rotation of both fluorene units in an achiral structure.[144]

[144] Kistemaker, J. C. M., Štacko, P., Visser, J. & Feringa, B. L. Unidirectional rotary motion in achiral molecular motors. *Nat. Chem.* **7**, 890-896 (2015).

Otherwise, this motor works similarly to the other generations of motors, proceeding with an isomerization of the double bond followed by a thermal helix inversion.

Over the last few years, other groups developed light-stimulated molecular motors inspired by Feringa's work. Among them, two noticeable examples were recently reported by the groups of Lehn and Dube (**Figure 53**).

Lehn and his collaborators described the unidirectional rotation of an imine base light-driven molecular motor (**Figure 53a,b**).[145] These motors can be obtained in one step from commercially available starting material, by titanium(III)tetrachloride catalyzed condensation of an amine and a ketone. They proved to work in a similar way as Feringa's molecular motor, undergoing a cis-trans isomerization of the imine followed by a thermal helix inversion, resulting in a unidirectional rotation (**Figure 53a**). However, by using a larger stator (*i.e.* the lower part), the energy barrier of the thermal step rises too high and induces another mechanism. It was demonstrated that in these bulky structures, the 180° rotations induced by the photoisomerization step are followed by an in-plane inversion of the nitrogen, yielding the starting material (**Figure 53b**). This kind of motors operate a two-steps unidirectional 180° rotation. An interesting feature of this class of motor is their constitutional dynamic, as ketone or amine exchange *in situ* could be used to access a dynamic library of molecular motors.

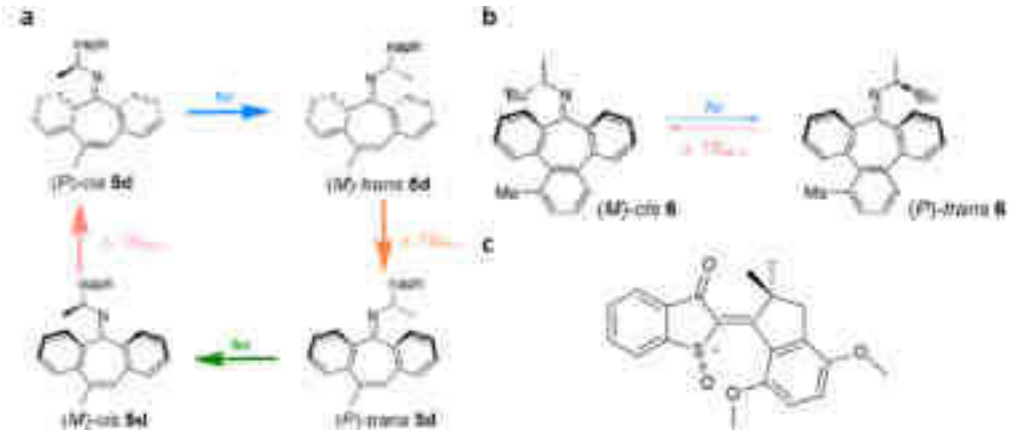

Figure 53 | New classes of light-driven molecular motors developed by a-b) Lehn[145] and c) Dube.[146]

Dube and his group developed hemithioindigo-based molecular motors, synthesized in six steps (**Figure 53c**)[146]; hemithioindigo are switches that can undergo a cis-trans isomerization

[145] Greb, L. & Lehn, J. M. Light-driven molecular motors: Imines as four-step or two-step unidirectional rotors. *J. Am. Chem. Soc.* **136**, 13114-13117 (2014).
[146] Guentner, M. *et al.* Sunlight-powered kHz rotation of a hemithioindigo-based molecular motor. *Nat. Commun.* **6**, 8406-8414 (2015).

of the central double bond upon irradiation around 400-500 nm. Addition of steric hindrance around the double bond and introduction of a chiral center by oxidation of the sulfur provided a unidirectional light-driven molecular motor, which, compared to the others, does not require intense UV light to operate. This opens the possibility to use these motors for *in vivo* application, something for which UV irradiation is far from ideal.

II. Molecular motors: applications

Light-driven molecular motors developed by the group of Feringa have been exploited to control various chemical systems, ranging from catalysis[147] to self-assembly.[148] However, in this section we will focus only on the few examples featuring control of the mechanical work created by the rotation of the motors.

Nanocars has been synthesized using four molecular motors as wheels, decorating a rigid aromatic core (**Figure 54**).[149] Electric stimulation of the molecule by an STM tip induces the excitation of electronic and vibrational states of the motors, thus activating their rotation (**Figure 54a**). The collective motions of the four motors propel the vehicle forward. As the stereochemical configuration of the motor controls the direction of its rotation, working using appropriate stereoisomers is important to predict the trajectory of the nanocar (**Figure 54b**). Indeed, the meso-isomer of the same chirality on each sides showed an almost straight motion of the molecular car. However, a meso isomer with opposite chirality on the front and the rear of the vehicle could not move. Using a purely *(S)* or *(R)* stereoisomer provided a nanocar only able to continuously rotate on itself.

[147] Wang, J. *et al.* Dynamic control of chiral space in a catalytic asymmetric reaction using a molecular motor. *Science* **331**, 1429-1432 (2011).
[148] van Dijken, D. J., Chen, J., Stuart, M. C. A., Hou, L. & Feringa, B. L. Amphiphilic molecular motors for responsive aggregation in water. *J. Am. Chem. Soc.* **138,** 660-669 (2016).
[149] Kudernac, T. *et al.* Electrically driven directional motion of a four-wheeled molecule on a metal surface. *Nature* **479**, 208-211 (2011).

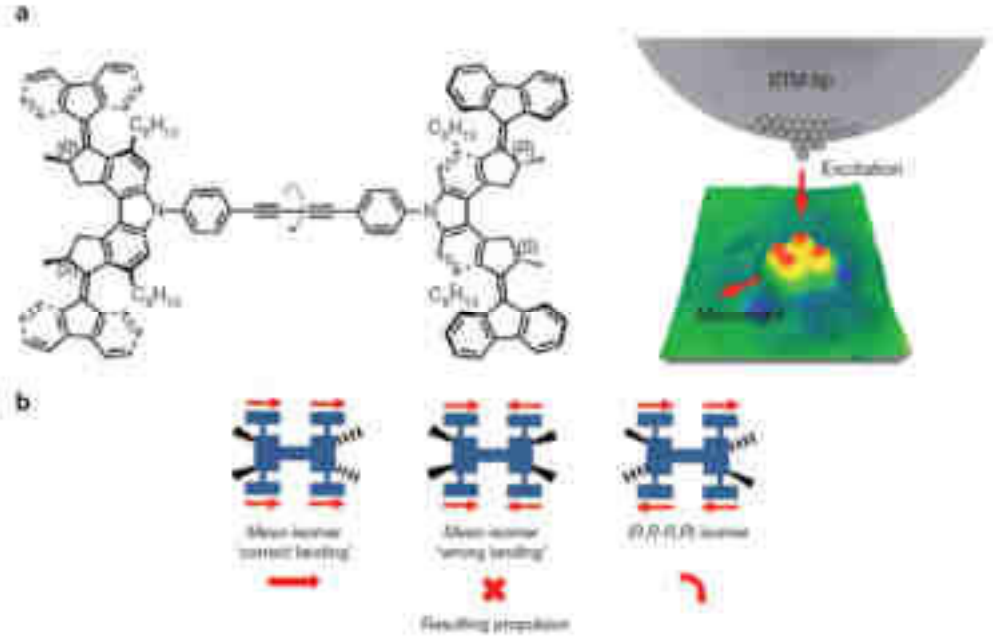

Figure 54 | a) Nanocar driven by the combined motions of four molecular motors, stimulated by the ejection of electrons by a STM tip, b) Influence of the configuration of the motors on the trajectory of the vehicle.[149]

The rotation of molecular motors has also been amplified to the microscopic scale, inducing motion of an object 10 000 times the size of one motor (**Figure 55**).[150] In this case, light-driven molecular motors were used as doping agents of a liquid crystalline film. Upon irradiation at 365 nm, the polygonal structure slowly rotates clockwise (during the photoisomerization step) and then anticlockwise (during the thermal step) when irradiation stops. The direction of the reorganization from the liquid crystalline texture could be tuned by choosing the appropriate enantiomer. The microscopic response triggered by the motions of the motors could be transferred to a microscopic glass rod dropped on the top of the film, which rotates in the same direction as the liquid crystalline texture. However, it should be noted that this motion is the result of an indirect influence of the motors, *i.e.* the rotation of the motors themselves does not induce the rotation of the glass rod. This example is therefore a case of indirect amplification of collective motions of molecular machines, analogous to what has been previously reported by Prof. Leigh.[113]

[150] Eelkema, R. *et al.* Molecular machines: nanomotor rotates microscale objects. *Nature* **440,** 163 (2006)

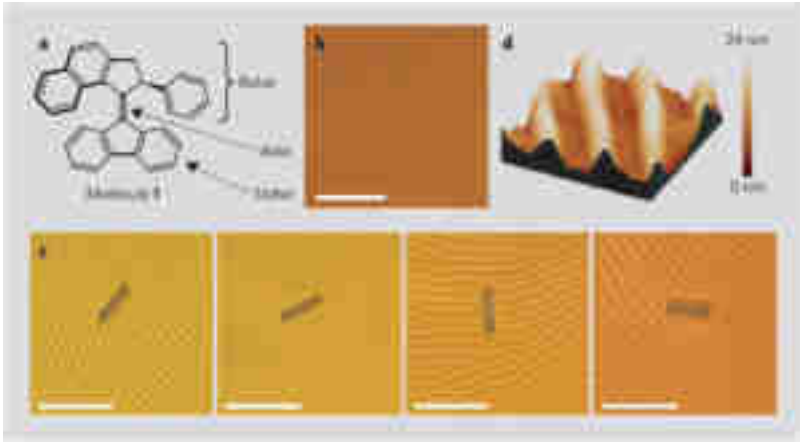

Figure 55 | Rotation of a microscopic glass rod induced by the rotation of molecular motors in a liquid crystal phase (scale bar: 50 µm). a) Molecular motor used to dope a b) Liquid crystalline phase. c) Rotation of a micrometric glass rod induced by reorganization of the liquid crystalline phase upon irradiation. d) Height profile of the liquid crystalline surface.[150]

The first direct macroscopic amplification of rotatory molecular motors was described by our group in 2015 (**Figure 56**).[7] An asymmetric molecular motor was functionalized with poly-ethylene glycol polymer chains bearing alkyne moieties on the top part and azide units on the bottom part (**Figure 56a**). A chemical gel was synthesized when this compound was engaged in a copper catalyzed 1,3-dipolar cycloaddition at high concentration. Upon light irradiation with UV (λ = 365 nm), a clear contraction of the gel was observed, reducing its size down to 20% of its original volume.

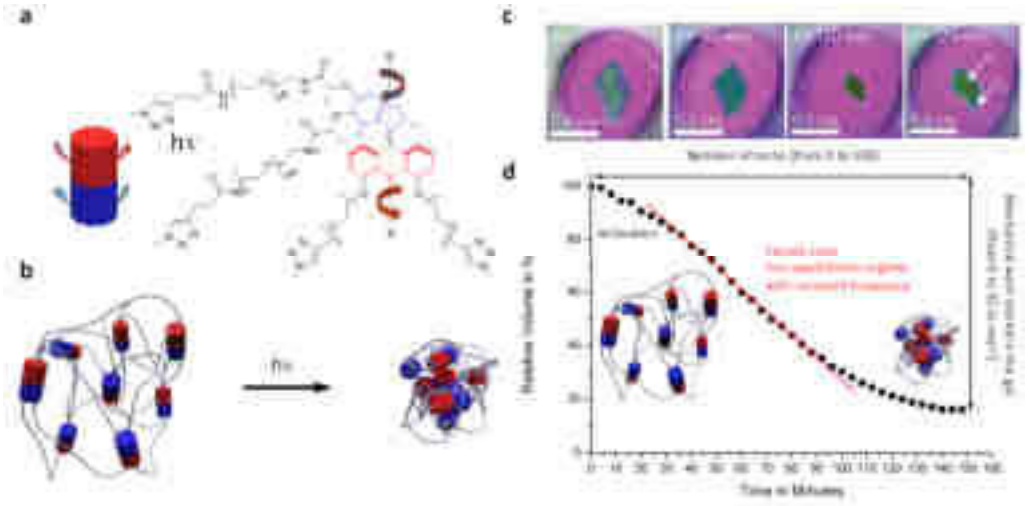

Figure 56 | a) Unidirectional rotational light-driven molecular motor/polymer conjugate, b) Representation of the motor/polymer gel and its contraction upon light irradiation, c) Snapshots of a movie of a contracting gel, d) Contraction kinetics of the gel.[7]

By pushing too much the system in presence of oxygen, the contraction can be so efficient that it leads to the breakage to the gel due to oxidation of the central double bond, whose

reactivity was enhanced by the tension applied by the entangled polymer chains (**Figure 56b-d**). This work represents the first example of artificial molecular machines directly producing a macroscopic mechanical work out of equilibrium.

General comment on the literature

From the first interlocked molecules to the amplification of the collective motions of nanomachines up to the macroscopic scale, at and out of equilibrium, molecular machines have gone a long way. Lessons learned from Nature and supramolecular chemistry provided powerful tools to design and synthesize molecular machines of growing complexity regarding their structure and functions, and this area of research is still very active. However, the careful organization of these molecules into materials that amplify their motions is still in its early development, and considerable efforts are required to synthesize stable, reversible and functional devices relying on molecular machines. The work developed in the following chapter of this manuscript is producing knowledge in these directions.

Results

Chapter IV: Poly[c2]daisy chains based on the 2,6-diacetylaminopyridine and N-hexyluracil recognition motifs

This work was carried out in collaboration with Dr. Guangyan Du for the chemistry part and Prof. Eric Buhler for the scattering experiments.

I. Objectives and retrosynthesis

The previously described system based on bis-terpyridine Fe(II) complexes[6] was characterized by a very high association constant and a low kinetic lability. In order to study how these parameters impact the structure of the poly[c2]daisy chains and the contraction/extension phenomena, we designed a DAD-ADA (D: Donor, A: Acceptor) hydrogen bonding supramolecular polymer made of N-hexyluracil functionalized [c2]daisy chain (the ADA part) and a complementary 2,6-diacetylaminopyridine functionalized [c2]daisy chain (the DAD part) (**Scheme 3**). The association of a 2,6-diacetylaminopyridine and N-hexyluracil units displays opposite characteristic to the metallic complex previously used: a low association constant but a high kinetic lability.[61] Formation of the contractile single chains hydrogen bonding supramolecular polymer should arise from the association of the two complementary [c2]daisy chains, allowing the comparison with the terpydidine-based system.

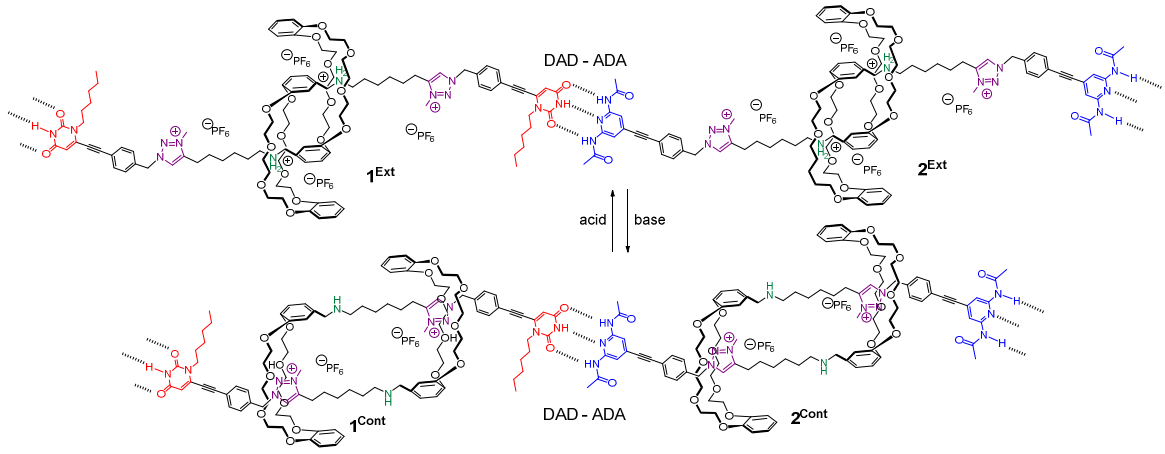

Scheme 3 | A telescopic hydrogen bonding supramolecular polymer using complementary [c2]daisy chains as monomers.

The synthesis of rotaxanes **1**^{Ext} and **2**^{Ext} was designed based on the retrosynthetic analysis described on **Figure 57**. Both ADA and DAD rotaxanes can be obtained from pseudo-rotaxane

12, which synthesis has been reported by Coutrot and his collaborators,[125] and azido precursors **21** (ADA) or **30** (DAD). For the ADA part $\mathbf{1^{Ext}}$, Boc-protected uracil **21** derivative was envisioned to avoid possible solubility issues and facilitate the purification of the [c2]daisy chains as the free uracil group is able to form weak dimers.[64] This compound will arise from a Sonogashira reaction between Boc-protected-1-hexyl-6-iodouracil **18** and 4-ethynylbenzyl acetate **15** which can be both obtained in 3 steps from commercially avalaible uracil and 4-bromobenzyl alcohol, respectively.

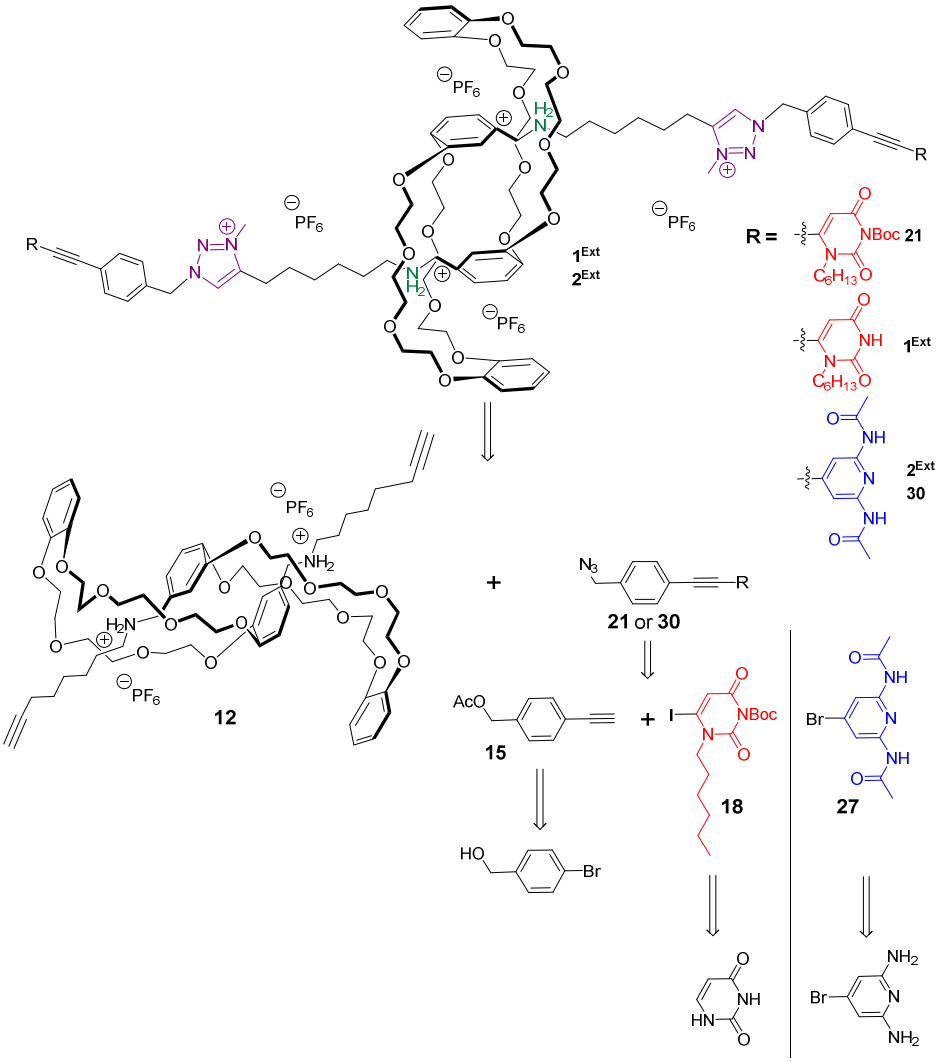

Figure 57 | Retrosynthetic analysis for the bis-N-hexyluracil and 2,6-diacetylaminopyridine functionalized [c2]daisy chains.

The complementary DAD unit $\mathbf{2^{Ext}}$ could be synthesized according to a similar pathway (**Figure 57**), *i.e.* by coupling 4-ethynylbenzyl acetate **15** with 4-bromo-2,6-diacetylaminopyridine **27**, which can be obtained in one step from the commercially available 4-bromo-2,6-diaminopyridine.

After studying the single chain polymer expected from a 1:1 mixture of $\mathbf{1}^{Ext}$ and $\mathbf{2}^{Ext}$, the next step would be to increase the degree of organization in order to form fibrous supramolecular assembly that would be good candidates for the amplification of molecular motions across several length scales.[5] The inclusion of a component able to introduce lateral interactions in the system was envisioned as an answer to this challenge. Such a system could be accessed by the synthesis of a supramolecular co-polymer, associating the previously mentioned 2,6-diacetylaminopyridine substituted [c2]daisy chains $\mathbf{2}^{Ext}$ and a rigid bis-uracil linker **3** (**Scheme 4**). The rotaxane unit would act as the functional unit of the assembly, being able to contract or extend upon pH stimulation, while the bis-uracil linker should behave as a structuring component. Indeed, according to several systems described in the literature,[36,64] the presence of long pending alkyl chains on aromatic moieties is expected to increase lateral interactions *via* π-stacking and Van-der-Waals interactions. Additionally, the mismatch between the polar character of the charged rotaxane and the relatively apolar linker (aromatic core and long branched alkyl chains) should induce a micro-phase separation,[151] leading to the hierarchical organization of the polymer chains into larger structures.

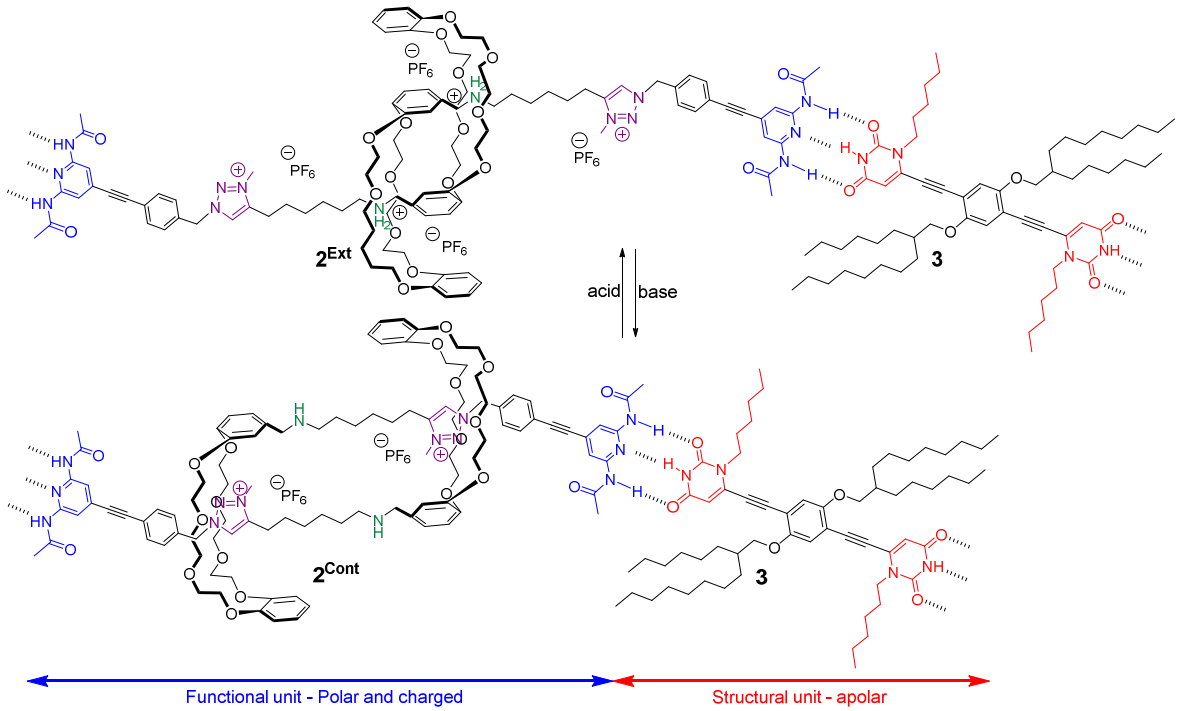

Scheme 4 | A supramolecular co-polymer based on the 2,6-diacetylaminopyridine substituted [c2]daisy chain and a complementary bis-N-hexyluracil linker.

[151] Chen, S. & Binder, W. H. Dynamic ordering and phase segregation in hydrogen-bonded polymers. *Acc. Chem. Res.* **49**, 1409-1420 (2016).

Compared to the bis-[c2]daisy chains system described above, this combination of non-covalent interactions should lead to the formation of fibers and/or highly organized supramolecular architectures. The bis-N-hexyl-uracil linker can be synthesized by coupling 1-hexyl-6-iodouracil **17** with bis-alkyne **26** which can be obtained in a few steps from 2,5-dibromohydroquinone (**Figure 58**).

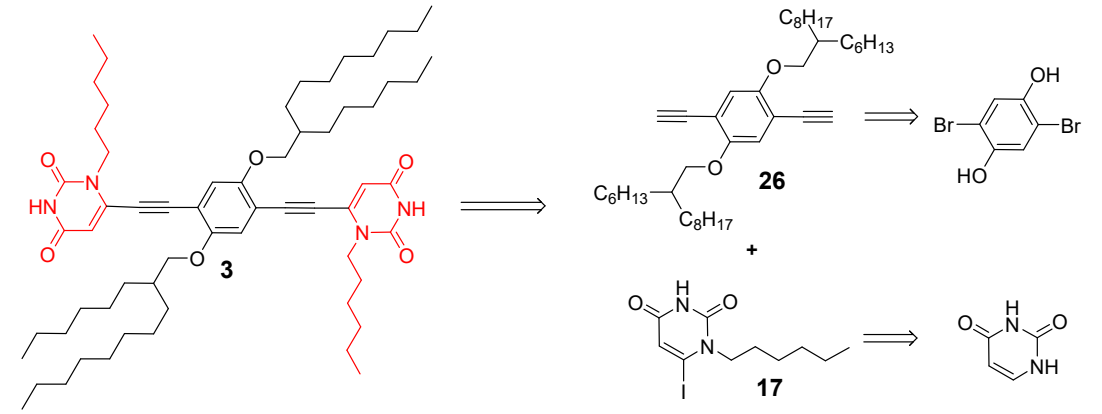

Figure 58 | Retrosynthetic scheme for the bis-N-hexyluracil linker

II. Results

A. Synthesis of pseudo-rotaxane 12

8-aminooct-1-yne **7** was obtained in four steps from commercially available oct-7-yne-1-ol (**Scheme 5**). First, acetylenic "zipper" isomerization reaction[152] was used to convert oct-7-yne-1-ol into the terminal alkyne **4**. This alcohol was converted into its bromo equivalent under Appel's conditions[153] yielding compound **5** as a colorless oil with a 91% yield. Amine **7** was obtained after substitution of the bromide using potassium phtalamide and deprotection with hydrazine monohydrate in good yields.

[152] Brown, C. A. & Yamashita, A. Saline hydrides and superbases in organic reactions. IX. Acetylene zipper. Exceptionally facile contrathermodynamic multipositional isomeriazation of alkynes with potassium 3-aminopropylamide. *J. Am. Chem. Soc.* **97**, 891-892 (1975).
[153] Appel, R. Tertiary phosphane/tetrachloromethane, a versatile reagent for chlorination, dehydration, and P-N linkage. *Angew. Chem. Int. Ed. Engl.* **14**, 801-811 (1975).

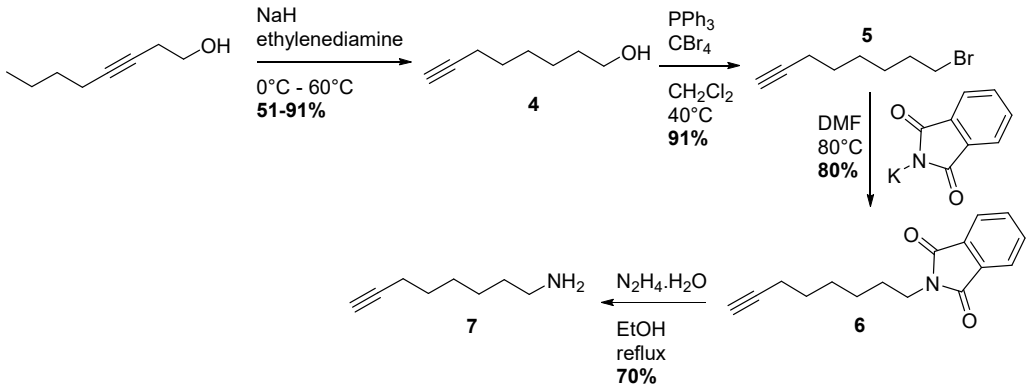

Scheme 5 | Synthesis of 8-aminooct-1-yne **7**.

The synthesis of the aldehyde-functionalized DB24C8 macrocycle was prepared according to the procedure reported by Stoddart and his collaborators[124] (**Scheme 6**). 3,4-dihydroxybenzaldehyde was reacted with commercially available 2-[2-(2-chloroethoxy)ethoxy]ethanol in basic conditions for three days to yield almost quantitatively diol **8**, which was further tosylated with a 70% yield. This bis tosylate **9** was then engaged in a macrocyclization reaction with catechol under high-dilution conditions, and cesium (II) cations as template to favor the formation of the macrocycle over unwanted oligomers/polymers. Macrocycle **10** was obtained at the gram scale, with a 52% yield after seven days of reaction at 100°C in dimethylformamide.

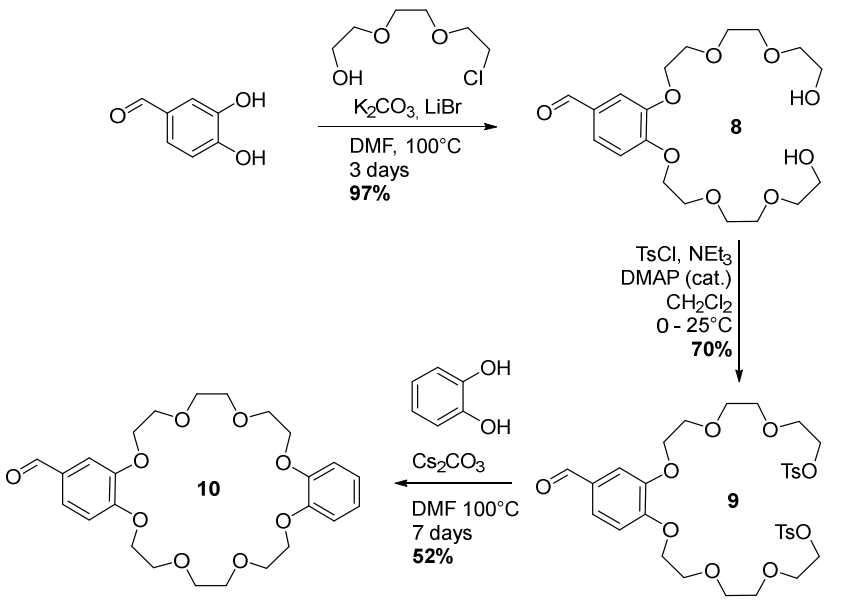

Scheme 6 | Synthesis of aldehyde-functionalized DB24C8 macrocyle **10**.

Aldehyde **10** and amine **7** were then engaged together in a reductive amination, yielding compound **11** with a 76% yield (**Scheme 7**). This amine-functionalized macrocycle can be efficiently protonated with a 2M solution of hydrochloric acid in ether and then washed with a saturated aqueous solution of ammonium hexafluorophosphate to yield the pseudo-rotaxane **12**, which will be an essential building block for several projects described in this manuscript.

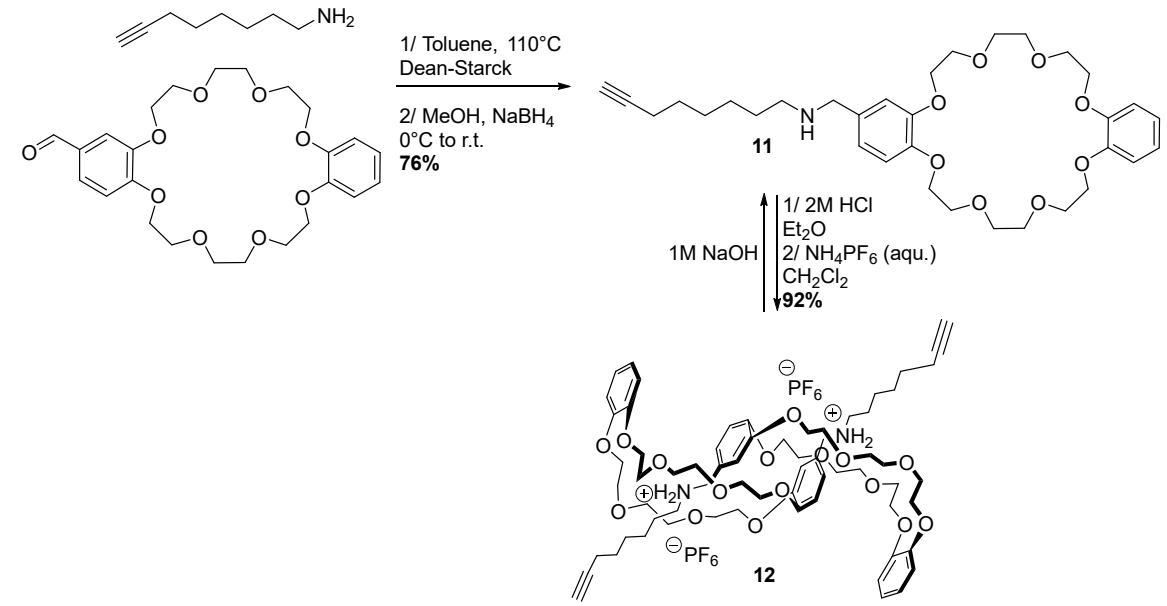

Scheme 7 | Synthesis of pseudo-rotaxane **12**.

B. Synthesis of bis-N-hexyluracil [c2]daisy chains 1^{Ext}

On the one hand, 4-ethynylbenzyl acetate **15** was prepared in three steps from commercially available 4-bromobenzyl alcohol (**Scheme 8**).[6] This molecule was first acylated in classic conditions to yield 4-bromobenzyl acetate **13** with an excellent yield. This compound was then engaged in a Sonogashira palladium-catalyzed cross-coupling reaction with trimethylsilylacetylene to give protected alkyne **14** with 80% yield. Free-alkyne **15** was obtained with an 85% yield by treating the protected compound with 1M tetrabutylammonium fluoride in THF.

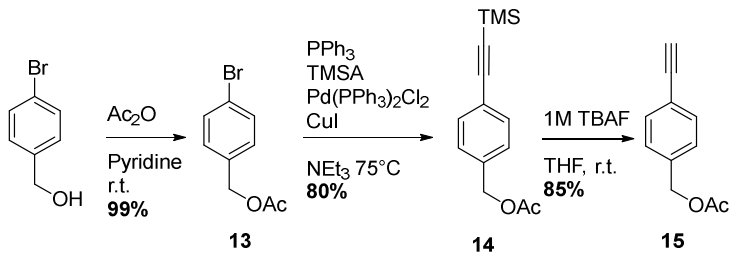

Scheme 8 | Synthesis of 4-ethynylbenzyl acetate **15**.

On the other hand, Boc-protected N-hexyl-6-iodouracil **18** was prepared following procedures described in the literature.[64,65] Commercially available uracil was alkylated under basic conditions using bromohexane in DMSO at 50°C with a moderate yield. Further treatment with freshly prepared LDA at -78°C followed by addition of iodine yielded N-hexyl-6-iodouracil **17** in 76% yield. This compound was protected with a Boc group to obtain **18**, which was engaged in a copper-free Sonogashira coupling reaction with 4-ethynylbenzyl acetate **15** to yield the acetate functionalized derivative **19** with 80% yield (**Scheme 9**). Copper was removed from the reactive medium as it seemed to greatly increase the formation of homo-coupling side-products, even in thoroughly degassed solvents.

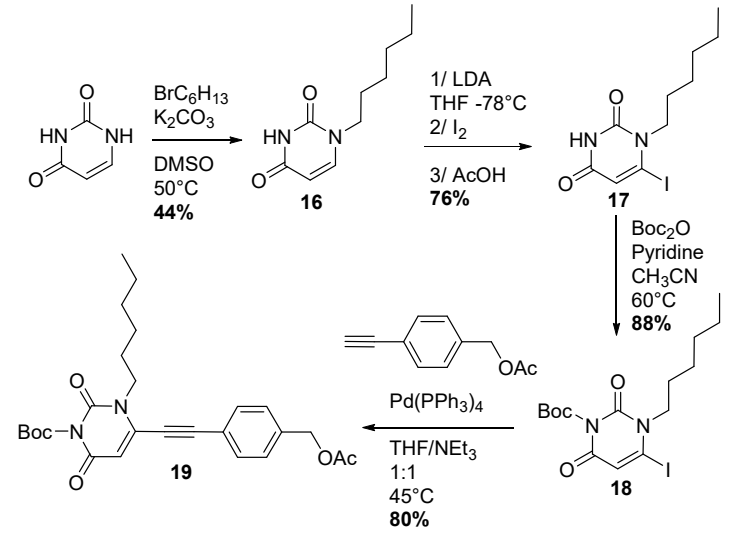

Scheme 9 | Synthesis of acetate derivative **19**.

Saponification of the acetate group proved more difficult than expected (**Figure 59**). The use of sodium hydroxide as a base or dichloromethane as a solvent yielded only decomposition compounds as determined by TLC and UPLC-MS. Using a mixture of tetrahydrofuran and methanol with two equivalents of potassium carbonate provided the alcohol **20** over an hour of

reaction, in a near quantitative yield and without any other purification required than a simple extraction.

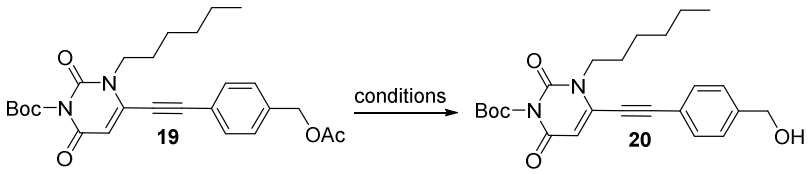

	T (°C)	Base	Solvent	Outcome
Conditions 1	25	K_2CO_3 (10 equiv.)	CH_2Cl_2/MeOH 9/1	Decomposition
Conditions 2	25	NaOH (2 equiv.)	CH_2Cl_2/MeOH 9/1	Decomposition
Conditions 3	25	K_2CO_3 (2 equiv.)	THF/MeOH 2.5/1	Product (95% yield)

Figure 59 | Conditions for the conversion of **19** into corresponding alcohol **20**.

Formation of azide **21** proceeded only with low yield when using the conditions developed for the terpyridine equivalent.[6] Satisfyingly, switching the solvent from dichloromethane to tetrahydrofuran allowed us to reach compound **21** with a good yield (**Scheme 10**).

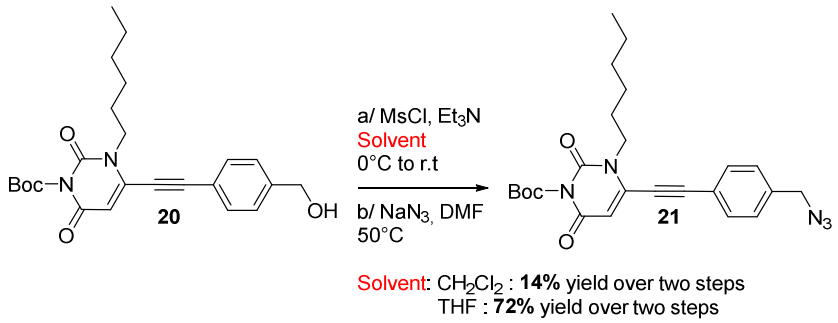

Scheme 10 | Conversion of primary alcohol **20** into the corresponding azide **21**.

Azide **21** was then engaged in a Huisgen 1,3-dipolar cycloaddition reaction with pseudo-rotaxane **12** (**Scheme 11**). The previously reported conditions for this reaction using 2,6-lutidine resulted only in the formation of traces of the expected rotaxane. The use of TMEDA as a base unfortunately led to the formation of a complex mixture composed of unreacted starting materials, protected, deprotected and partially-deprotected compound **22**, as the Boc protecting group appeared to be unstable under these conditions. However, after removal of the Boc group on the crude mixture using a 1:1 mixture of CH_2Cl_2/TFA, pure compound **22** was obtained after column chromatography using basic aluminum oxide in 37% yield.

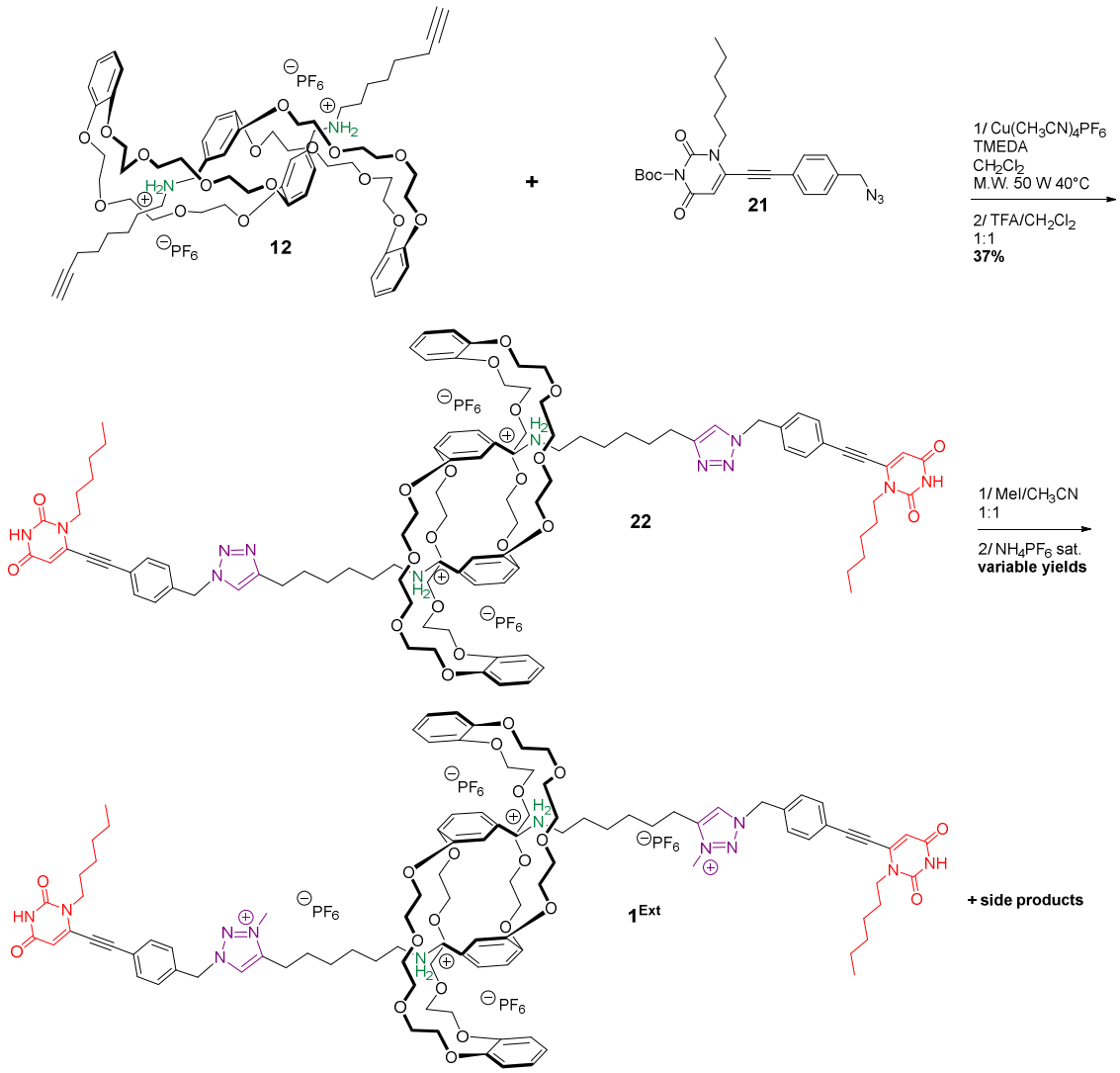

Scheme 11 | Synthesis of bis-uracil functionalized [c2]daisy chains $\mathbf{1^{Ext}}$.

The triazole groups still needed to be methylated in order to act as effective second stations in the deprotonated state of the [c2]daisy chains. The methylation was achieved once by stirring compound **22** in a large excess of methyl iodide and acetonitrile at room temperature over five days, yielding the final compound $\mathbf{1^{Ext}}$ quantitatively, which could be characterized by ^{1}H NMR in deuterated acetonitrile (**Figure 60**). Unfortunately, subsequent attempts led to partial methylation of the uracil unit, and reducing the amount of methyl iodide to two equivalents completely prevented the methylation of the triazole moieties.

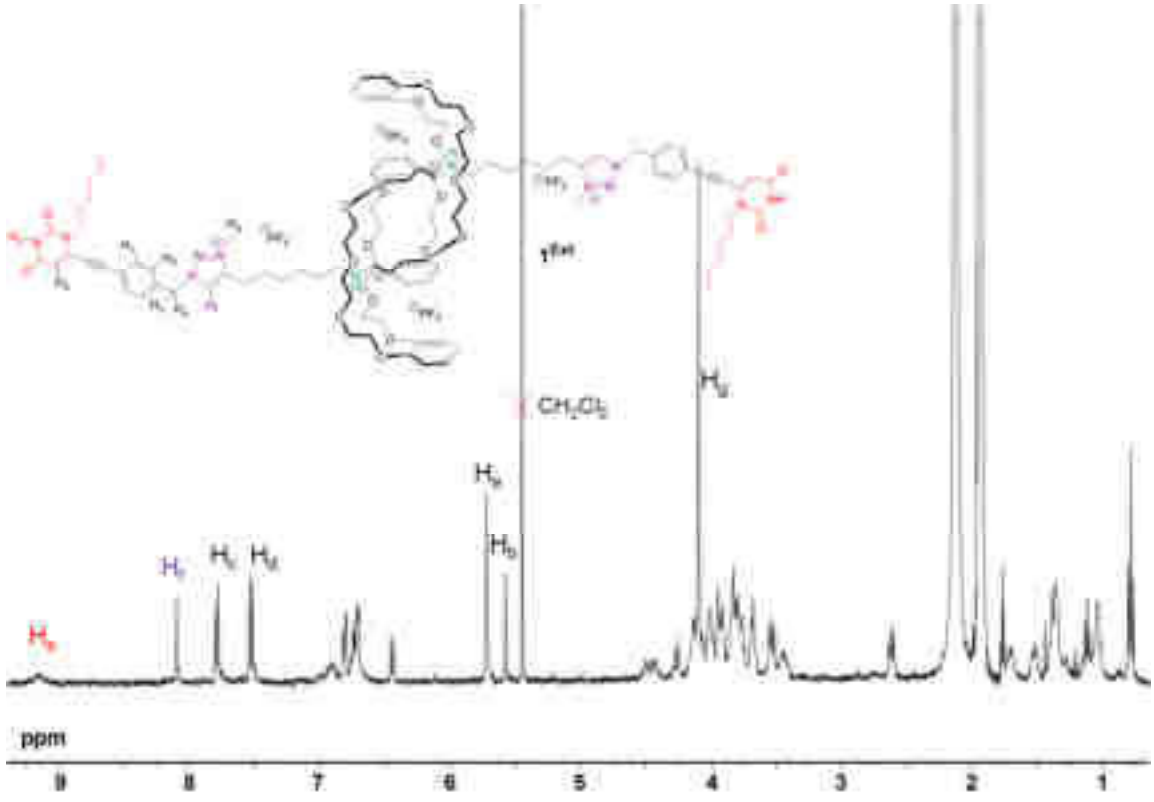

Figure 60 | ^{1}H NMR in CD_3CN of compound $\mathbf{1^{Ext}}$.

After several months of work and considering the length of the synthesis, the poor yields and the lack of reproducibility of the final steps, we decided to focus our efforts on the formation of a stimuli-responsive supramolecular fibrous system, as explained in the introduction of this chapter.

C. Synthesis of bis-uracil linker 3

2-hexyl-1-decanol was converted into its bromide equivalent **23** via an Appel reaction (**Scheme 12**). The purification of this intermediate proved difficult and a sufficiently pure compound was thus engaged right away into the following step. SN_2 reaction between 2,5-dibromohydroxyquinone and this bromide derivative **23** under basic conditions yielded compound **24** with 66% yield over two steps. A succession of Sonogashira coupling using trimethylsilylacetylene and deprotection under mild basic conditions provided bis-alkyne compound **26** in good yields. Compound **26** was finally coupled with the previously prepared 1-hexyl-6-iodouracil **17** using copper-free Sonogashira conditions to obtain the bis-uracil linker **3** with a decent yield, which was characterized by ^{1}H/^{13}C NMR and high resolution mass spectrometry.

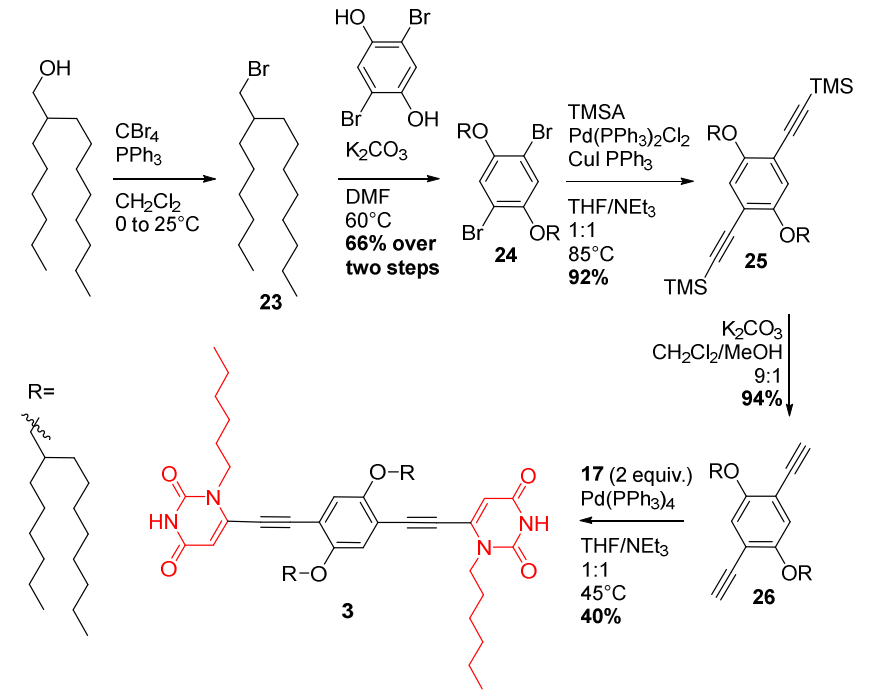

Scheme 12 | Synthesis of bis-uracil linker **3**.

D. Synthesis of bis-2,6-diacetylaminopyridine [c2]daisy chains

Based on the retrosynthesis analysis described in **Figure 57**, our next synthetic challenge was the formation of azide **30** to reach bis-2,6-diacetyaminopyridine [c2]daisy chain $\mathbf{2^{Ext}}$ (**Scheme 13**). Commercially available 4-bromo-1,6-diaminopyridine was acylated in classic conditions using acetyl chloride and triethylamine to give bis-amide compound **27** in a nearly quantitative yield. It was then coupled to 4-ethynylbenzyl acetate **15** in copper-free Sonogashira conditions to yield acetate-protected derivative **28** with an 81% yield. A sequence of deprotection under basic conditions, activation using mesityl chloride and nucleophilic substitution by sodium azide yielded azide **30** in excellent yield (86% after 3 steps) and even at the gram scale.

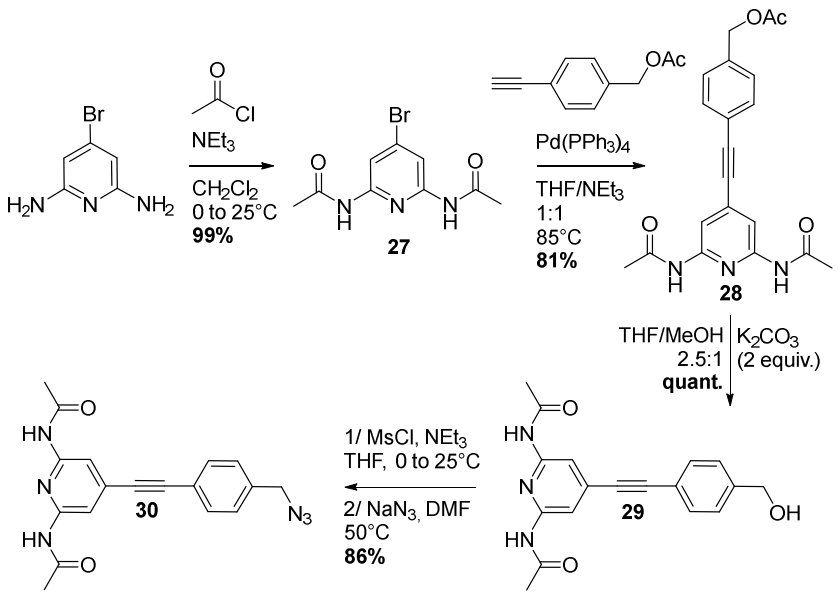

Scheme 13 | Synthesis of azide functionalized compound **30**.

This molecule was successfully coupled to pseudo-rotaxane **12** with a 69% yield (**Scheme 14**). The reaction was carried out in a microwave reactor irradiating at 50 W, which drastically reduced the reaction time, from several days to few hours. Subsequent methylation of the triazole unit using a large excess of methyl iodide in acetonitrile led to final compound $\mathbf{2}^{\mathbf{Ext}}$ in a quantitative yield without the formation of side-products even after four days of reaction. The [c2]daisy chain $\mathbf{2}^{\mathbf{Ext}}$ was characterized by $^{1}H/^{13}C$ NMR and high resolution mass spectrometry.

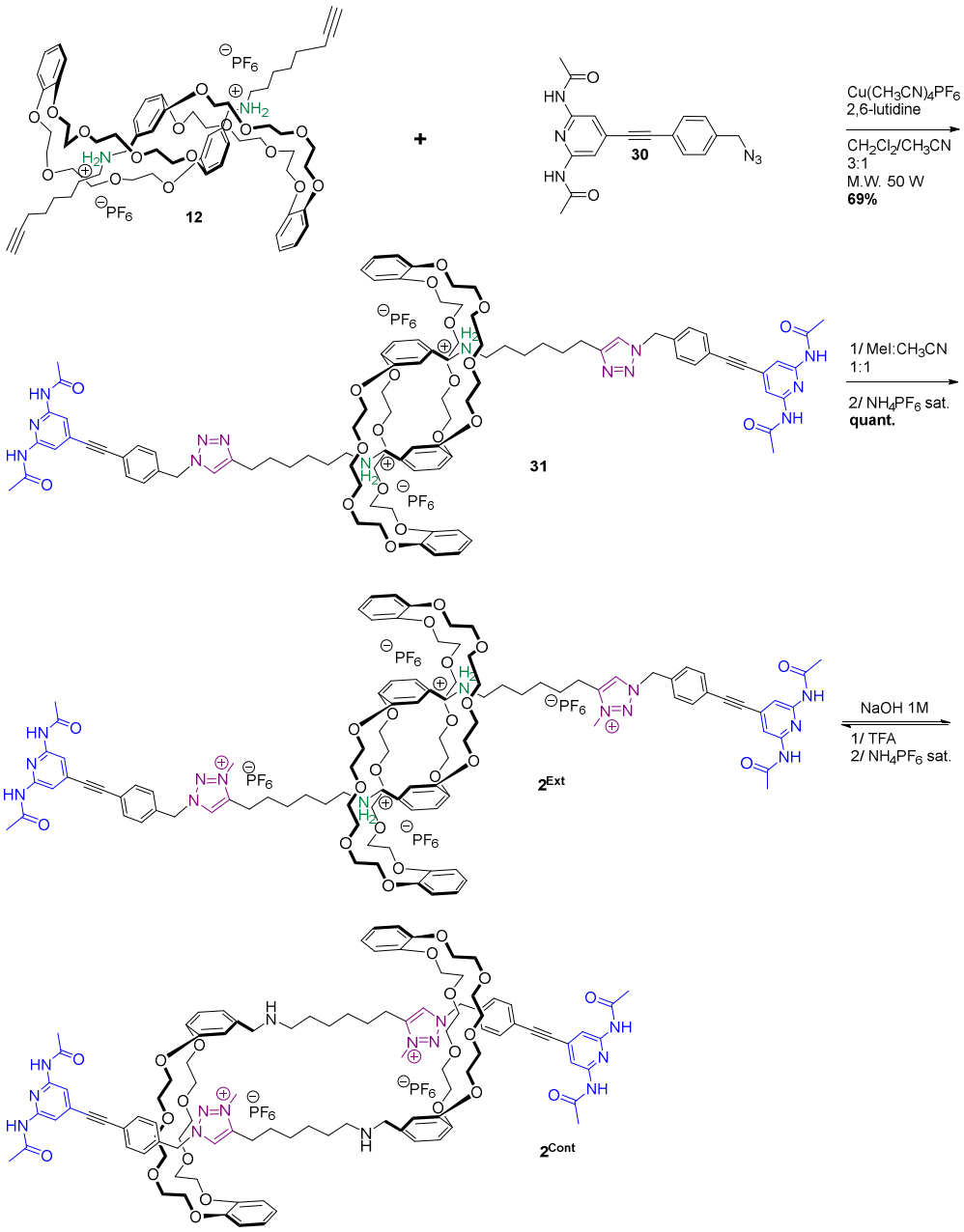

Scheme 14 | Synthesis of the bis-2,6-diacetylaminopyridine [c2]daisy chains $\mathbf{2^{Ext}}$ and its contraction into $\mathbf{2^{Cont}}$.

E. Characterization of the contraction/extension event of compound 2^{Ext}

The extended [c2]daisy chains $\mathbf{2^{Ext}}$ could be switched to its contracted state using a base (**Scheme 14**, **Figure 61**). Briefly shaking a solution of $\mathbf{2^{Ext}}$ in a 3:1 mixture of $CHCl_3/CH_3CN$ with a 1M NaOH aqueous solution yielded the contracted compound $\mathbf{2^{Cont}}$. This contraction event could be easily monitored by ^1H NMR. In the extended/protonated state $\mathbf{2^{Ext}}$, the electron-rich crown ether strongly binds the ammonium. In this state, the proton H_f from the triazolium group displays a characteristic resonance signal at δ = 7.81 ppm. Upon deprotonation of the

ammonium, the crown ether ring has a higher affinity for the electron-poor triazolium, and thus glides around it. This motion results in a reduction of the size of the molecule of around 1.2 - 1.6 nm, according to theoretical studies,[6,154] yielding the contracted state **2**$^{\mathbf{Cont}}$. This event is confirmed by i) the downfield shift of the triazolium signal H_f, moving from δ = 7.81 ppm to δ = 8.92 ppm as it becomes bound by the macrocycle, and ii) the broadening and downfield shifts of benzylic protons H_e and aromatic protons H_d located close to the triazolium unit.

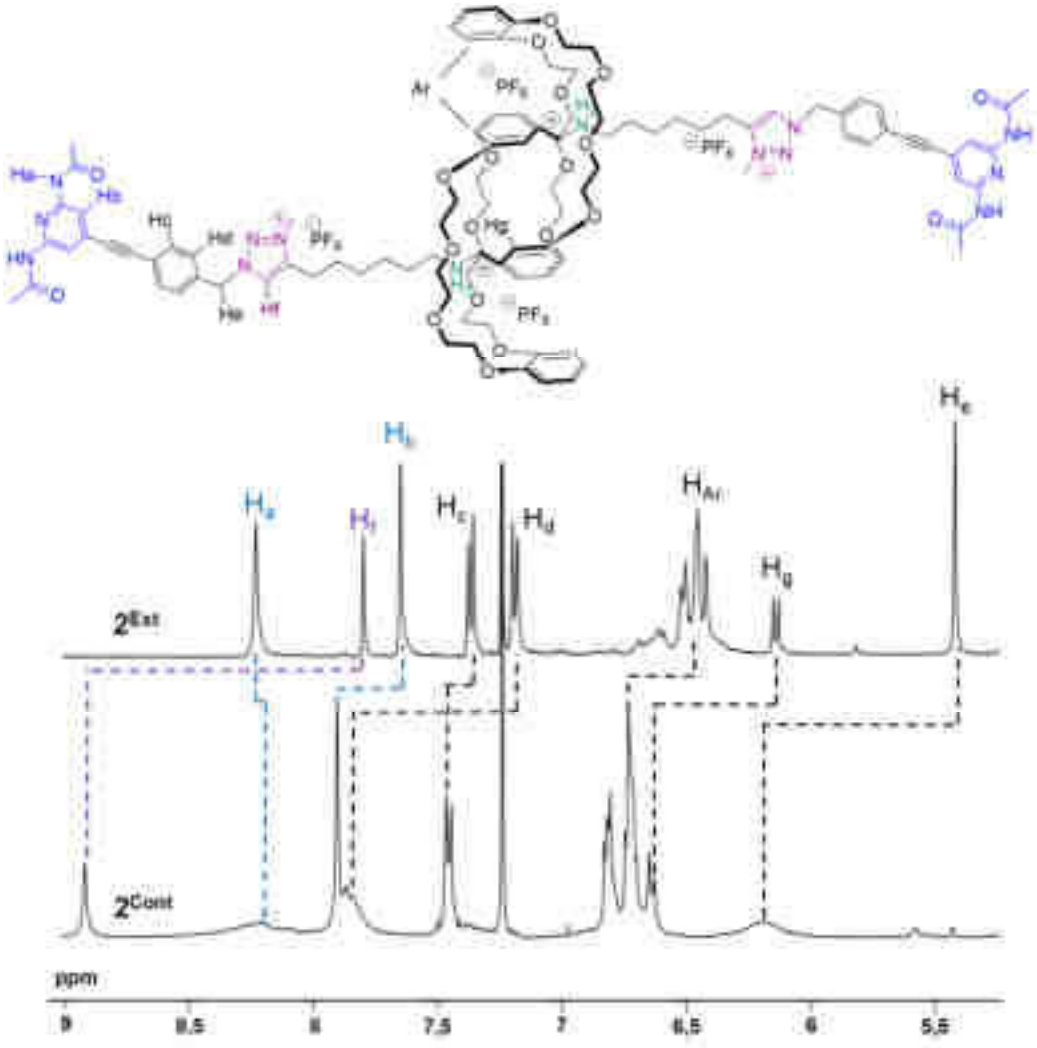

Figure 61 | ^{1}H NMR in a 4:1 mixture of $CDCl_3/CD_3CN$ of the extended and contracted [c2]daisy chains **2**$^{\mathbf{Ext}}$ (top) and **2**$^{\mathbf{Cont}}$ (down). The spectra displays a mixture of diastereoisomers.

It is important to note that the reversibility of this motion was confirmed by adding two equivalents of deuterated trifluoroacetic acid (TFA) to the contracted rotaxane **2**$^{\mathbf{Cont}}$. Further

[154] Zhao, Y.-L., Zhang, R.-Q., Minot, C., Hermann, K. & Hove, M. A. Van. Revealing highly unbalanced energy barriers in the extension and contraction of the muscle-like motion of a [c2]daisy chain. *Phys. Chem. Chem. Phys.* **17**, 18318-18326 (2015).

exchange of the counter anions using a saturated NH_4PF_6 solution resulted in a spectrum similar to the one obtained for the extended molecule $\mathbf{2^{Ext}}$ (**Figure 62**).

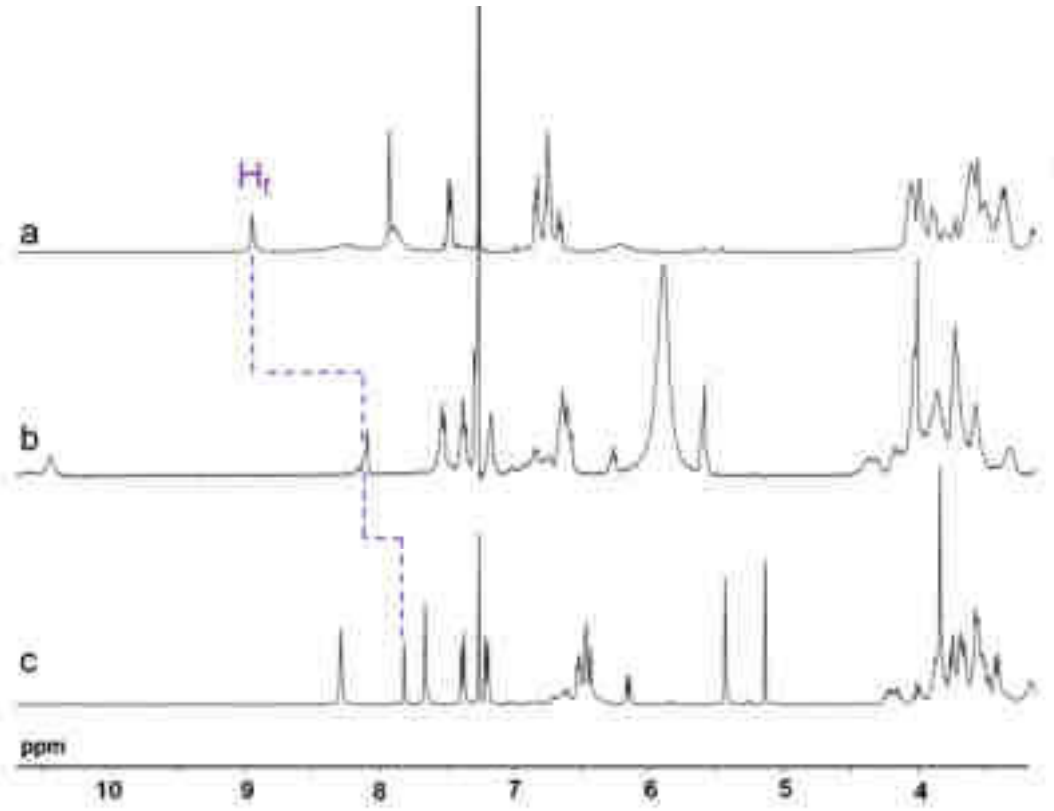

Figure 62 | ^{1}H NMR in a 4:1 mixture of $CDCl_3/CD_3CN$ showing a) the contracted compound $\mathbf{2^{Cont}}$, b) the extension of the compound $\mathbf{2^{Cont}}$ into $\mathbf{2^{Ext}}$ by addition of d-TFA, c) the extended compound $\mathbf{2^{Ext}}$ after anion exchange with NH_4PF_6.

F. Synthesis and characterization of a hydrogen bonding supramolecular polymer

The extended rotaxane $\mathbf{2^{Ext}}$ was dissolved in a 4:1 mixture of $CDCl_3/CD_3CN$ mixture along with linker **3** in a 1:1 ratio in order to form the corresponding hydrogen-bonded supramolecular complex $\mathbf{2^{Ext}}$:**3**. At a concentration of 1 mM, ^{1}H NMR spectroscopy displayed the characteristic features of the DAD-ADA association (**Figure 63**). Indeed, protons NH_a and NH_1 were significantly shifted downfield, a typical signature for this associated hydrogen-bonding pattern. This result demonstrates the formation of the expected supramolecular interactions in solution while not informing on the size of the polymer.

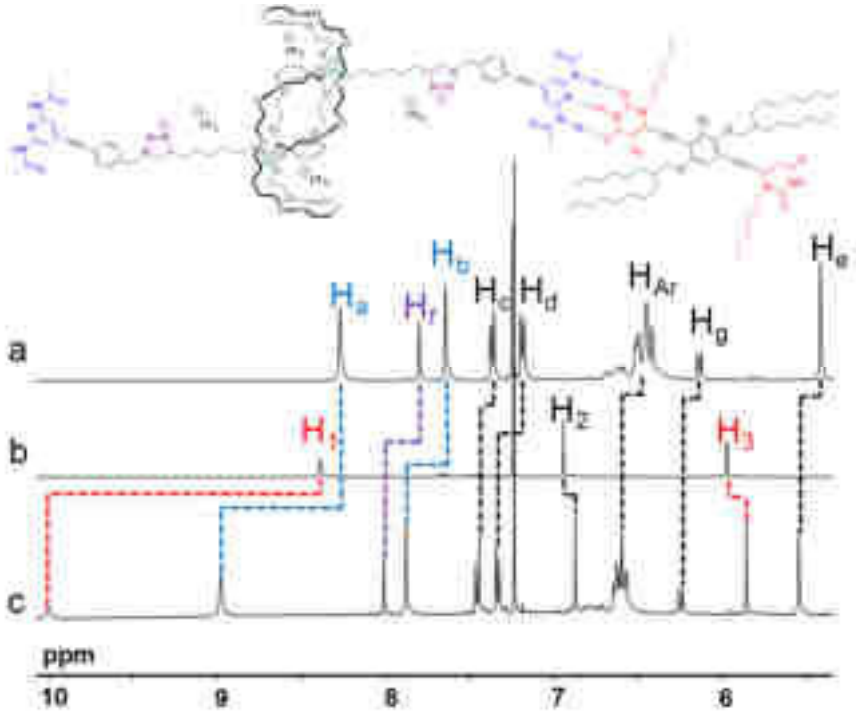

Figure 63 | ^{1}H NMR in a 4:1 mixture of $CDCl_3/CD_3CN$ of a) $\mathbf{2^{Ext}}$, b) **3**, c) the 1:1 $\mathbf{2^{Ext}}$**: 3** supramolecular polymer at 1 mM.

Similar observations were made when contracted rotaxane $\mathbf{2^{Cont}}$ was mixed with linker **3** in the same conditions (**Figure A 1**).

The formation of the supramolecular polymer did not seem to affect the viscosity of the solution, although no rigorous viscosity measurement was performed. However, when working at concentrations equal or higher than 4 mM, an important broadening of the signals was observed by ^{1}H NMR spectroscopy, which could be the sign of the growth and/or overlapping of polymer chains at this concentration. This behavior has been observed both for the extended (**Figure 64**) and the contracted (**Figure A 2**) supramolecular polymers.

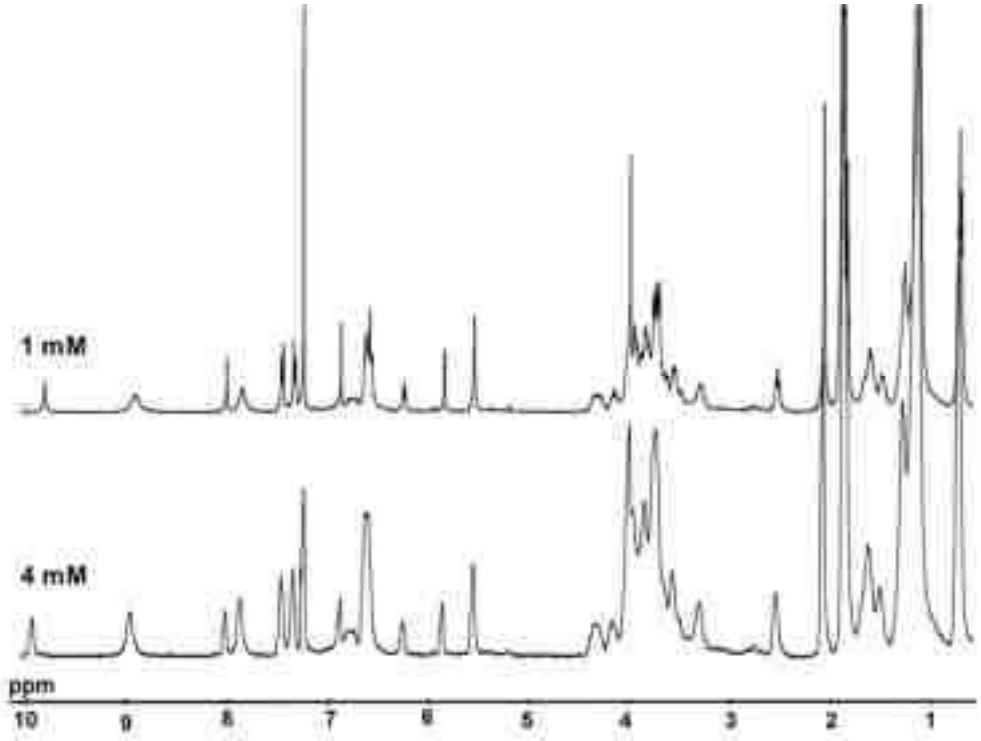

Figure 64 | Concentration dependent ^{1}H NMR spectra in a 4:1 mixture of $CDCl_3/CD_3CN$ of the **2^{Ext}:3** extended supramolecular polymer.

From these experiments, we can postulate that our [c2]daisy chain supramolecular polymer might aggregate into larger structures upon reaching a critical concentration. In order to probe and confirm the existence of these supramolecular polymers in solution, and elucidate their structure and size, we further combined static light scattering (SLS) and small-angle neutron scattering (SANS) experiments, which provide information in the range of 1 to 300 nm. Solutions were analyzed in a 4:1 mixture of $CDCl_3/CD_3CN$ at 4 mM, concentration at which the suspected aggregation seemed to occur. Although the samples seemed perfectly soluble and clear by observation with the naked eye, and did not show any sign of precipitation after several days, scattering experiments revealed the presence of a heterogeneous medium. Due to this heterogeneity, SLS data obtained for the contracted **2^{Cont}:3** supramolecular polymer were averaged over six different experiments, whereas only four averaged SLS experiments were necessary for the extended **2^{Ext}:3** supramolecular polymer, indicating a more homogeneous behavior in the 30 to 300 nm length scale in this state.

Qualitatively, for scattering vectors q ranging between 7 x 10^{-4} and 3 x 10^{-3} Å^{-1}, a pronounced increase in scattering intensity was observed, confirming the formation of aggregates larger than 200 nm, as no low-q Guinier regime associated to the finite size of the scattered objects is observed (**Figure 65**). The different slopes in these two experiments also

indicate that a structural change can be observed upon mechanical contraction/extension of the rotaxane. In the case of the extended state $\mathbf{2}^{\mathbf{Ext}}$:**3**, smooth two-dimensional objects (q^{-2} slope) were observed, whereas for the contracted state $\mathbf{2}^{\mathbf{Cont}}$:**3**, the q^{-3} slope is characteristic for three-dimensional assemblies with a rough interface. For q higher than 4 x 10^{-3} Å^{-1}, both solutions show the same behavior: they display only very low and almost flat scattering over the whole q range accessible by SANS. This observation highlights the formation of very dense aggregates, of which the internal structure could unfortunately not be determined by scattering experiments. Although these scattering experiments could not be used to determine quantitatively the full structural parameters of these polymers, they qualitatively indicate the formation of large, dense, but different self-assembled structures for $\mathbf{2}^{\mathbf{Ext}}$:**3** and $\mathbf{2}^{\mathbf{Cont}}$:**3** polymers in solution.

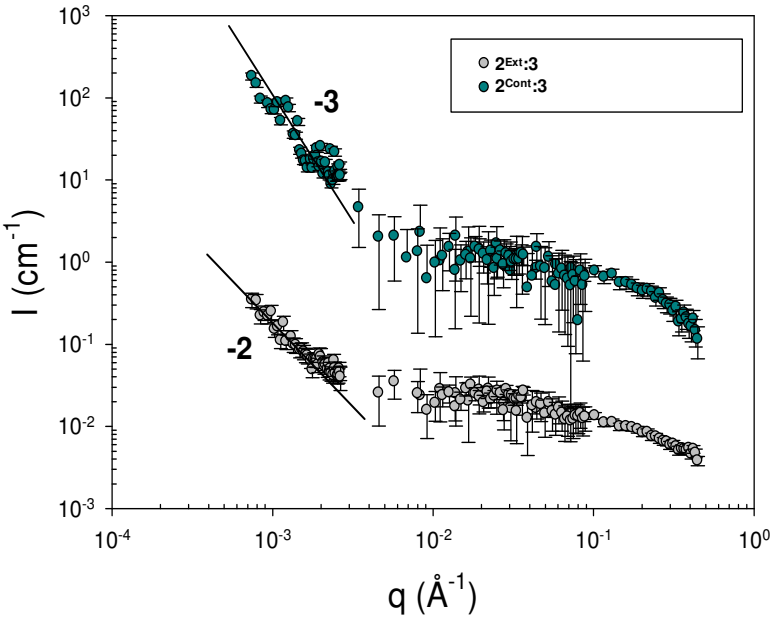

Figure 65 | Small Angle Neutron Scattering (SANS) and Static Light Scattering (SLS) of $\mathbf{2}^{\mathbf{Cont}}$:**3** (green dots) and $\mathbf{2}^{\mathbf{Ext}}$:**3** (grey dots) in a 4:1 mixture of $CDCl_3/CD_3CN$.

G. Imaging of supramolecular polymers $\mathbf{2}^{\mathbf{Ext}}$:3 and $\mathbf{2}^{\mathbf{Cont}}$:3 by TEM and AFM microscopy techniques

In order to determine the morphology of these supramolecular polymers, we performed microscopy experiments, in particular transmission electron microscopy (TEM) and atomic force microscopy (AFM). Classically, samples for these experiments are prepared by drop casting a solution on a carbon-coated copper grid (TEM). While often efficient, this method has one major disadvantage: while drying, the concentration in the drop increases, potentially leading to the formation of structures much different than what is actually in solution. In order

to observe structures as close as those existing in solution, we proceeded very rapidly for the preparation of the TEM grid. Namely, a TEM grid was placed on a piece of filtering paper, a drop of the solution was then casted onto the grid, and the paper instantly absorbs the excess of solution. By doing so, we expected that the carbon-coated copper grid "trap" the supramolecular structures on its surface, limiting, but not completely avoiding, concentration-related modification of their morphology. If not specified otherwise, all samples were prepared following this procedure.

For solutions of monomers $\mathbf{2}^{\mathbf{Ext}}$, $\mathbf{2}^{\mathbf{Cont}}$ and **3** and corresponding supramolecular polymers $\mathbf{2}^{\mathbf{Ext}}$:**3** and $\mathbf{2}^{\mathbf{Cont}}$:**3** at concentration lower than 4 mM, TEM experiments showed no large supramolecular organization or self-assembled architectures. However, for a concentration equal of higher than 4 mM, while the monomers still did not show any trace of supramolecular organization, both polymer $\mathbf{2}^{\mathbf{Ext}}$:**3** and $\mathbf{2}^{\mathbf{Cont}}$:**3** displayed very distinct mesoscopic structures. (**Figure 66**)

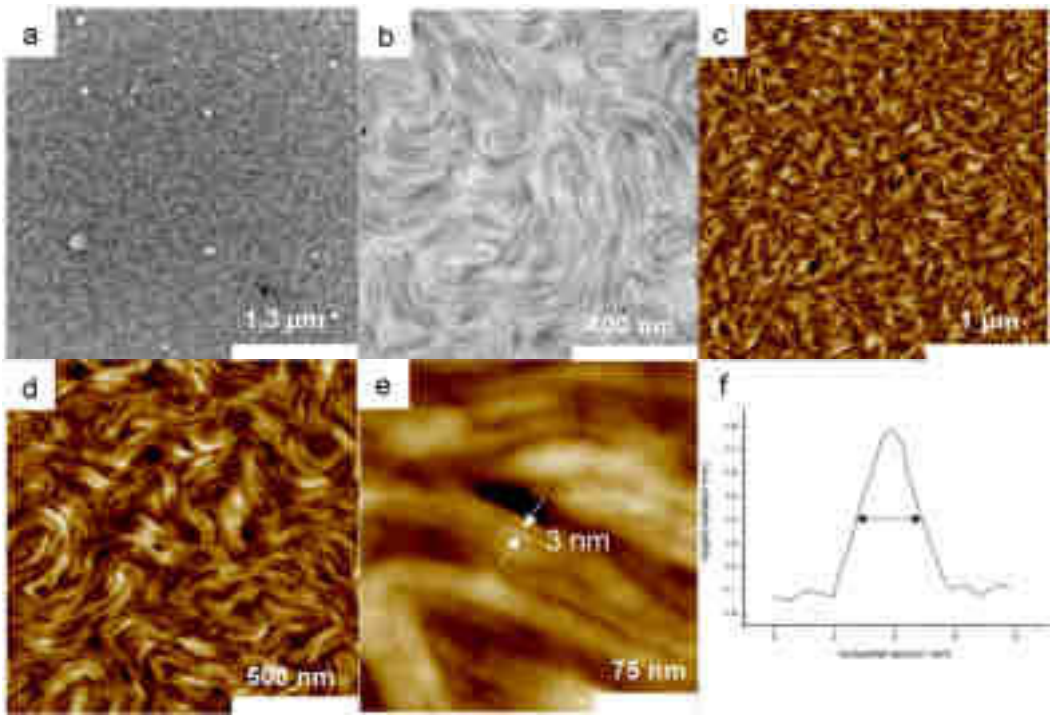

Figure 66 | TEM (a,b) and AFM (c,d,e) pictures of $\mathbf{2}^{\mathbf{Ext}}$:**3**. (f) Cross section of a single chain of $\mathbf{2}^{\mathbf{Ext}}$:**3** measured by AFM

For a 4 mM solution of the extended supramolecular polymer $\mathbf{2}^{\mathbf{Ext}}$:**3**, uniform and complete coating of the grid by structures made of relatively soft entangled fibers with extended lengths of several micrometers was revealed by TEM (**Figure 66a**). Zooming on the fibers revealed

that these large fibrous structures are indeed formed by the aggregation of several smaller fibers (**Figure 66b**).

AFM experiments (**Figure 66c,d**) allowed us to zoom further in these structures and reveal that they actually arise from the lateral aggregation of fibrils having a width of 3 nm (**Figure 66e,f**). According to molecular modeling data obtained from DFT calculation, such a diameter fits with that of a single chain of the expected supramolecular polymer (**Figure 67**). In a hierarchical structuring, these 3 nm wide single chains further bundle into wider fibers with a diameter ranging from 10 to 20 nm which further aggregate into the large micrometric structures observed by TEM and AFM.

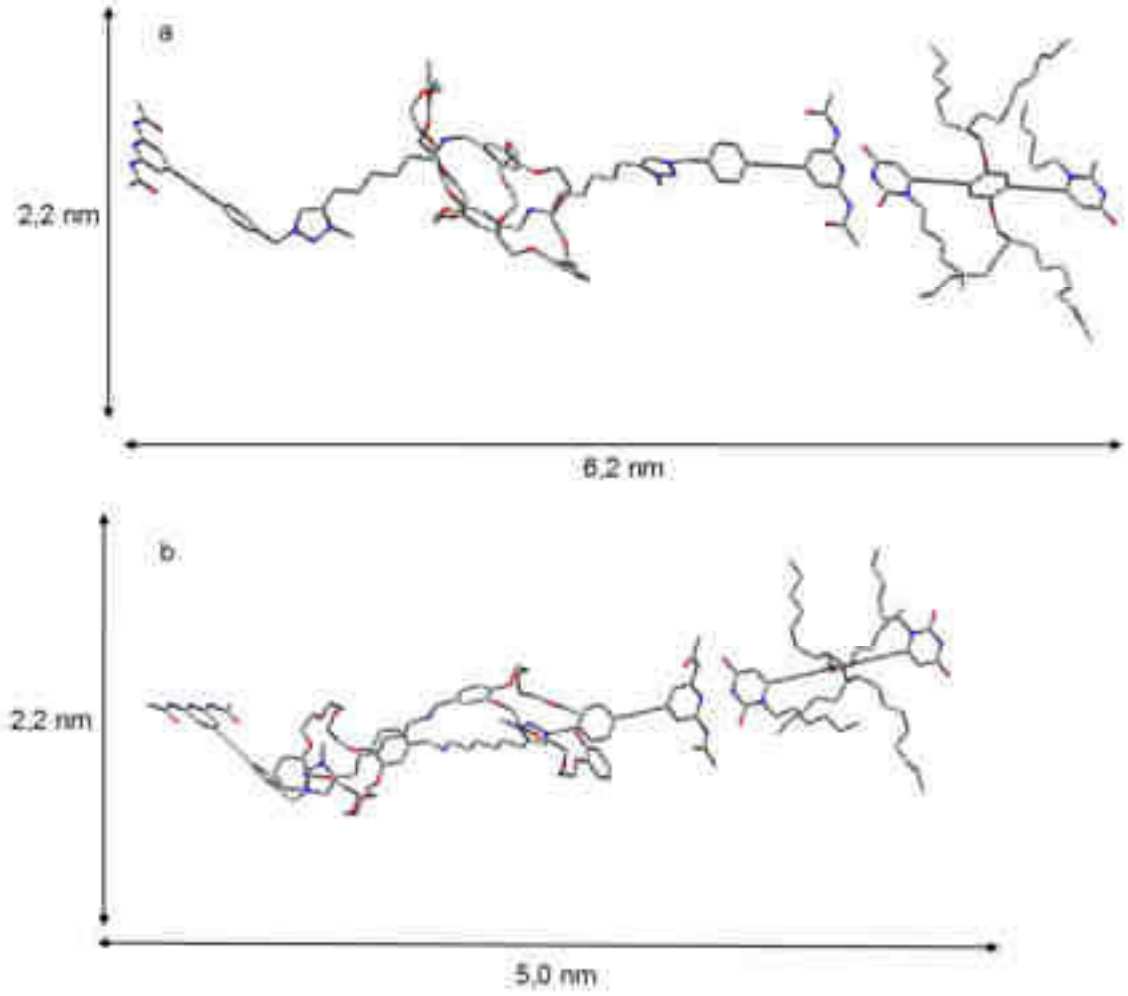

Figure 67 | Molecular modeling obtained by DFT for (a) $\mathbf{2}^{\mathbf{Ext}}$**:3** and (b) $\mathbf{2}^{\mathbf{Cont}}$**:3**.

Analysis of the contracted polymer $\mathbf{2}^{\mathbf{Cont}}$**:3** by TEM revealed also a homogeneous sample and the existence of very different morphologies compared to the extended one. Smaller and

discrete structures, with a size comprised between 200 and 400 nm in average length, were observed everywhere on the surface (**Figure 68a,b**). As a general comment, the objects were more straight and more rigid compared to the objects observed in the extended sample. Probing the internal structure of these objects by AFM (**Figure 68c,d**) revealed similar 3 nm chains as observed gor the extended sample $\mathbf{2}^{\mathbf{Ext}}$:**3**. The presence of similar single chains at the heart of both assemblies tends to prove that the extended and the contracted architectures have a similar internal structure.

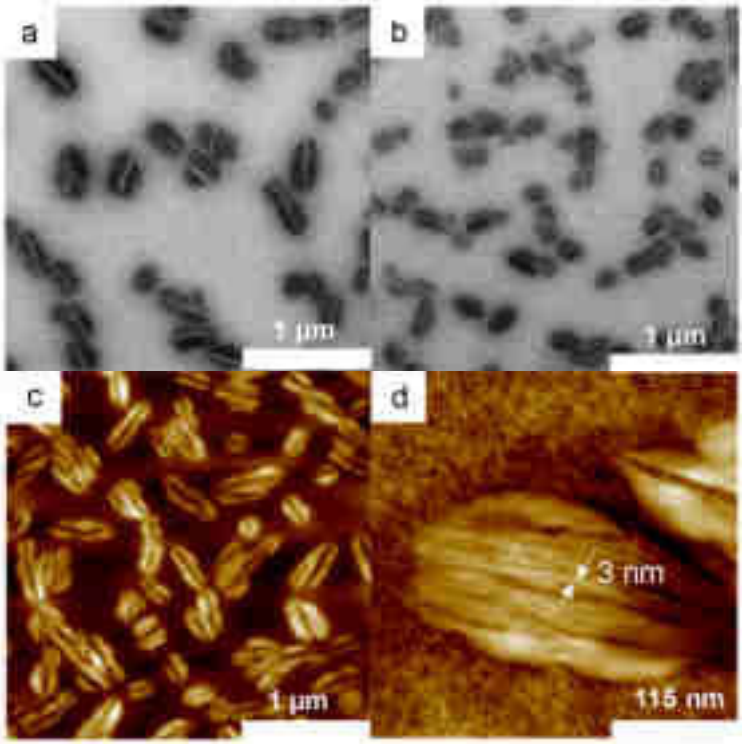

Figure 68 | TEM (a,b) and AFM (c,d) pictures of $\mathbf{2}^{\mathbf{Cont}}$:**3**.

Interestingly, these microscopy experiments qualitatively fit the trend described by light and neutron scattering data, so we can assume that the structures existing in solution are very close, even if shorter, to the one observed on the TEM grids and used for all the microcopy experiments. In both cases, dense and highly aggregated structures are observed at the nanoscopic scale, correlating the poor scattering from SANS experiments, while drastic differences were observed at the microscopic scale, thus in agreement with the change of q slopes in the low q range.

By comparison with the previously reported terpyridine-based single-chain polyrotaxane,[6] one may conclude that the formation of such large structures arises mainly from the addition of non-covalent lateral associations such as π-π stacking and Van der Waals interactions. Judging

by the relatively low concentration of the sample and the weak association constant of the 2,6-diacetylaminopyridine and N-hexyluracil recognition pattern, it can be assumed that the main chain polymerization process is strongly reinforced by a lateral growth/aggregation in a highly cooperative fashion.

The differences between the extended and contracted state can be confidently correlated to the global actuation of the individual mechanical bonds. According to previous work from the team,[6] and theoretical studies,[154] the length variation between the extended and the contracted state should be of around 1.2 - 1.6 nm. This change induces an overall size variation of the supramolecular polymer chains upon contraction/extension. Additionally, from the model obtained by DFT calculation, it can be assumed that the contracted rotaxane $\mathbf{2^{Cont}}$ is less flexible, more rigid than the extended one. This might explain why in the contracted architectures the structures are straighter. However, it has to be noted that the motion of the crown ether seems to affect not only the linear structure of the chains but also its faculty to aggregate laterally. That can be explain by the proximity of the crown ether near the recognition sites in the contracted state: the resulting steric hindrance of the macrocycles can reasonably be designated as the cause of a less efficient lateral aggregation for the structural linker **3**. As the chain-growth mechanism seems to be highly cooperative, decreasing the side interactions also decreases the overall size of the objects formed in the contracted state as observed by microscopy.

H. In situ contraction/extension experiments

Another challenge was to prove that the actuation of the mechanical bonds can be achieved *in situ* using pH modulation and affect the whole structure. Treatment of the extended polymer $\mathbf{2^{Ext}}$:**3 in** solution with two equivalents of 1,4-diazabicyclo[2.2.2]octane (DABCO) yielded small and rigid structures with a size comprised between 200 and 500 nm (**Figure 69a,b**). Treating the contracted polymer $\mathbf{2^{Cont}}$:**3** in solution with two equivalents of trifluoroacetic acid (TFA) yielded soft entangled fibers of several micrometers long (**Figure 69c,d**). The structures obtained from the *in situ* contraction and extension are noticeably close to the originally contracted polymer $\mathbf{2^{Cont}}$:**3** and extended polymer $\mathbf{2^{Ext}}$:**3**. These two experiments proved that the motions of the individual molecular machines can be integrated into large structures leading to the modification of their size and morphologies.

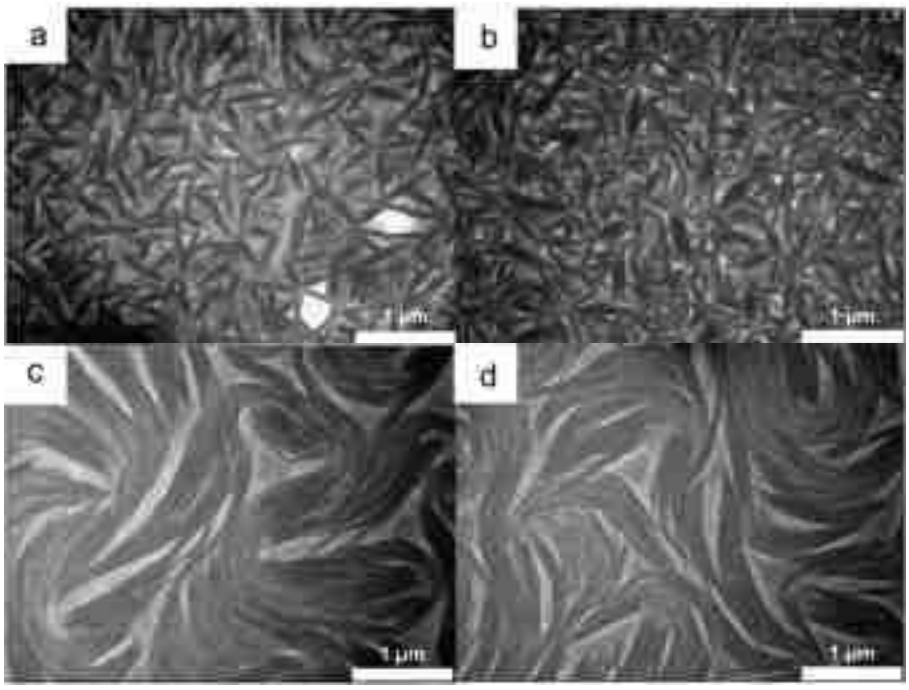

Figure 69 | TEM images obtained after (a,b) *in situ* contraction of $\mathbf{2^{Ext}}$**:3** and (c,d) *in situ* extension of $\mathbf{2^{Cont}}$**:3**.

I. Synthesis of a reticulated supramolecular polymer

The synthesis of a gel able to amplify the motions of these fibers required the formation of a 3D-network. For this reason, we decided to introduce a tris-uracil linker to act as a reticulating agent. Tris-uracil linker **4** was synthesized in three steps using procedures described in the literature (**Scheme 15**).[64] 1,3,5-tribromobenzene was coupled with trimethylsilylacetylene in Sonogashira's coupling conditions to yield compound **32**, which was deprotected in mild conditions to give tris-alkyne **33**. This molecule was engaged in another Sonogashira coupling with the previously prepared N-hexyl-iodouracil **17** to yield compound **4** which was soluble only in DMSO.

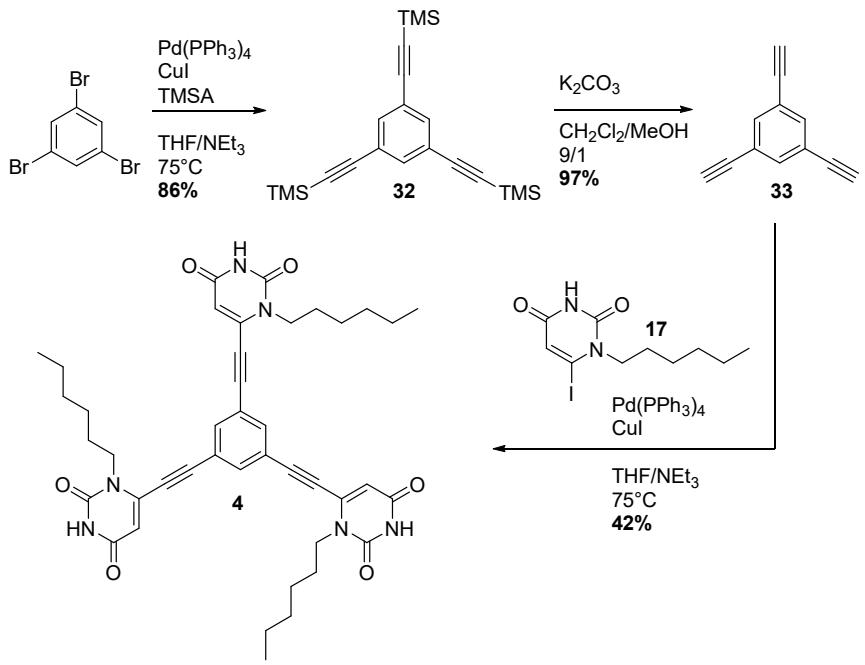

Scheme 15 | Synthesis of reticulating agent compound **4**.

The reticulated hydrogen-bonding supramolecular polymer was prepared using a 1:0.97:0.02 mixture of $\mathbf{2^{Ext}/3/4}$ in a 4:1 $CHCl_3/CH_3CN$ mixture at 4 mM. In the extended state, TEM images showed the presence of branched structures (**Figure 70**). In the contracted state, no satisfying images were obtained. Furthermore, increasing the concentration did not induce any visible increase of the viscosity nor triggered the transition to a gel phase. Upon drying a few drops of the solution on a Teflon mold, the reticulated supramolecular polymers formed only brittle films which could not be handle satisfactorily.

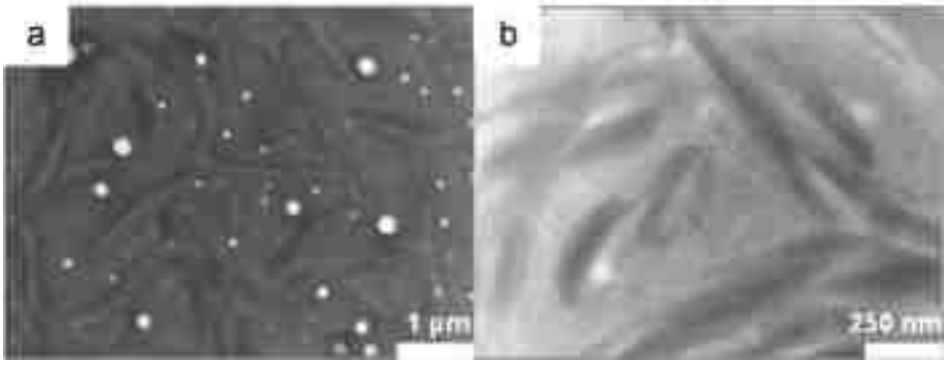

Figure 70 | TEM pictures of $\mathbf{2^{Ext}/3/4}$.

A possible explanation could be that the association constant of the chosen DAD-ADA recognition pattern is too weak to form a strong 3D network, and thus is unable to trap the solvent and form a gel. Furthermore, the structures we obtained with this tripodal unit are less

organized than in the linear system: the introduction of a branched component seems to disrupt the well-packed structures previously obtained. Interestingly, it confirms the crucial role of the lateral interactions induced by the bis-uracil linker in the self-assembly process.

III. Conclusion

To summarize, we have designed and synthesized the first example of muscle-like hydrogen-bonded supramolecular polymer, using a [c2]daisy chain rotaxane decorated with 2,6-diacetylaminopyridine stoppers as a functional unit and a complementary bis-uracil linker as a structural unit. In solution, a hierarchical structuring upon increase of the concentration occurs, as initially demonstrated by NMR spectroscopy and confirmed by SANS/SLS scattering and TEM/AFM microscopy experiments. More importantly, the local actuation between the contracted and extended state of the polymers gives rise to similar organization at the nanoscopic scale but morphological variations of the mesoscopic architectures: this is a demonstration that single chains of muscle-like supramolecular polymers can effectively be bundled into large fibers and integrate the molecular motion over several scale of magnitude. Overall, this is an important step toward the elaboration of muscle-like materials based on molecular machines using bottom-up approaches.

Although the formation of objects at the microscopic scale is noteworthy, we were still targeting the formation of soft materials like gels or films. Unfortunately, increasing the concentration, tuning the solvent mixture or even using a reticulating agent did not yield such materials. To overcome these issues and potentially reach even more ordered structures and stronger networks, we turned ourselves to another hydrogen bonding recognition group that might act both as a strong supramolecular connector and as a reticulating agent.

Chapter V: Poly[c2]daisy chains based on the ureidopyrimidinone recognition motif

This work was carried out in collaboration with Dr. Thomas Lang for the chemistry and Dr. Giacomo Mariani, Prof. Eric Bhler and Dr. Michel Rawiso for the scattering experiments.

I. Objectives and retrosynthesis

The use of ureidopyrimidinone (Upy) groups as supramolecular connectors for our [c2]daisy chains is attractive for several reasons, as explained in the first chapter of this manuscript. The most obvious one is related to the very high dimerization constant of this hydrogen bonding pattern (**Figure 71a**).[66,67] Additionally, careful selection of the Upy precursors, *i.e.* use of various R' groups, can allow to tune the solubility of the Upy groups and/or the ability of the Upy dimers to laterally interact. Indeed, under specific conditions, depending on the solvent and the R' groups, the Upy dimers have been shown to stack into helical columnar assembly (**Figure 71b**).[70,73] This phenomenon has been demonstrated to be at the origin of the physical crosslinking of single chains supramolecular polymers, turning them into a 3D network (**Figure 71c**).[74]

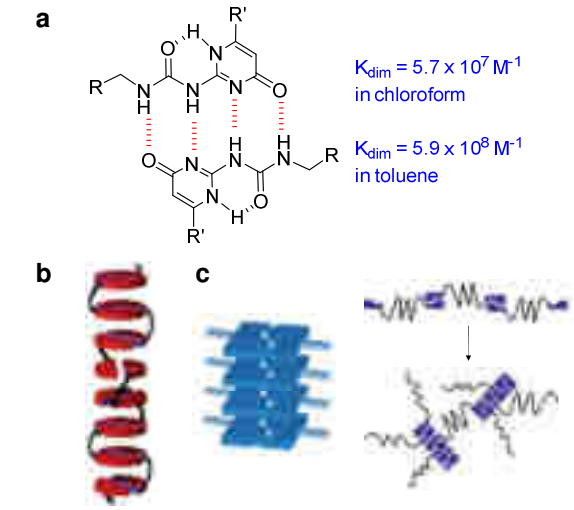

Figure 71 | a) Schematic representation of a ureidopyrimidinone (Upy) dimer with lateral R' groups.[70] b) Schematic representation of Upy dimers stacking into a helical column.[73] c) Schematic representation of the reticulation of single chain polymers into a 3D network *via* stacking of the Upy dimers.[74]

In order to take advantage of these properties to organize supramolecular polymer chains of molecular machines into a 3D network, we envisioned the synthesis of Upy-functionalized [c2]daisy chains, which required a carefully designed Upy connector (**Figure 72**). A 3,4,5-tris(dodecyloxy)benzene fragment was chosen as R' pending group. This group has been shown

to shield the Upy polar core from apolar solvents, triggering the formation of dimer stacks.[73] These chains should also prevent possible solubility issues of the targeted compounds. A photolabile *o*-nitrobenzyl group on the Upy moiety was introduced to prevent spontaneous polymerization of the targeted [c2]daisy chains **5**^{Ext} (**Figure 73**).

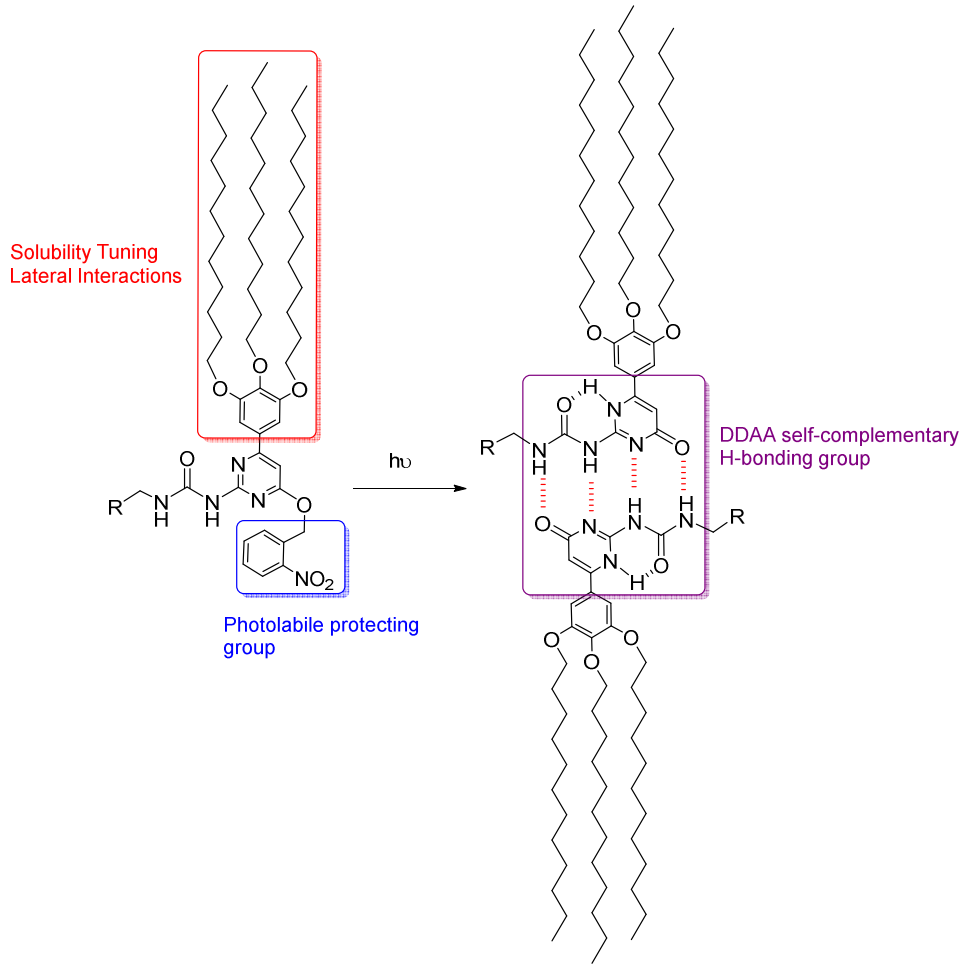

Figure 72 | Design of a multifunctional Upy connector.

The retrosynthetic strategy for rotaxane **5**^{Ext} is presented in **Figure 73**. This molecule can be accessed *via* [3+2] cycloaddition reaction between pseudo-rotaxane **12** and Upy-azide **45**, which can be syntheized from the corresponding Upy alcohol **43** after activation and nucleophilic substitution. This compound will arise from the carbonyldiimidazole mediated coupling of 6-aminohexanol with isocytosine **38**,[74] which can be synthesized in 5 steps from commercially available methyl 3,4,5-trihydroxybenzoate, also called methyl gallate.

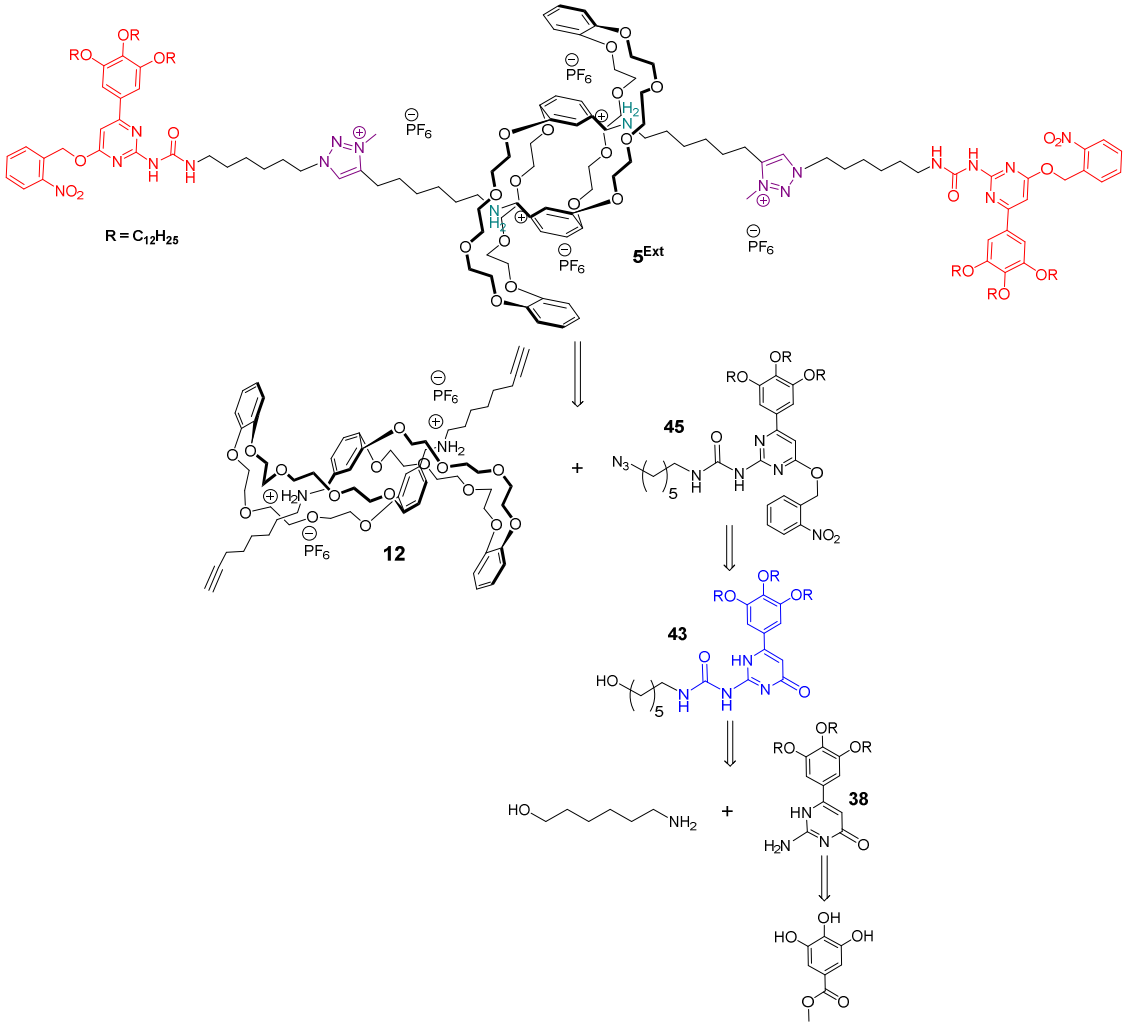

Figure 73 | Retrosynthetic scheme for protected bis-Upy [c2]daisy chain **5^{Ext}**.

II. Results

A. Synthesis of protected bis-Upy[c2]daisy chain

Isocytosine **38** has been prepared according to procedures described by E. W. Meijer and collaborators (**Scheme 16**).[73] Methyl 3,4,5-trihydroxybenzoate was reacted with bromododecane under basic conditions to give ester **34** in an almost quantitative yield. Saponification of this ester into its corresponding acid **35** using potassium hydroxide was achieved with a 95% yield. Compound **35** was converted into acyl chloride **36** by using oxalyl chloride with a catalytic amount of dimethylformamide, and was subsequently engaged without being isolated in a Knoevenagel/decarboxylation reaction with potassium ethylmalonate to provide compound **37** in excellent yield. Finally, this ethylmalonate was cyclized upon heating to reflux with guanidinium carbonate in ethanol to yield isocytosine **38** in moderate yield, but on gram scale quantities (1.7 g).

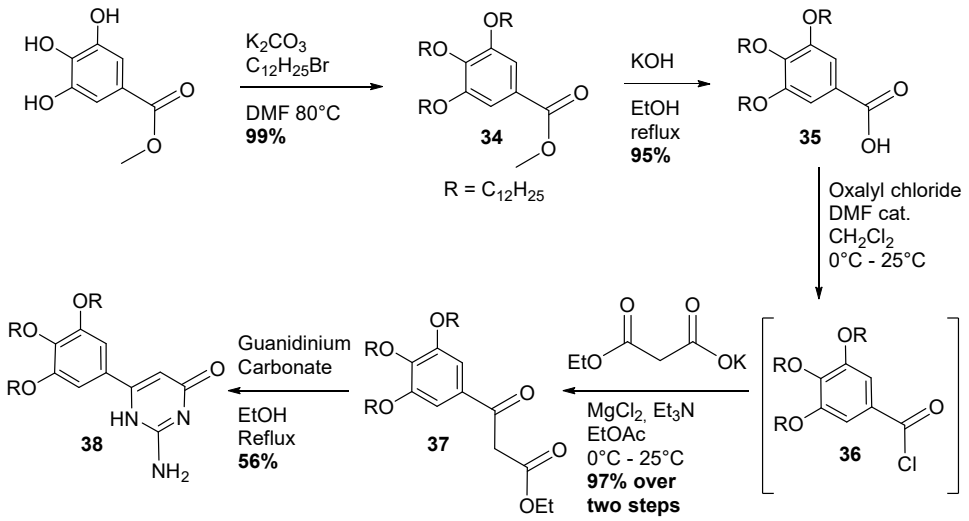

Scheme 16 | Synthesis of isocytosine **38**.

A widely reported procedure to synthesize ureidopyrimidinone derivatives is to generate an imidazolide intermediate[155] such as compound **39** pictured in **Scheme 17a**. This imidazolide can then be reacted with an amine to form the urea bridge of the Upy motif. Reaction of isocytosine **38** with an excess of carbonyldiimidazole (CDI) yielded a mixture of **39** with unreacted starting material **38**. The two compounds could not be separated without decomposition of compound **39**. For this reason, the crude mixture was engaged right away in the following step (**Scheme 17b**). Reaction with 6-aminohexanol did not provide the expected Upy **43** and only traces of compound **38** could be identified. As the unexpected instability of the imidazolide intermediate **39** seemed to be the problem, activation of 6-aminohexanol with CDI was envisioned as an alternative route (**Scheme 17c**). Imidazolide **40** was obtained quantitatively after reaction with one equivalent of CDI at room temperature and was then coupled to isocytosine **38**. Even at high temperature, no reaction of isocytosine **38** with intermediate **40** was observed as determined by UPLC-MS. However, compound **40** reacted on itself to yield small oligomers: this observation demonstrates that the primary alcohol, in these conditions, seemed to be more nucleophilic than isocytosine **38**, preventing the formation of the expected ureidopyrimidinone **43**.

[155] Keizer, H. M., Sijbesma, R. P. & Meijer, E. W. The convenient synthesis of hydrogen-bonded ureidopyrimidinones. *Eur. J. Org. Chem.* **12**, 2553-2555 (2004).

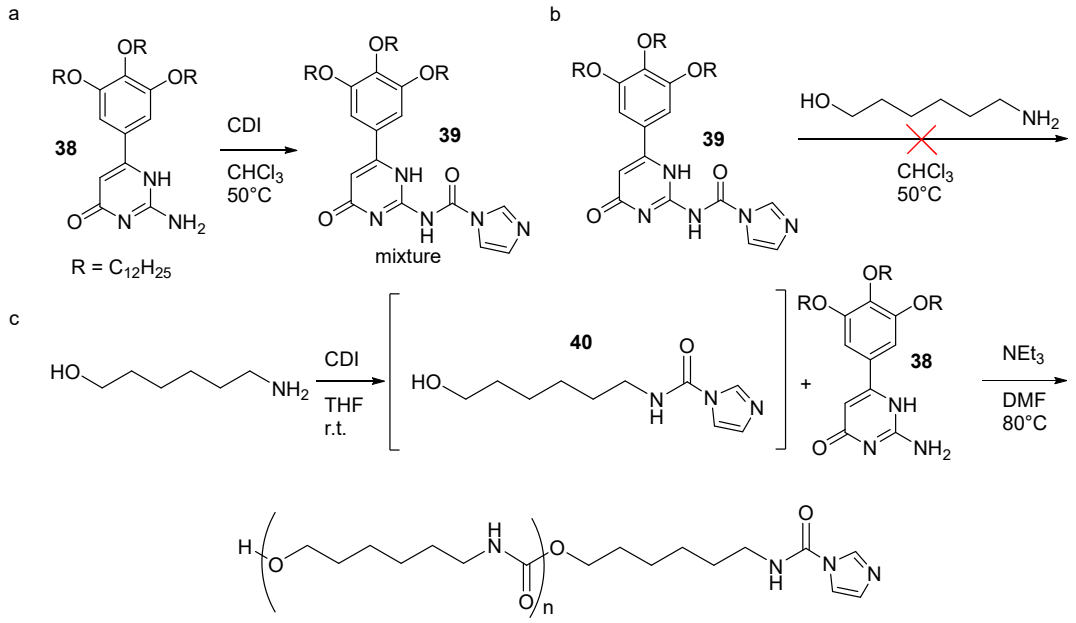

Scheme 17 | a) Activation of isocytosine **38** using carbonyldiimidazole, b) Reaction of activated isocytosine **39** with 6-aminohexanol, c) Activation of 6-aminohexanol with carbonyldiimidazole and reaction with isocytosine **38**.

For this reason, intermediate **40** was protected with *tert*-butyl(chloro)diphenylsilane on the primary alcohol, resulting in compound **41** with a very good yield over two steps (**Scheme 18**). The reaction of this molecule with isocytosine **38** proceeded efficiently to yield Upy **42**.

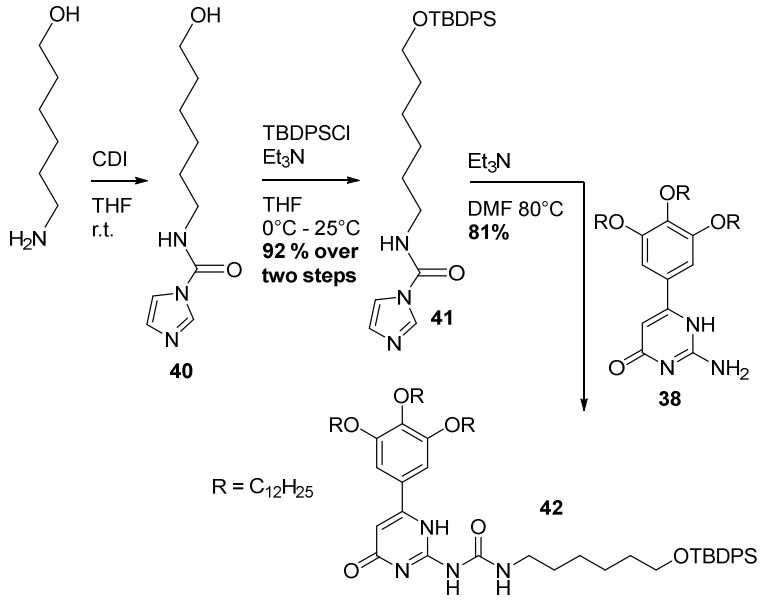

Scheme 18 | Synthesis of Upy **42**.

A sequence similar to the one described in the previous chapter was then used to obtained azide **44** (**Scheme 19**). Hydroxysilane **42** was deprotected using a 1 M tetrabutylammonium

fluoride solution in tetrahydrofuran to provide alcohol **43** in good yield. Activation of the alcohol using mesyl chloride followed by substitution with an excess of sodium azide gave access to azide **44**. The last step of this synthesis concerns the introduction of the photolabile protecting group, which was achieved by reaction of the enol form of Upy **44** with 1-(chloromethyl)-2-nitrobenzene under basic conditions, providing compound **45** with a good yield. This compound was not sensitive to ambient light and could be conveniently handle without any particular precaution.

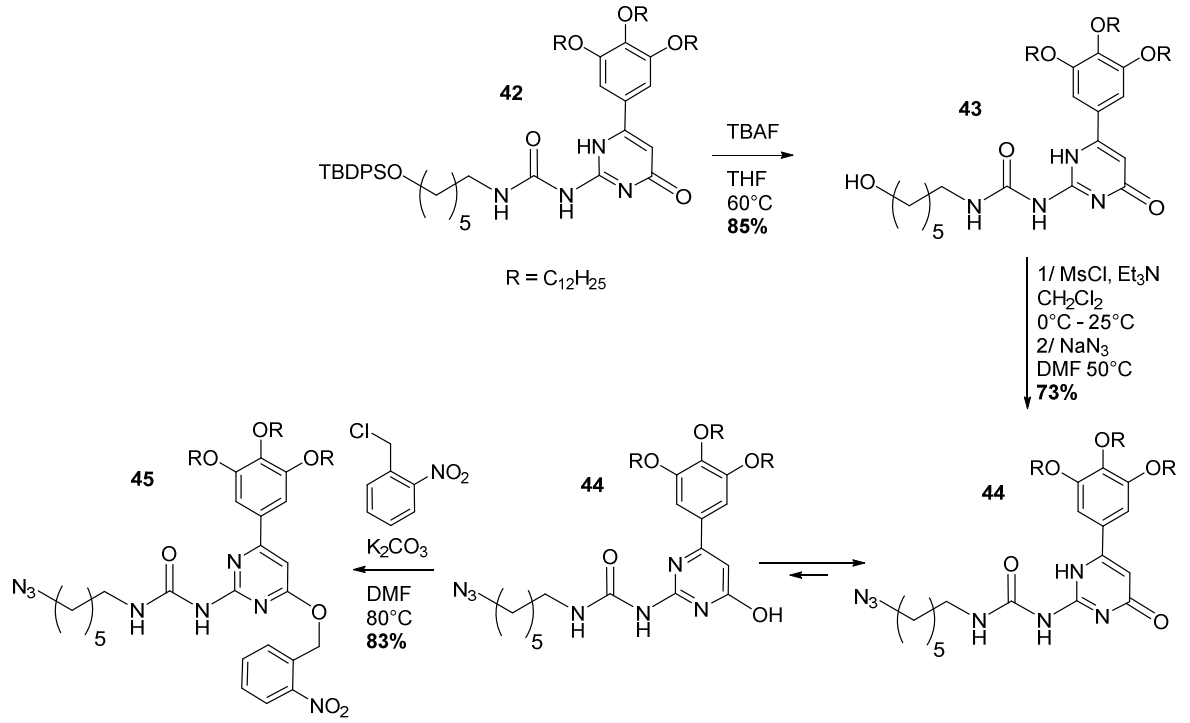

Scheme 19 | Synthesis of protected Upy-azide **45**.

Azide **45** was coupled with pseudo-rotaxane **12** under microwave irradiation to give rotaxane **46** with a moderate yield (**Scheme 20**). Final compound $\mathbf{5}^{\mathbf{Ext}}$ was obtained after quantitative methylation of the triazole moieties using a 2:1.5:0.5 mixture of methyl iodide/acetonitrile/chloroform. The contracted form $\mathbf{5}^{\mathbf{Cont}}$ was obtained by briefly shaking $\mathbf{5}^{\mathbf{Ext}}$ with a 1 M sodium hydroxide solution. This motion could be reversed by re-protonation of the secondary amine with trifluoroacetic acid.

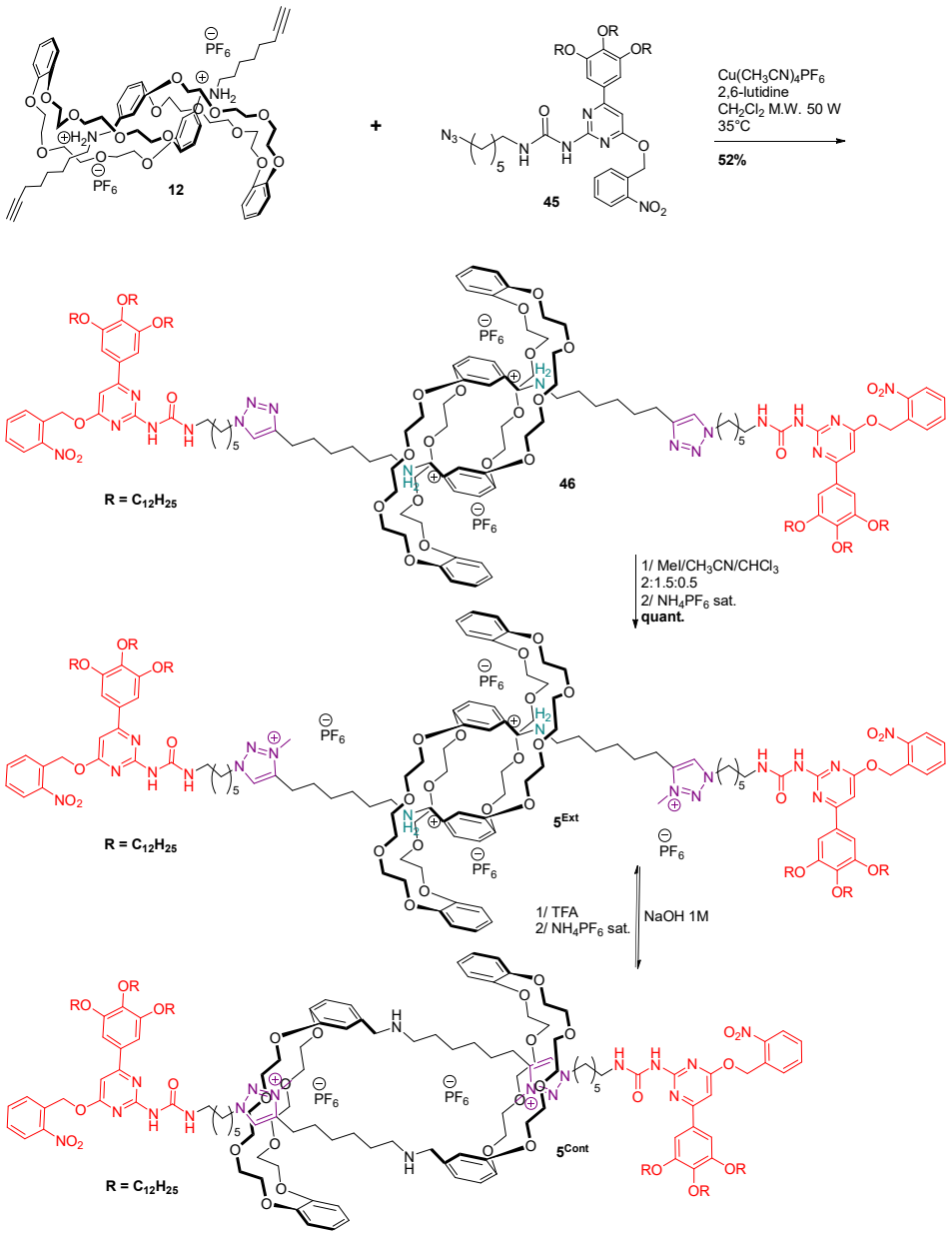

Scheme 20 | Synthesis of [c2]daisy chains $\mathbf{5^{Ext}}$ and its contraction into $\mathbf{5^{Cont}}$.

B. Characterization of the contraction/extension event of 5^{Ext}

The conversion of [c2]daisy chains $\mathbf{5^{Ext}}$ into $\mathbf{5^{Cont}}$ could be monitored by ^{1}H NMR in deuterated chloroform (**Figure 74**). The signal of the triazolium proton H_f, initially at δ = 8.20 ppm in $\mathbf{5^{Ext}}$, shifted downfield at δ = 8.45 ppm in the contracted state $\mathbf{5^{Cont}}$, as a consequence of its complexation by the crown ether. Similarly, the H_e signal from the CH_2 group next to the triazolium unit was strongly shifted downfield along with H_g, close to the crown ether moiety. The whole spectra of $\mathbf{5^{Ext}}$ and $\mathbf{5^{Cont}}$ can be found in **Figure A 3**. This motion and its reversibility prove that these new [c2]daisy chains should be useful for the synthesis of stimuli-responsive materials.

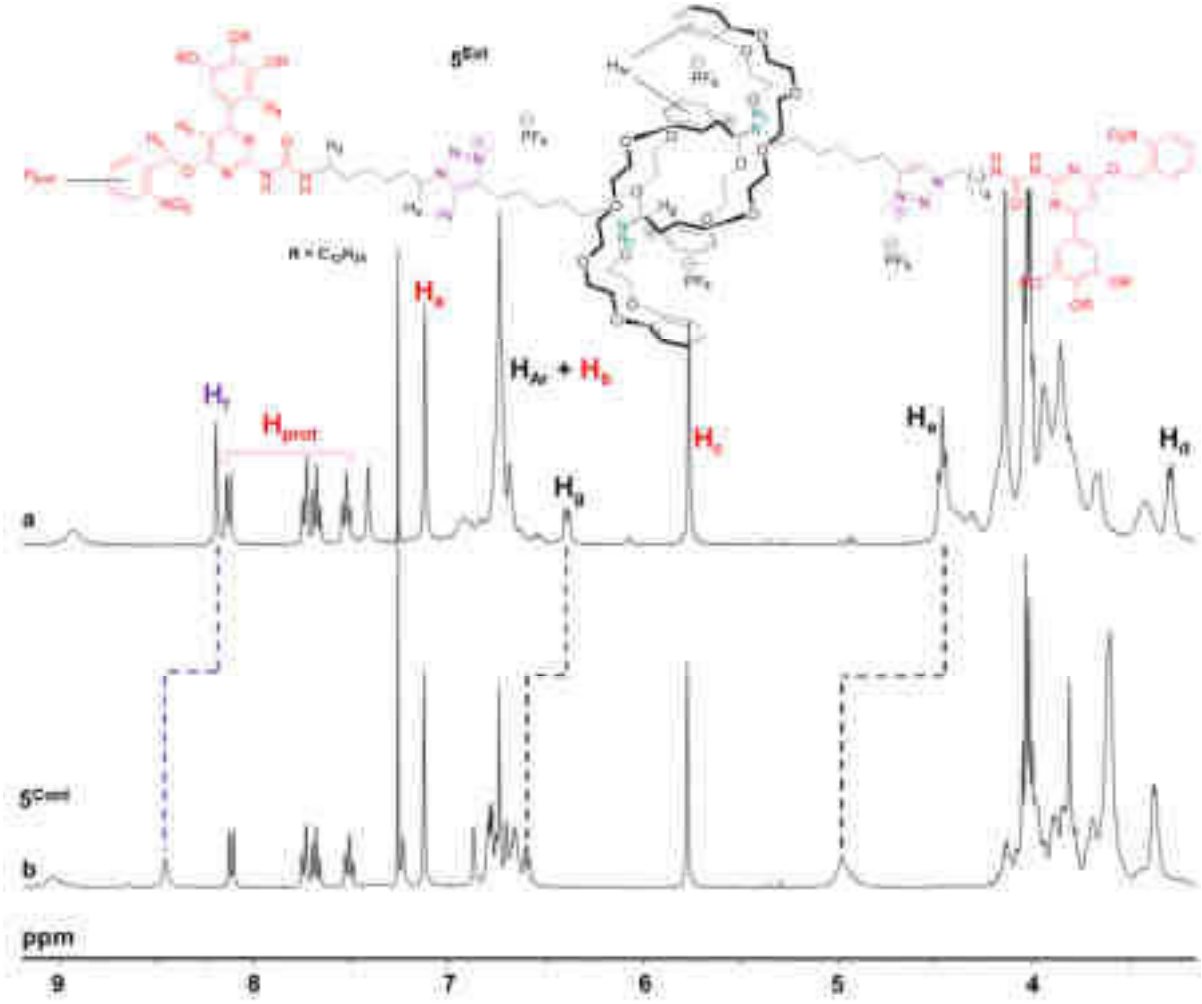

Figure 74 | ^{1}H NMR in $CDCl_3$ of a) a 5 mM solution of $\mathbf{5}^{Ext}$ and b) a 2 mM solution of its contracted state $\mathbf{5}^{Cont}$.

C. Photo-triggered supramolecular polymerization of $\mathbf{5}^{Ext}$ and $\mathbf{5}^{Cont}$

The photo-triggered deprotection of compound $\mathbf{5}^{Ext}$ and $\mathbf{5}^{Cont}$ was achieved by using a 150 W Xenon-Mercury lamp with a 320-375 nm filter. A 18 wt. % solution of $\mathbf{5}^{Ext}$ in toluene was irradiated for 4 hours to yield supramolecular polymer $\mathbf{6}^{Ext\text{-}G}$, resulting in a dark-orange gel (**Figure 75**). Interestingly, irradiation of a 16.6 wt. % of solution of $\mathbf{5}^{Cont}$ in toluene resulted in a dark orange solution of supramolecular polymer $\mathbf{6}^{Cont\text{-}S}$, which never produces a gel, even at higher concentration.

Figure 75 | Deprotection of an 18 wt. % solution in toluene of $\mathbf{5^{Ext}}$ or $\mathbf{5^{Cont}}$ into $\mathbf{6^{Ext\text{-}G}}$ and $\mathbf{6^{Cont\text{-}S}}$.

After drying the material under vacuum, polymer $\mathbf{6^{Ext}}$ was taken back in deuterated chloroform, in which it remained as a solution. ^{1}H NMR spectroscopy showed the complete disappearance of the signals corresponding to the protecting group (**Figure 76**). Broadening of all the signals and displacement of the NH signals at chemical shifts typical of the Upy-Upy dimerization proved the formation of a supramolecular polymer. Similar results were obtained for supramolecular polymers $\mathbf{6^{Cont}}$ and non-methylated control $\mathbf{46^{Ext}}$ (**Figure A 5** and **Figure A 6).**

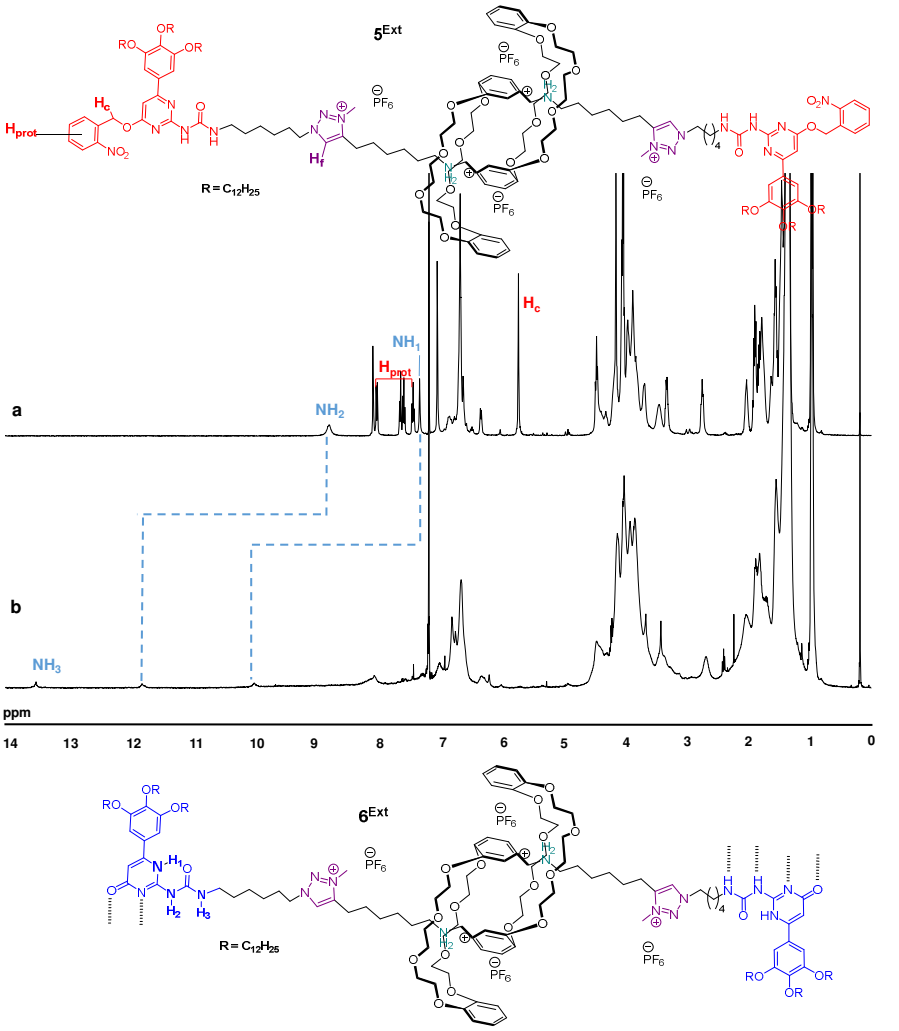

Figure 76 | ^{1}H NMR in $CDCl_3$ of a 5 mM solution of a) $\mathbf{5^{Ext}}$ and b) $\mathbf{6^{Ext}}$ after 4 hours of irradiation and 4 hours of vacuum.

While the assignment of all ^{1}H NMR signals proved difficult because of the broadening of the peaks upon polymerization (**Figure 76**), HRMS (ESI+) experiments on $\mathbf{6^{Ext}}$, $\mathbf{6^{Cont}}$ and $\mathbf{46^{Ext}}$ confirmed their formation (**Figure 77**, **Figure A 7**, **Figure A 8**).

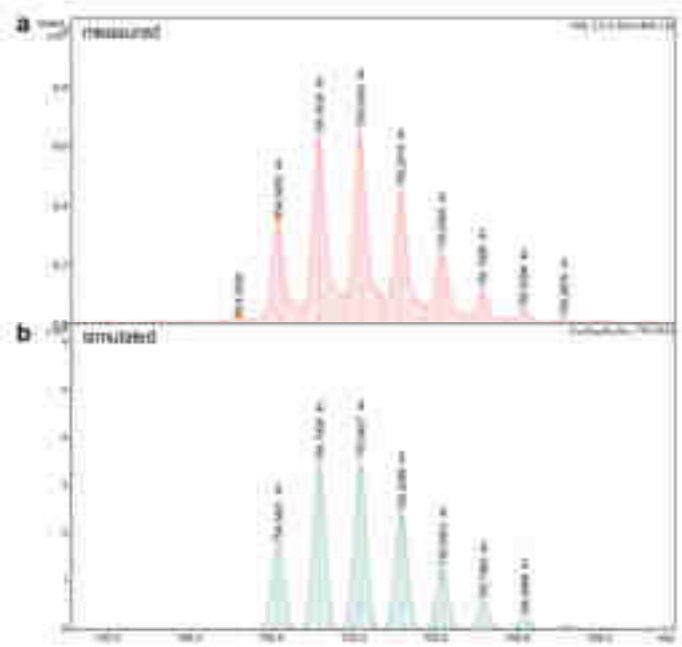

Figure 77 | a) Measured and b) simulated HRMS (ESI+) spectra of $\mathbf{6^{Ext}}$ (m/z calcd. for $C_{174}H_{288}F_{24}N_{16}O_{26}P_4$: 754.5421 $[M\text{-}4PF_6]^{4+}$, found: 754.5430).

D. Stimuli-responsive behavior of supramolecular polymers 6^{Ext} and 6^{Cont}

Supramolecular polymers $\mathbf{6^{Ext}}$ and $\mathbf{6^{Cont}}$ were dissolved in various solvents to study their gelation properties. For all solvents, the solution was heated to its boiling point before being allowed to gently cool down to room temperature. The results are displayed in **Figure 78b**. Both supramolecular polymers displayed a very similar behavior, while the only difference came from the dissolution in apolar solvents. Although they were both completely insoluble in apolar aliphatic solvents, $\mathbf{6^{Ext}}$ formed a gel in aromatic apolar solvents while $\mathbf{6^{Cont}}$ remained in solution. When a sample of gel $\mathbf{6^{Ext\text{-}G}}$ in toluene was treated with two equivalents of triethylamine to induce the contraction of the [c2]daisy chain units, it quickly turned into a solution $\mathbf{6^{Cont\text{-}S}}$ (**Figure 78a**).

This gel-sol transition could be safely attributed to the base-triggered molecular motions of the monomers. Indeed, non-methylated compound **46** was deprotected using the same conditions and yielded a dark-orange gel $\mathbf{46^{Ext\text{-}G}}$ similar to the one observed for polymer $\mathbf{6^{Ext\text{-}G}}$ (**Figure A 4**). However, deprotonation of gel $\mathbf{46^{gel\text{-}G}}$ did not trigger the formation of a solution, as it was the case for $\mathbf{6^{Ext\text{-}G}}$ upon addition of base. A reasonable explanation might be that compound $\mathbf{46^{Ext}}$ lacks a well-defined second station for the crown ether macrocycle in the contracted state, and thus could not be converted into a fully contracted state. Furthermore, the reverse phase transition from $\mathbf{6^{Cont\text{-}S}}$ to $\mathbf{6^{Ext\text{-}G}}$ was observed after reprotonation of the rotaxane

using a 2 M hydrochloric acid solution in diethyl ether. Additionally, gel $\mathbf{6}^{\mathbf{Ext\text{-}G}}$ showed thermoreversible properties with a melting point around 40 °C.

a

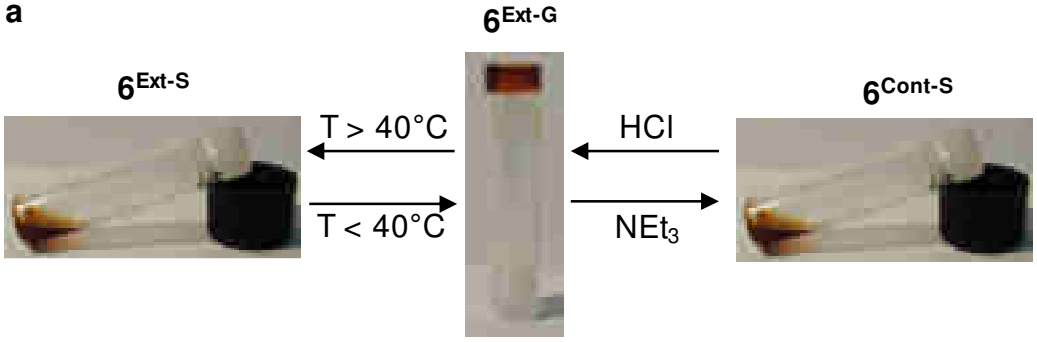

b

Solvent	6^{Ext}	6^{Cont}
Chloroform	S	S
Dichloromethane	S	S
Dimethylformamide	S	S
Dimethylsulfoxyde	S	S
Acetonitrile	S	S
Tetrahydrofuran	PS	PS
Diethylether	I	I
1,6-dioxane	I	I
Methanol	I	I
Ethanol	I	I
Water	I	I
Cyclohexane	I	I
1-methylcyclohaxane	I	I
Heptane	I	I
Toluene	G	S
Xylene	G	S

I = Insoluble, PS = Partialy soluble, S = Solution, G = Gel

Figure 78 | a) Stimuli-responsive behavior of an 18 wt. % $\mathbf{6}^{\mathbf{Ext}}$ gel in toluene, b) Physical state of $\mathbf{6}^{\mathbf{Ext}}$ and $\mathbf{6}^{\mathbf{Cont}}$ in various solvents.

E. Characterization of supramolecular polymers 6^{Ext} and 6^{Cont}

Investigations of the properties of supramolecular polymers $\mathbf{6}^{\mathbf{Cont\text{-}S}}$ and $\mathbf{6}^{\mathbf{Ext\text{-}G}}$ were further performed using various techniques.

First, infrared (IR) spectroscopy was performed on both supramolecular polymers to demonstrate the presence of absorption bands typical of hydrogen bonding formation and the absence of those typical of free N-H bonds (**Figure 79**). In the case of $\mathbf{6}^{\mathbf{Ext\text{-}G}}$, IR spectrum displayed N-H stretching bands at 3172 and 3070 cm^{-1}, and C-O stretching band at 1692 and 1648 cm^{-1}. For the solution made of $\mathbf{6}^{\mathbf{Cont\text{-}S}}$, the spectrum displayed N-H stretching bands at

3174 and 3071 cm^{-1}, and C-O stretching bands at 1687 and 1661 cm^{-1}. These values are similar to the one reported in the literature for Upy dimers.[156,157] The absence of peaks between 3700-3500 cm^{-1} proves the absence of free N-H moieties. Overall, these two measurements showed very similar profile for both supramolecular polymers, confirming the formation of hydrogen bonds in both cases.

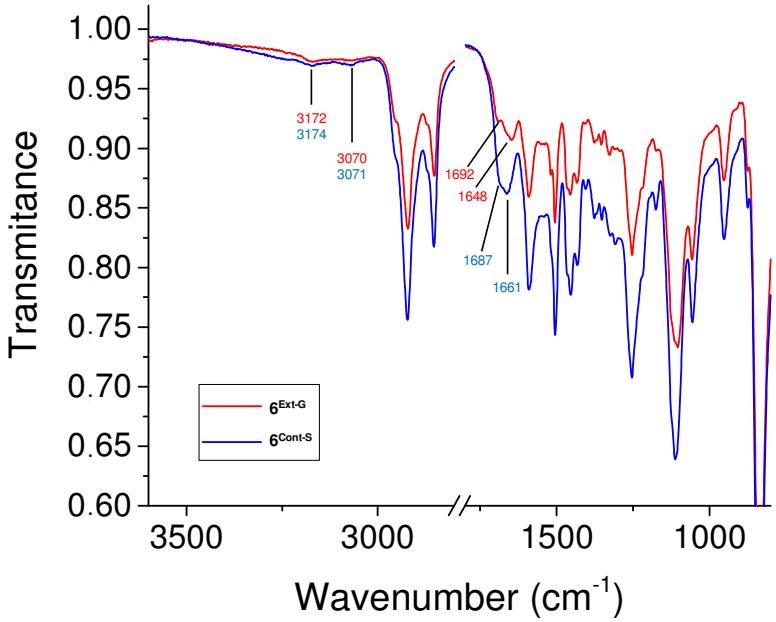

Figure 79 | Partial infrared spectra of a 50 mM solution in toluene of $\mathbf{6}^{\text{Cont-S}}$ and a 50 mM gel of $\mathbf{6}^{\text{Ext-G}}$ in toluene.

Then, both supramolecular polymers were further characterized by Differential Scanning Calorimetry (DSC). A 16.6 wt. % solution of polymer $\mathbf{6}^{\text{Cont-S}}$ in toluene was heated and cooled down several times between 10 and 80 °C, but no transition was observed. A 18 wt. % gel of polymer $\mathbf{6}^{\text{Ext-G}}$ in toluene was then analyzed in the same conditions. Upon heating, two exothermic peaks appeared at 39.6 °C and 74.9 °C, while when cooling down, a hysteresis was observed as the two peaks appeared at lower temperatures, 35.1 and 65.5 °C respectively (**Figure 80**). Thanks to thermogravimetric analysis (TGA), we were able to confirm that these peaks do not arise from an eventual thermal decomposition of the compound (**Figure A 9**). The first peak observed by DSC can be related to the melting point previously observed by simply heating a sample of the gel (**Figure 78a**). The second peak might arise from lateral ordering of

[156] Van Beek, D. J. M., Spiering, A. J. H., Peters, G. W. M., Te Nijenhuis, K. & Sijbesma, R. P. Unidirectional dimerization and stacking of ureidopyrimidinone end groups in polycaprolactone supramolecular polymers. *Macromolecules* **40**, 8464-8475 (2007).
[157] Armstrong, G. & Buggy, M. Thermal stability of a ureidopyrimidinone model compound. *Mater. Sci. Eng. C* **18**, 45-49 (2001).

the polymer chains, as the temperature seemed too low to arise from the dissociation of ureidopyrimidinone dimers.[157]

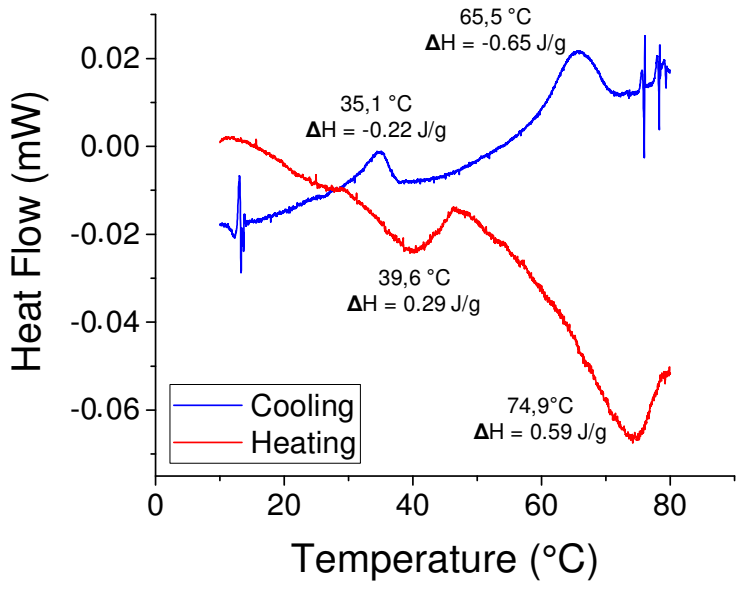

Figure 80 | Differential Scanning Calorimetry (DSC) performed on an 18 wt. % $\mathbf{6}^{\mathbf{Ext\text{-}G}}$ gel in toluene between 10 and 80 °C.

Isothermal Titration Calorimetry (ITC) experiments were finally performed on a solution made of $\mathbf{6}^{\mathbf{Cont}}$. This technique has been used to measure the association constant of the interactions involved in the cohesion of a supramolecular polymer.[158] Here, 20 x 5 µL aliquots of a 1% wt. solution of $\mathbf{6}^{\mathbf{Cont\text{-}S}}$ in toluene were added into pure toluene and the associated heat effect was measured, resulting in the enthalpogram displayed in **Figure 81a**. The positive heat flux indicates that the dissociation process is endothermic ($\Delta H_{diss} > 0$). The data could be fitted using a dimer dissociation model, as displayed on **Figure 81b**, leading to the value of $K_d = 9.0 \times 10^5$ M, and the enthalpy associated to this dissociation $\Delta H_{diss} = 2.5 \times 10^1$ kJ/mol, which means that ΔH_{ass} is negative. The association being an exothermic process is compatible with the expected formation of hydrogen bonding by the ureidopyrimidinone moieties. Finally, we noticed that the association constant $K_a = 1.1 \times 10^4$ M^{-1} is four orders of magnitude lower than what has been predicted for Upy dimers in toluene.[67] We can postulate that this is a consequence of the proximity of the macrocycles hindering the association of the Upy derivatives, which are in this work substituted with large and bulky groups.

[158] Arnaud, A. & Bouteiller, L. Isothermal Titration Calorimetry of supramolecular polymers. *Langmuir* **20**, 6858-6863 (2004).

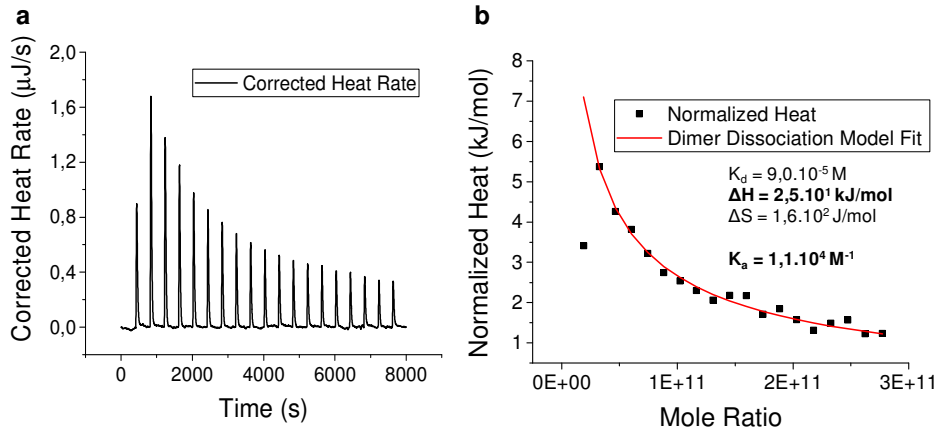

Figure 81 | Isothermal Titration Calorimetry (ITC) experiment performed on a 2.66 mM solution of $\mathbf{6}^{\mathbf{Cont\text{-}S}}$ in toluene. a) Enthalpogram obtained by injecting 20 c 5 µL aliquots of a 2.66 mM solution of $\mathbf{6}^{\mathbf{Cont\text{-}S}}$ in toluene into pure toluene (T = 25°C). b) Normalized heat obtained from ITC experiments fitted with a dimer dissociation model.

F. Characterization of monomers 5^{Ext} and 5^{Cont} by Small Angle Neutron Scattering (SANS)

Monomers $\mathbf{5}^{\mathbf{Cont}}$ and $\mathbf{5}^{\mathbf{Ext}}$ were characterized by SANS prior to the polymers, as data extracted from these experiments are needed for the elucidation of the structure of polymers $\mathbf{6}^{\mathbf{Cont\text{-}S}}$ and $\mathbf{6}^{\mathbf{Ext\text{-}G}}$. Solution of monomers $\mathbf{5}^{\mathbf{Cont}}$ and $\mathbf{5}^{\mathbf{Ext}}$ in toluene were analyzed by SANS to obtain the scattering profile displayed in **Figure 82**. Both shows an increase of the scattered intensity at low q, probably the sign of the presence of aggregates due to the partial solubility of the monomers in toluene. In both cases, the curves were fitted accordingly to the Guinier approximation. The gyration radius extracted from these fit were R_g = 2.3 ± 0.2 nm for $\mathbf{5}^{\mathbf{Cont}}$ and R_g = 3.4 ± 0.2 nm for $\mathbf{5}^{\mathbf{Ext}}$, which confirmed the reduction of the size of the molecule in the contracted state.

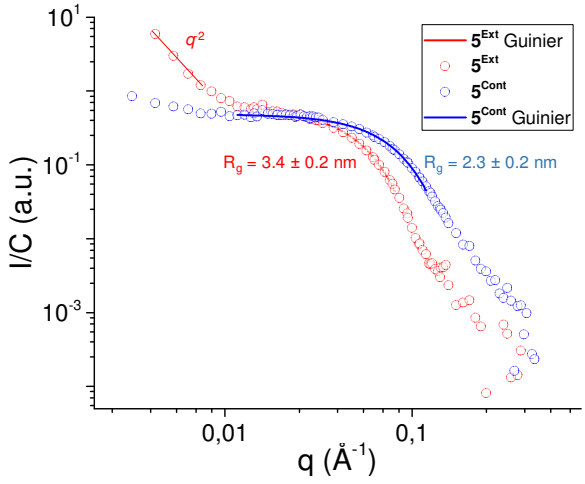

Figure 82 | Scattering profile for toluene solutions of $\mathbf{5}^{\mathbf{Cont}}$ at 3.24 x 10^{-3} M and $\mathbf{5}^{\mathbf{Ext}}$ at 3.15 x 10^{-3} M normalized by the concentration.

G. Characterization of supramolecular polymers 6^{Ext} and 6^{Cont} by Small Angle Neutron Scattering (SANS) and Small Angle X-ray Scattering (SAXS)

Supramolecular polymers $\mathbf{6}^{\mathbf{Cont\text{-}S}}$ and $\mathbf{6}^{\mathbf{Ext\text{-}G}}$ were analyzed respectively as a solution and a gel at 4.32 x 10^{-2} M in toluene. The curves are displayed in **Figure 83**, the data obtained for $\mathbf{6}^{\mathbf{Cont\text{-}S}}$ and $\mathbf{6}^{\mathbf{Ext\text{-}G}}$ are very different, showing a completely different organization of the two supramolecular polymers in the solution and the gel phase.

For $\mathbf{6}^{\mathbf{Cont\text{-}S}}$, the signal is completely flat at low scattering vector q, indicating objects with a finite size, and rather smooth at high q indicating no structural ordering (**Figure 83a**). It should be noted that the scattering intensity of $\mathbf{6}^{\mathbf{Cont\text{-}S}}$ decays at lower q values compared to $\mathbf{5}^{\mathbf{Cont}}$, which indicates object of different dimensions in the polymer and the monomer solution. The Guinier approximation was not able to fit the data obtained for $\mathbf{6}^{\mathbf{Cont\text{-}S}}$, which is an indication that the plateau observed is in fact not really related to the finite size of the polymer, but can rather be linked to structural ordering. However, the intensities at q = 0 from the monomer and the polymer curves provided information about the number of monomers associated in the polymer: $\mathbf{6}^{\mathbf{Cont\text{-}S}}$ has a degree of polymerization of 22. This number was in perfect agreement with what can be predicted using the association constant obtained from ITC experiments. If we assume that polymerization occurs *via* an isodesmic mechanism,[39] the expected degree of polymerization should be: $n = [C.K_a]^{1/2} = [4.32 \times 10^{-2} \times 1.1 \times 10^{4}]^{1/2} \approx 22$.

Supramolecular gel $\mathbf{6}^{\mathbf{Ext\text{-}G}}$ displayed a much more complex behavior (**Figure 83b**). At low q, a slope with a decay between q^{-3} and q^{-2} was observed with no plateau (no Guinier region) for the scattered intensities, indicating the presence of large assemblies. The monomer and polymer scattering intensity decay at the same q value, indicating that they have the same cross section. Interestingly, in the high q regime, several fluctuations are observed, which can be considered as structural peaks associated with ordering of the molecules inside the gel and which were not visible in the $\mathbf{6}^{\mathbf{Cont\text{-}S}}$ measurements. The general aspect of the curve at high q shows that some inter-chains interactions are specific to the extended state, and are not present in the contracted one.

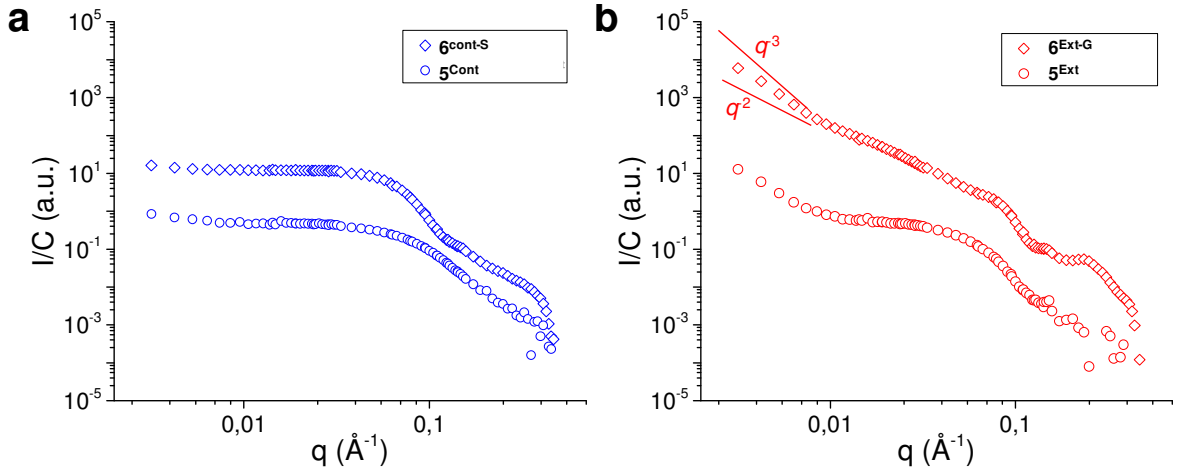

Figure 83 | Superimposition of the respective monomers curves with a) a $\mathbf{6}^{\text{Cont-S}}$ solution (4.32 x 10^{-2} M in toluene) and b) a $\mathbf{6}^{\text{Ext-G}}$ gel (4.32 x 10^{-2} M in toluene).

To investigate the structure of the gel with more precision, a new and original approach was developed by Dr. Mariani and Prof. Buhler, our collaborators for all scattering experiments. Monomer $\mathbf{5}^{\text{Ext}}$ and polymer $\mathbf{6}^{\text{Ext-G}}$ have the same cross-section, allowing the signal of the first to be removed from the second, by simple subtraction and normalization. As a consequence, such a mathematical treatment removes the contribution of the monomer to the signal, leaving only the structural characteristics of the gel and the 3D structure it describes (**Figure 84**). The q^{-3} slope observed at low q is thus replaced by a plateau corresponding to a size of around 20 nm, which could correspond to the mesh size of the network which forms the gel. Additionally, at high q, three structural peaks associated with lengths of 8.5 nm, 4.3 nm and 2.7 nm are clearly visible. These peaks provide precious information on the internal structure of the gel. The first one might correspond to the average inter-reticulating distance in the gel, while the second one could be attributed to the second order fluctuation of the first one. The peak at 2.7 nm support the piling of Upy dimers into columnar aggregates. Indeed, according to theoretical studies, Upy dimers stacks are characterized by a shift between two planes of about 45°. Considering that their typical inter-plane distance is around 3.5 Å or 0.35 nm, and that eight rotations of 45° each would be required to achieve a complete rotation, the predicted helical arrangement resulting from the stacking of Upy dimers would have a helical pitch of about 8 x 0.35 = 2.8 nm, which fits quite well the value of the last peak.

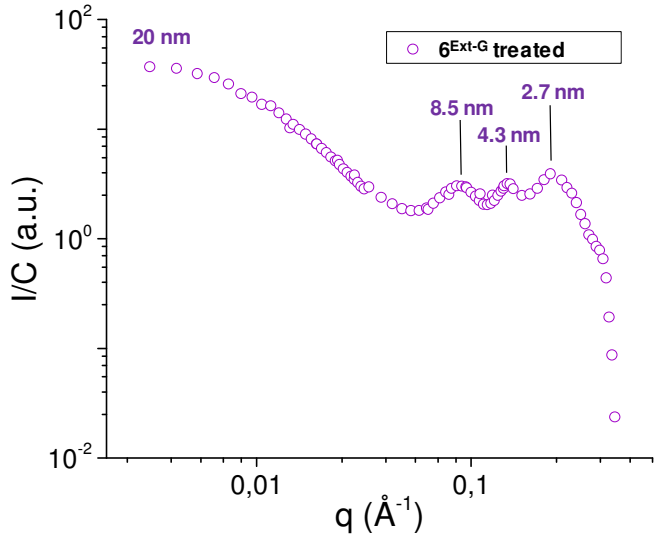

Figure 84 | New $\mathbf{6}^{\text{Ext-G}}$ treated scattering curve, displaying three structural peaks.

Small Angle X-ray Scattering (SAXS) was also performed to confirm these results (**Figure 85**). Although these two techniques usually provide different information on the structure of the analyte,[159] the scattering curves obtained for polymers $\mathbf{6}^{\text{Ext-G}}$ and $\mathbf{6}^{\text{Cont-S}}$ showed an identical behavior by SANS and SAXS. In the contracted polymer, SAXS confirmed the presence of a plateau at low *q* and a smooth decay at high *q* (**Figure 85a**), while in the extended one, peaks similar to the one revealed by mathematical treatment of the SANS data are visible (**Figure 85b**).

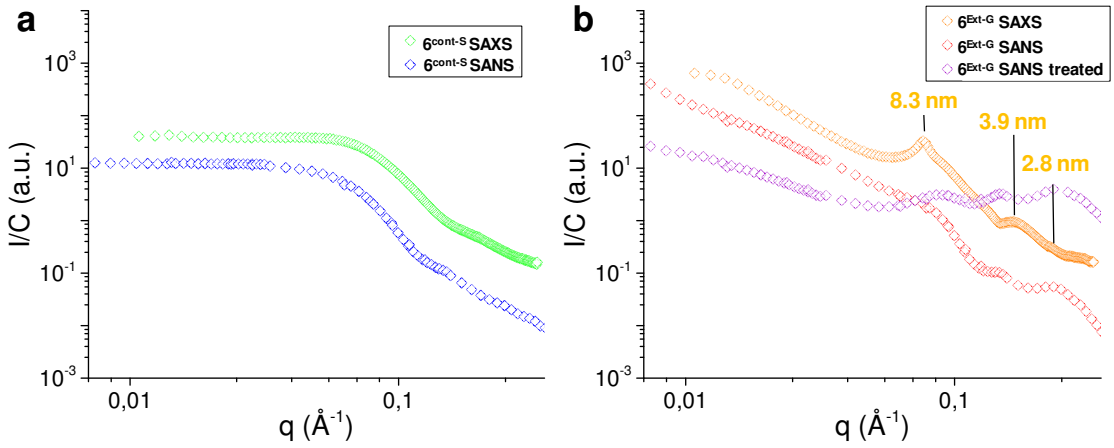

Figure 85 | Superimposition of the SANS and SAXS scattering curves of a) a solution of $\mathbf{6}^{\text{Cont-S}}$ in toluene (4.32×10^{-2} M in toluene) and b) a gel of $\mathbf{6}^{\text{Ext-G}}$ (4.32×10^{-2} M in toluene).

[159] Patterson, J. P. *et al.* The analysis of solution self-assembled polymeric nanomaterials. *Chem. Soc. Rev.* **43**, 2412-2425 (2014).

Overall, scattering experiments demonstrate that precise ordering of the polymer chains by lateral interaction for $\mathbf{6}^{\mathbf{Ext\text{-}G}}$ is responsible for the difference of physical state observed in toluene, compared to the polymer made of $\mathbf{6}^{\mathbf{Cont\text{-}S}}$. We proposed that this is due to the ability of Upy dimers to stack in $\mathbf{6}^{\mathbf{Ext\text{-}G}}$, which is prevented in polymer $\mathbf{6}^{\mathbf{Cont\text{-}S}}$ because of the proximity of the crown ether macrocycles, combined with the overall reduction of the size of the chains, in a cooperative fashion.

III. Conclusion

In this work, we successfully synthesized and characterized ureidopyrimidinone functionalized [c2]daisy chains $\mathbf{5}^{\mathbf{Ext}}$ and $\mathbf{5}^{\mathbf{Cont}}$. These two compounds were used as building blocks for a photo-triggered supramolecular polymerization process, yielding two hydrogen-bonded polymers $\mathbf{6}^{\mathbf{Ext}}$ and $\mathbf{6}^{\mathbf{Cont}}$ which respectively formed a gel and a solution in toluene/xylene. Deprotonation of the extended gel yielded a solution of the contracted supramolecular polymer, a stimuli-responsive behavior which can be reversed by addition of acid. IR spectroscopy and ITC experiments confirmed the formation of hydrogen bonds between the Upy moieties, while scattering experiments revealed an inter-chains ordering only for $\mathbf{6}^{\mathbf{Ext\text{-}G}}$ which explains why $\mathbf{6}^{\mathbf{Ext\text{-}G}}$ forms a gel and $\mathbf{6}^{\mathbf{Cont\text{-}S}}$ gives rise to a solution.

According to the association constant measured by ITC, polymer $\mathbf{6}^{\mathbf{Cont\text{-}S}}$ forms unusually weak hydrogen bonds for Upys. We propose that the presence of the macrocycles, closer to the Upy than in the extended state, hinder the approach of another Upy group in close proximity, destabilizing the formation of the dimer. For this reason, in solution, $\mathbf{6}^{\mathbf{Cont\text{-}S}}$ was shown to only form short polymer chains (22 monomers, around 73 000 $g.mol^{-1}$) in solution, which do not present any noticeable ordering.

On the other hand, $\mathbf{6}^{\mathbf{Ext\text{-}G}}$ was proved to form long polymer chains that interact with each other and turn the chains into a network. The formation of Upy dimer stacks create physical cross-linking nodes which are prerequisite for the gelation of the system, as demonstrated by scattering experiments. These experiments suggest that helices with a step of 2.7 nm are formed from the Upy dimer stacks, acting as reticulating nodes, separated by a 8.5 nm average distance. From this organization arise a network which mesh size is around 20 nm.

This work confirms that supramolecular polymers of complex molecules such as [c2]daisy chains can be ordered into a 3D network able to form physical gels. Although deprotonation of the extended rotaxane did not trigger the contraction of the gel but a transition to a liquid phase, this work illustrates how the conformation of [c2]daisy chains can affect the main chain

polymerization process but also the lateral ordering into a network. The cooperative motions of the rotaxanes are amplified and trigger a reorganization of the system, which is translated into a macroscopic response in the form of a physical state transition.

Chapter VI: Covalent poly[c2]daisy chains and their associated chemical gels

This work was carried out with the collaboration of Dr Guangyan Du and Dr. Prasad Polavarapu for the covalent polymer and Dr. Thomas Lang for the chemical gels, in addition to Dr. Giacomo Mariani and Prof. Eric Buhler for the scattering experiments.

I. Objectives and retrosynthesis

The synthesis of covalent muscle-like polymers has been described by the group of Stoddart[127] and Grubbs[128] (**Figure 45**); in both cases, a Huisgen 1,3-dipolar cycloaddition was used to covalently polymerize the pH-switchable [c2]daisy chains. While being conceptually interesting, these two systems exhibit several limitations. The degree of polymerization reached for these polymers is too low for good candidates as muscle-like materials. In the case of Grubbs, the motion is not reversible without heavy a chemical modification. Additionally, in both cases, no study on their structural parameters in solution has been performed. Although, at first, this covalent approach seems to be less effective than the supramolecular one developed by ourselves, large assemblies of covalently linked [c2]daisy chains present some advantages. In supramolecular polymers, the degree of polymerization depends on the concentration, and solvents/additives can prevent/disrupt the elongation process. From these ascertainments, the synthesis of a covalent polymer with a high degree of polymerization and/or lateral organization would be a great candidate for the elaboration of muscle-like materials made of [c2]daisy chain units.

Based on a design similar to what has been described in previous sections, we envisioned the synthesis of covalent polymer $\mathbf{7^{Ext}}$ (**Figure 86**). A long apolar linker bearing large alkyl chains is planned to be introduced between each [c2]daisy chain unit to 1) ensure solubility in common organic solvents, 2) increase lateral interaction *via* Van-der-Waals and π-stacking interactions, and 3) induce a mismatch between polar and apolar segments to induce lateral organization *via* microphase separation. Polymer $\mathbf{7^{Ext}}$ can be obtained from pseudo-rotaxane **12** and bis-azide **53** in two steps. The precursor of this last compound can be synthesized by coupling the previously prepared 4-bromobenzyl acetate **13** with bis-alkyne **51** using Sonogashira's conditions. This bis-alkyne can be accessed by another Sonogashira coupling reaction between protected alkyne **49** that can be prepared from previously described compound

24 and small bis-alkyne **48** which can be obtained in two steps from commercially available 1,4-dibromobenzene.

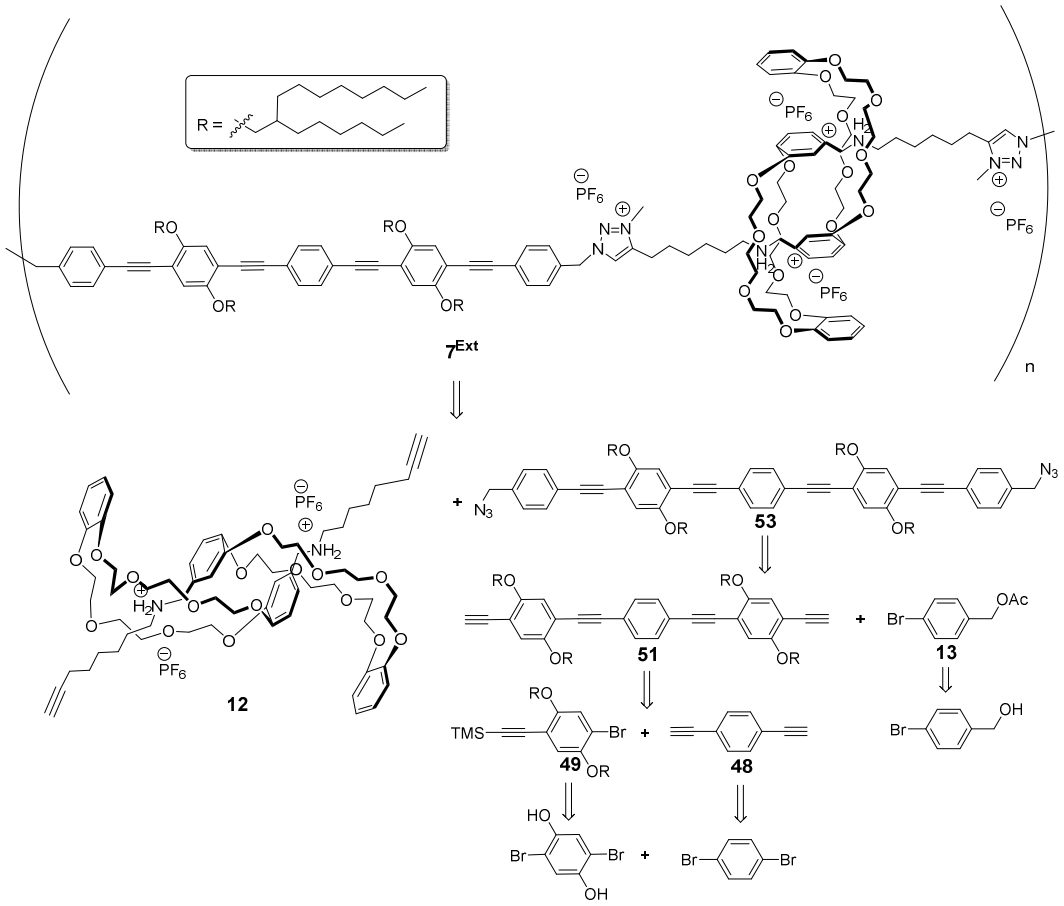

Figure 86 | Retrosynthetic scheme for covalent polymer $\mathbf{7^{Ext}}$.

Later on, the formation of covalent 3D networks made of [c2]daisy chains subunits was considered. The synthesis of these architectures should lead to the formation of chemical gels, which volume should be switchable between a contracted and an extended state. To achieve this goal, the complex linker **53** was no more required and replaced by bis-azide **46** and tris-azide **48**. They can be synthesized in three steps from 2-[2-(2-chloroethoxy)ethoxy]ethanol and hydroquinone in the case of **56** and from 1,3,5-trihydroxybenzene in the case of **58** (**Figure 87**).

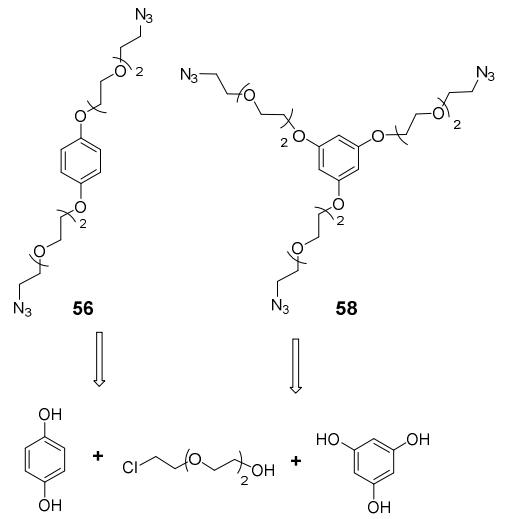

Figure 87 | Retrosynthetic scheme for bis-azide **56** and tris-azide **58**.

II. Results

A. Synthesis of covalent polymer 7^{Ext}

1,4-dibromobenzene was coupled to trimethylsilylacetylene under Sonogashira's conditions to access compound **47** in a very good yield (**Scheme 21**). The alkyne moieties were deprotected under mild basic conditions to quantitatively yield compound **48**, which had to be stored in the fridge as its color slowly turned to black over time at room temperature.

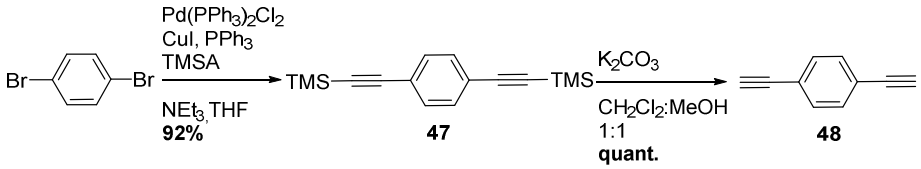

Scheme 21 | Synthesis of bis-alkyne **48**.

Previously prepared compound **24** was coupled to one equivalent of trimethylsilylacetylene to obtained mono-TMS compound **49** (**Scheme 22**). Another Sonogashira coupling reaction was performed to attach this compound to bis-alkyne **48**. The resulting compound **50** was deprotected under basic conditions to yield bis-alkyne **51** in an excellent yield.

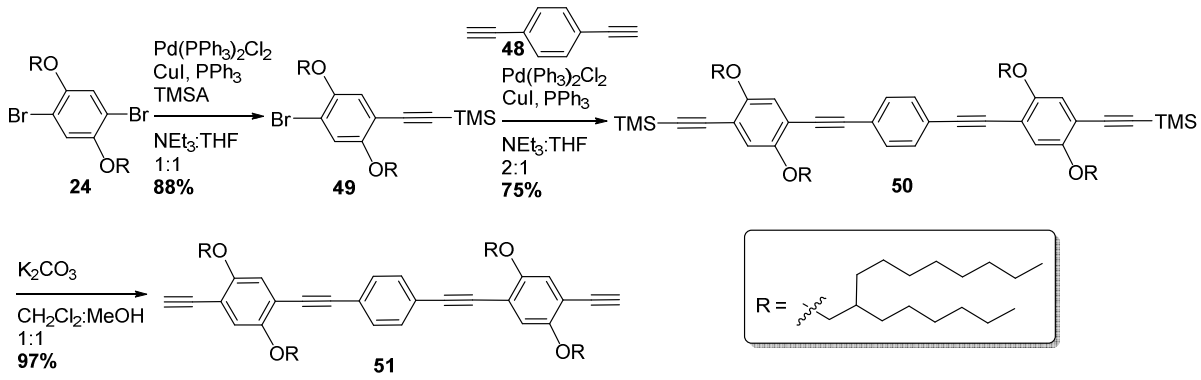

Scheme 22 | Synthesis of bis-alkyne **51**.

Compound **51** was coupled under copper-free Sonogashira's conditions with previously prepared 4-bromobenzyl acetate **13** to yield bis-acetate linker **52** with a 75% yield (**Scheme 23**). Finally, the acetyl protected benzyloxy units were converted into azide moieties in 3 steps. After quantitative deprotection, the alcohols were activated using mesyl chloride and then reacted with sodium azide in a SN_2 reaction to yield bis-azide **53** with a good yield of 58% over three steps.

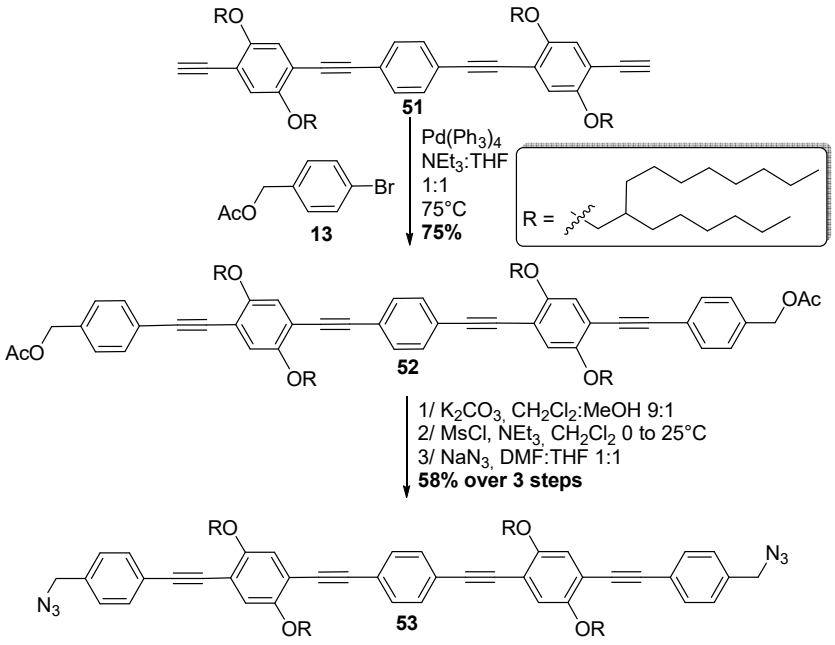

Scheme 23 | Synthesis of bis-azide **53**.

Compound **53** was co-polymerized with pseudo-rotaxane **12** *via* a copper catalyzed 1,3-dipolar cycloaddition under microwave irradiation (**Scheme 24**). The resulting bright-yellow solid was gently washed with cold dichloromethane and diethyl ether to remove remaining reagents and starting materials. ^{1}H NMR spectroscopy in a 4:1 mixture of chloroform and

acetonitrile showed broad peaks and a triazole signal but no alkyne signal, proving the success of the reaction. No starting materials were detected. This polymer was then methylated using a large excess of methyl iodide to quantitatively yield methylated polymer **7^{Ext}**, which can be contracted into **7^{Cont}** by brief treatment with a 1 M sodium hydroxide solution.

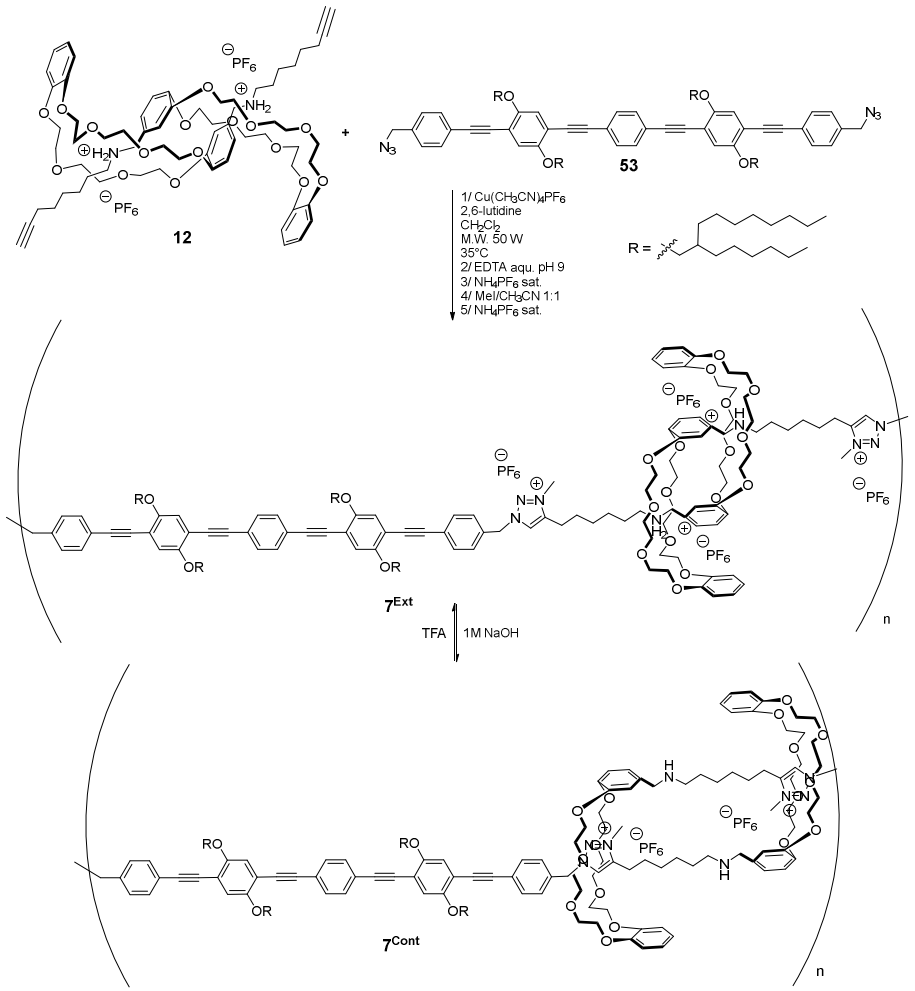

Scheme 24 | Synthesis of polymer **7^{Ext}** and its contraction into **7^{Cont}**.

B. Characterization of the contraction/extension event of 7^{Ext}

The contraction event of **7^{Ext}** was monitored by ^{1}H NMR and Gel Permeation Chromatography (GPC). ^{1}H NMR spectra were performed in a 4:1 mixture of $CDCl_3$ and CD_3CN (**Figure 88**). Upon contraction, typical shift of the triazole signal H_t from δ = 8.07 ppm to 8.93 ppm was observed. Other signals around the new position of the crown ether were also affected, such as protons H_{ar} and H_{ben}. This contraction could be reversed by the addition of acid.

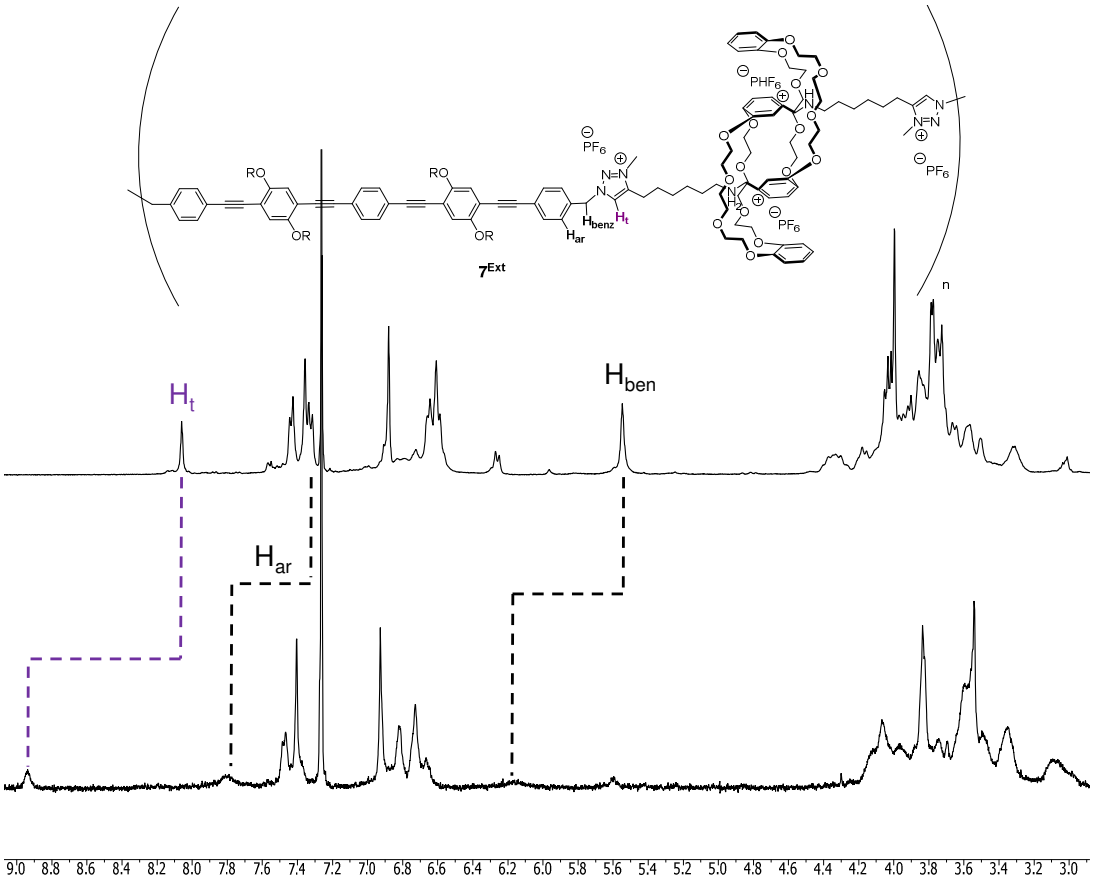

Figure 88 | ^{1}H NMR in a 4:1 mixture of $CDCl_3/CH_3CN$ of a) a 2 mM solution of $\mathbf{7^{Ext}}$ and b) a 2 mM solution of its contracted state $\mathbf{7^{Cont}}$.

The contraction event should be accompanied by a reduction of the overall size of the polymer chains. GPC experiments should show differences of retention times depending on the position of the crown ether, and provide us with an estimate of the molecular weight and degree of polymerization of our polymer. These experiments were carried out using a 0.5 M lithium bromide dimethylformamide solution as the eluent, and with 5 $mg.mL^{-1}$ solution of $\mathbf{7^{Ext}}$ and $\mathbf{7^{Cont}}$. The polymers were detected using a right angle scattering detector (RALS; 90° detection). The results are reported in **Figure 89**.

a

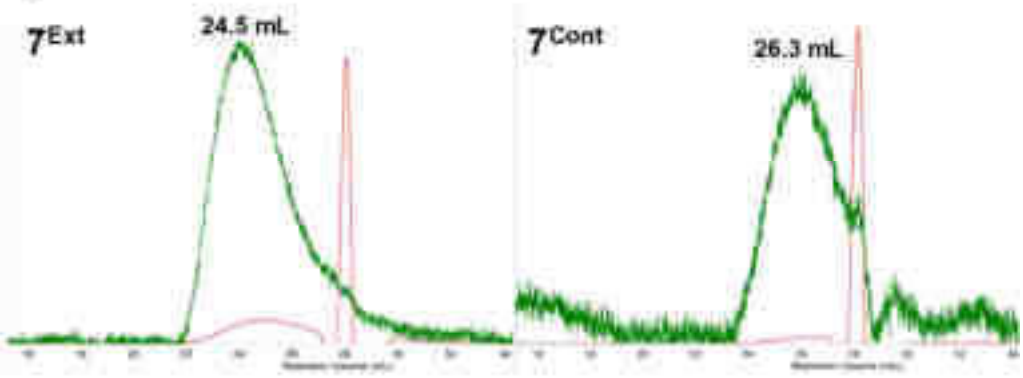

b

	Retention volume (mL)	Intrinsic viscosity (L.g^{-1})	R_g (nm)	M_w (g/mol^{-1})
7^{Ext}	24.5	0.0591	4.6	109 997
7^{Cont}	26.3	0.0355	2.3	47 584

Figure 89 | a) Chromatogram obtained for GPC experiments on **7^{Ext}** and **7^{Cont}**. The red curves represent the signals of the viscosity detector, the green ones the ones of RALS detector. The flow of elution was of 1 mL.min^{-1}. b) Characteristic parameters obtained for **7^{Ext}** and **7^{Cont}** from GPC experiments.

Elution of each polymer displayed different retention volume: 24.46 mL for **7^{Ext}** and 26.31 mL for **7^{Cont}** which is in agreement with a smaller size for **7^{Cont}** (**Figure 89a**). The measured intrinsic viscosities can be used to estimate the gyration radius R_g from a spherical model, giving values of 4.6 nm for the extended polymer and 2.3 nm for the contracted one. From comparison with a polystyrene standard, a molecular weight of M_w = 109 997 g.mol^{-1} was estimated for **7^{Ext}**. From this value, a degree of polymerization of 33 was calculated, which is 33% higher than Grubbs covalent [c2]daisy chains polymer, the longest to date. The contracted polymer however displayed smaller R_g and M_w because these values were estimated from a smaller intrinsic viscosity. Overall, these experiments proved that the combined actuations of the [c2]daisy chains constituting the polymer induced noticeable change of physical properties.

C. Characterization of polymers 7^{Ext} and 7^{Cont} by scattering techniques

Polymers **7^{Ext}** and **7^{Cont}** were characterized by a combination of SANS and SLS in order to determine their structural parameters in solution. The resulting scattered intensities are displayed in **Figure 90**.

Both polymers are almost undistinguishable by comparing their respective scattered intensities for high and mid scattering vectors q, which can be due to the low contrast of these polymers chains. The similarities at high q indicate that the cross section remains unchanged in the contracted and extended states. However, the dimension of this cross-section cannot be calculated due to the lack of a clear decay, indicating dimensions smaller than 1.5 nm. For

medium scattering vectors q, the two curves seem identical. As the scattered intensity in this region is directly proportional to the linear mass density M_L of the polymer, **7**^{Ext} and **7**^{Cont} have very similar or identical M_L values. This can be explained by the small difference expected for both polymers: M_L(**7**^{Ext}) = 560 g.mol^{-1}.nm^{-1} and M_L(**7**^{Cont}) = 640 g.mol^{-1}.nm^{-1}. Indeed, such a small variation of 14% is comparable with the resolution of the SANS technique and might simply not be measurable.

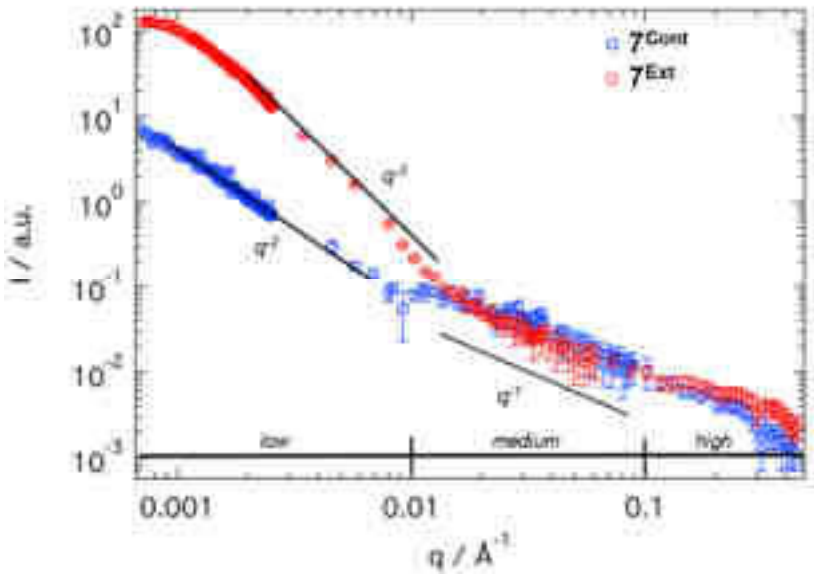

Figure 90 | Scattering intensities measured by SANS for **7**^{Cont} and **7**^{Ext} 2.5 mmol solutions in a 4:1 mixutre of $CDCl_3/CD_3CN$.

On the other hand, behaviors at low q are very different for the extended and the contracted polymers. In this region, **7**^{Ext} displays a scattered intensity increasing proportionally to a q^{-3} slope typical of 3D objects, before ending with a Guinier plateau. This observation allows us to estimate the finite size of these objects, which have a gyration radius R_G of 200 ± 10 nm, corresponding to the size of compact 3D spherical aggregates. For polymer **7**^{Cont}, the increase of the intensity at low q follows a q^{-2} slope. The q^{-1} slope at medium q followed by a q^{-2} one at low q corresponds to the typical scattering pattern of a wormlike chain, which size has to be very long since no decrease of the scattered intensity can be observed over the whole q region. The point at which the transition between the q^{-1} slope turns into a q^{-2} can be used to calculate the persistence length of polymer **7**^{Cont} which is l_P = 19 ± 2 nm. The contour length could not be calculated as the Guinier plateau seems to be located at q values outside the range accessible by static light scattering.

To summarize, while the precise characteristics of the polymer chains such as their linear mass density seemed impossible to distinguish from one polymer to the other, $\mathbf{7^{Ext}}$ and $\mathbf{7^{Cont}}$ displayed a very different behavior for low scattering vectors q. While $\mathbf{7^{Ext}}$ seemed to bend over itself to form spherical aggregates associated with a R_G of 200 ± 10 nm, $\mathbf{7^{Cont}}$ displayed the typical signature of a wormlike chain, which dimension was too large to be determined by these scattering experiments.

The differences between the two conformations adopted by the polymer chains have to be related to the position of the crown ethers on the [c2]daisy chains units. We suggest that, in the extended state, the aromatic linkers aggregate thanks to a combination of π-stacking and Van-der-Waals interactions from their large aromatic core bearing four branched alkyl chains, thus inducing the folding of $\mathbf{7^{Ext}}$ covalent polymer into pseudo-spherical structures, which size could be estimated by scattering experiments. This stacking might be distributed by the proximity of the crown ether macrocycle in polymer $\mathbf{7^{Cont}}$, preventing its organization beyond a wormlike chain structure.

D. Synthesis of a chemical gel 8^{Gelx}

Films made of the previously prepared covalent polymer does not show macroscopic upon contraction/extension of its sub-components. For this reason, we turned ourselves to the synthesis of a 3D chemical network, which gelation should provide a stimuli-responsive material.

Diol **55** was obtained by nucleophilic substitution between dihydroquinone and 2-[2-(2-chloroethoxy)ethoxy]ethanol under basic conditions and using lithium bromide as a catalyst (**Scheme 25**). The free alcohols were then converted into azides using a well known sequence, *i.e.* activation by mesityl chloride followed by nucleophilic substitution with sodium azide, to yield compound **56** in good yields.

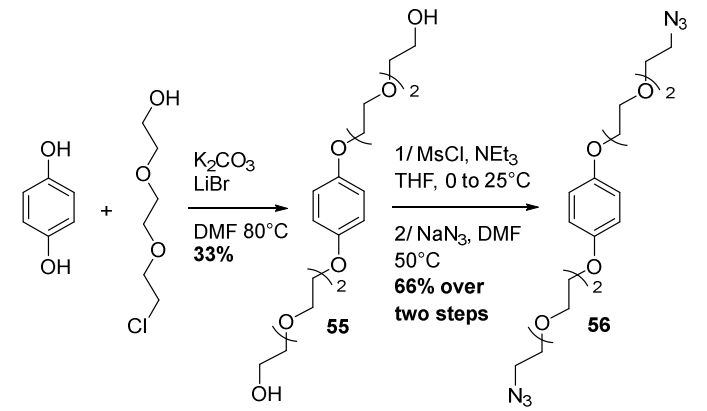

Scheme 25 | Synthesis of bis-azide **56**.

The conversion of 1,3,5-trihydroxybenzene into tris-hydroxy compound **57** was achieved in low yield using a procedure identical to the one used for compound **55** (**Scheme 26**). However, its conversion into compound **58** after activation of the alcohol and substitution with sodium azide was performed with 80% yield over two steps.

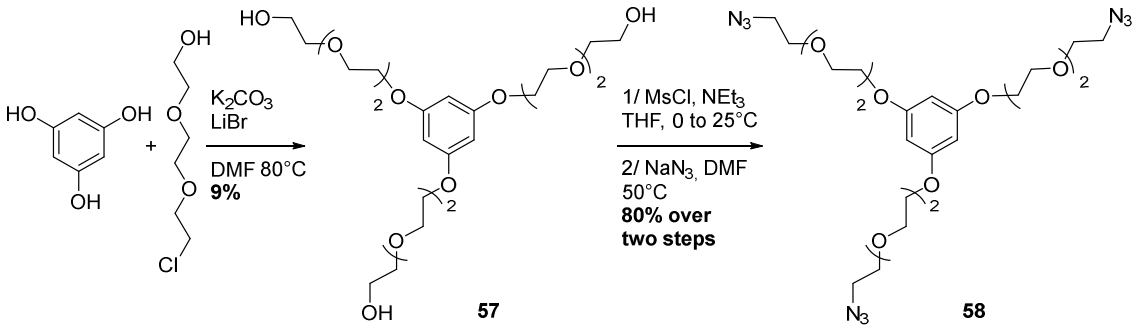

Scheme 26 | Synthesis of tris-azide **58**.

These two compounds were then engaged in a 1,3 dipolar cycloaddition with compound **12** in various proportions depicted on **Figure 91**. The reaction was first performed in a microwave vessel. To our surprise, the formation of a gel-like material was observed after a few seconds of stirring even before using the microwave reactor. The gel could be extracted from the reactor but its shape made it hard to process and purify. As an answer to these issues, the reaction was then performed in a metallic mold, ensuring the formation of a rectangular gel (**Figure 91a**). The reaction provided a plastic-like material which could be swollen up to around 1900% compared to its dry volume in most organic solvents but drastically shrank in aqueous solutions.

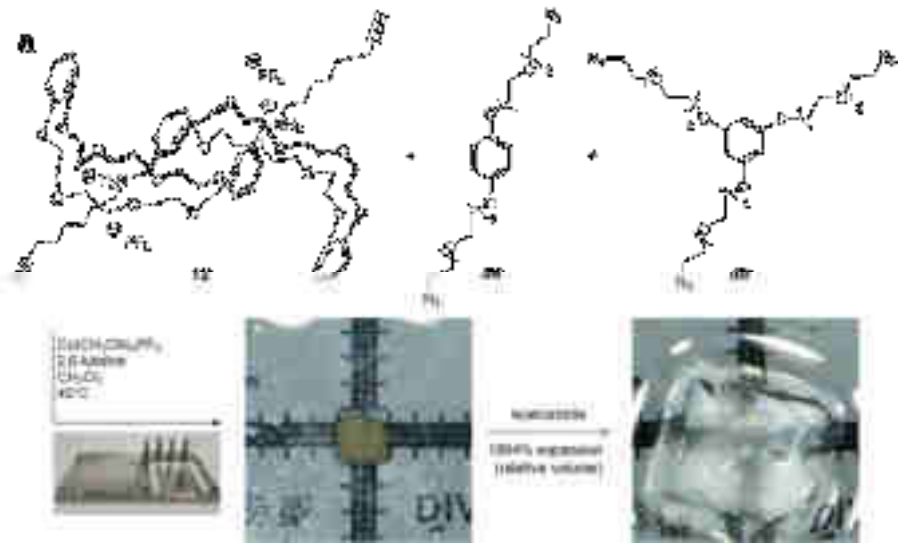

b

Gel	12	56	58
$\mathbf{8}^{\mathbf{Gel1}}$	1	0.33	0.44
$\mathbf{8}^{\mathbf{Gel2}}$	1	0.5	0.33
$\mathbf{8}^{\mathbf{Gel3}}$	1	0.66	0.22

Figure 91 | a) Synthesis of [c2]daisy chains based chemical networks, b) Proportion of components in $\mathbf{8}^{\mathbf{GelX}}$.

While the reaction conditions for $\mathbf{8}^{\mathbf{Gel1}}$ and $\mathbf{8}^{\mathbf{Gel2}}$ resulted in the formation of robust gels, $\mathbf{8}^{\mathbf{Gel3}}$ was too soft and fragile to be manipulated and further studied. Successive immersions in dichloromethane were performed in order to remove possibly remaining starting materials and copper salts were extracted using a pH 8 aqueous solution of ethylenediaminetetraacetic acid. Gel $\mathbf{8}^{\mathbf{Gel1}}$ and $\mathbf{8}^{\mathbf{Gel2}}$ were methylated into $\mathbf{8}^{\mathbf{Gel1M}}$ and $\mathbf{8}^{\mathbf{Gel2M}}$ by immersion in a 1:1 solution of acetonitrile/methyl iodide followed by anion exchange with ammonium hexafluorophosphate. The success of this step will be proven in the following section, by triggering the contraction/extension of the gels.

E. Stimuli-responsive behavior of gels $\mathbf{8}^{\mathbf{GelxM}}$

In its initial protonated state, the [c2]daisy chains constituting the gel are extended. The addition of two equivalents of triethylamine to $\mathbf{8}^{\mathbf{Gel1M}}$ or $\mathbf{8}^{\mathbf{Gel2M}}$ in acetonitrile triggers an obvious reduction of its volume but, unexpectedly, the subsequent addition of trifluoroacetic acid led to the same observation. This result can be explained by the accumulation of salts in the medium. While the gels are well swollen in acetonitrile, it might be possible that an increase of charged species reduces the solvent ability to swell the gel. In order to get around these issues, the gels were treated as follow: a square piece of gel was imaged and measured, before being immersed in a 1 M solution of sodium hydroxide to deprotonate the [c2]daisy chains units. The resulting shrunk gel was swollen back in acetonitrile and measured again. It was then

immersed in an aqueous ammonium hexafluorophosphate solution to protonate the [c2]daisy chains, before being swollen back in acetonitrile and measured again. The pictures are displayed in **Figure 92a**.

To evaluate the size change after each step, a reference ruler was placed next to the gel and used to measure the area of the gel thanks to the software ImageJ. To compare the volume of a gel from one picture to another, we made the approximation that if a contraction/extension process is happening, it occurs in an isotropic manner, so that Equation (2) can be used to estimate the relative volume:

$$V_{rel} = \left(\frac{A_f}{A_i}\right)^{\frac{3}{2}} \quad (2)$$

V_{rel} being the relative volume, A_f the volume after protonation or deprotonation, and A_i the volume before starting the experiment. The results are presented on **Figure 92b**. The volume of $\mathbf{8}^{\mathbf{Gel1M}}$ changed from 100% to 61% after deprotonation and went back to 98% after protonation. The volume of $\mathbf{8}^{\mathbf{Gel2M}}$ decreased from 100% to 68% after deprotonation and went back to 111% after protonation. The fact that the final size exceeds the original size here can be explained by the possible exchange of counter anions of the [c2]daisy chains during the experiments, modifying its swelling ability. In both cases, the volume variation observed is in agreement with the expected response of the [c2]daisy chains units, which proved their successful incorporation in the material and the integration of their nanoscopic motions to the macroscopic scale. Additionally, control experiments with non-methylated gels $\mathbf{8}^{\mathbf{Gel1}}$ and $\mathbf{8}^{\mathbf{Gel2}}$ confirmed this trend. Indeed, only small variation of their volume were observed after the same experiments: 100-99-100% for $\mathbf{8}^{\mathbf{Gel1}}$ and 100-95-105% for $\mathbf{8}^{\mathbf{Gel2}}$ (**Figure 92c**). It confirms that the presence of a second station on the rotaxane is a prerequisite to observe size variations of the gel, confirming the relationship between volume variation at the macroscopic scale and contraction/extension of the [c2]daisy chains at the molecular one. The small variations observed for the non-methylated gels may be due to the slight motions of the macrocycles, due to Brownian motion, but never truly a contracted conformation.

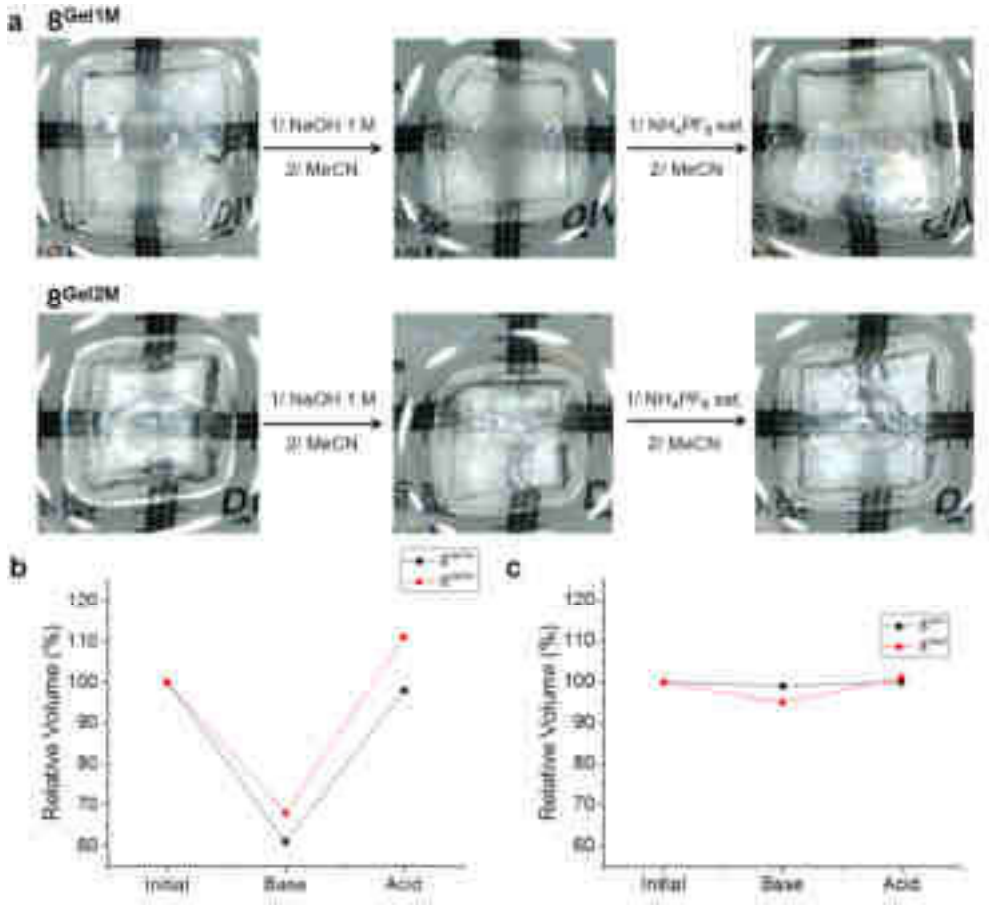

Figure 92 | a) Pictures taken from gels $\mathbf{8}^{\mathbf{Gel1M}}$ and $\mathbf{8}^{\mathbf{Gel2M}}$ during the contraction/extension process. b) Relative volume calculated at each step of the experiment on gels $\mathbf{8}^{\mathbf{Gel1M}}$ and $\mathbf{8}^{\mathbf{Gel2M}}$ c) Relative volume calculated at each step of the experiment on non-methylated gels $\mathbf{8}^{\mathbf{Gel1}}$ and $\mathbf{8}^{\mathbf{Gel2}}$.

Repetitive contraction/extension events were performed on gel $\mathbf{8}^{\mathbf{Gel1M}}$ (**Figure 93**), without degradation of the material and showing successful repeated contraction/extension cycles. Once again, the final size exceeding 100% might be due to the progressive exchange of [c2]daisy chains counter anions.

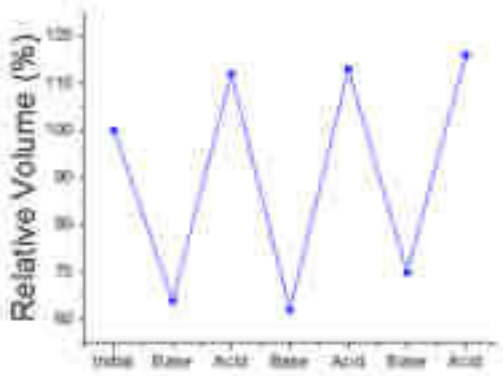

Figure 93 | Relative volume variation upon successive contraction/extension performed on $\mathbf{8}^{\mathbf{Gel1M}}$.

F. Characterization of the contraction/extension event of 8^{Gel1M} by SANS

SANS experiments were performed on gel $\mathbf{8^{Gel1M}}$ swollen in deuterated acetonitrile in its extended and contracted states as shown in **Figure 94**. The signal at mid and high scattering vectors q corresponds to the scattering of the polymer chains composing the chemical network of the gel. Both curves decay at the same q value in the high q region, which is an indication that the cross-section of the chains remains unchanged during extension or contraction. Applying the Guinier approximation for elongated objects to these curves yields a cross-section radius R_{Gc} of 0.49 ± 0.02 nm. Around the medium q region, both curves increase according to a q^{-1} slope, but at different intensities. The difference between the two curves here is crucial, as the signal intensity in this region is only proportional to the linear mass density M_L from the measured polymer. A higher scattered intensity corresponds to a higher linear mass density. Therefore, we clearly observe that the contracted version of $\mathbf{8^{Gel1M}}$ has a higher linear mass density, which is a clear proof that a contraction of the polymer chains occurred upon deprotonation of the [c2]daisy chains. For the extended $\mathbf{8^{Gel1M}}$ gel, a linear mass density M_L = 325 g.mol^{-1}.nm^{-1} was recorded, while for the contracted $\mathbf{8^{Gel1M}}$ gel we measured M_L = 480 g.mol^{-1}.nm^{-1}, corresponding to a noticeable increase of almost 50% upon contraction. The continuous increase of the scattered intensity at low q following a q^{-3} slope also indicates the presence of homogeneities in the network with a size larger than the q range accessible by small angle neutron scattering.

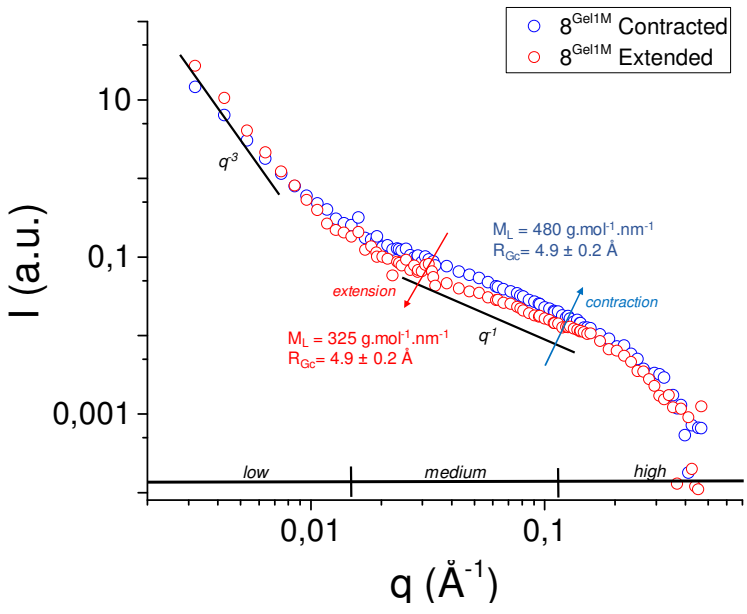

Figure 94 | Scattering intensities measured for extended $\mathbf{8^{Gel1M}}$ and contracted $\mathbf{8^{Gel1M}}$ gels by SANS in acetonitrile.

The fact that the cross-section remains the same in both states and that the linear mass density shows a 50% increase in the contracted version is a clear signature that the macroscopic contraction/extension pictured on **Figure 92** can be directly related to the collective actuation of the [c2]daisy chains and the amplification of their motion up to the millimeter scale.

III. Conclusion

Single chain covalent polymers and chemical gels based on covalent poly[c2]daisy chains were synthesized and characterized, and their stimuli-responsive behavior was investigated by several techniques.

Polymer $\mathbf{7^{Ext}}$ proved to reversibly contract into $\mathbf{7^{Cont}}$ upon deprotonation of the [c2]daisy chains units. GPC experiments indicated that both polymers have different physical properties, *i.e.* different retention times, intrinsic viscosities and gyration radii. From this experiment, a degree of polymerization of 33 corresponding to a molecular weight Mw = 109 997 g.mol^{-1} could be estimated. Then, scattering experiments showed that the conformation of the [c2]daisy chains units have a noticeable influence on the polymer structure in solution. While $\mathbf{7^{Ext}}$ seemed to fold on itself, leading to spherical objects associated to a R_G of 200 ± 10 nm, $\mathbf{7^{Cont}}$ showed the signature of a wormlike chain which length was too large to be estimated. The difference of tertiary structure for these polymers might originate from the ability of the aromatic linkers to stack in the case of $\mathbf{7^{Ext}}$, a phenomenon prevented by the proximity of the crown ether macrocycle in the case of $\mathbf{7^{Cont}}$. The contraction of the polymer chains could not be characterized in details as the contrast of the scattering experiments was not good enough to distinguish the potential difference of linear mass density between the two systems.

Covalent [c2]daisy chains chemical networks were then synthesized from pseudo-rotaxane **9** and two smaller components namely a ditopic and a tritopic azide. The resulting materials were swollen upon addition of organic solvent, providing robust and stable chemical gels. Immersion into a basic solution followed by washing with acetonitrile showed a reduction of the volume of the gel of about 39% in the case of $\mathbf{8^{Gel1M}}$. The gel could retrieve its original volume by immersion into a saturated solution of ammonium hexafluorophosphate and washing with acetonitrile. This contraction-extension cycle could be reproduced several times without degradation of the material. Non-methylated gels did not show noticeable change of volume when treated in a similar way. Moreover, SANS experiments confirmed an increase of 50% of the linear mass density of the polymer chains of the network upon contraction, proving that the macroscopic change of volume observed can be directly correlated to the motions of the

[c2]daisy chains. This work corresponds to the first reversible macroscopic amplification of nanoscopic motions in covalent rotaxanes-based polymeric materials.

Chapter VII: Dual light control of a contractile gel that integrates molecular motors and modulators subunits

This work was carried out with the collaboration of Quan Li, Dr. Justin T. Foy, Jean-Remy Collard-Itté, and of Dr. Olivier Schiffman for the elaboration of a mathematical model.

I. Objectives and retrosynthesis

The integration of molecules able to continuously produce mechanical work when fueled with energy into materials is of great interest for the development of functional devices based on molecular machines. Our group successfully demonstrated in 2015 that light-driven molecular motors reticulated in a polymer network produces gels that contract upon light irradiation (**Figure 95a**).[7] The collective rotations of the motors entangle the polymer chains, reducing the size of the network. However, in such a system, the contraction event cannot be reversed, as the unidirectional nature of the rotation of the molecular motors prevents them to unwind the polymer chains. The elaboration of materials based on molecular machines which motions can be reversed is essential for the development of potential applications. Herein, we propose to include a second component, *i.e.* a modulating unit, that can bypass this issue by releasing the tension energy stored in the entangled chains allowing unwinding. Such a component should have two key features: 1) its releasing capacity should operate under stimuli orthogonal to those which make the motor rotate; 2) the modulator, when irradiated at the same wavelength as the motor, should not prevent the contraction of the gel, while it should operate when the motor is not rotating. Diarylethene switches appear as good candidates for the role of modulating unit: this class of compound can undergo a 6 electrons electrocyclisation to adopt a "closed" state when irradiated in the UV range, while they can be switched back to the original "opened" state when exposed to visible light (**Figure 95d**).[160] We postulated that, in the closed state, formed upon irradiation at similar wavelength to which make the motor turn, this switch should not prevent the entangling of polymer chains, as it lacks single bonds between the right and left parts. However, after contraction of the gel and upon exposure to visible light, rotation around the single bonds of the diarylethene core should unwind the polymer chains, thanks to the tension energy stored by the system (**Figure 95b**). Collaboration with mathematician Dr.

[160] Irie, M., Fukaminato, T., Matsuda, K. & Kobatake, S. Photochromism of Diarylethene Molecules and Crystals: Memories, Switches, and Actuators. *Chem. Rev.* **114**, 12174-12277 (2014).

Olivier Schiffman yielded the elaboration of a complex mathematical model which will not be detailed in this manuscript. However, his most important conclusion is that the network should unwind even with a small quantity of modulating unit, after an infinite amount of time, going back to thermodynamic equilibrium.

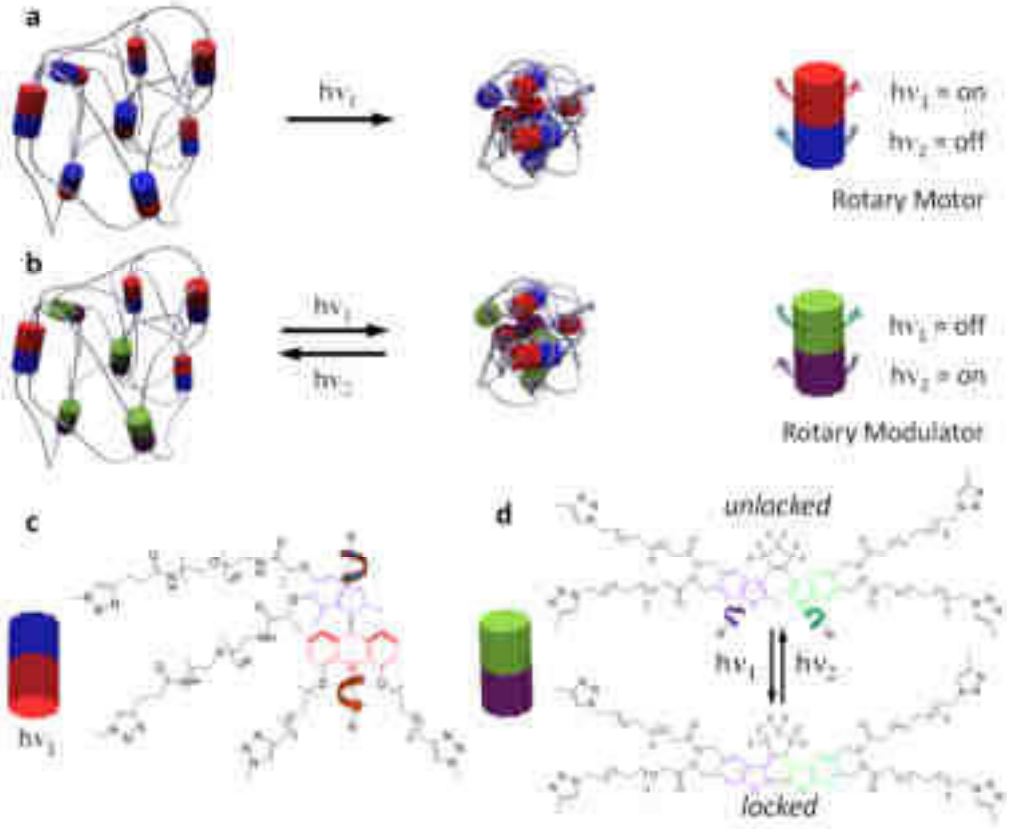

Figure 95 | a) Polymer network with molecular motors as reticulating nodes, which contracts upon light irradiation at a wavelength of energy $h\nu_1$. b) Polymer network with molecular motors and regulating units as reticulating units. The motors rotate at a wavelength of energy $h\nu_1$ while the rotary modulator operates at a wavelength of energy $h\nu_2$. c) Motor/PEG conjugate and its schematic representation. d) Modulating unit included in a polymer network, which can be switched between its opened (unlocked) and closed (locked) form. In the unlocked form, rotation around the single bonds of the diarylethene motif is possible.

The elaboration of such gels requires the synthesis of three components: a tetra-alkyne motor **M-9** and a complementary modulator tetra-azide **R-11** (**Figure 96** and **Figure 97**). These two compounds can be used to access a 1:1 mixture of motor/modulator gel. However, the synthesis of tetra-azide motor **M-10** is also envisioned to vary the proportions of motor/modulator in the material.

The synthesis of both motors has been partially described by Prof. Feringa[161,162] and our group.[7] Motors **M-9** and **M-10** can be obtained from motor **69**, after selective deprotection and functionalization of the bottom and top parts (**Figure 96**). This motor can be obtained from a Barton-Kellogg reaction[141,142] between thioketone **58** and hydrazone **67**. Thioketone **58** can be obtained in four steps from commercially available methacrylic acid and 2,3-dimethoxytoluene, after cleavage of the methoxy group and a Mitsunobu reaction[163] as the main steps.

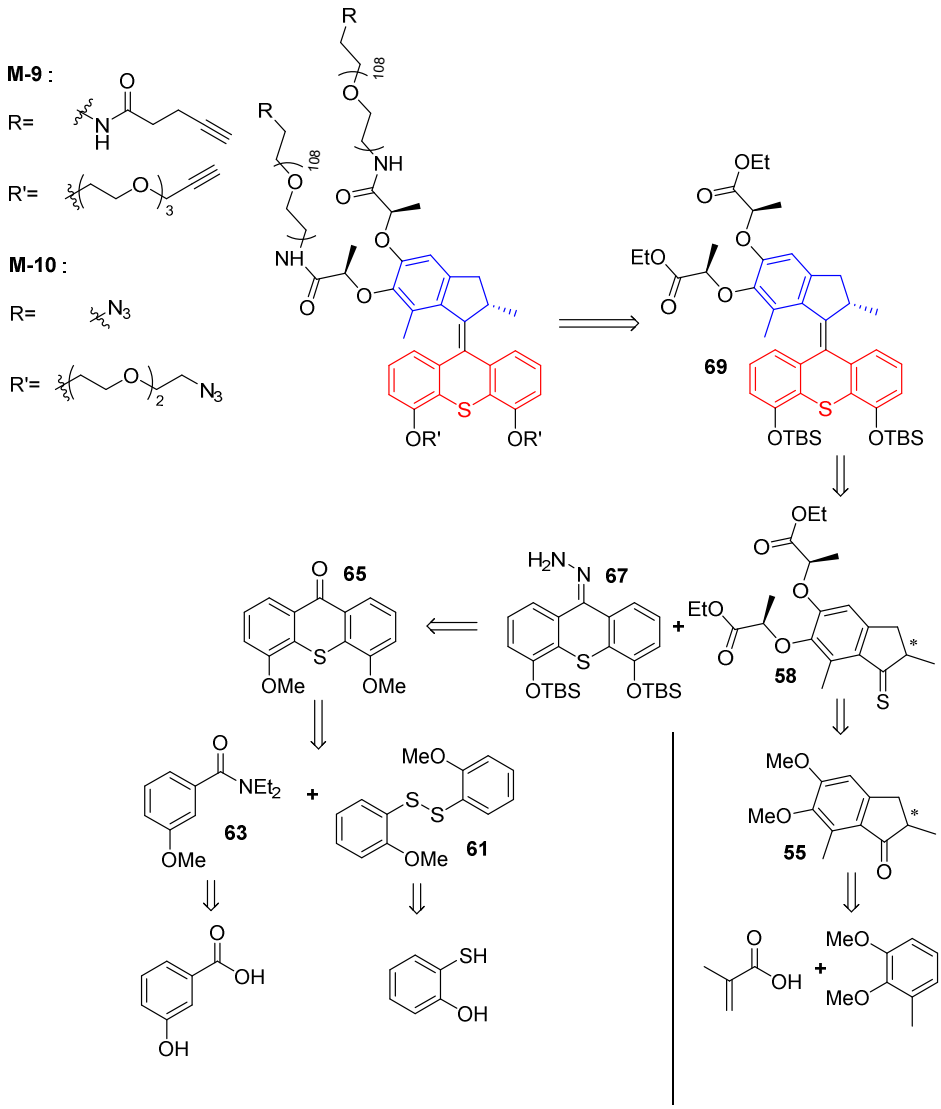

Figure 96 | Retrosynthetic scheme for tetra-alkyne **M-9** and tetra-azide **M-10** motor/PEG conjugates.

Hydrazone **67** can be obtained in three steps from ketone **65** after a series of deprotection and protection reactions. This thioxanthenone could be synthesized from tertiary amide **63** and

[161] London, G. *et al.* Light-driven altitudinal molecular motors on surfaces. *Chem. Commun.* **41**, 1712-1714 (2009)
[162] Pollard, M. M. *et al.* Light-driven rotary molecular motors on gold nanoparticles. *Chem. Eur. J.* **14**, 11610-11622 (2008).
[163] Fletcher, S. The Mitsunobu reaction in the 21 st century. *Org. Chem. Front.* **2**, 739-752 (2015).

disulfide **61** by sequential orthometallation and cyclisation. Intermediates **63** and **61** can be synthesized in two steps from commercially available 3-hydroxybenzoic acid and 2-mercaptophenol, respectively.

The modulating unit **R-11** can be synthesized in 9 steps from 4-bromo-2-methylthiophene (**Figure 97**). Final compound **R-11** can be accessed from tetra-alcohol switch **84** which should be accessible in two steps from compound **82** and perfluorocyclopentene. Compound **82** can be synthesized from acrylic compound **78** after a four-step sequence involving a 6 electrons electrocyclisation, bromination, reduction and protection of terminal alcohols. Bis-alkene **78** is then produced by a sequential bromination and a Heck reaction as main steps from commercially available 4-bromo-2-methylthiophene.

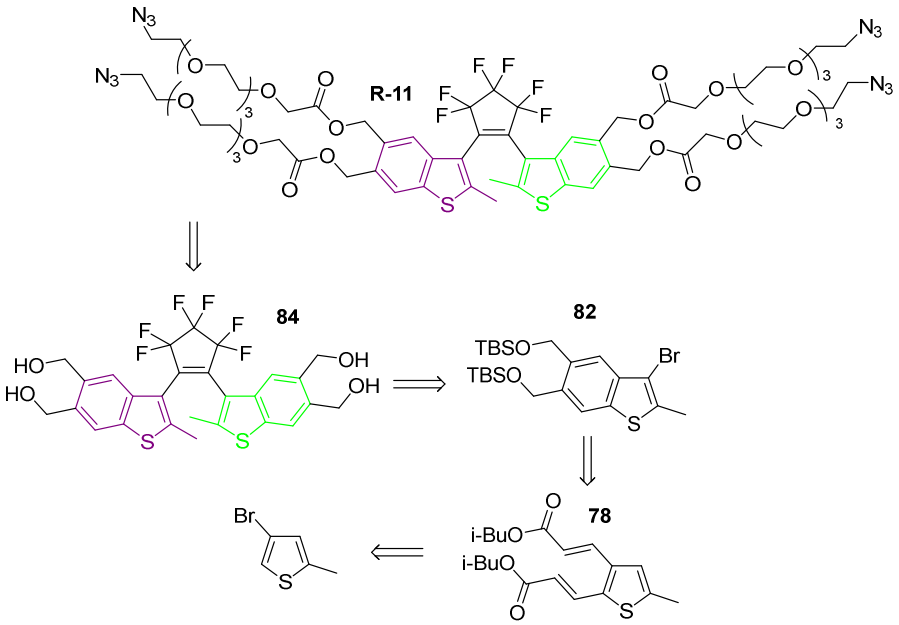

Figure 97 | Retrosynthetic scheme for modulating unit **R-11**.

II. Results

A. Synthesis of motor/polymer conjugates tetra-alkyne M-9 and tetra-azide M-10

Thioketone **58** was synthesized in four steps (**Scheme 27**). First, methacrylic acid and 2,3-dimethoxytoluene were mechanically stirred in hot polyphosphoric acid to yield compound **55**. The methoxy groups were cleaved by the addition of boron tribromide to access the bis-phenol **56**. This compound was engaged in a Mitsunobu reaction to attach lactic acid moieties to the aromatic core. This crucial step turns the two enantiomers of the top part of the motor into diastereoisomers, which will allow separation of the (*R*) and (*S*) episulfides **58** at a later stage.

Finally, ketone **57** was turned into its thioketone equivalent **58** using phosphorus pentasulfide, a reaction which should be performed only prior to the Barton-Kellogg reaction with **67**.

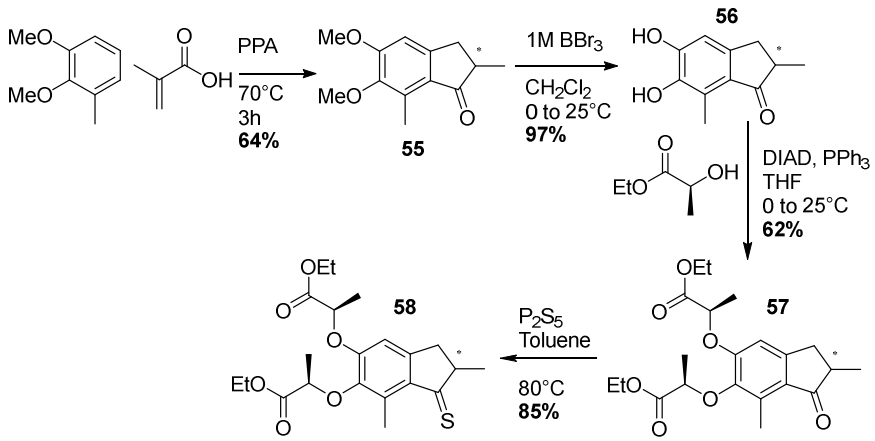

Scheme 27 | Synthesis of thioketone **58**.

The two key intermediates **61** and **63** of the bottom part of the motor were synthesized in two steps as described in **Scheme 28**. On one hand, 2-mercaptophenol was oxidized to give disulfide **60**, which was methylated under basic conditions to yield **61** with excellent yields for each step. On the other hand, 3-hydroxybenzoic acid was converted into its diethylamide equivalent **62** by successive activation of the acid with thionyl chloride and substitution of the chloride by diethylamine, with an excellent yield, and further methylation of the phenol group using methyl iodide provided intermediate **63**.

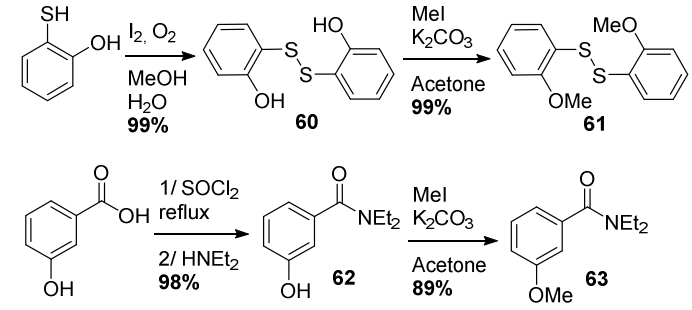

Scheme 28 | Synthesis of disulfide **61** and amide **63**.

Amide **63** was orthometallated in Snieckus conditions[164] before addition of compound **61** yielding intermediate **64** (**Scheme 29**). Treatment of this amide with freshly prepared lithium diisopropylamide (LDA) provided compound **65** in an almost quantitative yield. Methoxy groups were then removed by using boron tribromide and replaced with *tert*-butyldimethylsilyl

[164] Snieckus, V. Directed ortho metalation. Tertiary amide and O-carbamate directors in synthetic strategies for polysubstituted aromatics. *Chem. Rev.* **90**, 879-933 (1990).

groups, yielding compound **66**. The ketone was converted into a thioketone using phosphorus pentasulfide before being treated with hydrazine hydrate at reflux in ethanol to obtain hydrazone **67**.

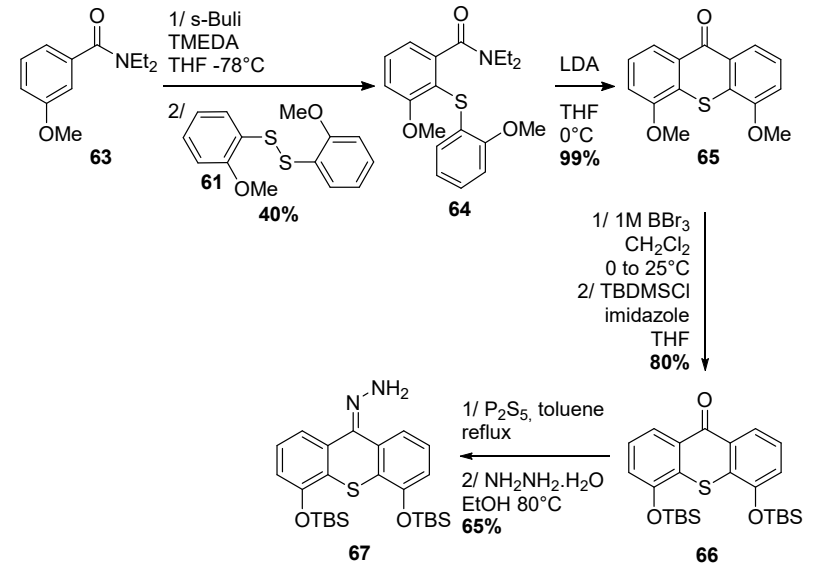

Scheme 29 | Synthesis of hydrazone **67**.

Hydrazone **67** was oxidized in its corresponding diazo derivative before reaction with thioketone **67**, under Barton-Kellogg conditions (**Figure 98a**). This reaction yielded a mixture of stereoisomers **68-(*R*)** and **68-(*S*)** which could be separated by silica gel column chromatography. Subsequent reduction of the episulfide thanks to triphenylphosphine provided motor **69** with a very good yield. The configuration of intermediates **69-(*S*)** and **68-(*R*)** was attributed after X-ray diffraction on crystals obtained by Dr. Quan Li (**Figure 98b**,**c**).

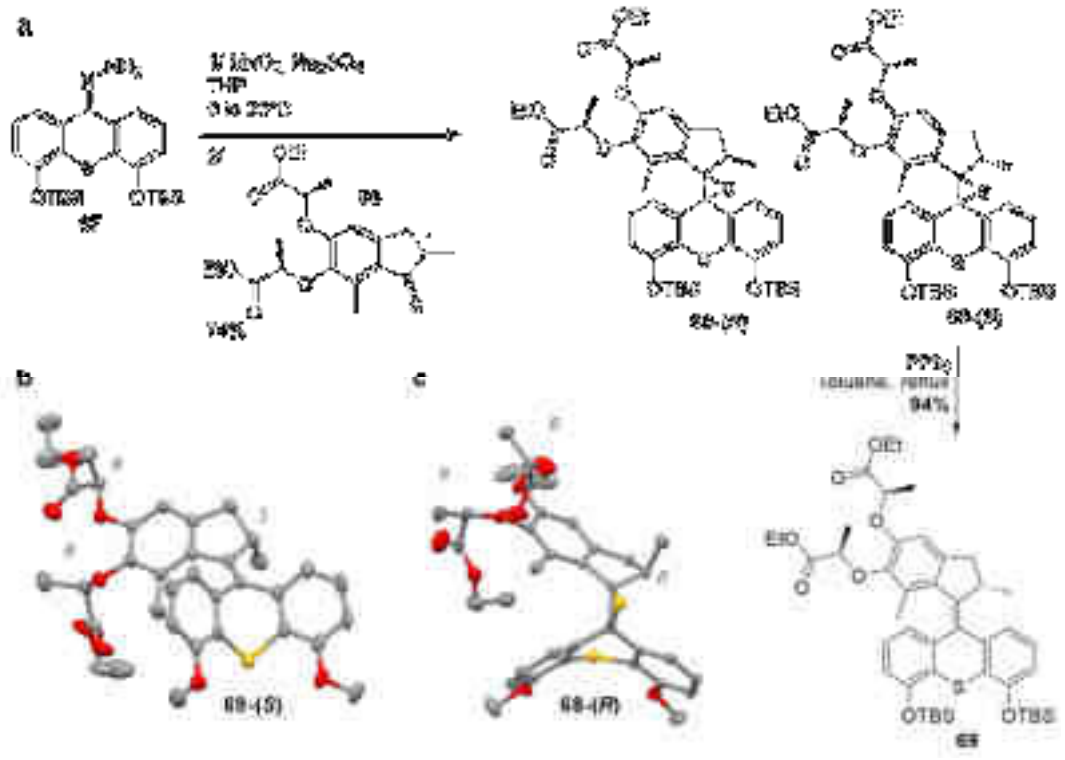

Figure 98 | a) Synthesis of motor **69**, b) Crystal structure of motor **69-(S)**, c) Crystal structure of episulfide **68-(R)**.

The remaining synthetics steps necessary to access motor **M-9** were performed on motor **(S)-69** (**Scheme 30**). The phenol units of motor **69** were first selectively deprotected by using a 1M solution of tetrabutylammonium fluoride in tetrahydrofuran at low temperature, with a 98% yield. A triethyleneglycol chain bearing an alkyne group **71**[165] was grafted on these free phenol units under basic conditions to yield compound **72**, before saponification of the esters into acids to provide bis-acid **73**. Finally, insertion of large commercially available PEG chains presenting two other alkynes *via* a peptidic coupling, yielded tetra-alkyne motor **M-9** after purification by reverse-phase column chromatography.

[165] Michel, O. & Ravoo, B. J. Carbohydrate microarrays by microcontact 'click' chemistry. *Langmuir* **24**, 12116-12118 (2008).

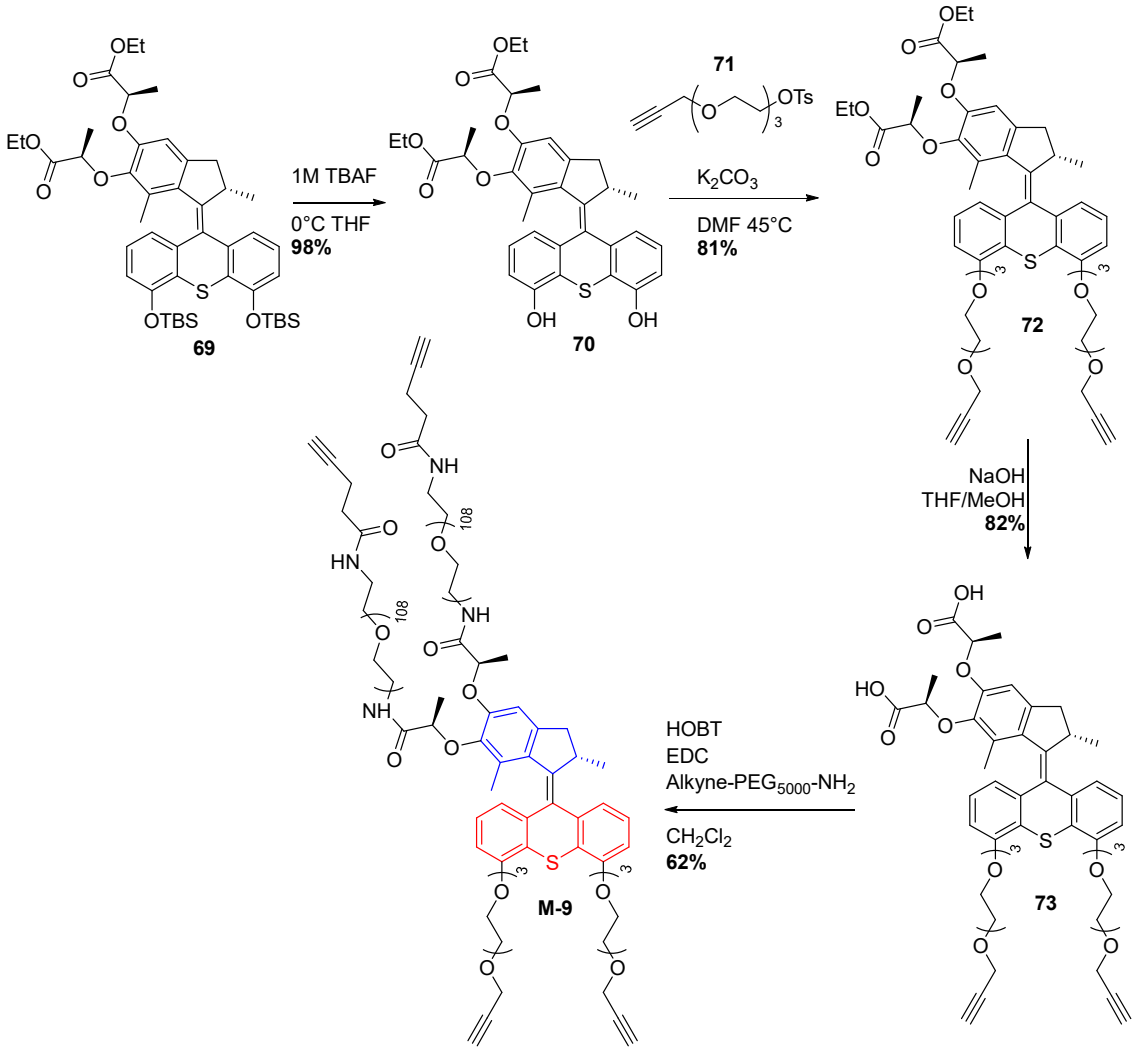

Scheme 30 | Synthesis of tetra-alkyne motor **M-9**.

A similar strategy was used to access **M-10** from bis-phenol **70** (**Scheme 31**). The deprotected compound was reacted with alkyne-tosylate **74**[166] under basic conditions to yield compound **75**, which was saponified to provide the bis-acid **76** in a nearly quantitative yield. Peptidic coupling between the two carboxylic acids with a large commercially available PEG chain ending with an azide yielded motor/PEG conjugate **M-10**, after purification by reverse phase column chromatography.

[166] Reibel, A. T. *et al.* Fate of linear and branched polyether-lipids in vivo in comparison to their liposomal formulations by ^{18}F-radiolabeling and positron emission tomography. *Biomacromolecules* **16,** 842-851 (2015).

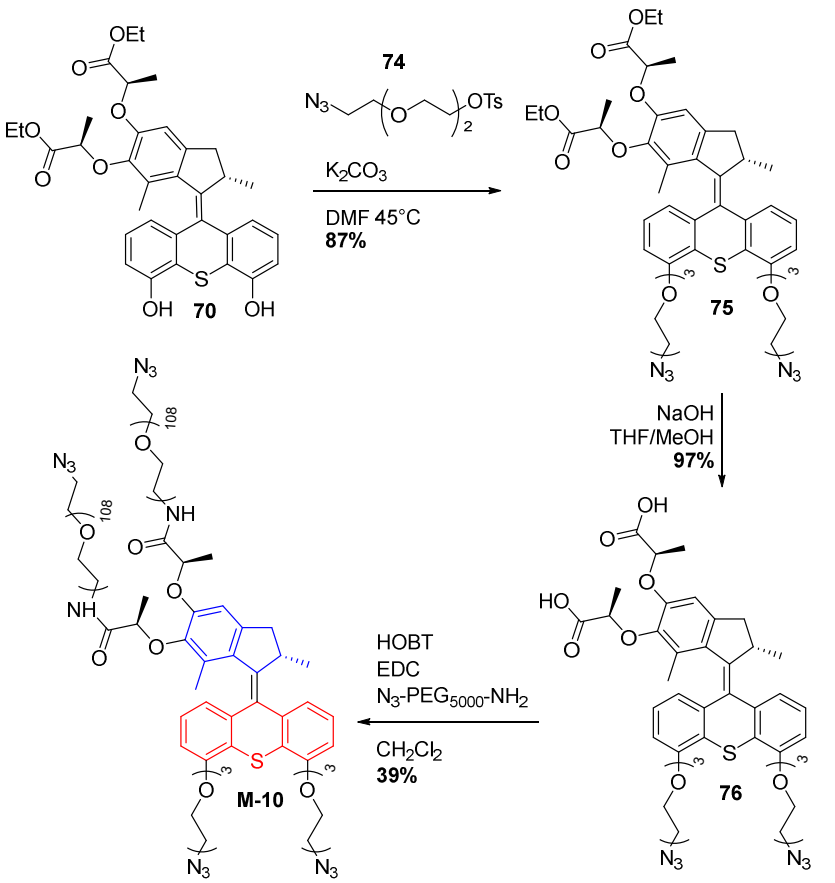

Scheme 31 | Synthesis of tetra-alkyne motor **M-10**.

B. Study of the regulating unit R-11

The synthesis of the modulating unit was first achieved by Dr. Justin T. Foy, post doc in our group, after a nine-step of synthetic sequence (**Figure A 10**). The key steps were an electrocyclisation followed by an oxidation to access compound **79**, and the formation of the switch **83** by lithiation of **82** followed by reaction with perfluorocyclopentene. Final compound **R-11** was isolated as a colorless oil, and its dynamic and photochromic properties were then investigated by ^{1}H NMR, DFT calculations and UV-visible spectroscopy.

In order to operate as an elastic releaser in our system, the modulator **R-11** should have his left and right parts rotating around the single bonds linked to the perfluorocyclopentene moiety, a phenomenon associated to an energetic barrier ideally low enough to perform these rotations at room temperature. The ^{1}H NMR of compound **84** and **R-11** in acetonitrile displayed two sets of signals, indicating that these molecules adopt two distinct conformations in solution. As displayed on **Figure 99a**, these switches can either be in a parallel conformation (P) in which the two "arms" face each other's, or in an anti-parallel conformation (AP) corresponding to a "flat" molecule. The presence of the anti-parallel conformation was confirmed by

crystallization of **84** as showed in **Figure 99b**. Variable temperature NMR was performed in deuterated acetonitrile in order to determine the frequency of interconversion between the two conformations. A solution of **R-11** was heated up to 343 K, revealing a coalescence temperature at 338 K for the aromatic signals around δ = 7.8 ppm (**Figure 99c**). The Gibbs activation energy $\Delta G^{\ddagger}$ was estimated to be 72 kJ.mol^{-1} using the following equations:[167]

$$k_c = \pi \Delta \nu / \sqrt{2} \tag{3}$$

$$\Delta G^{\ddagger} = a T_c \, [10.32 + \log\left(\frac{T_c}{k_c}\right)] \tag{4}$$

Where a = 1.914 x 10^{-2} kJ.mol^{-1}, T_c is the temperature at coalescence in Kelvin, $\Delta \nu$ the change in frequency in Hz, and k_c = π x 19/√2 = 42.2 s^{-1} being the interconversion rate constant.

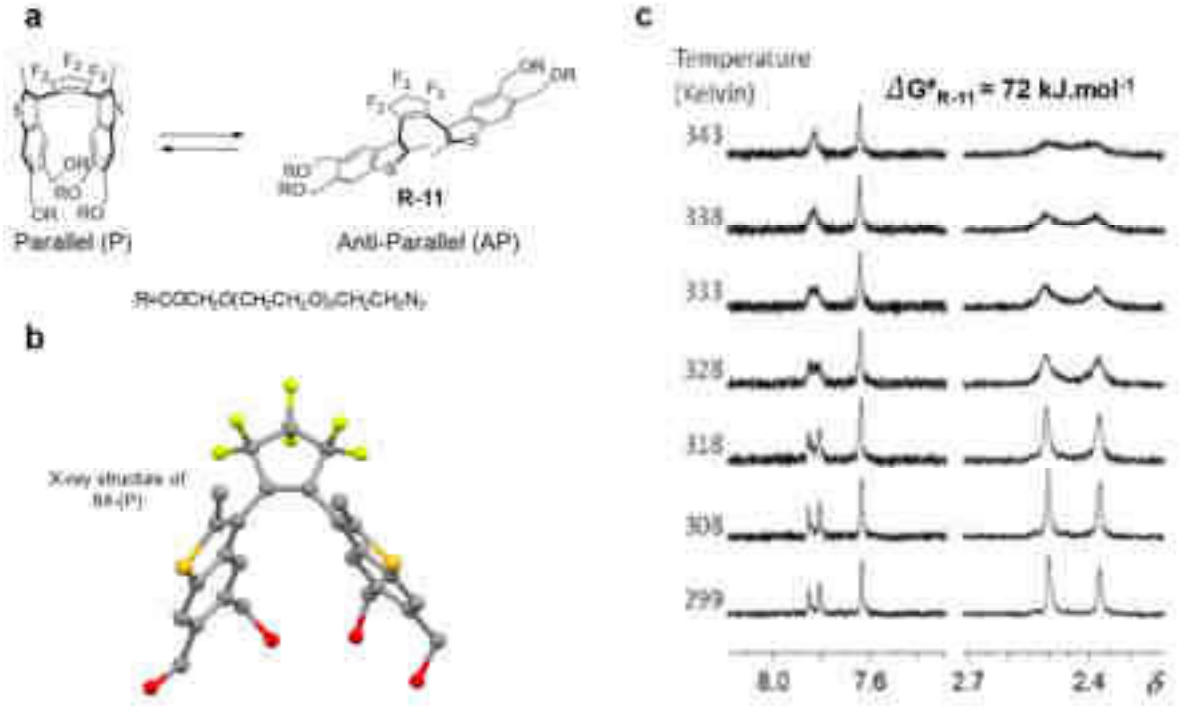

Figure 99 | a) Parallel (P) and anti-parallel (A) conformations adopted by modulator **R-11** in solution. b) Crystal structure of tetra-alcohol **84** in the parallel (P) conformation, c) Variable temperature ^{1}H NMR of the switch **R-11** in deuterated acetonitrile.

This experiment allowed us to evaluate the frequency at which the switch interconverts between (P) and (AP) conformations at room temperature, using the following equation:

$$k = \left(\frac{k_B T}{h}\right) e^{-\Delta G^{\ddagger}/RT} \tag{5}$$

[167] Sandström, V. J. *Dynamic NMR spectroscopy*. (Acedemic Press, 1982).

Where k is the rate, k_b = 1.38 x 10^{-23} J.K^{-1} is the Boltzman constant, h = 6.63 × 10^{-34} J.s^{-1}·is the Planck constant, $\Delta G^{\ddagger}$ the activation energy, R = 8.31 J.mol^{-1}.K^{-1} is the gas constant and T the temperature (293 K).

Based on the previously evaluated activation energy from the NMR experiments, we estimated that the frequency associated with the interconversion between the (P) and (AP) conformations is around 1.5 Hz.

We then performed DFT calculations to evaluate the rotation speed of the arms of the switch (**Figure 100**). A tetra-methoxy model compound was studied, to avoid complex calculation associated with the size of **R-11** and perturbation by intra-molecular hydrogen bonding between the alcohols in **84**. The structures of the parallel and anti-parallel conformations were first optimized with the Avogadro software before being refined with Gaussian using a 6-31 G (d,p) basis.[168] Plotting the energy as a function of the dihedral angle between the five and the six member rings revealed the presence of two different transition states TS1 at 63.2 kJ.mol^{-1} and TS2 at 66.7 kJ.mol^{-1} (**Figure 100a**). Each intermediate was then optimized again to provide the minimized structures of each intermediate, as displayed in **Figure 100b**. TS1 occurs when the methyl from the thiophene is coplanar with the perfluorocyclopentene ring. TS2 occurs when the phenyl group from the benzothiophene is coplanar with the perfluorocyclopentene group. These two transition states were associated with frequencies using equation (5), giving k_{TS1} = 51.9 Hz and k_{TS2} = 12.6 Hz, allowing us to estimate the overall frequency ω_{tot} = 10.1 Hz for a 360° rotation at room temperature. This results indicates that this switch should efficiently release the tension stored in the polymer chain and unwind them.

[168] M. J. Frisch, G. W. Trucks, H. B. Schlegel, G. E. Scuseria, M. A. Robb, J. R. Cheeseman, G. Scalmani, V. Barone, B. Mennucci, G. A. Petersson, H. Nakatsuji, M. Caricato, X. Li, H. P. Hratchian, A. F. Izmaylov, J. Bloino, G. Zheng, J. L. Sonnenberg, M. H. Gaussian 09, Revision D.01. (2009).

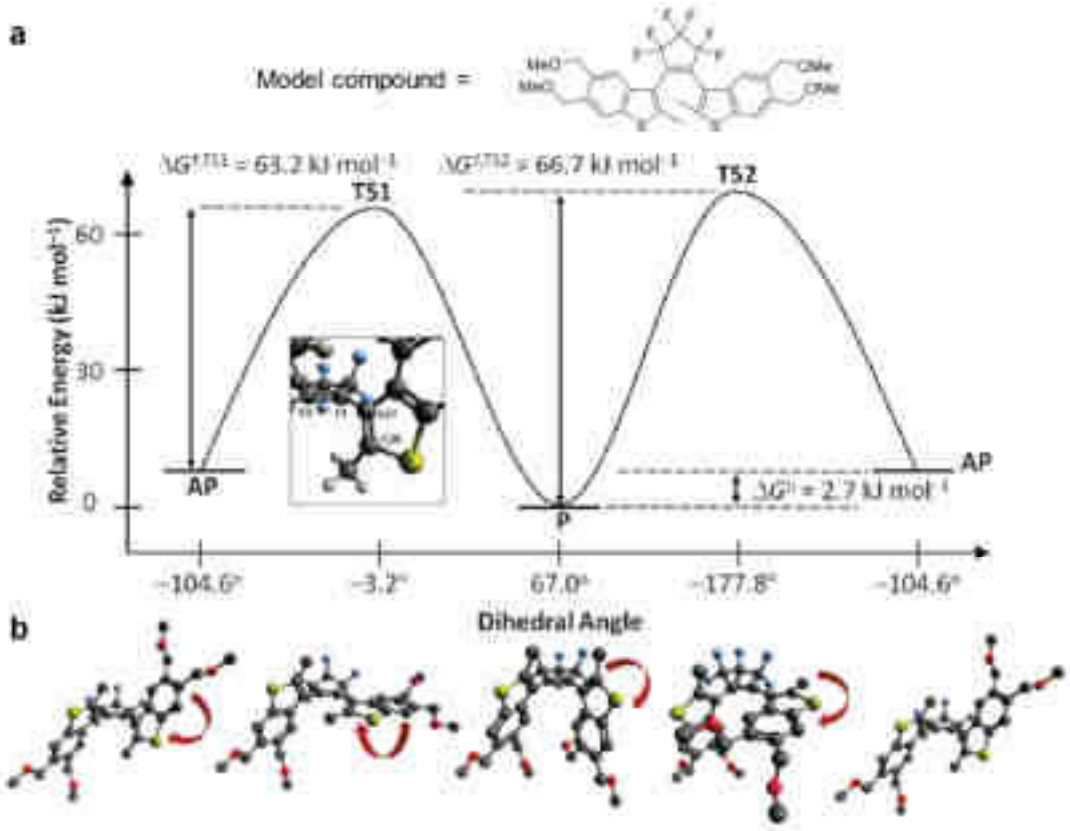

Figure 100 | a) Energetic profile of the rotation around the single bond of a tetra-methoxy model compound. b) Models associated with each conformation studied in these calculations.

Finally, the photochromic properties of compound **84** were evaluated in solution (**Figure 101**). A sample in DMSO-d_6 was irradiated at 300 nm, immediately triggering a change of color typically associated with the closing of the diarylethene switches (**Figure 101b**). UV-Vis spectroscopy showed the appearance of a band at 530 nm, in agreement with the deep purple colour of the sample (**Figure 101a**). No evolution was observed for 5 minutes of irradiation, which means that the system reached the photostationary state. After 5 minutes exposure to visible light, the solution returned to its original yellow color, and the disappearance of the band at 530 nm concomitantly occurred as observed by UV-Vis spectroscopy. This reaction was also monitored by ^{1}H NMR spectroscopy, allowing us to estimate a proportion of 40% of the closed state when irradiated with UV at 300 nm (**Figure 101c**). A similar behavior was observed for modulator **R-11** although minor side products appeared, probably due to the relative instability of the azide moieties under sustained UV irradiation.

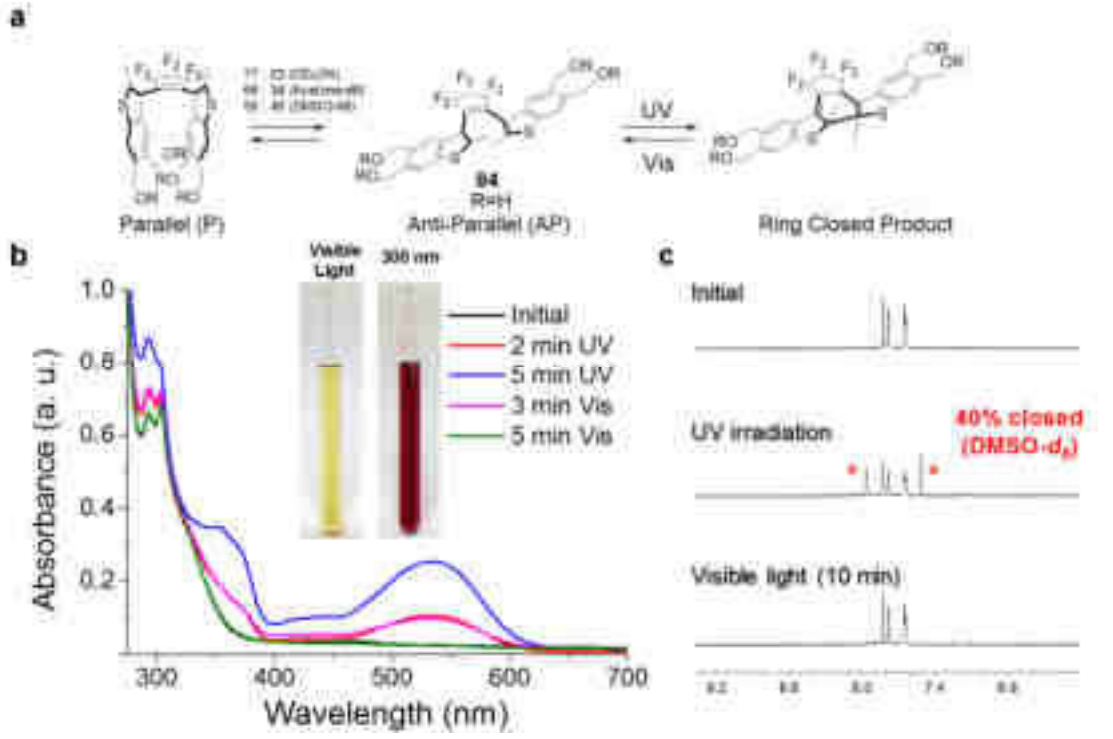

Figure 101 | a) UV-triggered ring closing reaction of compound **84** and reversible opening process under visible light. b) UV-Visible spectra of **84** in DMSO after exposure to UV and visible light. c) Monitoring of the closing/opening process by ^{1}H NMR in DMSO-*d6*.

These experiments prove that, upon irradiation with UV light, the modulator **R-11** should indeed be in a "locked" state, preventing unwinding of the chains. However, under visible light, the "unlocked" state rotates at room temperature and should efficiently unwind the polymer chains.

C. Synthesis and contraction/extension experiments of Gel-XX

The motor/PEG conjugates **M-9**/**M10** and the modulator **R-11** were then engaged in a 1,3-dipolar cycloaddition reaction to synthesized stimuli-responsive chemical gels (**Figure 102a**). After half an hour of reaction, the product was recovered as a robust gel-like material. The reaction can be performed in a vial or in a rheology mold to access gels of precise dimensions, 500 nm thick if not specified otherwise (**Figure 102b**). Varying the proportion of the different components in the reaction allowed the formation of four different motor/modulator **Gel XX** and one control motor **Gel 0** (**Figure 102c**). The gels were then washed by successive immersion into an aqueous EDTA solution, water, ethanol, and finally acetonitrile in which they were stored, in order to ensure complete removal of remaining starting materials and copper catalyst. They were stored under argon at low temperature and hidden from light.

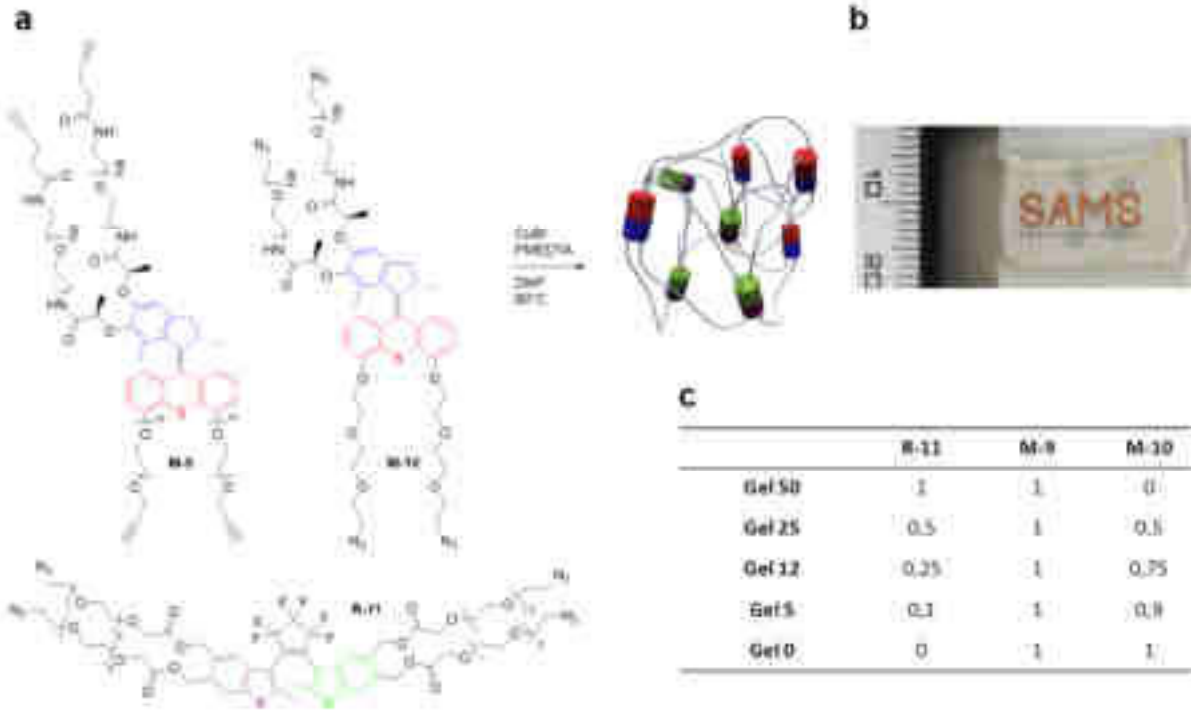

	R-11	M-9	M-10
Gel 50	1	1	0
Gel 25	0.5	1	0.5
Gel 12	0.25	1	0.75
Gel 5	0.1	1	0.9
Gel 0	0	1	1

Figure 102 | a) Synthesis of motor/modulator gels by 1,3-dipolar cycloaddition. b) Picture of a gel synthesized in a rheology mold. c) Proportion of motor and modulator in each synthesized gel.

Pieces of gels were cut with a razor blade and laid down at the bottom of a glass vial, filled with argon-degassed dry acetonitrile. First, irradiation of these gels was performed using a 150W Xenon-Mercury lamp equipped with a 300 ± 10 nm filter. At this wavelength, both the motors and the modulating units absorb, meaning that these conditions should trigger both the rotation of the motor and the closure of the switches. The gels were irradiated and thus contracted until no evolution of their size was observed. Their size was estimated at various times using equation (2) from **Chapter VI**. The event was recorded by a camera and the size of the bottom of the vial was used as an internal reference. **Figure 103** shows the relative size of a piece of **Gel 50** a) at the start of the irradiation at 300 nm, b) after three hours and a half of irradiation and c) after 24h under visible light. As expected, irradiation with UV light triggers the contraction of the gel down to 63% of its original volume, a less pronounced contraction that in the previously reported system. **Gel 50** displays a purple color confirming the closing of the modulating units **R-11** when exposed to UV light. Upon exposure to visible light, **Gel 50** quickly retrieved its colorless aspect, confirming opening of **R-11**. After 24 hours in these conditions, the size measured was the same as before the experiment started.

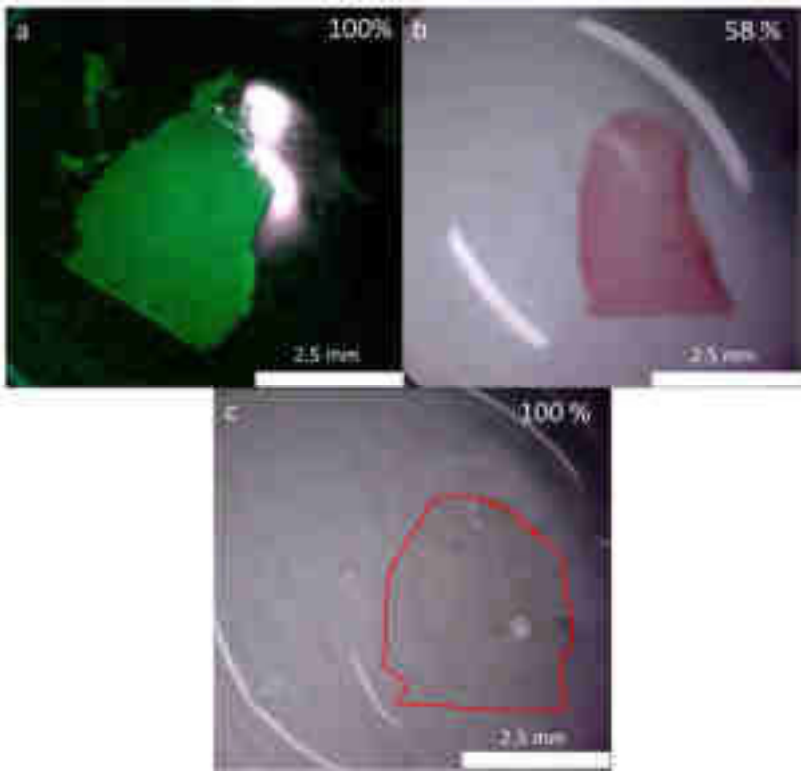

Figure 103 | Snapshots of the **Gel 50** a) irradiated at 300 nm before the start of the experiment, b) after three hours and a half of irradiation, displaying the purple color typical of the closed state of **R-11**, and c) after 24 hours exposure to visible light.

Similar experiments were repeated on the other gels. The results are displayed in **Figure 104**. All gels contract in about three hours and a half of irradiation (**Figure 104a**), while the control gel lacking modulator, **Gel 0**, reaches its minimum size after five hours and a half. Gels containing the modulator subunit contract less that the previously reported systems, contracting only to 68-56% of their initial volume. Decreasing the amount of modulating unit **R-11** improves the initial speed of contraction, which is close to the gel without modulating unit in the case of **Gel 12**. **Gel 50** shows an activation period within its first hour under UV, which presumably can be associated to the two conformations the switch **R-11** can adopt. Indeed, one could imagine that as the motors start pulling on the polymer chains, the force applied to the modulating unit could slightly favor the (AP) conformation over the (P) one. As the (AP) conformation is required to perform the 6-electrons electrocyclisation, such a behavior could explain the late increase of the contraction speed. All the gels approximatively return to their initial volume if given enough time (**Figure 104b**). The gels containing the largest amount of modulating unit **R-11**, **Gel 50** and **Gel 25**, extend at a much higher rate compared to **Gel 12** and **Gel 5**.

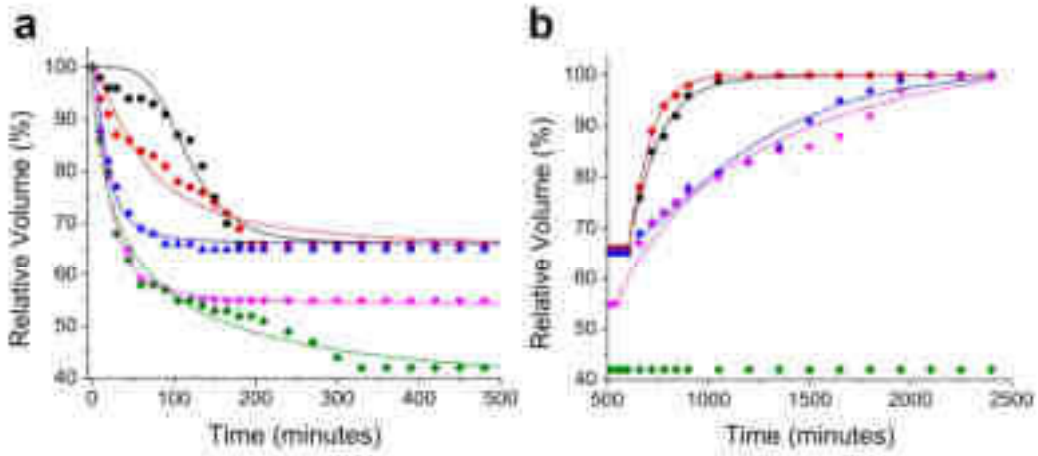

Compound	R-11	M-9	M-10
Gel 50 ■	1	1	0
Gel 25 ●	0,5	1	0,5
Gel 12 ▲	0,25	1	0,75
Gel 5 ▼	0,1	1	0,9
Gel 0 ◆	0	1	1

Figure 104 | Kinetics of a) the contraction of the gels when exposed at 300 nm light and b) the extension of the gels when exposed to visible light.

No extension was observed in the case of **Gel 0**, proving that modulating unit **R-11** is essential to the extension. The fact that the gels reach a less impressive contraction percentage than the previously reported system can be explained as follow: when a certain level of contraction is reached, the tension stored in the polymer chains increases rotation around the central single bonds of **R-11**, a phenomenon that competes with the entanglement induced by the motors **M-9** and **M-10**. Indeed, as previously demonstrated, closing of the switch is not complete under irradiation at 300 nm: thus, there is always remaining free-rotating modulator in the system. This small amount can effectively unwind the polymer chains, as seen in a control experiment in which a contracted gel was left to extend in the dark: a small extension was observed overnight (less than 5%), illustrating the action of the remaining opened switches. The consequence of this observation during the contraction event is that the final volume observed is the result of a steady state bound to the ratio of rotational frequency between the motor and the switch, which are both competing with each other.

D. Dual-light control of Gel 50

To illustrate the modulation of frequencies between the two sub-components of the gel, we performed a dual irradiation of the system, with both visible and UV light (**Figure 105**). While irradiated with UV such as in the previous experiments at a fixed distance, the visible light source, a white LED at 300 Lumen, was placed from 5 to 35 cm away from the sample. A 1 mm thick **Gel 50** was chosen for this experiment as the influence of the modulating unit should be more obvious compared to the gels containing less compound **R-11**. For each position, three hours were given to the gel to reach the steady state (**Figure 105a-e**). A reduction of the volume was observed until 69% of the initial volume when the visible source was 35 cm away from the gel, and accompanied with a progressive increase of the purple color. Putting the visible source back to 5 cm away from the sample allows progressive extension until 93% of its original size after twelve hours.

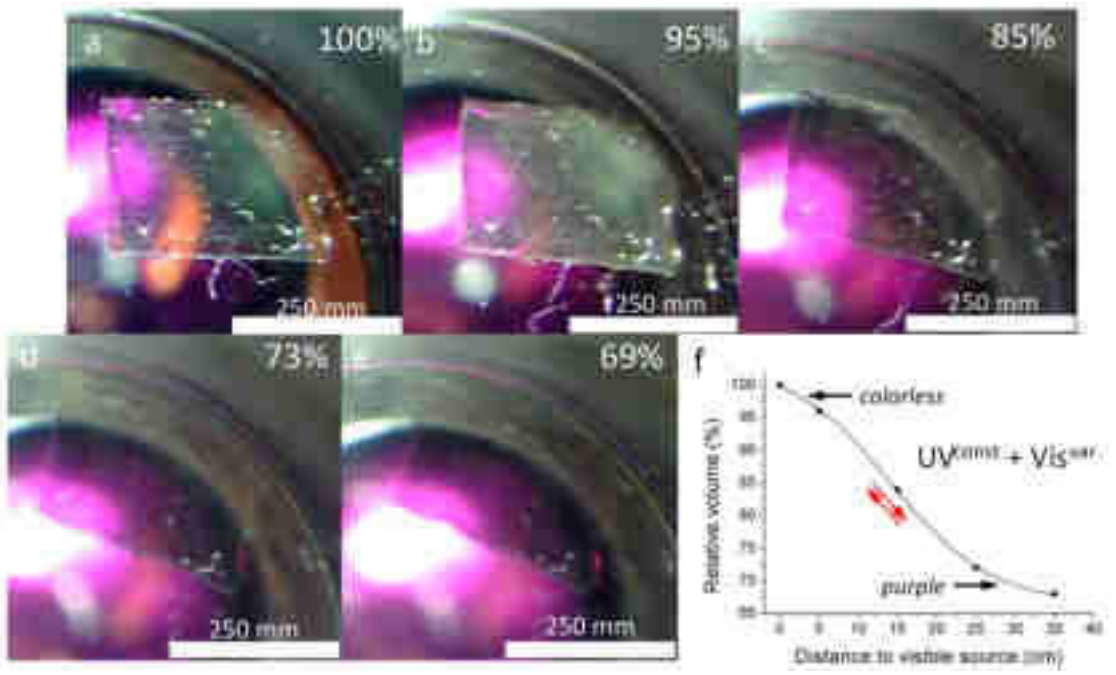

Figure 105 | a-e) Snapshots of a movie of the contraction of **Gel 50** when simultaneously exposed to UV and visible lights, f) Relative volumes of **Gel 50** depending of the distances to the visible light source.

This experiment demonstrates the existence of original non-equilibrium dynamics in a system combining molecular motors and switches. The size of the material seems to be tunable by fine tuning of the proportion of modulating unit operational.

Unfortunately, after these experiments, reproducibility issues appeared, either coming from the progressive decay of the intensity of our light source, degradation of the 300 nm filter, or

other non-identified phenomena. This pushed us to revise our experimental conditions in order to achieve a better understanding and control over this system.

E. Contraction/extension of Gel XX using a TLC lamp

Alternative light sources were tested in order to retrieve perfectly reproducible conditions. It rapidly turned out that only irradiating with a 300 nm 40 mW LED was not enough to contract our gel. Interestingly, adding the irradiation from a 365 nm TLC tube to this experimental setup did trigger the expected contraction of the gel. Going back to the 300 nm filter conjointly used with the 150W Xenon Mercury lamp, careful examination revealed that the filter did not completely prevent some wavelength above 300 nm to go through, especially around 360 nm. Irradiation around 360-365 nm is often the wavelength of choice to activate light driven molecular motors described by Prof. Feringa in the literature. We concluded that, to obtain efficient contraction of our gel, both wavelengths might be required: irradiation around 300-310 nm should close the modulating unit **R-11** while irradiation around 365 nm should trigger the rotational activity of motors **M-9** and **M-10**. Indeed, irradiation of gels at 365 nm using a 4 W TLC tube yielded only minor contraction after three hours of experiment (around 5 to 10% depending on the gels), while irradiation at 300 nm using the LED did not yield any visible change aside from the purple coloring. Irradiations performed using both wavelengths at the same time, with a 300 nm LED and a 4 W 365 nm TLC tube, indeed yielded contractions followed by extensions similar to what was previously observed.

However, the use of a small LED with a small cone of irradiation did not allow for perfectly homogeneous closing of the switches **R-11** in the irradiated gels, as proven by the clear gradient of color observed at their surface. To overcome this issue, a modified TLC lamp was engineered to contain a 6 W 312 nm tube and a 6 W 365 nm one. Irradiation with the 6 W 312 nm tube showed clear purple coloring of the gel. Using both tubes at the same time, behavior similar to what has been previously described was observed for all the gels, as illustrated on **Figure 106**.

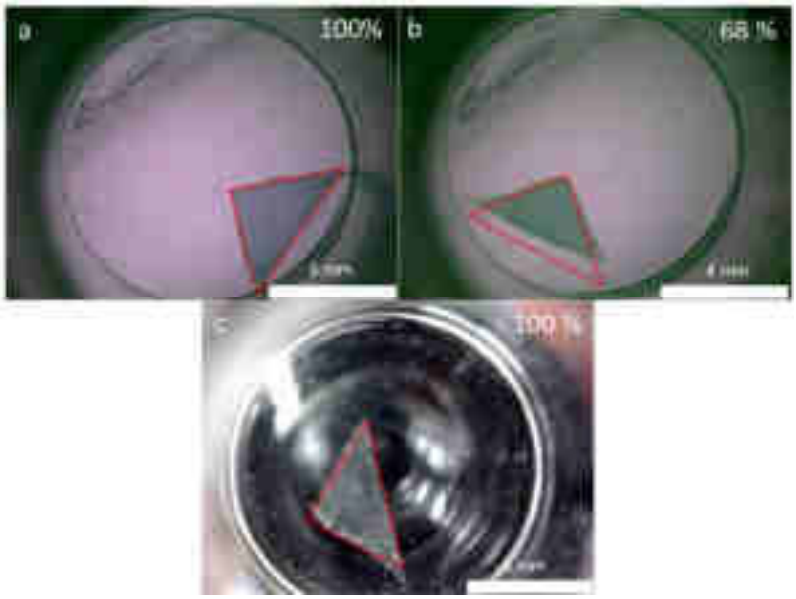

Figure 106 | Snapshots from a video of the contraction of a piece of **Gel 25** under irradiation at 312 and 365 nm, with their relative volume, a) before experiment, b) after contraction, c) after extension when exposed to visible light. The red triangle represents the size of the original piece of gel, and has the same dimension on every picture.

.However, some issues are still unsolved at that time. Indeed, the quite intense irradiation received by the gel in these conditions sometimes colors it in yellow. As this happen, only partial extension follows the contraction. It seems that side products preventing unwinding of the polymer chains are formed,[169] or new cross-linking nodes are created thanks to undesired photo-triggered processes. Indeed, although the diarylethene switches and Feringa's motors are described as resilient toward UV irradiation,[160,170] it often refers to repeated short irradiation times, while our experiments involve several hours-long irradiations. Continuous irradiation also sometime induces curling of the films, which prevents accurate measurement. This issue has been solved by synthesizing amorphous gels in vials, and using non-perfectly flat pieces in experiments. Work toward the resolution of these issues is in good progress at the time this manuscript is being written.

III. Conclusion and perspectives

Tetra-substituted molecular motors/PEG conjugates **M-9** and **M-10**, as well as modulating unit **R-11** were successfully synthesized and used to produce chemical gel *via* 1,3 dipolar cycloadditions. The modulator **R-11** was proven to perform the typical 6-electrons cyclization

[169] Fredrich, S., Göstl, R., Herder, M., Grubert, L. & Hecht, S. Switching diarylethenes reliably in both directions with visible light. *Angew. Chem. Int. Ed.* **55**, 1208-1212 (2016).
[170] Feringa, B. L. The art of building small: from molecular switches to molecular motors. *J. Org. Chem.* **72**, 6635-6652 (2007).

expected for this class of molecules, and to display freely rotating extremities in the open state as demonstrated by DFT calculations. This last characteristic made it an efficient modulating unit, able to unwind polymer chains in the open state.

Chemical gels containing various proportion of modulating unit **R-11** were synthesized. They were all proven to contract upon UV light irradiation and extend upon exposure to visible light, while a gel containing no amount of **R-11** did not show any variation of its volume when exposed to visible light after contraction, confirming the releasing properties of the modulating unit. The orthogonal frequencies used to stimulate one component or another allowed for tuning the activity of each component in the gel, as proven by the dual-light experiments.

Despite the still ongoing investigations to reach perfect experimental conditions, these results describe the first report of a fully non-equilibrium system combining two types of components, *i.e.* a light driven rotary molecular motor and a modulating unit in the form of a photochromic switch. As proven by the extensions observed for these systems, the inclusion of the modulator indeed appears as a solution to overcome the unidirectional limitation intrinsic to a molecular ratchet-based stimuli responsive material.

General Conclusion and Perspectives

The inclusion of functional molecular machines in materials has been a challenge for chemists over the last years. Combining the motions of thousands of molecular machines at the same time is an exciting perspective in nanotechnology and for the elaboration of new classes of stimuli-responsive materials. Following the work initiated by our group in 2012 for the [c2]daisy chains[6] and in 2015 for the molecular motors,[7] the work described in this thesis proves that such stimuli-responsive materials can be produced by combining supramolecular chemistry, ambitious molecular design and demanding organic synthesis.

The three first chapters show how [c2]daisy chain units can be used to synthesize stimuli-responsive materials and architecture responding at a scale several orders of magnitude above the size of these molecular machines. The progression described in this manuscript shows the inclusion of [c2]daisy chains in first, supramolecular fibers showing response upon contraction/extension at the microscopic scale.[171] Then, a macroscopic response was obtained in the form of a physical state transition in the case ureidopyrimidinone-based [c2]daisy chains. The high level of organization of molecular machines in this system allows for the gelation of the polymer chains, a state in which the rotaxanes remained responsive toward chemically-induced contraction/extension. Finally, a covalent strategy was used to synthesize stimuli responsive polymer chains but, more noticeably, chemical gels which size could be changed by concerted contraction/extension of the [c2]daisy chain units, as proven by neutron scattering experiments. This example represent the first macroscopic reversible contraction/extension of a [c2]daisy chain-based covalent material.

Future work on improving the [c2]daisy chains sytems should focus on 1) the use of rotaxanes responding to different stimuli such as light or redox processes and 2) the orientation of the polymer chains in order to obtain an anisotropic response upon contraction/extension of the material.

The last chapter describes how the inclusion of a modulating unit in a contractile network based on light-driven molecular motors allows the reversibility of the contraction. Both components can be independently controlled by orthogonal signals which allows for tuning the macroscopic response upon light irradiation with two light sources. This unprecedented success

[171] Goujon, A. *et al.* Hierarchical Self-Assembly of Supramolecular Muscle-Like Fibers. *Angew. Chem. Int. Ed.* **55**, 703-707 (2016).

is the first example of molecular motor-based out of equilibrium materials showing a reversible behavior, by the careful design of its nanoscopic components.

Ongoing research on this topic includes the synthesis of oscillating out-of-equilibrium systems. Indeed, taking advantage of reversible links such as supramolecular association, dynamic covalent bonds or mechanosensitive moieties could allow the synthesis of a system in which the system unwind itself by mechanically induced transient dissociation of the network. We should also aim for the synthesis of gels able to produce an anisotropic contraction, for example by using liquid crystalline polymer chains instead of polyethylene glycol ones.

It is clear that the materials and supramolecular systems described in this thesis, resulting from a work at the interface between supramolecular chemistry, polymer chemistry, organic synthesis and nanotechnologies, are not yet potential candidates for commercially available artificial molecular muscles. However, this work provides interesting insight about the consequences of molecular motions over the physical properties of materials. Even if widely accessible molecular machines-based materials are still a lasting objective, we believe that some of the achievements reported in this thesis are the first steps toward a new class of materials, which properties and size can be tuned by controlled molecular motions.

Experimental Part

1) General procedures

I. Solvent and chemical reagents

All *reagents and solvents* were purchased at the highest commercial quality and used without further purification unless otherwise noted. Dry solvents were obtained using a double column SolvTech purification system. Water was deionized by using a milli-gradient system (Millipore, Molsheim, France). All reactions were carried out under argon atmosphere except for when water was used as solvent. Microwave reactions were carried out with a single mode cavity Discover SP Microwave Synthesizer (CEM Corporation, NC, USA), producing continuous irradiation at 2455 MHz and equipped with simultaneous external air-cooling system. Yields refer to spectroscopically purified (^{1}H NMR) homogeneous materials.

II. Chromatographic methods

Thin Layer Chromatographies were performed using silica on TLC Al foils (silica gel matrix with fluorescent indicator 254 nm, thickness: 500 µm, Sigma-Aldrich). In most cases, irradiation using a *Bioblock VL-4C* UV-Lamp (6 W, 254 nm and/or 365 nm) as well as *p*-anisaldehyde, phosphomolybdic acid and Cerium ammonium molybdate stainings were used for visualization. *Ultra Performance Liquid Chromatographies coupled to Mass Spectroscopy* (UPLC-MS) were carried out on a *Waters Acquity UPLC-SQD* apparatus equipped with a PDA detector (190–500 nm, 80Hz), using a reverse phase column (Waters, BEH C_{18} 1.7 µm, 2.1 x 50 mm), the MassLynx 4.1 – XP software and a gradient (water-acetonitrile + 0.1% TFA) as eluent.

III. Analytical methods and instruments

A. Nuclear Magnetic Resonnance

^{1}H NMR spectra were recorded on a Bruker Avance 400 spectrometer at 400 MHz and ^{13}C spectra at 100 MHz, and on a *Bruker Avance I* spectrometer at 500 MHz for ^{1}H NMR and 125 MHz for ^{13}C at the Service de Résonnance Magnétique Nucléaire at the Faculté de Chimie. The spectra were internally referenced to the residual proton solvent signal ($CDCl_3$: 7.26 ppm, CD_3CN: 1.94 ppm, CD_3OD: 3.31 ppm for ^{1}H spectrum, and $CDCl_3$: 77.16 ppm and CD_3OD: 49.15 ppm for ^{13}C spectrum). For ^{1}H NMR assignments, the chemical shifts are given in ppm. Coupling constants *J* are given in Hz. Peaks are described as singlet (s), doublet (d), triplet (t), quartet (q), multiplet (m), broad (br), broad singlet (brs) and broad multiplet (brm).

B. Mass spectrometry

ESI-MS mass spectra were recorded on a SQD apparatus from Waters. MALDI-TOF mass spectra were recorded on a Bruker Daltonics AutoflexII TOF spectrometer. HRMS mass spectra were recorded on a Micro-Q-TOF apparatus from Bruker.

C. UV-vis-NIR-experiments

UV-Vis-NIR spectra were recorded on a UV-Vis-NIR spectrophotometer Perkin Elmer – Lambda 25.

D. Elemental analyses

Elemental analyses were performed by the Service de Microanalyse at the Institut Charles Sadron.

E. Gel Permeation Chromatography (GPC)

GPC experiments were performed at the Institut Charles Sadron at the Plateforme de caractérisation des polymers, on three PLgel-B columns (granulometry: 10 µm, length: 30 cm, internal diameter: 7.5 mm, separation in the $10^3 – 10^7$ g.mol^{-1}). A triple detector from Viscotek was used (light scattering, viscometer, refractometer). A 0.5 M lithium bromide solution of HPLC-grade dimethylformamide was used as solvent. Rate of flow: 1 mL/min. The samples were dissolved in the solvent 24 h prior to experiment and heated up to 50°C before being filtered on a 0.45 µm PTFE and injected.

F. Transmission Electron Microscopy (TEM)

TEM experiments were performed using a CM12 Philips microscope equipped with a MVIII (SoftImaging System) CCD camera. Samples were analyzed in Bright Field Mode with a LaB_6 cathode and 120 kV tension. Image treatments were performed by using analySIS (Soft Imaging System) software. For the sample preparation, a carbon-coated copper grid was placed on a Whatman filter paper. Then, a 5 µL drop was casted on the grid and the grid was left to dry at air before analysis.

G. Atomic Force Microscopy (AFM)

Atomic force microscopy (AFM) images were obtained by scanning the samples using a Nanoscope 8 (Bruker) operated in Peak-Force tapping mode. Peak-Force AFM is based on Peak force tapping technology, during which the probe is oscillated in a similar fashion as it is in tapping mode, but at far below the resonance frequency. Each time the tip and the sample are brought together, a force curve is captured. These forces can be controlled at levels much lower

than contact mode and even lower than tapping mode allowing operation on even the most delicate soft samples, as is the case here. Ultra-sharp silicon tips on nitride levers were used (Bruker, Scanasyst with spring constant of 0,4 N/m). During AFM imaging, the force was reduced in order to avoid dragging of molecules by the tip. All analyses of the images were conducted in integrated software. Images were recorded directly on previously prepared TEM grids.

H. DFT Calculations – Geometric optimizations

All calculations were performed using the PBEPBE method. The 6-31G(d) split valence plus polarization basis set was used and all calculations were carried out using the Gaussian 09.2 software.[90]

I. Differential Scanning Calorimetry (DSC)

DSC experiments were performed on a Nano-DSC III from Setaram at the Institut Charles Sadron.

J. Isothermal Titration Calorimetry (ITC)

Isothermal titration calorimetry (ITC) experiments were performed at 25 °C using a nano-ITC titration calorimeter from TA Instruments with a standard sample cell volume of 1 mL, following standard procedures. A 100 μL injection syringe was used with stirring at 250 rpm. Supramolecular polymers were dissolved in dry toluene and the solutions were degassed gently under vacuum before use. Each titration comprised an initial 4.8 μL preinjection followed by 19 × 5 μL aliquots of a solution of the supramolecular polymer.

General principle:

Injecting a solution of a supramolecular polymer into pure solvent leads to its dissociation. This event is accompanied by absorption and/or emission of heat. The heat measured by the machine is the heat that has to be supplied to the measurement cell to keep it at the same temperature as the reference cell. Injection after injection, the concentration in the cell rises, until no dissociation can be observed anymore. The resulting enthalpogram can be used to access K_d, the dissociation constant associated to the dilution of our supramolecular polymer.

K. Small angle neutron scattering (SANS)

SANS spectra were performed on the PACE spectrometers at the Laboratoire Leon Brillouin (LLB, CEA Saclay).

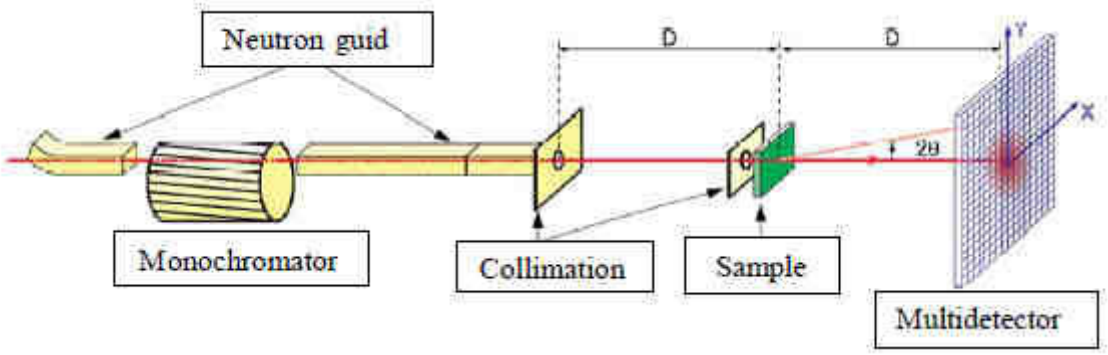

Figure 107 | Principle of the neutron scattering method

On PACE, three configurations were used: typically the first was set with a distance sample to detector of 4.7 m, a wavelength of 12 Å and a collimation distance of 5.00 m, the second at 3 m and 4.6 Å and the last at 1 m and 4.6 Å with a collimation distance of 2.50 m, providing a large accessible q-range from 3 x 10^{-3} to 0.3 $Å^{-1}$. For data reported in chapter IV (ADA-DAD), two configurations were used: the first with a distance sample to detector of 4.7 m and a wavelength of 10 Å, the second with a distance sample to detector of 1.5 m and a wavelength of 6 Å. Data treatment has been done with a homemade program (Pasinet) following standard procedures.

L. Small angle X-ray scattering (SAXS)

Small angle X-ray scattering experiments were performed at the Institut Charles Sadron by using both a diffractometer developed by Molecular Metrology (Elexience in France), and the Nanostar diffractometer from Bruker-Anton Paar. Both operate with a pinhole collimation of the X-ray beam and a two-dimensional gas-filled multiwire detector. For the Elexience diffractometer, a monochromatic (λ = 1.54 Å with Dl/l < 4%) and focused X-ray beam is obtained through a multilayer optic designed and fabricated by Osmic. For the Nanostar, a monochromatic and almost parallel X-ray beam (divergence better than 0.03°) is obtained through a confocal mirror with advanced W/Si multilayer coating from Xenocs. The size of the incident beam on the sample was close to 600 and 300 µm, respectively. The sample to detector distance was set at 0.70 m for the Elexience diffractometer and 0.20 m for the Nanostar one, allowing to explore scattering vectors ranging from q = 0.01 $Å^{-1}$ to 0.9 $Å^{-1}$, with $q = 4\pi\sin(\theta/2)/\lambda$, where λ and θ are the wavelength of the incident beam and the scattering angle, respectively. The q-resolution related to the beam size on the sample and the beam divergence was close to 0.005 $Å^{-1}$. Cells of 1 mm thickness and calibrated Mica windows were used as sample holders. Measurements were performed at room temperature. All data were treated

according to standard procedures for isotropic small angle X-ray scattering. After radial averaging, the spectra were corrected from electronic noise of the detector, empty cell, absorption and sample thickness. A ^{55}Ir source was used for the corrections of geometrical factors and detector cells efficiency as well as a Silver Behenate sample, for the q-calibration. After all these data treatments, the scattered intensities were corrected from the scattering of the solvent. According to such a procedure, the scattered intensity I(q) containing all the structural information is obtained for each solution.

M. Static Light scattering experiments (SLS)

DLS and SLS spectra were performed at the University Paris Diderot on the 3D DLS spectrometer (LS Instruments, Fribourg, Switzerland) equipped with a 25 mW HeNe laser (JDS uniphase) operating at λ = 632.8 nm, a two channel multiple tau correlator (1088 channels in autocorrelation), a variable-angle detection system, and a temperature-controlled index matching vat (LS Instruments). The scattering spectrum was measured using two single mode fibre detections and two high sensitivity APD detectors (Perkin Elmer, model SPCM-AQR-13-FC). Solutions were directly filtered through 0.22 μm Millipore filter into the scattering cell.

Static light scattering

In SLS experiment, the scattering intensity $I(q)$ is measured as a function of scattering wave vector q defined by:

$$q = \frac{4\pi}{\lambda} n_0 \sin\left(\frac{\theta}{2}\right) \quad (6)$$

where n_0 is the refractive index of the solvent (1.33 for water, 1.44 for chloroform, 1.34 for acetonitrile, 1.49 for toluene at 20 °C), λ is the wavelength of light under vacuum and θ is the scattering angle, which has been varied from 30° to 140° providing a q-range from 7×10^{-4} Å^{-1} to 2.4×10^{-3} Å^{-1}. Corrections to the absolute scattering intensities $I(q)$ (called also Rayleigh ratio R(q)) were made using a toluene sample reference for which the excess Rayleigh ratio is well-known ($R_{toluene}$=1.3522×10^{-5} cm^{-1} at λ = 632.8 nm) and R(q) can thus be written as:

$$R(q) = \frac{I - I_0}{I_{toluene}} \left(\frac{n_0}{n_{toluene}}\right)^2 R_{toluene}(q) \quad (7)$$

where I is the scattering intensity of the solution sample, I_0 the scattering intensity of the solvent, and $n_{toluene}$ is the refractive index of the toluene ($n_{toluene}$ = 1.49 at 20 °C). The usual

equation for absolute light scattering combines the form factor *P(q)*, the structure factor *S(q)* and the weight average molecular weight M_w of the scattered objects:

$$R(q) = \frac{4\pi^2 n_0^2}{N_a \lambda^4}\left(\frac{dn}{dc}\right)^2 CM_w P(q)S(q) \quad (8)$$

where d*n*/d*c* is the refractive index increment and N_a is the Avogadro's number.

N. Gel Irradiation Studies for chapter VII

Typical procedure for sequential light irradiation experiments:

Gel irradiation studies were conducted in dry, degassed acetonitrile, at the wavelength specified. Gels were cut in small pieces, and swollen in a glass vial filled with acetonitrile. All gel manipulations were performed in a room with fluorescent light bulbs emitting > 400 nm so as not to activate the rotation of the motor. The samples were placed 1 cm from the UV lamp and maintained at a constant aspect ratio relative to the camera. After contraction, exposure to ambient room light caused the closed, red colored, form of the switch to fade within 10 min (a flash with halogen lamp for instance accelerate this process to a few seconds).

When gels are imaged after expansion for long periods of time, for sake of measurement they were flashed with UV light for 30 seconds to appear red colored for a more accurate area measurement. The surface area of the gels was measured using ImageJ software.

Procedure for dual-light irradiation experiments:

A vial containing a piece of gel in acetonitrile was placed 6 cm above the UV-light source. Perpendicular to this was installed a white LED CREE XP-G 300 Lumen used as a visible light source. The sample was irradiated by both lamps at the same time, and the distance between the white LED and the sample was modulated. When the size of the gel stopped evolving, we considered the steady state was reached (up to three hours for each contraction, ten hours for extensions). The volume variation in each situation was calculated using ImageJ the same way it was performed in the previous experiments.

2) Syntheses and analyses of compounds

*Oct-7-yn-1-ol (**4**)*

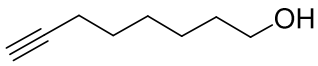

4

To dry ethylene-1,2-diamine (120 mL) at 0°C was added portionwise sodium hydride (60% suspension in oil, 7.0 g, 175 mmol). The grey cloudy mixture was allowed to warm slowly to 60°C and stirred for 1 hour to give a deep blue mixture. After cooling down the mixture to 45°C, 3-octyn-1-ol (6.25 mL, 43.6 mmol) was added dropwise. The solution was stirred at 60°C for 1 hour and cooled to 0°C, turning from red to purple. Water (200 mL) and diethylether (200 mL) were then added slowly and the solution was acidified using 12 M hydrochloric acid slowly until pH 1. The aqueous layer was extracted with diethylether (4 x 200 mL) and the organic layers were combined, dried over sodium sulfate and concentrated. The crude residue was purified by column chromatography (SiO_2, cyclohexane → cyclohexane/EtOAc 1/1) to provide product **4** (5.1 g, 91 %) as a yellow oil.

R_f = 0.3 (cyclohexane/ EtOAc 3/1).

^{1}H NMR ($CDCl_3$, 400 MHz, 25°C): δ = 3.63 (t, *J* = 6.7 Hz, 2H), 2.19 (td, *J* = 7.0, 2.7 Hz, 2H), 1.91 (t, *J* = 2.6 Hz, 1H), 1.61-1.51 (m, 4H), 1.49-1.33 (m, 4H).

^{13}C NMR ($CDCl_3$, 100 MHz, 25°C): δ = 84.7, 68.3, 63.0, 32.7, 28.6, 28.5, 25.4, 18.5.

ESI-MS: m/z calcd. for $C_8H_{14}O$: 127.11 $[M+H]^+$, found: 127.18.

*8-bromooct-1-yne (**5**)*

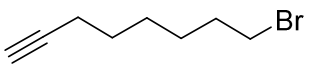

5

To a solution of oct-7-yn-1-ol **4** (1.4 g, 11.1 mmol) in dichloromethane (35 mL) were added carbon tetrabromide (5.2 g, 15.5 mmol) and triphenylphosphine (4.1 g, 15.5 mmol). The solution was stirred at 45°C for an hour. Diethylether (100 mL) was added and the resulting precipitate was filtered and washed abundantly with cold cyclohexane. The filtrate was

evaporated and the crude residue was purified by column chromatography (SiO_2, cyclohexane → cyclohexane/EtOAc 9/1) to give compound **5** (1.9 g, 91%) as a colorless oil.

R_f = 0.23 (cyclohexane/EtOAc 9/1).

^{1}H NMR ($CDCl_3$, 400 MHz, 25°C): δ = 3.39 (t, *J* = 6.8 Hz, 2H), 2.18 (td, *J* = 6.8, 2.7 Hz, 2H), 1.92 (t, *J* = 2.6 Hz, 1H), 1.89-1.82 (m, 2H), 1.56-1.47 (m, 2H), 1.46-1.34 (m, 4H).

^{13}C NMR ($CDCl_3$, 100 MHz, 25°C): δ = 84.5, 68.5, 33.9, 32.8, 28.3, 27.9, 27.8, 18.5.

*2-(oct-7-yn-1-yl)isoindoline-1,3-dione (**6**)*

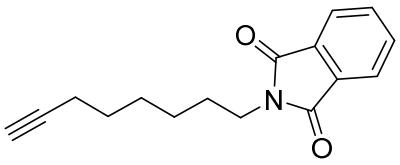

6

Potassium phtalimide (5.4 g, 29.4 mmol) was added to a solution of **5** (3.7 g, 19.6 mmol) in dimethylformamide (25 mL). The solution was stirred at 80°C for an hour, and then the solvent was evaporated. The solid residue was taken back in dichloromethane (50 mL) and filtered through a pad of silica. Evaporation of the filtrate yielded compound **6** (4.0 g, 80%) as a colorless oil that slowly solidified over time.

^{1}H NMR ($CDCl_3$, 400 MHz, 25°C): δ = 7.85-7.83 (m, 2H), 7.71-7.69 (m, 2H), 3.68 (t, *J* = 7.3 Hz, 2H), 2.17 (td, *J* = 6.8, 2.6 Hz, 2H), 1.92 (t, *J* = 2.7 Hz, 1H,), 1.69 (tt, *J* = 7.5, 7.5 Hz, 2H), 1.54-1.34 (m, 6H).

^{13}C NMR ($CDCl_3$, 100 MHz, 25°C): δ = 168.6, 134.0, 132.4, 123.3, 84.6, 68.4, 38.1, 28.6, 28.5, 28.4, 26.5, 18.5.

ESI-MS: m/z calcd. for $C_{16}H_{17}NO_2$: 256.13 $[M+H]^+$, found: 256.26.

*Oct-7-yn-1-amine (**7**)*

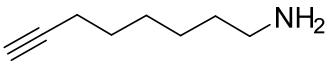

7

To a solution of **6** (1.5 g, 5.9 mmol) in ethanol (60 mL) was added hydrazine hydrate (1 mL, 20.6 mmol) and the mixture was stirred at reflux for 4 hours (after 1 hour, a white precipitate appears) and then cooled down to room temperature. After removal of the solvent the residue is taken back in a 1 M potassium hydroxide solution (40 mL). The solution was extracted three times with dichloromethane (3 x 50 mL) and then the organic layers were dried over sodium sulfate and concentrated to yield compound **7** (514 mg, 70%) as a yellow oil.

^{1}H NMR ($CDCl_3$, 400 MHz, 25°C): δ = 2.69 (t, *J* = 7.0 Hz, 2H), 2.19 (td, *J* = 7.2, 2.7 Hz, 2H), 1.93 (t, *J* = 2.7 Hz, 1H), 1.56-1.46 (m, 2H), 1.40-1.26 (m, 6H).

^{13}C NMR ($CDCl_3$, 100 MHz, 25°C): δ = 84.6, 68.1, 41.9, 33.6, 28.5, 28.4, 26.4, 18.4.

*3,4-bis(2-(2-(2-hydroxyethoxy)ethoxy)ethoxy)benzaldehyde (**8**)*

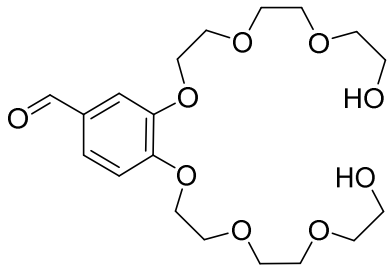

8

3,4-Dihydroxybenzaldehyde (9.0 g, 65.2 mmol), potassium carbonate (22.2 g, 161 mmol) and lithium bromide (5.7 g, 65.9 mmol) were suspended in dimethylformamide (250 mL). 2-[2-(2-Chloroethoxy)ethoxy]ethanol (20.8 mL, 144 mmol) was dissolved in dimethylformamide (100 mL) and added dropwise under argon at 100°C. The reaction mixture was stirred at 100 °C for 3 days. Then, the mixture was filtered and the solvents evaporated. The residue was taken back in dichloromethane (500 mL) and washed with potassium carbonate 10% (4 x 500 mL). The organic layer was then dried over sodium sulfate and concentrated to yield compound **8** (24.4 g, 97%) as a yellow oil, which pure enough to be used as such for the next step.

R_f = 0.1 ($MeOH/CH_2Cl_2$ 1/99).

^{1}H NMR ($CDCl_3$, 400 MHz, 25°C): δ = 9.83 (s, 1H), 7.46-7.43 (m, 2H), 6.98 (d, *J* = 8.6 Hz, 1H), 4.27-4.22 (m, 4H), 3.94-3.89 (m, 4H), 3.78-3.62 (m, 16H), 3.60 (brs, 2H).

^{13}C NMR ($CDCl_3$, 100 MHz, 25°C): δ = 190.8, 154.0, 148.9, 130.1, 126.7, 112.2, 111.5, 72.6, 70.8, 70.7, 70.2, 69.3, 69.2, 68.5, 61.5.

*3,4-bis(2-{2-[2-(p-toluenesulfonyloxy)ethoxy]ethoxy}ethoxy)benzaldehyde (**9**)*

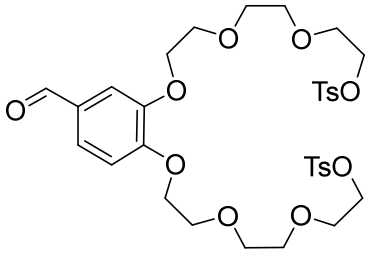

9

Compound **8** (24.4 g, 60.6 mmol), triethylamine (84.3 mL, 606 mmol) and a catalytic amount of 4-(dimethylamino)pyridine (1.1 g, 9.1 mmol) were dissolved in dichloromethane (250 mL), and the solution was cooled down to 0°C using a cryostat. A solution of *p*-toluenesulfonyl chloride (57.8 g, 303 mmol) in dichoromethane (100 mL) was then added dropwise over a period of 1 hour while at 0°C. The reaction mixture was stirred overnight at room temperature. Then, it was acidified with a 5 M hydrochloric acid solution (100 mL), washed with 2 M hydrochloric acid (150 mL) and brine (2 × 150 mL), dried over sodium sulfate, and the solvent was removed under vacuum. The residue was purified by column chromatography (SiO_2, EtOAc/cyclohexane 1/1 → 4/1) to yield compound **9** (30.1 g, 70%) as a brown oil.

R_f = 0.2 (EtOAc/cyclohexane 2/1).

^{1}H NMR ($CDCl_3$, 400 MHz, 25°C): δ = 9.84 (s, 1H), 7.78 (d, *J* = 8.2 Hz, 4H), 7.45-7.41 (m, 2H), 7.32 (d, *J* = 8.2 Hz, 4H), 6.99 (d, *J* = 8.2 Hz, 1H), 4.24-4.13 (m, 8H), 3.90-3.83 (m, 4H), 3.70-3.59 (m, 12H), 2.42 (s, 6H).

^{13}C NMR ($CDCl_3$, 100 MHz, 25°C): δ = 190.9, 154.3, 149.2, 144.8, 133.0, 130.3, 129.9, 128.0, 126.8, 112.5, 111.8, 111.3, 70.8, 69.6, 69.5, 69.3, 69.2, 68.7, 21.6.

*(2-Formyl)dibenzo[24]crown-8 (**10**)*

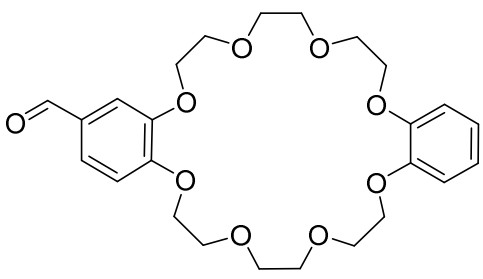

10

Cesium carbonate (2.3 g, 7.0 mmol) was placed in a 3-neck 2 L round-bottomed flask fitted with a condenser, a pressure-equalized dropping funnel and a thermometer, before anhydrous dimethylformamide (500 mL) was added. The ditosylate **9** (9.4 g, 13.2 mmol) and cathecol (1.5 mg, 13.2 mmol) were dissolved in dimethylformamide (1 L) and the resulting solution was added to the dropping funnel after the suspension in the flask has been heated to 100°C. Under vigourous stirring, the ditosylate/catechol mixture was added dropwise over twelve hours. The mixture was stirred at 100°C during 7 days. Then, the solvent was removed under vacuum and the residue taken back in toluene (1 L) and washed with 10% potassium carbonate (750 mL). The aqueous layer was further extracted with toluene (3 × 500 mL) and the combined organic layers were washed with 10% potassium carbonate (35 mL). The organic phase was dried over sodium sulfate and the solvents were removed under vacuum. The residue was purified by column chromatography (SiO_2, EtOAc → EtOAc/MeOH 99/1) to yield compound **10** (3.2 g, 52%) as a white solid.

R_f = 0.35 (EtOAc).

^{1}H NMR ($CDCl_3$, 400 MHz, 25°C): δ = 9.81 (s, 1H), 7.41 (dd, *J* = 8.1, 1.9 Hz, 2H), 7.37 (d, *J* = 8.2 Hz, 1H), 6.94 (d, *J* = 8.2 Hz, 1H), 6.89-6.86 (m, 4H), 4.22-4.18 (m, 8H), 3.96-3.92 (m, 8H), 3.84-3.82 (m, 8H).

^{13}C NMR ($CDCl_3$, 100 MHz, 25°C): δ = 190.9, 154.4, 149.3, 149.0, 130.3, 126.9, 121.5, 114.2, 112.0, 111.2, 71.7, 71.5, 71.4, 70.1, 69.7, 69.8, 69.7.

ESI-MS: m/z calcd. for $C_{25}H_{32}O_9$: 499.20 $[M+Na]^+$, found: 499.16.

*Compound (**8**)*

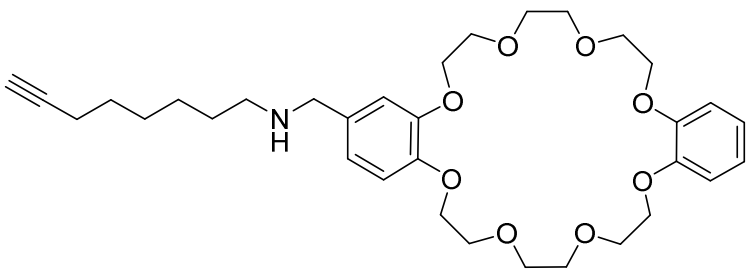

8

Compound **10** (1.0 g, 2.1 mmol) and compound **7** (260 mg, 2.1 mmol) were heated overnight at reflux in toluene (60 mL) using a Dean-Stark apparatus. The solvent was then evaporated, giving a yellow oil. This oil was dissolved in methanol (50 mL), and then sodium borohydride (793 mg, 21 mmol) was added portionwise at 0°C. The solution was stirred at room temperature for 4 hours, then a 5 M aqueous solution of hydrochloric acid (50 mL) was added to the reaction mixture. The solvent was evaporated, and the residue was taken back with dichloromethane (100 mL) and washed with a 5 M aqueous solution of sodium hydroxyde (75 mL). The aqueous layer was back extracted with dichloromethane (2 x 100 mL) and the organic layers were dried over sodium sulfate and concentrated. The crude compound was purified by column chromatography (SiO_2, MeOH/CH_2Cl_2/NH_4OH 19/80/1) to yield compound **11** (957 mg, 76 %) as a pale yellow oil that slowly solidify over time.

R_f = 0.8 (MeOH/CH_2Cl_2/NH_4OH 19/80/1).

^{1}H NMR ($CDCl_3$, 400 MHz, 25°C): δ = 6.91-6.74 (m, 7H), 4.18-4.08 (m, 8H), 3.96-3.84 (m, 8H), 3.84-3.77 (m, 8H), 3.67 (s, 2H), 2.58 (t, *J* = 7.0 Hz, 2H), 2.15 (t, *J* = 7.2 Hz, 2H), 1.92 (brs, 1H), 1.54-1.24 (m, 8H).

^{13}C NMR ($CDCl_3$, 100 MHz, 25°C): δ = 149.0, 148.9, 147.9, 133.9, 121.5, 120.9, 114.2, 114.2, 114.0, 114.0, 84.7, 71.3, 70.0, 69.6, 69.5, 68.3, 53.8, 49.4, 30.0, 28.7, 28.4, 26.9, 18.4.

ESI-MS: m/z calcd. for $C_{33}H_{47}NO_8$: 586.33 $[M+H]^+$, found: 586.34.

*Pseudo-rotaxane (**12**)*

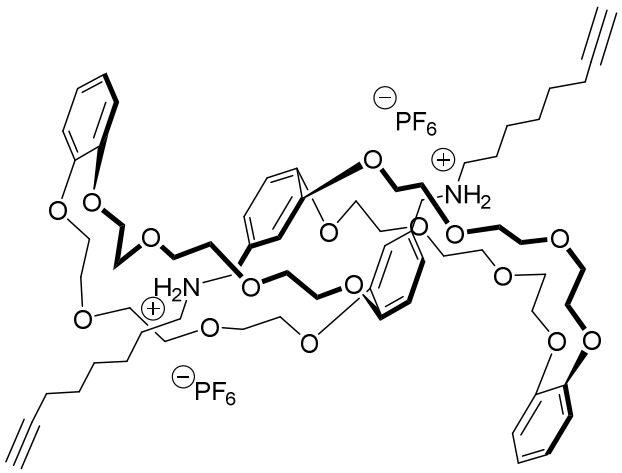

12

To a solution of compound **11** (500 mg, 1.6 mmol) in diethylether (10 mL) was slowly added 2 M hydrochloric acid in diethylether (2.5 mL). The suspension was stirred for 30 min at room temperature. The solvent was evaporated and the solid taken back in a biphasic mixture of water (12 mL) and dichloromethane (12 mL), to which was added ammonium hexafluorophosphate (1.0 g, 6.1 mmol). The mixture was stirred vigorously for 1 hour before being extracted with dichloromethane (3 x 15 mL). The organic layer was dried over sodium sulfate and concentrated to yield compound **12** (575 mg, 92%) as a white solid.

^{1}H NMR ($CDCl_3$, 400 MHz, 25°C): δ = 6.91 (d, *J* = 8.3 Hz, 2H), 6.84-6.71 (m, 10H), 6.57 (s, 2H), 4.44-4.38 (m, 2H), 4.35-4.29 (m, 2H), 4.23-3.63 (m, 48H), 3.56-3.36 (m, 4H), 2.09 (td, *J* = 6.9, 1.8 Hz, 4H), 1.92 (brs, 2H), 1.48-1.14 (m, 16H).

^{13}C NMR ($CDCl_3$, 100 MHz, 25°C): δ = 147.9, 147.8, 147.8, 147.0, 146.5, 146.3, 124.8, 123.2, 121.4, 121.2, 113.4, 112.7, 112.1, 112.0, 84.4, 72.6, 72.0, 71.3, 71.0 (x3), 70.6, 70.5, 68.8, 68.7, 67.8, 67.2, 67.1 (x2), 66.9, 52.4, 49.0, 28.2, 26.8, 26.4, 18.4.

ESI-MS: m/z calcd. for $C_{66}H_{96}N_2O_{16}P_2F_{12}$: 586.84 $[M\text{-}2PF6]^{2+}$, found: 586.45.

*4-bromobenzyl acetate (**13**)*

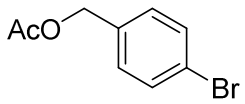

13

4-bromobenzyl alcohol (3.4 g, 18.0 mmol) and 4-dimethylaminopyridine (226 mg, 1.9 mmol) were dissolved in 1:1 mixture of acetic anhydride/pyridine (38 mL) and the solution was stirred overnight at room temperature overnight. Water (10 mL) and ethyl acetate (10 mL) were then added, and the layers were separated. The organic layer was washed with 1 M hydrochloric acid (10 mL) and brine (10 mL). The organic phase was then dried over sodium sulfate and the solvents were removed. Further purification by column chromatography (SiO_2, cyclohexane/EtOAc 95/5) afforded compound **13** (4.1 g, 99%) as a white solid.

R_f = 0.45 (cyclohexane/EtOAc 20/1).

^{1}H NMR ($CDCl_3$, 400 MHz, 25°C): δ = 7.48 (d, *J* = 8.4 Hz, 2H), 7.23 (d, *J* = 8.3 Hz, 2H), 5.05 (s, 2H), 2.10 (s, 3H).

^{13}C NMR ($CDCl_3$, 100 MHz, 25°C): δ = 170.9, 135.1, 131.8, 130.1, 122.4, 65.6, 21.1.

ESI-MS: m/z calcd. for $C_9H_9BrO_2$: 228.99 $[M+H]^+$, found: 229.13.

*4-((trimethylsilyl)ethynyl)benzyl acetate (**14**)*

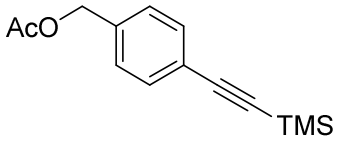

14

Compound **13** (4.0 g, 17.5 mmol), copper iodide (665 mg, 3.5 mmol), bis(triphenylphosphine)palladium(II) dichloride (1.2 g, 1.8 mmol), triphenylphosphine (92 mg, 3.5 mmol) were dissolved in triethylamine (60 mL) under argon. The mixture was degassed doing freeze-thaw cycles, and trimethylsilylacetylene (2.9 mL, 20.1 mmol) was added and the solution was heated up to 70 °C for 2 days. The solvents were removed and further purification by column chromatography (SiO_2, cyclohexane/EtOAc 20/1) yielded compound **14** (3.4 g, 80%) as a pale orange solid.

R_f = 0.2 (cyclohexane /EtOAc 20/1).

^{1}H NMR ($CDCl_3$, 400 MHz, 25°C): δ = 7.44 (d, *J* = 8.4 Hz, 2H), 7.30 (d, *J* = 8.4 Hz, 2H), 5.07 (s, 2H), 2.08 (s, 3H), 0.25 (s, 9H).

^{13}C NMR ($CDCl_3$, 100 MHz, 25°C): δ = 170.9, 136.4, 132.3, 128.0, 123.2, 104.8, 94.8, 65.9, 21.1, 0.1.

ESI-MS: m/z calcd. for $C_{14}H_{18}O_2Si$: 247.12 $[M+H]^+$, found: 247.15.

*4-ethynylbenzyl acetate (**15**)*

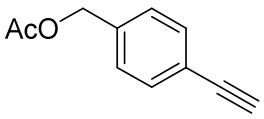

15

Compound **14** (2.8 g, 11.4 mmol) in tetrahydrofuran (28 mL) was treated with 1M tetrabutylammonium fluoride in tetrahydrofuran (3.3 mL, 11.4 mmol). The mixture was stirred at room temperature for 30 min and the solvent was removed. Further purification of the black

residue by column chromatography (SiO_2, cyclohexane/EtOAc 20/1) yielded compound **15** (1.1 g, 85%) as a yellow solid.

R_f = 0.2 (cyclohexane/EtOAc 20/1).

^{1}H NMR ($CDCl_3$, 400 MHz, 25°C): δ = 7.48 (d, *J* = 8.2Hz, 2H), 7.31 (d, *J* = 8.4 Hz, 2H), 5.09 (s, 2H), 3.09 (s, 1H), 2.11 (s, 3H).

^{13}C NMR ($CDCl_3$, 100 MHz, 25°C): δ = 170.9, 136.8, 132.5, 128.2, 122.2, 83.4, 77.7, 65.9, 21.1.

Anal. calcd. for $C_{11}H_{10}O_2$: C 75.84, H 5.79; found C 75.17, H 5.86.

*1-hexyl-uracil (**16**)*

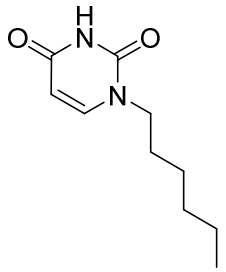

16

To a solution of uracil (4.0 g, 35.7 mmol) in dimethylsulfoxyde (55 mL) was added potassium carbonate (5.4 g, 39.7 mmol). The suspension was stirred at room temperature for 20 min. and then 1-bromohexane (5.0 mL, 35.7 mmol) was added. The mixture was heated up to 40 °C and stirred overnight. After 24 h, the mixture was diluted with chloroform (60 mL), and washed with 0.1 M hydrochloric acid (3 x 50 mL), water (2 x 50 mL) and brine (50 mL). The organic phase was dried on sodium sulfate and concentrated to 5 mL under vacuum, and then poured in cold hexane (40 mL) until a white precipitate formed. After washing with hexane, pure 1-hexyluracil **16** (3.1 g, 44%) was recovered by filtration as a white powder.

^{1}H NMR ($CDCl_3$, 400MHz, 25°C): δ = 9.34 (s, 1H), 7.14 (d, *J* = 7.9 Hz, 1H), 5.67 (d, *J* = 7.9 Hz, 1H), 3.71 (t, *J* = 7.3 Hz, 2H), 1.69-1.61 (m, 2H), 1.34-1.26 (m, 6H), 0.88 (t, *J* = 6.8 Hz, 3H).

^{13}C NMR ($CDCl_3$, 100MHz, 25°C): δ = 164.0, 151.0, 144.5, 102.1, 49.1, 31.4, 29.1, 26.2, 22.6, 14.1.

ESI-MS: m/z calcd. for $C_{10}H_{16}N_2O_2$: 197.13 $[M+H]^+$, found: 197.01.

*1-hexyl-6-iodouracil (**17**)*

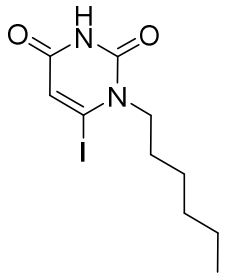

17

To a solution of 1-hexyluracil **16** (1.0 g, 5.1 mmol) in tetrahydrofuran (25 mL) cooled at -78 °C was added a freshly prepared solution of lithium diisopropylamide (0.556 M, 46 mL, 25.5 mmol). The solution was stirred at -78 °C for 1.5 h. Then, powdered iodine was added (6.5 g, 25.5 mmol) and the solution was stirred at -78 °C for 2 h. Glacial acetic acid (0.4 mL) was added and the solution was diluted with chloroform (20 mL), washed with a saturated solution of sodium bicarbonate (3 x 20 mL), a saturated solution of sodium thiosulfate (3 x 20 mL) and brine (20 mL). The organic phase was dried over sodium sulfate and the solid residue was purified by column chromatography (SiO_2, cyclohexane → cyclohexane/EtOAc 1/3) to yield compound **17** (1.24 g, 76%) as a white solid.

R_f = 0.2 (cyclohexane/EtOAc 2/1).

m.p.: 122°C.

^{1}H NMR ($CDCl_3$, 400MHz, 25°C): δ = 9.40 (s, 1H), 6.39 (s, 1H), 4.03 (d, *J* = 7.3 Hz, 2H), 1.70-1.65 (m, 2H), 1.34-1.28 (m, 6H), 0.88 (t, *J* = 7.0 Hz, 3H).

^{13}C NMR ($CDCl_3$, 100MHz, 25°C): δ = 161.0, 148.4, 115.9, 113.9, 53.8, 31.4, 28.8, 26.1, 22.6, 14.1.

HRMS (ESI+): m/z calcd. for $C_{10}H_{15}IN_2O_2$: 323.0251 $[M+H]^+$, found: 323.0264.

*1-hexyl-3-tertbutylcarboxylate-6-iodouracil (**18**)*

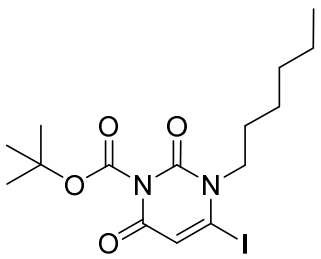

18

To compound **17** (550 mg, 1.7 mmol) in acetonitrile (2.5 mL) was added pyridine (0.5 mL) and the mixture was stirred for 10 min. Di-*tert*-butyl dicarbonate (1.1 g, 5.1 mmol) was added and the solution was stirred overnight at 40 °C. The solution was diluted with chloroform (5 mL) and washed with water (10 mL) and brine (10 mL). The organic phase was dried over sodium sulfate and after evaporation of the solvent the residue was purified by column chromatography (SiO_2, cyclohexane/EtOAc 1/0 → 80/20) to yield the product **18**(634 mg, 88%) as a brown oil that slowly solidify over time.

^{1}H NMR ($CDCl_3$, 400MHz, 25°C): δ = 6.41 (s, 1H), 4.03 (d, *J* = 8.0 Hz, 2H), 1.74-1.68 (m, 2H), 1.64 (s, 9H) 1.58-1.33 (m, 6H), 0.89 (t, *J* = 6.6 Hz, 3H).

^{13}C NMR ($CDCl_3$, 100MHz, 25°C): δ = 158.6, 147.4, 146.5, 115.4, 113.1, 87.2, 54.3, 31.4, 28.7, 27.7, 26.1, 22.6, 14.1.

ESI-MS: m/z calcd for $C_{15}H_{23}IN_2O_4$: 445.06 $[M+Na]^+$, found: 445.30.

*4-(1-hexyl-3-tertbutylcarboxylateuracil)-ethynylbenzyl acetate (**19**)*

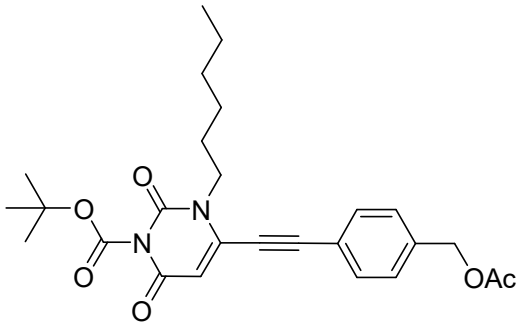

19

Compound **18** (350 mg, 0.8 mmol) and alkyne **15** (144 mg, 0.8 mmol) were dissolved in a 1:1 mixture of tetrahydrofuran/triethylamine (9 mL). The mixture was degassed two times by freeze-thaw cycle and tetrakis(triphenylphosphine)palladium(0) (289 mg, 25 μmol) was introduced under argon. The solution was degassed by 2 more freeze-thaw cycles, and then heated up to 45°C for 24 hours. The resulting dark solution was evaporated under vacuum and the solid residue was purified by column chromatography (SiO_2, cyclohexane/EtOAc, 1/0 → 1/5) to yield the desired product **19** (310 mg, 80%) as a yellow solid.

^{1}H NMR ($CDCl_3$, 400MHz, 25°C): δ = 7.45 (d, *J* = 8.2 Hz, 2H), 7.34 (d, *J* = 8.2 Hz, 2H), 5.99 (s, 1H), 5.12 (s, 2H), 3.97 (t, *J* = 7.8 Hz, 2H), 2.11 (s, 3H), 1.74-1.68 (m, 2H), 1.60 (s, 9H), 1.35-1.30(m, 6H), 0.84 (t, *J* = 7.0 Hz, 3H).

^{13}C NMR ($CDCl_3$, 100 MHz, 25°C): δ = 170.8, 151.7, 149.0, 147.9, 139.0, 137.9, 132.4, 128.4, 119.9, 106.6, 100.4, 87.0, 80.6, 65.5, 47.4, 31.6, 28.8, 27.6, 27.0, 26.6, 22.7, 14.1.

ESI-MS: m/z calcd. for $C_{26}H_{32}N_2O_6$: 429.21 $[M+Na]^+$, found: 492.40.

*4-(1-hexyl-3-tertbutylcarboxylateuracil)-ethynylbenzyl azide (**21**)*

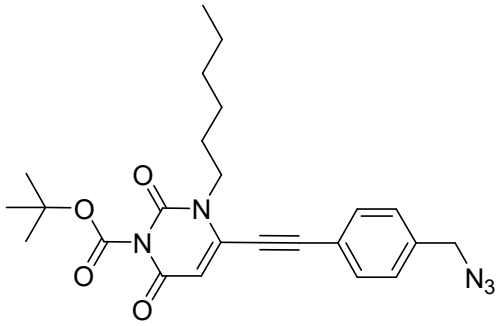

21

Compound **19** (500 mg, 1.1 mmol) was dissolved in a 2.5:1 mixture of tetrahydrofuran/methanol (20 mL) and potassium carbonate (295 mg, 2.13 mmol) was added. The solution was stirred at room temperature for 1 hour. The mixture was diluted with dichloromethane (10 mL) and the mixture was washed with water (2 x 20 mL). The organic phase was dried on sodium sulfate and the solvent evaporated under vacuum to yield the desired product **20** (432 mg, 95%) as a yellow sticky solid which was pure enough to be used as such in the next step.

The previously prepared alcohol **20** was dissolved in tetrahyrofuran (12 mL) and cooled to 0°C. Then, triethylamine (210 µL, 1.5 mmol) and mesityl chloride (12 µL, 1.5 mmol) were added dropwise. The solution was stirred at room temperature for 1 hour. The reaction mixture was diluted with chloroform (10 mL) and washed with water (2 x 20 mL). The organic phase was dried on sodium sulfate and the solvents were evaporated to obtain a sticky yellow residue. The crude mesylated product was pure enough to be used as such in the next step.

The crude mesylated product was dissolved in dimethylformamide (10 mL) and sodium azide (658 mg, 10.1 mmol) was added. The solution was stirred at 50 °C overnight. Then, chloroform was added (20 mL) and the mixture was washed with water (3 x 30 mL). The organic phase

was dried on sodium sulfate and the solvents evaporated under vacuum to yield a yellow residue. The crude product was purified by column chromatography (SiO_2, cyclohexane/EtOAc, 1/0 → 5/1) to yield azide **21** (330 mg, 72% over two steps) as a yellow pale sticky solid.

^{1}H NMR ($CDCl_3$, 400 MHz, 25°C): δ = 7.64 (d, *J* = 8.2 Hz, 2H), 7.40 (d, *J* = 8.2 Hz, 2H), 5.77 (s, 1H), 4.39 (s, 2H), 3.59 (t, *J* = 7.8 Hz, 2H), 1.64 (s, 9H), 1.42-1.38 (m, 2H), 1.09-1.01 (m, 6H), 0.76 (t, *J* = 7.0 Hz, 3H).

^{13}C NMR ($CDCl_3$, 100 MHz, 25°C): δ = 159.2, 149.4, 147.7, 145.9, 137.9, 137.5, 129.0, 127.9, 127.6, 105.7, 87.2, 68.0, 54.3, 46.2, 30.9, 28.4, 27.5, 26.0, 22.7, 14.1.

*Bis-uracil[c2]daisy chains (**22**)*

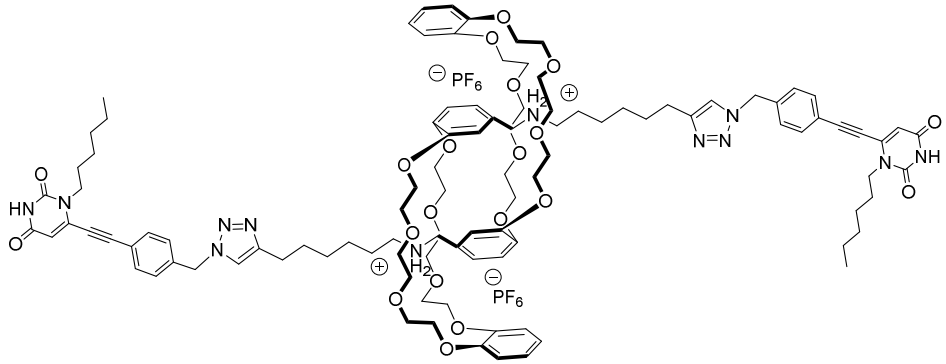

22

In an oven-dried schlenck tube, compound **21** (150 mg, 0.33 mmol) and pseudo-rotaxane **12** (225 mg, 0.15 mmol) were dissolved in dry dichloromethane (6 mL) under argon. After two freeze-thaw cycles, tetrakis(acetonitrile)copper(I) hexafluorophosphate (112 mg, 0.33 mmol) was added. The solution was stirred at room temperature 2 minutes and tetramethylethylenediamine (45 µL, 0.30 mmol) was added. The mixture was heated up to 35°C and stirred under argon for two days. After this time, trifluoroacetic acid (2 mL) was added and the solution was stirred 12 hours at room temperature. The solvents were removed under vacuum, and the yellow residue was taken back in dichloromethane (5 mL) and stirred with an ethylenediaminetetraacetic acid solution (5 mL) at pH 9 for 1 hour. The organic phase was isolated and stirred with a saturated ammonium hexafluorophosphate solution (5 mL). The organic phase was separated, dried over sodium sulfate and the solvent was evaporated under vacuum. The residue was purified several time over column chromatography (Al_2O_3, CH_2Cl_2/MeOH 99.5/0.5) to yield rotaxane **22** (121 mg, 37%) as a sticky yellow solid.

^{1}H NMR (CD_3CN, 400 MHz, 25°C): δ = 7.69 (d, *J* = 8.1 Hz, 4H), 7.54 (s, 2H), 7.36 (d, *J* = 8.1 Hz, 4H), 6.82-6.68 (m, 12H), 6.42 (d, *J* = 8.3 Hz, 2H), 5.58 (s, 2H), 5.53 (s, 4H), 4.55-4.36 (m, 4H), 4.30-4.18 (m, 4H), 4.17-4.05 (m, 8H), 4.03-3.95 (m, 8H), 3.94-3.87 (m, 10H), 3.85-3.72 (m, 16H), 3.70-3.60 (m, 8H), 3.57-3.50 (m, 4H), 3.46-3.38 (m, 4H), 2.59 (t, *J* = 7.3 Hz, 4H), 1.78-1.65 (m, 4H), 1.60-1.50 (m, 4H), 1.45-1.22 (m, 12H), .1.14-0.95 (m, 10H), 0.76 (t, *J* = 7.3 Hz, 6H).

^{13}C NMR (CD_3CN, 100 MHz, 25°C): δ = 173.5, 163.3, 152.4, 149.0, 148.6, 148.5, 147.1, 147.0, 138.3, 129.5, 128.6, 126.2, 123.5, 122.5, 114.1, 113.0, 112.7, 106.1, 72.9, 71.5, 71.3, 71.2, 71.0, 68.5, 68.2, 68.0, 67.9, 53.7, 52.8, 49.7, 46.0, 31.6, 30.3, 29.8, 29.0, 28.9, 27.0, 26.8, 26.5, 25.9, 22.9, 22.5, 14.1.

*1-bromo-2-hexyldecane (**23**)*

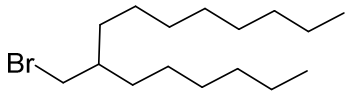

23

A solution of 2-hexyl-1-decanol (5.0 g, 20.6 mmol) and carbon tetrabromide (10.3 g, 30.9 mmol) in dichloromethane (300 mL) was cooled to 0 °C. Triphenylphosphine (10.8 g, 41.2 mmol) was added in portions over 30 min at 0 °C and stirring was continued overnight at room temperature. Dichloromethane (200 mL) was added to the reaction mixture and the organic phase was washed with water (3 × 400 mL), and dried over sodium sulfate. Further evaporation of the solvent and purification by column chromatography (SiO_2, n-hexane) yielded compound **23** as a colorless oil (6.1 g) whose purity was sufficient to be used in the next step.

^{1}H NMR ($CDCl_3$, 400 MHz, 25°C): δ = 3.45 (d, *J* = 4.8 Hz, 2H), 1.61-1.57 (m, 1H), 1.45-1.18 (m, 24H), 0.89 (t, *J* = 6.8 Hz, 6H).

^{13}C NMR ($CDCl_3$, 100 MHz, 25°C): δ = 39.9, 39.7, 32.8, 32.7, 32.1, 32.0, 29.9, 29.7, 29.6, 29.5, 26.7, 26.7, 22.8, 22.8, 14.3, 14.2.

*1,4-dibromo-2,5-bis((2-hexyldecyl)oxy)benzene (**24**)*

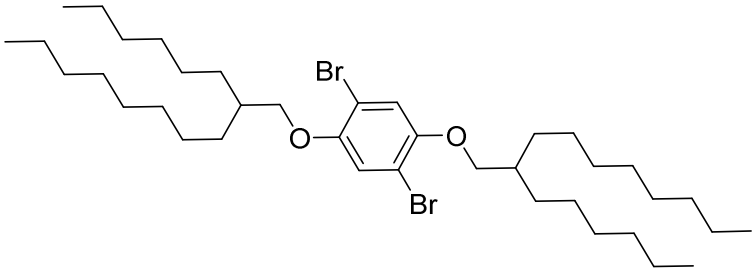

24

To a solution of 1-bromo-2-hexyldecane **23** (2.5 g, 8.25 mmol) in dimethylformamide (60 mL) was added potassium carbonate (6.8 g, 49.5 mmol) and a solution of 2,5-dibromohydroquinone (884 mg, 3.30 mmol) in dimethylformamide (50 mL) was then added dropwise over 1 hour. The dark brown solution was stirred overnight at 60 °C. Diethyl ether (120 mL) was added to the reaction mixture and the organic phase was washed with citric acid 5% in water (3 × 120 mL) and dried over sodium sulfate. Evaporation of the solvent and further purification by column chromatography (SiO_2, n-hexane) provided compound **24** (1.6 g, 66%) as a colorless oil.

R_f = 0.25 (n-hexane).

^{1}H NMR ($CDCl_3$, 400 MHz, 25°C): δ = 7.07 (s, 2H), 3.82 (d, *J* = 5.6 Hz, 4H), 1.82-1.78 (m, 2H), 1.56-1.19 (m, 48H), 0.89-0.86 (m, 12H).

^{13}C NMR ($CDCl_3$, 100 MHz, 25°C): δ = 150.3, 118.3, 111.2, 73.1, 38.1, 32.1, 32.0, 31.5, 31.5, 30.1, 29.8, 29.7, 29.5, 27.0, 26.9, 22.8, 14.3.

Anal. calcd. for $C_{38}H_{68}Br_2O_2$: C 63.68, H 9.56, O 4.46, found: C 63.76, H 9.78, O 4.5.

HRMS (ESI+): m/z calcd. for $C_{38}H_{68}Br_2O_2$: 734.3908 $[M+NH_4]^+$, found: 734.3922.

*((2,5-bis((2-hexyldecyl)oxy)-1,4-phenylene)bis(ethyne-2,1-diyl))bis(trimethylsilane) (**25**)*

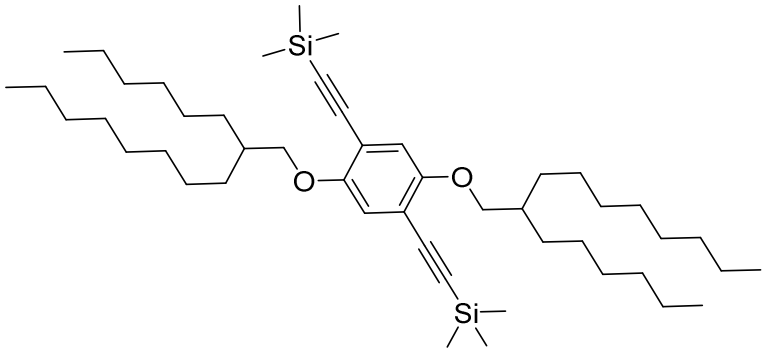

25

Compound **24** (300 mg, 0.41 mmol) in a 1:1 solution of triethylamine and tetrahydrofuran (5 mL) was degassed by freeze-thaw cycles. Tetrakis(triphenylphosphine)palladium(0) (72.0 mg, 63.0 µmol) and copper iodide (12.0 mg, 63.0 µmol) were then added, and the solution was degassed one more time. Trimethylsilylacetylene was then added (130 µL, 0.92 mmol) and the solution was stirred overnight at 75°C. The solvent was then evaporated and purification by column chromatography (SiO_2, cyclohexane → cyclohexane/EtOAc 98/2) provided the bis protected alkyne compound **25** (289 mg, 92%) as a bright yellow oil.

R_f = 0.3 (cyclohexane/EtOAc 4/96).

^{1}H NMR ($CDCl_3$, 400 MHz, 25°C): δ = 6.85 (s, 2H), 3.80 (d, *J* = 5.4 Hz, 4H), 1.83-1.72 (m, 2H), 1.55-1.20 (m, 48H), 0.91-0.82 (m, 12H), 0.23 (s, 18H).

^{13}C NMR ($CDCl_3$, 100 MHz, 25°C): δ = 154.6, 117.2, 114.3, 101.7, 100.3, 72.4, 38.7, 32.4, 31.8, 30.6, 30.3, 30.2, 29.9, 27.4, 23.2, 14.6, 0.6.

HRMS (ESI+): m/z calcd. for $C_{48}H_{86}O_2Si_2$: 751.6239 $[M+H]^+$, found: 751.6206.

*1,4-diethynyl-2,5-bis((2-hexyldecyl)oxy)benzene (**26**)*

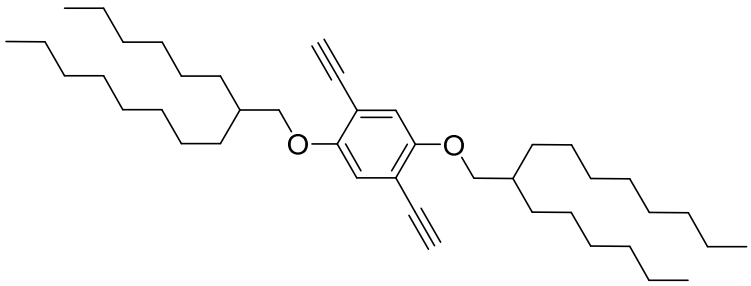

26

Bis protected alkyne compound **25** (2.10 g, 2.79 mmol) and potassium carbonate (3.86 g, 27.95 mmol) were stirred overnight at room temperature in a 2.5:1 mixture of tetrahydrofuran/methanol (28 mL). Solvents were evaporated under vacuum, and the residue was taken back in dichloromethane (100 mL). The organic phase was washed with water (3 x 100 mL), dried over sodium sulfate, and the solvents were evaporated to yield bis alkyne **26** (1.6 g, 94%) as an orange oil which was pure enough to be used as such in the next step.

^{1}H NMR ($CDCl_3$, 400 MHz, 25°C): δ = 6.92 (s, 2H), 3.81 (d, *J* = 5.9 Hz, 4H), 3.29 (s, 2H), 1.85-1.72 (m, 2H), 1.55-1.12 (m, 48H), 0.95-0.80 (m, 12H).

^{13}C NMR ($CDCl_3$, 100 MHz, 25°C): δ = 154.8, 118.1, 113.8, 82.9, 80.4, 73.1, 38.5, 32.5, 32.4, 31.9, 30.6, 30.2, 30.1, 29.9, 27.3, 23.2, 14.7.

HRMS (ESI+): m/z calcd. for $C_{42}H_{70}O_2$: 607.5449 $[M+H]^+$, found: 607.5425.

*Bis-uracil linker (**3**)*

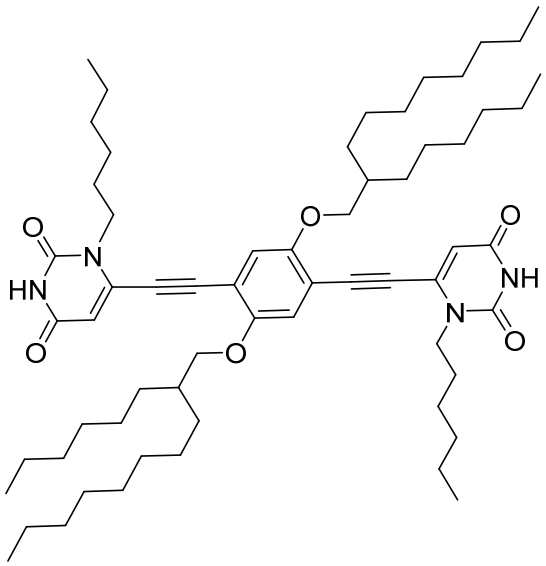

3

A solution of compound **17** (75 mg, 0.23 mmol) and compound **26** (64 mg, 0.1 mmol) in a 1:1 mixture of triethylamine and tetrahydrofuran (2 mL) was degassed by freeze-thaw cycles. Tetrakis(triphenylphosphine)palladium(0) (7.3 mg, 6.0 µmol) was then added, and the solution was degassed one more time and then stirred overnight at 40°C. The solvent was then evaporated and purification by column chromatography (SiO_2, cyclohexane → cyclohexane/EtOAc 2/1) yielded compound **3** (42 mg, 40%) as a very bright yellow solid.

R_f = 0.6 (n-hexane/EtOAc 2/1).

m.p.: 188°C.

^{1}H NMR ($CDCl_3$, 400 MHz, 25°C): δ = 8.99 (s, 2H), 6.96 (s, 2H), 5.99 (d, *J* = 2.6 Hz, 2H), 4.09 (t, *J* = 7.4 Hz, 4H), 3.88 (d, *J* = 5.4 Hz, 4H), 1.81-1.75 (m, 6H), 1.43-1.25 (m, 60H), 0.90-0.83 (m, 18H).

^{13}C NMR ($CDCl_3$, 100 MHz, 25°C): δ = 162.4, 154.5, 150.7, 138.8, 116.4, 113.0, 107.0, 96.8, 86.2, 72.4, 46.8, 38.2, 32.0, 31.9, 31.6, 31.4, 30.2, 29.8, 29.7, 29.50, 29.0, 26.9, 26.5, 22.8, 22.7, 14.2, 14.1.

HRMS (ESI+): m/z calcd. for $C_{62}H_{98}N_4O_6$: 995.7559 $[M+H]^+$, found: 995.7521.

*4-bromo-2,6-diacetylaminopyridine (**27**)*

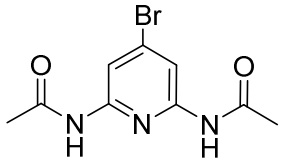

27

4-bromo-2,6-diaminopyridine (750 mg, 3.99 mmol) was dissolved in dichloromethane (50 mL) along with triethylamine (1.39 mL, 9.97 mmol). The solution was cooled down to 0°C and acetyl chloride (0.68 mL, 9.57 mmol) was added dropwise. The solution was stirred at room temperature overnight. The mixture was diluted with dichloromethane (100 mL) and washed with 1 M sodium hydroxide (100 mL). The aqueous phase was washed with a 8:2 dichloromethane/methanol solution (2 x 100mL) and the organic phase were combined, dried on sodium sulfate, before the solvents were evaporated to yield compound **27** (1.07 g, 99%) as a white compound.

^{1}H NMR ($CD_3OD/CDCl_3$ 1:1, 400MHz, 25°C): δ = 7.70 (s, 2H), 4.30 (s, 2H), 1.90 (s, 6H).

^{13}C NMR ($CD_3OD/CDCl_3$ 1:1, 100 MHz, 25°C): δ = 171.1, 151.2, 135.5, 112.7, 23.9.

*4-(2,6-diacetylaminopyridine)benzylethynyl acetate (**28**)*

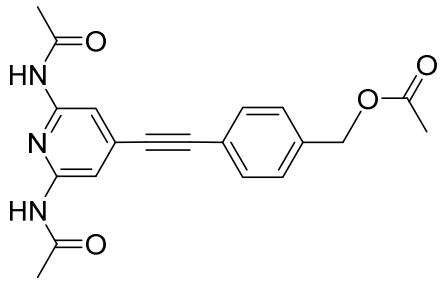

28

In a Teflon® sealed Schlenck tube, a solution of 4-bromo-2,6-diacetylaminopyridine **27** (930 mg, 3.42 mmol) and compound **15** (655 mg, 3.76 mmol) in a 1:1 mixture of dry tetrahydrofuran/triethylamine (35 mL) was degassed by freeze-thaw cycles (3 times) and tetrakis(triphenylphosphine)palladium(0) (237 mg, 205 μmol) was added under argon. The solution was degassed by 2 freeze-thaw cycles, and then heated up to 85°C for 24 hours. The resulting yellow solution was concentrated to dryness and further purification by column

chromatography (SiO_2, cyclohexane/EtOAc 1/1 → 1/5) yielded compound **28** (1.0 g, 81%) as a pale yellow solid.

R_f = 0.4 (n-hexane/EtOAc 1/1).

m.p.: 176°C.

^{1}H NMR ($CDCl_3$, 400 MHz, 25°C): δ = 7.98 (bs, 2H), 7.70 (bs, 2H), 7.51 (d, *J* = 8.0 Hz, 2H), 7.33 (d, *J* = 8.0 Hz, 2H), 5.01 (s, 2H), 2.18 (s, 6H), 2.10 (s, 3H).

^{13}C NMR ($CDCl_3$, 100 MHz, 25°C): δ = 171.1, 169.0, 149.5, 137.2, 136.3, 133.5, 128.0, 122.2, 111.5, 94.8, 88.0, 66.1, 25.0, 21.1.

HRMS (ESI+): m/z calcd. for $C_{20}H_{19}N_3O_4$: 372.1531 $[M+Li]^+$, found: 372.1540.

*4-(2,6-diacetylaminopyridine)benzylethynyl azide (**30**)*

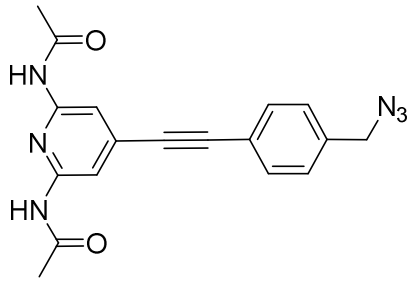

30

Potassium carbonate (757 mg, 5.54 mmol) was added to a solution of compound **28** (1.01 g, 2.77 mmol) in a 2.5:1 mixture of tetrahydrofuran/methanol (70 mL). The solution was stirred at room temperature for 1 hour and then chloroform was added (50 mL). The organic phase was washed with water (2 x 50 mL) and then dried over sodium sulfate. Further evaporation of the solvent under reduced pressure yielded the corresponding alcohol **29** (878 mg, 2.71 mmol) as a yellow/white solid which was pure enough to be used as such in the next step.

A solution of the freshly prepared alcohol **29** (877 mg, 2.71 mmol) in a mixture of dry tetrahydrofuran (12 mL) and dry dimethylformamide (18 mL) was cooled to 0°C. Triethylamine (565 µL, 4.07 mmol) and methanesulfonyl chloride (314 µL, 4.07 mmol) were then sequentially added dropwise. The solution was allowed to warm slowly to room temperature for around one hour, and was then diluted with chloroform (25 mL) and washed with water (2 x 50 mL). The organic phase was dried over sodium sulfate and concentrated under reduced pressure to yield the mesylated derivative as a sticky orange residue which was pure enough to be used as such in the next step without any further purification.

A solution of the crude mesylated product in dry dimethylformamide (20 mL) was treated with sodium azide (1.76 g, 27.1 mmol) and then stirred at 50 °C for 24 hours. Chloroform was added (50 mL). The organic phase was washed with water (2 x 50 mL), dried on sodium sulfate and concentrated under reduced pressure. Further purification by column chromatography (SiO_2, cyclohexane → cyclohexane/EtOAc 5/1) yielded compound **30** (810 mg, 86% over three steps) as a yellow pale solid.

R_f = 0.2 (cyclohexane/AcOEt 1/4).

m.p.: 146°C.

^{1}H NMR ($CDCl_3$, 400 MHz, 25°C): δ = 7.87 (bs, 2H), 7.48 (d, *J* = 7.6 Hz, 2H), 7.28 (d, *J* = 7.6 Hz, 2H), 4.39 (s, 2H), 2.12 (s, 6H).

^{13}C NMR ($CDCl_3$, 100 MHz, 25°C): δ = 170.0, 150.1, 137.5, 136.1, 132.8, 128.6, 122.6, 111.8, 92.2, 88.4, 54.8, 31.2.

HRMS (ESI+): m/z calcd. for $C_{18}H_{16}N_6O_2$: 349.1408 $[M+H]^+$, found: 349.1418.

*Bis-2,6diacetylaminopyridine[c2]daisy chains (**31**)*

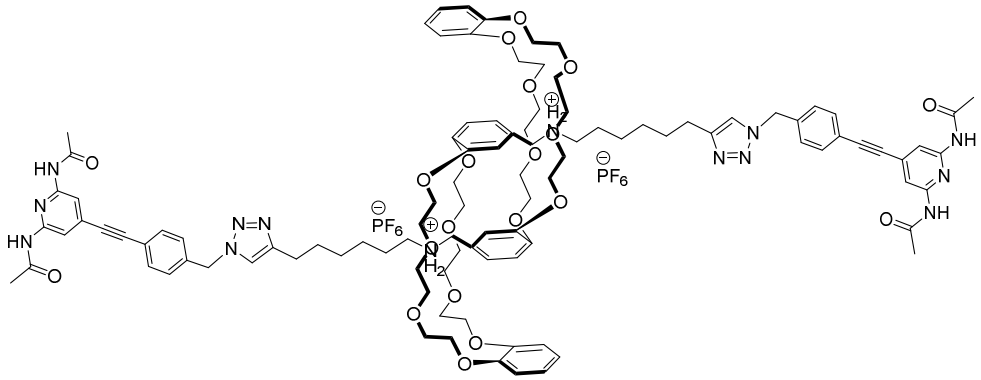

31

To a solution of compound **30** (89 mg, 0.25 mmol) and pseudo-rotaxane **12** (152 mg, 0.1 mmol) in dry dichloromethane (4 mL) were added successively tetrakis(acetonitrile)copper(I) hexafluorophosphate (76.2 mg, 0.2 mmol) and 2,6-lutidine (23 µL, 0.2 mmol). The reaction mixture was stirred for 5 min, then heated by microwave irradiation (50 W) for two hours at 35°C and finally, stirred with an aqueous ethylenediaminetetraacetic acid solution adjusted to pH 9 (6 mL). The aqueous phase was then extracted with a 3:1 mixture of dichloromethane/acetonitrile (3 × 10 mL). The organic phases were combined, dried over sodium sulfate and finally evaporated in vacuo. Further purification by column chromatography

(SiO_2, CH_2Cl_2 → CH_2Cl_2/MeOH 99:1) yielded compound **31** (152 mg, 69%) as a yellow solid. R_f = 0.15 (CH_2Cl_2/methanol 99/1).

m.p.: 190°C.

^{1}H NMR (CD_3CN, 400 MHz, 25°C): δ = 8.52 (s, 4H), 7.88 (s, 4H), 7.55 (d, *J* = 8.0 Hz, 4H), 7.49 (s, 2H), 7.28 (d, *J* = 8.0 Hz, 4H), 6.80-6.64 (m, 12H), 6.37 (d, *J* = 8.9 Hz, 2H), 5.50 (s, 4H), 4.35-4.52 (m, 4H) 4.27-4.17 (m, 4H), 4.15-4.02 (m, 8H), 4.00-3.95 (m, 8H), 3.94-3.86 (m, 8H), 3.80-3.71 (m, 16H), 3.68-3.60 (m, 4H), 3.42-3.35 (m, 4H), 2.58 (t, *J* = 7.4 Hz, 4H), 2.10 (s, 12H), 1.73-16.2 (m, 4H), 1.61-1.51 (m, 4H), 1.42-1.25 (m, 8H).

^{13}C NMR (CD_3CN, 100 MHz, 25°C): δ = 170.8, 151.1, 148.5, 148.1, 146.6, 146.4, 138.0, 134.6, 132.7, 128.6, 123.0, 122.9, 121.0, 113.6, 112.4, 112.2, 110.6, 92.3, 88.2, 72.4, 71.0, 70.8, 70.5, 68.0, 67.7, 67.5, 67.4, 53.3, 52.2, 49.1, 29.2, 28.3, 26.6, 26.4, 25.4, 24.0.

HRMS (ESI+): m/z calcd. for $C_{102}H_{128}N_{14}O_{20}P_2F_{12}$: 934.4709 $[M-2PF_6]^{2+}$, found: 934.4717.

*Bis-Me-2,6-diacetylaminopyridine[c2]daisy chains (**2**^{Ext})*

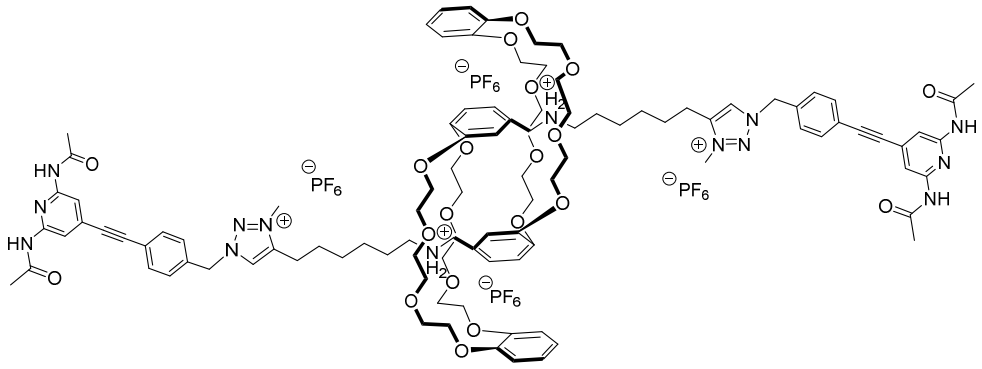

2^{Ext}

Compound **31** (100 mg, 0.46 mmol) was dissolved in a 1:1 mixture of methyl iodide and acetonitrile (6 mL). The mixture was stirred for 4 days at room temperature and then, solvents were evaporated in vacuo. The resulting solid was washed with diethyl ether (5 mL) to give a brown solid. The residue was dissolved in a biphasic mixture of 3:1 dichloro-methane/acetonitrile (5 mL) and a saturated aqueous ammonium hexafluorophosphate solution (5 mL) and the resulting solution was stirred for 1 hour. The aqueous layer was extracted with chloroform (3 × 5 mL). The organic layers were combined, dried over sodium sulfate and concentrated in vacuo to give product **2**^{Ext} (114 mg, quantitative) as a yellow solid.

m.p.: 202°C.

^{1}H NMR ($CDCl_3/CD_3CN$ 4:1, 400 MHz, 25°C): δ = 8.23 (s, 4H), 7.81 (s, 2H), 7.65 (s, 4H), 7.37 (d, *J* = 8.4 Hz, 4H), 7.19 (d, *J* = 8.4 Hz, 4H), 6.58-6.38 (m, 12H), 6.14 (d, *J* = 8.1 Hz, 2H), 5.42 (s, 4H), 4.23-4.12 (m, 4H) 4.07-3.97 (m, 2H), 3.92-3.90 (m, 10H), 3.85 (s, 6H), 3.77-3.65 (m, 16H), 3.62-3.48 (m, 16H), 3.45-3.38 (m, 4H), 3.25-3.12 (m, 4H), 2.35 (t, *J* = 8.0 Hz, 4H), 1.84 (s, 12H), 1.50-1.40 (m, 4H), 1.35-1.25 (m, 4H), 1.15-1.05 (m, 8H).

^{13}C NMR ($CDCl_3/CD_3CN$ 4:1, 125 MHz, 25°C): δ = 168.9, 149.8, 147.4, 146.0, 145.9, 144.8, 132.5, 131.9, 129.2, 127.5, 124.8, 123.7, 122.4, 120.8, 113.1, 111.7, 111.6, 110.9, 91.6, 88.7, 77.0, 71.8, 70.5, 70.2, 70.0, 67.3, 66.8, 66.6, 56.6, 51.8, 50.1, 48.6, 37.3, 29.4, 27.9, 25.9, 24.3, 22.8.

HRMS (ESI+): m/z calcd. for $C_{104}H_{134}N_{14}O_{20}P_4F_{24}$: 948.4866 $[M\text{-}4PF_6\text{-}2H^+]^{2+}$, found: 948.4840.

*Bis-Me-2,6-diacetylaminopyridine[c2]daisy chains (**2**^{cont})*

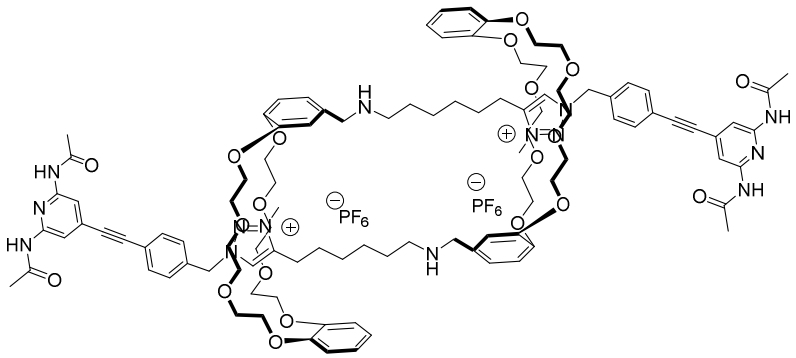

2^{cont}

A solution of compound **2**^{Ext} (10 mg, 4.03 µmol) in chloroform (6 mL) was washed with a 1 M aqueous solution of sodium hydroxide (6 mL). The organic phase was dried over sodium sulfate and then evaporated in vacuo to provide compound **2**^{Cont} (8.8 mg, quantitative) as a yellow solid.

m.p.: 170°C.

^{1}H NMR ($CDCl_3/CD_3CN$ 4:1, 400 MHz, 25°C): δ = 8.92 (s, 2H), 8.22 (brs, 4H), 7.91 (s, 4H), 7.86 (d, *J* = 8.3 Hz, 4H), 7.46 (d, *J* = 8.3 Hz, 4H), 6.86-6.79 (m, 4H), 6.78-6.71 (m, 6H), 6.66 (d, *J* = 8.2 Hz, 2H), 6.64 (d, *J* = 8.5 Hz, 2H), 6.19 (s, 4H), 4.12-4.02 (m, 8H), 4.02-3.94 (m, 8H), 3.92-3.85 (m, 4H), 3.84-3.70 (m, 4H), 3.67-3.45 (m, 22H), 3.43-3.39 (m, 10H), 3.20-2.95 (m, 8H), 2.52-2.32 (m, 4H), 2.11 (s, 12H), 1.45-1.27 (m, 8H), 1.17-1.05 (m, 8H).

^{13}C NMR ($CDCl_3/CD_3CN$ 4:1, 125 MHz, 25°C): δ = 168.9, 149.7, 147.3, 146.2, 134.7, 133.5, 132.5, 131.2, 130.8, 130.3, 129.3, 128.6, 121.0, 120.9, 120.3, 111.7, 111.2, 110.8, 91.5, 88.1, 70.6, 69.6, 68.2, 56.1, 53.3, 49.1, 38.5, 37.4, 31.7, 30.1, 29.4, 28.7, 26.4, 25.9, 24.3, 23.5, 22.7, 22.4.

HRMS (ESI+): m/z calcd. for $C_{104}H_{132}N_{14}O_{20}P_2F_{12}$: 948.4866 $[M-2PF_6]^{2+}$, found: 948.4907.

*1,3,5-tris((trimethylsilyl)ethynyl)benzene (**32**)*

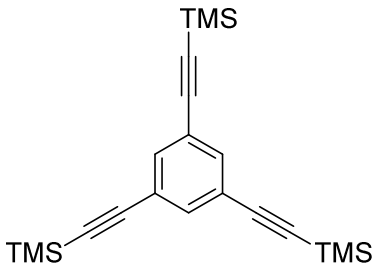

32

1,3,5-Tribromobenzene (600 mg, 1.90 mmol) was dissolved in dry tetrahydrofuran (10 mL) and triethylamine (7 mL) was added. The mixture degassed by doing two freeze-thaw cycles. Then, tetrakis(triphenylphosphine)palladium(0) (132 mg, 0.11 mmol), copper iodide (43.6 mg, 0.23 mmol) and trimethylsilylacetylene (1.1 mL, 7.62 mmol) were added and the reaction mixture was degassed again. The reaction mixture was stirred overnight at 85°C. The crude was then filtered over celite and the solvent evaporated. Purification of the residue by column chromatography (SiO_2, cyclohexane) yielded compound **32** (602 mg, 86 %) as a yellow oil.

^{1}H NMR ($CDCl_3$, 400 MHz, 25°C): δ = 7.50 (s, 3H), 0.25 (s, 27 H).

^{13}C NMR ($CDCl_3$, 100 MHz, 25°C): δ = 135.9, 129.8, 103.0, 95.6, 0.02.

ESI-MS: m/z calcd for $C_{21}H_{30}Si_3$: 367.73 $[M-H]^+$, found: 367.63.

*1,3,5-triethynylbenzene (**33**)*

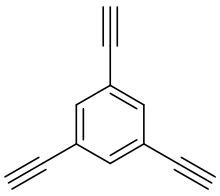

33

Compound **32** (580 mg, 1.59 mmol) was dissolved in a 1:1 mixture of tetrahydrofuran/methanol (30 mL) along with potassium carbonate (1.31 g, 9.5 mmol) and the reaction mixture was stirred for one hour at room temperature. The reaction mixture was then diluted with chloroform (60 mL) and filtered through a pad of silica. The organic phase was then extracted with water (2 x 100 mL) and dried over sodium sulfate. Evaporation of the solvent yielded compound **33** (230 mg, 97 %) as a slightly yellow solid.

^{1}H NMR ($CDCl_3$, 400 MHz, 25°C): δ = 7.58 (s, 3H), 3.16 (s, 3H).

^{13}C NMR ($CDCl_3$, 100 MHz, 25°C): δ = 135.1, 123.2, 81.5, 79.0.

*Tris-uracil linker (**4**)*

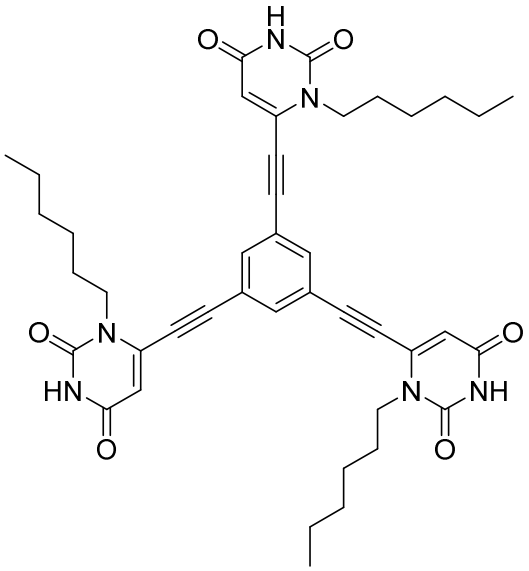

4

Compound **17** (375 mg, 1.17 mmol) and tris-alkyne **33** (43.7 mg, 0.30 mmol) were dissolved in a 1:1 mixture of dry tetrahydrofyran/triethylamine (10 mL). The solution was degassed performing freeze-thaw cycles, and tetrakis(triphenylphosphine)palladium(0) (33.6 mg, 3 μmol) was added to the mixture. It was degassed one more time and then gently heated to 45 °C overnight. The solution was filtered on celite and then cooled down to 0°C and chloroform (20 mL) was added. A yellow precipitate formed overnight, which was recovered by filtration to isolate compound **4** (90 mg, 42%), which proved to be soluble only in DMSO.

^{1}H NMR (d_6-DMSO, 400 MHz, 25°C): δ = 11.53 (s, 3H), 8.06 (s, 3H), 6.04 (d, *J* = 1.8 Hz, 3H), 3.94 (t, *J* = 6.9 Hz, 6H), 1.68-1.63 (m, 6H), 1.31-1.27 (m, 18H), 0.79 (t, *J* = 6.6 Hz, 9H).

*Methyl 3,4,5-tris(dodecyloxy)benzoate (**34**)*

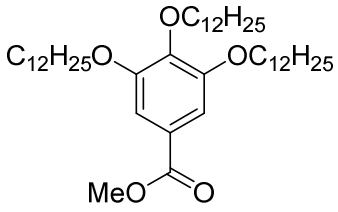

34

Methyl 3,4,5-trihydroxybenzoate (5.0 g, 27.2 mmol) and potassium carbonate (43.9 g, 317 mmol) were suspended in dry dimethylformamide (160 mL) under argon and the solution was stirred for 5 min. at room temperature. Then, 1-bromododecane (25 mL, 103 mmol) was added and the mixture was stirred at 80°C overnight. The solvent was evaporated, and the residue was taken back in a 1:1 mixture of water/ethyl acetate (300 mL). The organic phase was separated and the aqueous phase was extracted with ethyl acetate (4 x 100 mL). The combined organic phases were washed with brine (150 mL), water (100 mL), and dried on sodium sulfate. The solution was filtered through a small pad of silica, concentrated under vacuum and cooled with an ice bath. The precipitate was filtered and carefully washed with cold ethyl acetate and cold cyclohexane to yield compound **34** (18.0 g, 99%) as a white solid.

^{1}H NMR ($CDCl_3$, 400 MHz, 25°C): δ = 7.26 (s, 2H), 3.99 (t, *J* = 6.7 Hz, 6H), 3.88 (s, 3H), 1.83-1.27 (m, 60H), 0.88 (t, *J* = 6.8 Hz, 9H).

^{13}C NMR ($CDCl_3$, 100 MHz, 25°C): δ = 167.0, 152.9, 142.4, 124.8, 108.0, 73.6, 69.3, 52.2, 2.1, 30.5, 29.9, 29.8, 29.7, 29.5, 29.4, 26.2, 22.8, 14.2.

*3,4,5-tris(dodecyloxy)benzoic acid (**35**)*

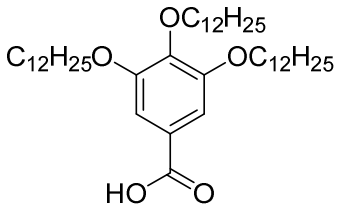

35

Compound **34** (13.0 g, 18.9 mmol) and potassium hydroxyde (2.1 g, 37.7 mmol) were suspended in ethanol (130 mL). The reaction was stirred overnight at reflux. To the cooled solution was added water (200 mL), and the pH was adjusted to 1 using a 10 M hydrochloric acid solution. The precipitate was filtered and washed with water (500 mL). The solid was taken back in dichloromethane (200 mL), dried with sodium sulfate, filtered and evaporation of the solvent yielded acid **35** (12.2 g, 95%) as an orange pale solid.

^{1}H NMR ($CDCl_3$, 400 MHz, 25°C): δ = 7.10 (s, 2H), 4.15-4.06 (m, 6H), 1.93-1.89 (m, 4H), 1.85-1.80 (m, 2H), 1.53 (m, 6H), 1.80-1.22 (m, 48H), 0.89 (t, *J* = 6.8 Hz, 9H).

*6-[3,4,5-Tri(dodecyloxy)phenyl]isocytosine (**38**)*

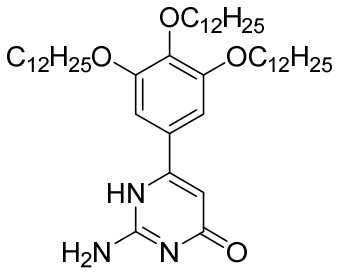

38

Carboxylic acid **34**(3.0 g, 4.44 mmol) was dissolved in dichloromethane (20 mL) with a few drops of dimethylformamide. The solution was cooled down using an ice bath and oxalyl chloride (0.57 mL, 6.66 mmol) was added dropwise. The solution was stirred overnight at room temperature. Then, solvents were evaporated *via* azeotropic distillation using toluene. The resulting solid was dried for 1 hour under vacuum.

Meanwhile, potassium ethyl malonate (1.02 g, 6.0 mmol) and magnesium chloride (780 mg, 8.21 mmol) were dissolved under argon in ethyl acetate (12 mL). The mixture was cooled to 0°C using an ice bath and triethylamine (2.23 mL, 16.1 mmol) was added dropwise. After stirring at 35°C for 6 hours, a solution of the previously prepared acyl chloride dissolved in dry dichloromethane (12 mL) was added dropwise *via* a cannula. The solution was stirred overnight at room temperature. The solution was then cooled down to 0°C and 13% hydrochloric acid (20 mL) was added dropwise. The aqueous phase was separated and extracted with toluene (20 mL) and ethylacetate (20 mL). The combined organic layers were washed with 13% hydrochloric acid (20 mL), water (20 mL), and 5% sodium carbonate (20 mL). The solvents were evaporated

to yield the corresponding ethyl malonate **37** (3.00 g, 97%) as an orange compound, which was used as such in the next step without further purification or characterization.

The previously prepared compound **37** (3.0 g, 4.02 mmol) was dissolved in ethanol (35 mL) and guanidinium carbonate (0.9 g, 5.03 mmol) was added. The solution was stirred for two days at reflux. The solvent was then removed under vacuum and the residue taken back in chloroform (50 mL). The organic phase was washed with water (50 mL), dried on sodium sulfate and evaporated under vacuum. The residue was purified by column chromatography (SiO_2, CH_2Cl_2/EtOH 1/0 → 96/5), yielding compound **38** (1.7 g, 56%) as a white sticky solid.

^{1}H NMR ($CDCl_3$, 400 MHz, 25°C): δ = 12.35 (br, 1H), 7.13 (s, 2H), 6.19 (s, 1H), 5.84 (brm, 2H) 4.05-3.97 (m, 6H), 1.75-1.67 (m, 6H), 1.58-1.43 (m, 6H),1.42-1.16 (m, 48H), 0.89 (brt, *J* = 6.5 Hz, 9H).

^{13}C NMR ($CDCl_3$, 100 MHz, 25°C): δ =159.8, 155.1, 153.5, 151.7, 142.0, 123.6, 106.0, 100.2, 72.0, 68.0, 32.0, 30.6, 29.7, 29.6, 29.5, 29.4, 29.3, 26.2, 26.0, 22.4, 14.0.

*N-(6-((tert-butyldiphenylsilyl)oxy)hexyl)-1H-imidazole-1-carboxamide (**41**)*

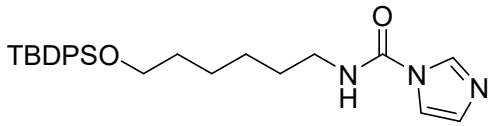

41

6-aminohexanol (3.3 g, 28.0 mmol) was dissolved in dry tetrahydrofuran (85 mL), and carbonyldiimidazole (5.0 g, 30.8 mmol) was added. The solution was stirred for 5 hours at room temperature and then diluted with water (150 mL). The aqueous solution was and extracted with ethyl acetate (4 x 50 mL). The combined organic phases were concentrated under vacuum and cooled down to trigger precipitation of imidazole. Evaporation of the filtrate yielded compound **40** a sticky colorless oil which was used as such in the next step.

The previously prepared intermediate **40** was dissolved in tetrahydrofuran (150 mL) along with triethylamine (2.7 mL, 19.9 mmol). The solution was cooled down to 0°C using an ice bath and *tert*-butyl(chloro)diphenylsilane (5.1 mL, 19.9 mmol) was added dropwise. The solution was allowed to come back to room temperature and stirred overnight. Then the mixture was diluted with water (150 mL), and extracted with chloroform (3 x 75 mL). The combined organic phases were dried over sodium sulfate and evaporated under vacuum. The residue was purified by

column chromatography (SiO_2, cyclohexane/CH_2Cl_2/MeOH 1/0/0 → 0/98/2) to yield the compound **41** (8.2 g, 92% over two steps) as a colorless sticky oil.

^{1}H NMR ($CDCl_3$, 400 MHz, 25°C): δ = 8.14 (s, 1H), 7.69-7.64 (m, 4H), 7.44-7.34 (m, 6H), 7.04 (s, 1H), 6.78 (s, 1H), 3.66 (t, *J* = 6.2 Hz, 2H), 3.38 (dt, *J* = 6.7 Hz, 2H), 1.65-1.53 (m, 4H), 1.45-1.30 (m, 4H), 1.05 (s, 9H).

^{13}C NMR ($CDCl_3$, 100 MHz, 25°C): δ = 149.1, 135.9, 135.7, 134.2, 129.7, 127.7, 116.3, 76.8, 63.9, 41.2, 32.5, 29.6, 27.0, 26.7, 25.6, 19.4.

HRMS (ESI+): m/z calcd. for $C_{26}H_{35}N_3O_2Si$: 450.2571 $[M+H]^+$, found: 450.2574.

*Compound **42***

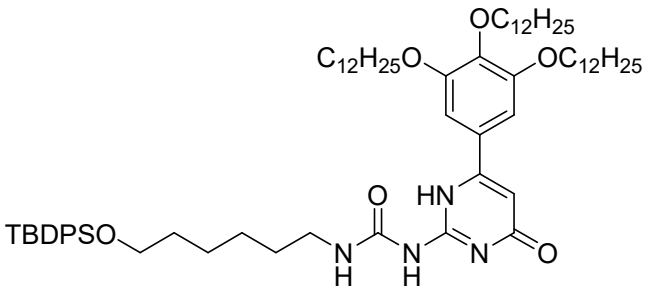

42

Compound **38** (2.5 g, 3.38 mmol) and **41** (1.8 g, 4.05 mmol) were suspended in dry dimethylformamide (50 mL). Triethylamine (0.6 mL, 4.05 mmol) was added to the mixture and the flask was heated up to 80°C for 3 days. After this time, methanol (80 mL) was added and the solution was cooled down to 0°C. The solution was then filtered to recover the crude compound **3** as a white precipitate. The solid was washed with cold acetone (20 mL) and methanol (20 mL). If the crude compound was not clean, purification by column chromatography (SiO_2, CH_2Cl_2/MeOH 1/0 → 98.5/1.5) was performed to obtain compound **42** (3.1 g, 81%) as a pure white solid.

^{1}H NMR ($CDCl_3$, 400 MHz, 25°C): δ = 13.85 (s, 1H), 12.03 (s, 1H), 10.18 (t, *J* = 5.1 Hz, 1H), 7.67-7.63 (m, 4H), 7.42-7.33 (m, 6H), 6.81 (s, 2H), 6.25 (s, 1H), 4.06-3.97 (m, 6H), 3.65 (t, *J* = 6.2 Hz, 2H), 3.27 (td, *J* = 5.4 Hz, 2H), 1.87-1.71 (m, 6H), 1.68-1.53 (m, 6H), 1.53-1.44 (m, 6H), 1.42-1.19 (m, 50H), 1.03 (s, 9H), 0.87 (t, *J* = 6.9 Hz, 9H).

^{13}C NMR ($CDCl_3$, 100 MHz, 25°C): δ = 173.5, 156.8, 155.2, 154.0, 149.4, 141.2, 135.7, 134.3, 129.6, 127.7, 126.2, 104.5, 73.8, 69.5, 64.1, 40.3, 32.7, 32.1, 30.5, 29.9-29.4, 27.0, 26.2, 25.7, 22.9, 19.4, 14.3.

HRMS (ESI+): m/z calcd. for $C_{69}H_{112}N_4O_6Si$: 1121.8424 $[M+H]^+$, found: 1121.8390.

*Compound **44***

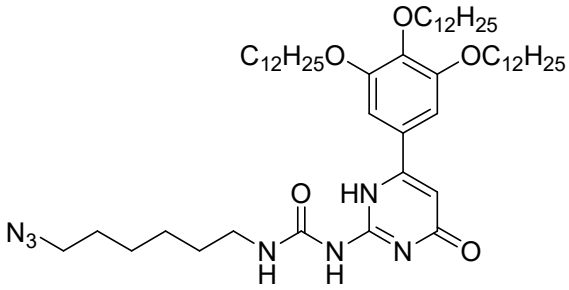

44

Compound **42** (1.5 g, 1.34 mmol) was suspended in tetrahydrofuran (15 mL) and 1 M tetrabutylammonium fluoride in tetrahydrofuran (6.7 mL) was added to the solution. The mixture was stirred at 60°C overnight. Methanol (25 mL) was added, and the solution was cooled down to 0°C. The solution was then filtered to recover a white precipitate. The solid was washed with cold methanol (15 mL) and cold acetone (10 mL). The white precipitate was taken back in chloroform (50 mL) and washed with water (3 x 25 mL). The solution was dried over sodium sulfate, filtered, and evaporated under vacuum to yield the corresponding alcohol **43** as a white compound (1.01 g, 85%) pure enough to be used as such in the next step.

The previously prepared alcohol **43** (1.01 g, 1.13 mmol) was suspended in dry dichloromethane (30 mL) with triethylamine (236 µL, 1.70 mmol). The solution was cooled down to 0°C and methanesulfonyl chloride (131 µL, 1.70 mmol) was added dropwise. The solution was stirred at room temperature overnight. Dichloromethane (20 mL) was added and the organic phase was washed with a saturated solution of ammonium chloride (20 mL) and water (50 mL). The organic phase was dried over sodium sulfate, filtered, and evaporated under vacuum to yield the mesylated compound as a yellow solid, which was pure enough to be used as such in the next step.

The mesylated compound was taken back in dry dimethylformamide (20 mL) and treated with sodium azide (735 mg, 11.3 mmol). The solution was stirred for 12 hours at 50°C. Then, the mixture was diluted with chloroform (25 mL) and the organic phase was washed with water (3 x 25 mL). The organic phase was dried over sodium sulfate, filtered, and evaporated under vacuum. The residue was purified by column chromatography (SiO_2, CH_2Cl_2/MeOH 98.5/1.5) to yield compound **44** (812 mg, 73% over 3 steps) as a white solid.

^{1}H NMR ($CDCl_3$, 400 MHz, 25°C): δ = 13.83 (s, 1H), 12.04 (s, 1H), 10.19 (s, 1H), 6.81 (s, 2H), 6.25 (s, 1H), 4.07-3.99 (m, 6H), 3.34-3.27 (m, 2H), 3.25 (t, *J* = 7.0 Hz, 2H), 1.87-1.70 (m, 6H), 1.68-1.52 (m, 6H), 1.52-1.41 (m, 6H), 1.40-1.15 (m, 50H), 0.88 (t, *J* = 6.9 Hz, 9H).
^{13}C NMR ($CDCl_3$, 100 MHz, 25°C): δ = 173.5, 156.9, 155.2, 154.0, 149.5, 141.3, 126.2, 104.5, 103.9, 100.1, 73.8, 69.6, 40.0, 32.1, 32.1, 30.5, 29.9-28.9, 26.6, 26.6, 26.2, 22.9, 14.3.
HRMS (ESI+): m/z calcd. for $C_{53}H_{93}N_7O_5$: 908.7311 $[M+H]^+$, found: 908.7347.

*Compound **45***

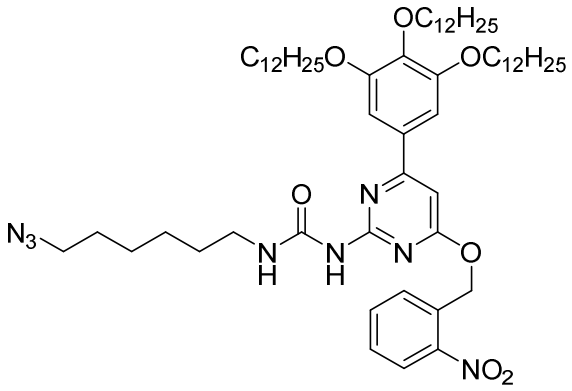

45

Compound **44** (1.2 g, 1.32 mmol), 1-(chloromethyl)-2-nitrobenzene (340 mg, 1.98 mmol) and potassium carbonate (292 mg, 2.11 mmol) were mixed in dry dimethylformamide (35 mL) under argon and the solution was stirred at 80°C overnight. After the reaction, dimethylformamide was removed under vacuum, and the residue was taken back in chloroform (30 mL), washed with water (30 mL) and brine (30 mL). The organic phase was dried over sodium sulfate and filtered. After evaporation of the solvent under vacuum, the residue was purified by column chromatography (SiO_2, cyclohexane/CH_2Cl_2 1/1 → 0/1) to yield the protected compound **45** (1.1 g, 83%) as a yellow solid.
^{1}H NMR ($CDCl_3$, 400 MHz, 25°C): δ = 9.13 (bs, 1H), 8.14 (dd, *J* = 8.2, 1.3 Hz, 1H), 7.72 (dd, *J* = 8.0, 1.6 Hz, 1H), 7.66 (td, *J* = 7.6, 1.3 Hz, 1H), 7.53-7.48 (m, 1H), 7.41 (s, 1H), 7.10 (s, 2H), 6.72 (s, 1H), 5.79 (s, 2H), 4.06-4.00 (m, 6H), 3.36 (dt, *J* = 6.7 Hz, 2H), 3.20 (t, *J* = 6.9 Hz, 2H), 1.88-1.62 (m, 8H), 1.65-1.42 (m, 12H), 1.43-1.18 (m, 48H), 0.87 (t, *J* = 6.9 Hz, 9H).
^{13}C NMR ($CDCl_3$, 100 MHz, 25°C): δ = 170.5, 166.0, 161.5, 157.9, 154.6, 153.9, 148.0, 141.6, 134.2, 132.7, 131.7, 129.5, 129.3, 125.5, 106.2, 97.3, 74.1, 69.9, 65.4, 51.7, 40.4, 32.4, 30.8, 30.6, 30.2-29.7, 29.2, 27.0, 26.9, 26.6, 23.1, 14.5.
HRMS (ESI+): m/z calcd. for $C_{60}H_{98}N_8O_7$: 1043.7631 $[M+H]^+$, found: 1043.7665.

*Bis-UPyProtected[c2]daisy chains (**46**)*

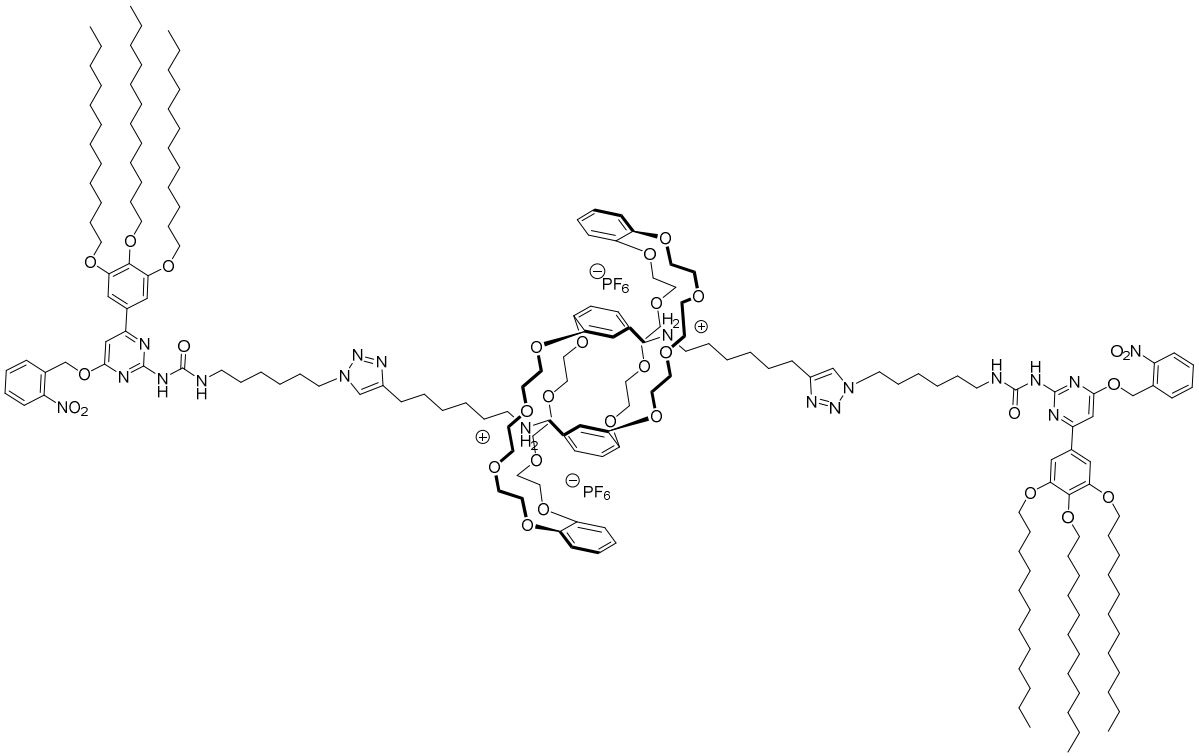

46

Compound **45** (437 mg, 0.42 mmol) and compound **12** (250 mg, 0.17 mmol) were mixed in dry dichloromethane (10 mL) in a microwave vessel, flushed with argon. Then, tetrakis(acetonitrile)copper(I) hexafluorophosphate (250 mg, 0.67 mmol) was added and the mixture was stirred overnight at 35°C, under microwave irradiation (50 W). Dichloromethane (10 mL) was added, along with an aqueous ethylenediaminetetraacetic acid solution at pH 9 (20 mL). The biphasic mixture was stirred for 2 hours. The organic phase was separated, the aqueous phase extracted with dichloromethane (2 x 20 mL). The combined organic phases were stirred with a saturated aqueous ammonium hexafluorophosphate solution (30 mL). The organic phase was separated and the aqueous phase extracted with dichloromethane (2 x 15 mL). The combined organic phases were dried with sodium sulfate and filtered, and the solvent evaporated under vacuum. Column chromatography of the residue (SiO_2, CH_2Cl_2/MeOH 100/0 → 99/1) yielded compound **46** (310 mg, 52%) as a yellow solid.

^{1}H NMR ($CDCl_3$, 400 MHz, 25°C): δ = 9.04 (s, 2H), 8.15 (dd, *J* = 8.1, 1.1 Hz, 2H), 7.73 (d, *J* = 8.1 Hz, 2H), 7.68 (td, *J* = 7.4, 1.1 Hz, 2H), 7.53 (td, *J* = 8.0, 1.1 Hz, 2H), 7.24 (s, 2H), 7.21 (s, 2H), 7.11 (s, 4H), 6.84-6.69 (m, 14H), 6.61 (d, *J* = 1.3 Hz, 2H), 5.79 (s, 4H), 4.50 – 4.39

(m, 4H), 4.38-4.29 (m, 4H), 4.27 (t, *J* = 7.3 Hz, 4H), 4.24-4.07 (m, 12H), 4.07-4.00 (m, 16H), 4.00-3.65 (m, 30H), 3.52-3.42 (m, 2H), 3.33 (td, *J* = 6.33 Hz, 4H), 2.62 (t, *J* = 7.3 Hz, 4H), 1.90-1.81 (m, 10H), 1.79-1.73 (m, 4H), 1.66 (m, 8H), 1.64-1.55 (m, 8H), 1.53-1.44 (m, 12H), 1.42-1.17 (m, 110H), 0.91-0.83 (m, 18H).

^{13}C NMR ($CDCl_3$, 100 MHz, 25°C): δ = 170.1, 165.8, 157.6, 154.2, 153.6, 147.9, 147.8, 147.7, 147.6, 146.4, 146.2, 141.2, 134.1, 132.3, 131.3, 129.1, 125.2, 124.8, 123.1, 121.2, 121.1, 120.6, 113.3, 112.7, 112.0, 111.9, 105.9, 96.9, 73.8, 72.4, 71.9, 71.2, 70.9, 70.5, 69.5, 67.7, 67.1, 67.1, 66.9, 65.2, 52.3, 50.2, 48.9, 40.0, 32.1, 30.5, 30.4, 30.2, 29.9-29.4, 29.4, 28.8, 26.8, 26.6, 26.5, 26.3, 26.2, 25.6, 22.8, 14.2.

HRMS (ESI+): m/z calcd. for $C_{186}H_{292}F_{12}N_{18}O_{30}P_2$: 1631.1043 $[M-2PF_6]^{2+}$, found: 1631.1231.

*Bis-Me-UPyProtected[c2]daisy chains (**5**^{Ext})*

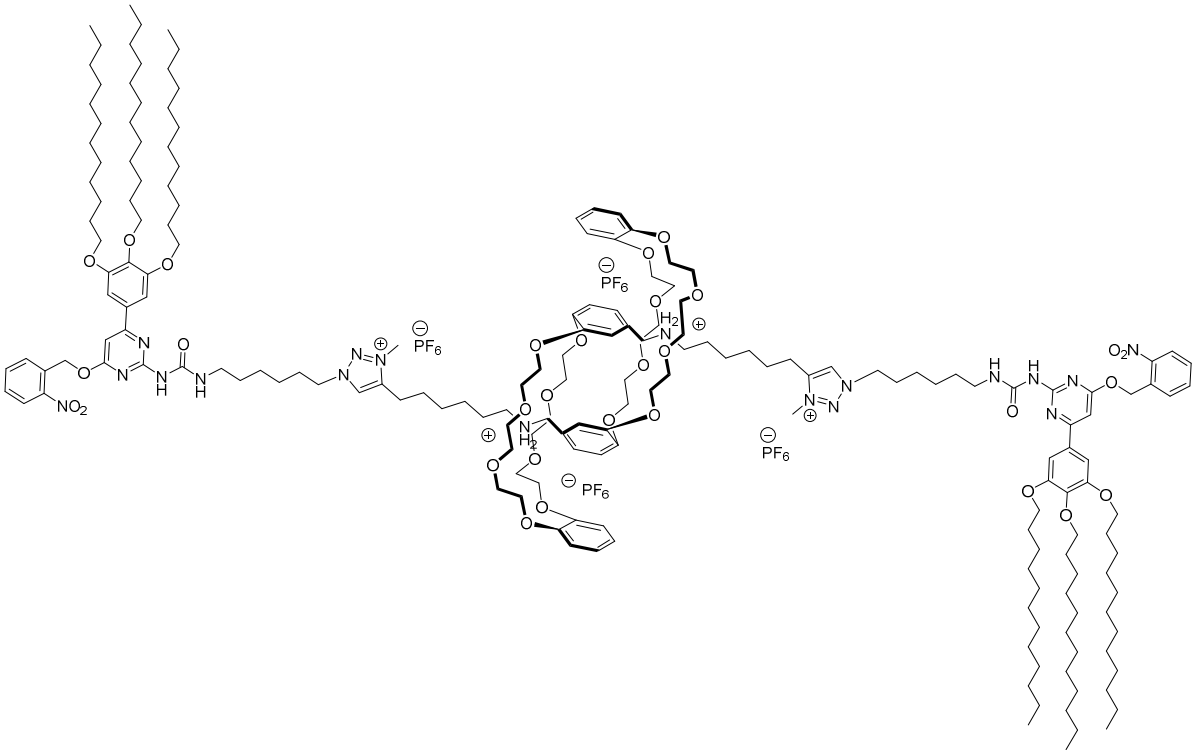

39^{Ext}

Compound **46** (28.0 mg, 8 µmol) was dissolved in a 2:1.5:0.5 mixture of methyl iodide/chloroform/acetronitrile (2.5 mL) and stirred at room temperature for 5 days. After the reaction, solvents were evaporated and the residue was taken back in dichloromethane (5 mL). The solution was stirred with a saturated aqueous ammonium hexafluorophosphate solution (5 mL). The organic phase was separated, the aqueous phase extracted with dichloromethane (2 x

5 mL). The combined organic phases were dried with sodium sulfate and filtered, and the solvent evaporated under vacuum to yield the methylated compound **5^{Ext}** (30.5 mg, quantitative) as a yellow solid.

^{1}H NMR ($CDCl_3$, 400 MHz, 25°C): δ = 8.94 (s, 2H), 8.21 (s, 2H), 8.13 (dd, *J* = 8.2, 1.1 Hz, 2H), 7.74 (d, *J* = 7.8 Hz, 2H), 7.68 (td, *J* = 7.4, 1.1 Hz, 2H), 7.53 (td, *J* = 7.0, 1.1 Hz, 2H), 7.41 (s, 2H), 7.12 (s, 4H), 6.80-6.66 (m, 14H), 6.39 (d, *J* = 8.0 Hz, 2H), 5.77 (s, 4H), 4.50-4.36 (m, 4H), 4.46 (t, *J* = 7.2 Hz, 4H), 4.34-4.26 (m, 2H), 4.22-4.08 (m, 6H), 4.14 (s, 6H), 4.08-4.00 (m, 6H), 4.02 (dt, *J* = 7.0 Hz, 12H), 3.97-3.89 (m, 12H), 3.89-3.73 (m, 16H), 3.73-3.60 (m, 6H), 3.49-3.37 (m, 4H), 3.33-3.29 (m, 4H), 2.70 (t, *J* = 7.2 Hz, 4H), 2.01-1.92 (m, 4H), 1.87-1.63 (m, 24H), 1.60-1.42 (m, 16H), 1.42-1.17 (m, 110H), 0.91-0.83 (m, 18H).

^{13}C NMR ($CDCl_3$, 100 MHz, 25°C): δ = 170.1, 166.0, 157.6, 154.3, 153.6, 147.8, 147.7, 147.5, 146.5, 146.3, 144.9, 141.3, 134.2, 132.3, 131.3, 129.2, 128.0, 125.3, 125.2, 122.8, 121.2, 121.0, 113.7, 112.1, 111.9, 105.9, 100.1, 96.9, 73.8, 72.1, 70.9, 70.6, 69.5, 67.2, 66.9, 65.2, 53.9, 52.2, 49.0, 39.8, 37.4, 32.1, 30.5, 29.9-29.4, 29.1, 28.3, 26.3, 26.3, 26.1, 25.6, 23.1, 22.8, 14.2.

HRMS (ESI+): m/z calcd. for $C_{188}H_{298}F_{24}N_{18}O_{30}P_4$: 822.0581 $[M-4PF_6]^{4+}$, found: 822.0608.

Bis-Me-UPyProtected[c2]daisy chains (5^{Cont})

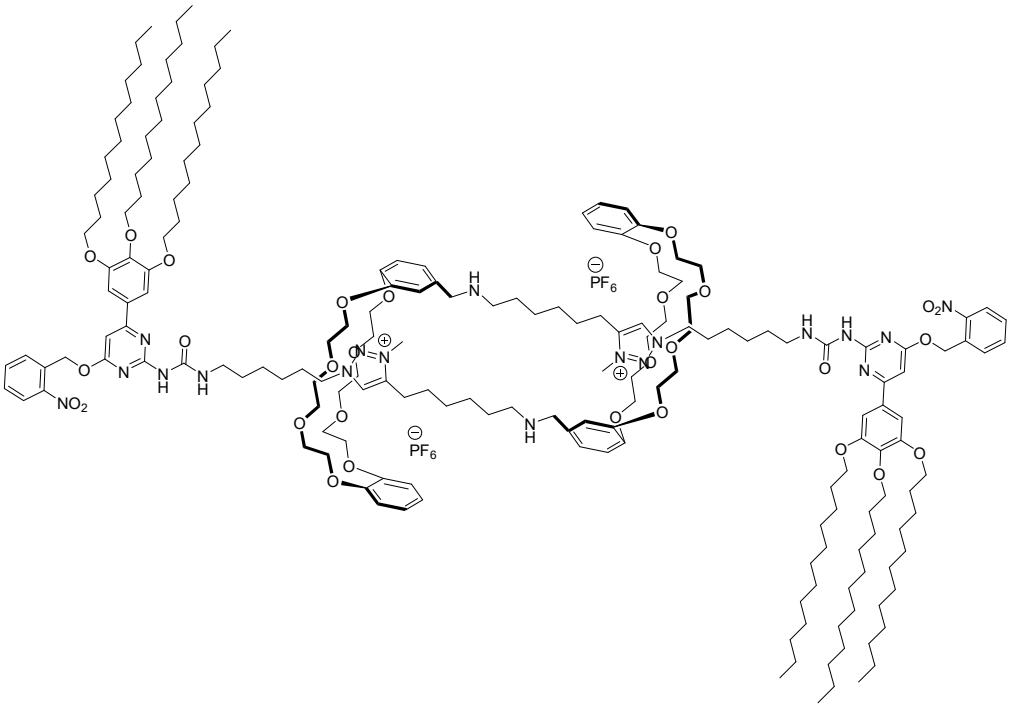

5^{Cont}

Compound **5^{Ext}** (50.0 mg, 13 µmol) was dissolved in chloroform (5 mL) and briefly shaken with a 1 M sodium hydroxyde solution (1 mL). The organic phase was separated, and the aqueous phase washed with chloroform (2 x 5 mL). The combined organic phases were combined and dried over sodium sulfate. Evaporation of the solvent yielded the pure contracted rotaxane **5^{Cont}** (48 mg, quantitative).

^{1}H NMR ($CDCl_3$, 400 MHz, 25°C): δ = 9.03 (s, 2H), 8.46 (s, 2H), 8.11 (dd, *J* = 8.5, 1.1 Hz, 2H), 7.74 (d, *J* = 7.3 Hz, 2H), 7.68 (td, *J* = 7.3, 1.1 Hz, 2H), 7.51 (td, *J* = 8.56, 1.1 Hz, 2H), 7.24 (s, 2H), 7.13 (s, 4H), 6.87 (s, 2H), 6.83-6.67 (m, 14H), 5.77 (s, 4H), 5.06-4.88 (m, 4H), 4.18-4.10 (m, 4H), 4.10-3.92 (m, 10H), 4.02 (dt, *J* = 7.0 Hz, 12H), 3.92-3.75 (m, 16H), 3.75-3.67 (m, 6H), 3.67-3.53 (m, 18H), 3.42-3.33 (m, 8H), 2.61-2.52 (m, 4H), 2.30-2.17 (m, 4H), 1.88-1.71 (m, 14H), 1.67-1.58 (m, 4H), 1.55-1.41 (m, 24H), 1.40-1.19 (m, 110H), 0.91-0.82 (m, 18H).

^{13}C NMR ($CDCl_3$, 100 MHz, 25°C): δ = 170.1, 165.8, 157.5, 154.1, 153.6, 149.1, 147.8, 147.6, 146.4, 141.3, 134.2, 133.8, 132.2, 131.2, 129.1, 128.4, 125.2, 121.6, 121.2, 121.0, 120.5, 112.1, 111.8, 111.7, 111.3, 105.8, 96.8, 73.8, 71.3, 71.1, 70.1, 69.5, 68.3, 68.2, 68.0, 65.2, 53.6, 49.4, 40.1, 40.0, 36.0, 33.9, 32.1, 30.5, 29.9-29.4, 28.9, 27.4, 27.3, 26.7, 26.6, 26.3, 22.8, 14.2.

HRMS (ESI+): m/z calcd. for $C_{188}H_{296}F_{12}N_{18}O_{30}P_2$: 1643.1089 $[M-2PF_6]^{2+}$, found: 1643.1082.

*Bis-UPy[c2]daisy chains (**46^{Ext}**)*

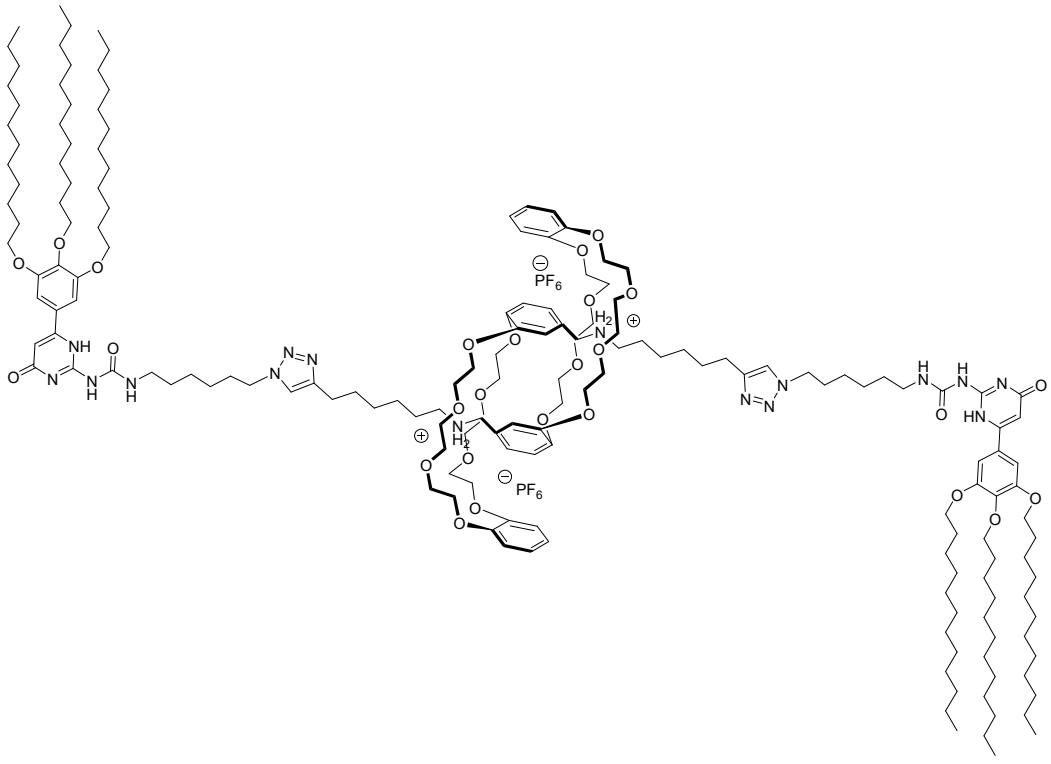

40

Protected compound **46** (50.0 mg, 15 µmol) was dissolved in dry toluene (250 µL) in a vial and degassed with using argon. The vial was tightly closed and irradiated under stirring using a 150W Xenon-Mercury lamp with a 320-375 nm filter. After six hours, a gel phase appeared when the sample was left unstirred. The solvents were removed under vacuum and the dark orange residue was dried overnight. The solid residue was then taken back in $CDCl_3$ for ^1H NMR analysis

The spectrum displays NH shifts typical of hydrogen bonding and the disappearance of peaks from the protecting group. The drastic broadening of the peaks confirms the formation of a supramolecular polymer.

HRMS (ESI+): m/z calcd. for $C_{172}H_{282}F_{12}N_{16}O_{26}P_2$: 1494.0613 $[M-2PF_6]^{2+}$, found: 1494.0622.

*Bis-Me-UPy[c2]daisy chains (**6**^{Ext})*

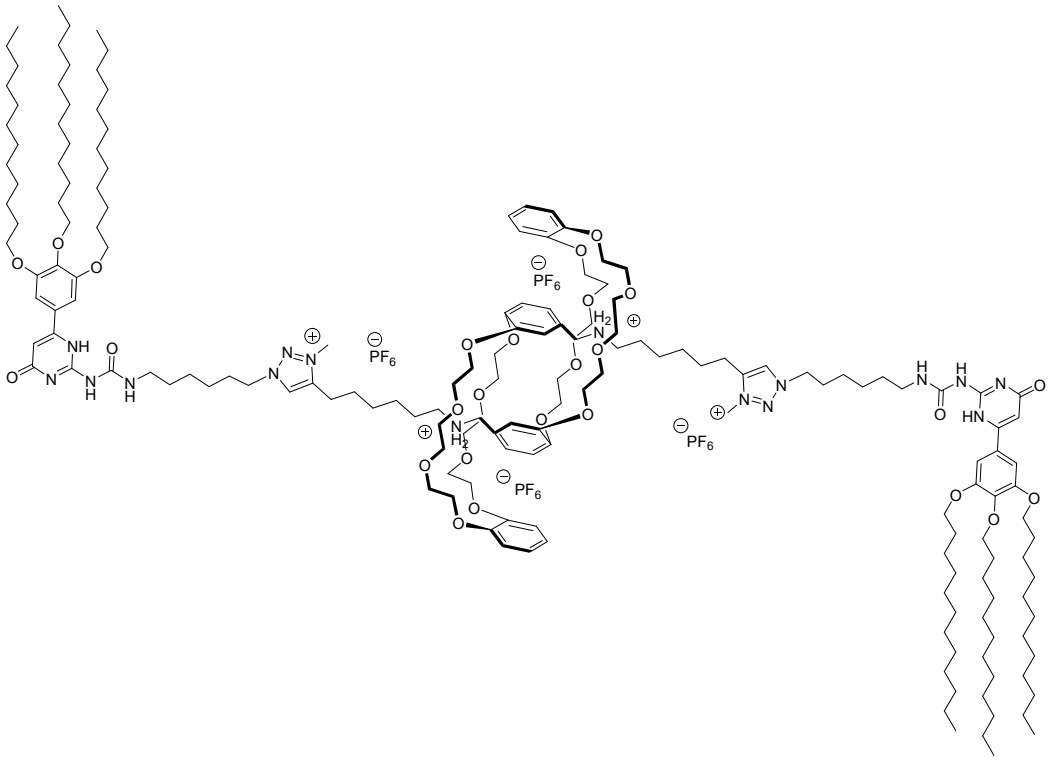

6^{Ext}

Protected compound **5**^{Ext} (50 mg, 15µmol) was dissolved in dry toluene (250 µL) in a vial and degassed with using argon. The vial was tightly closed and irradiated under stirring using a 150W Xenon-Mercury lamp with a 320-375 nm filter. After six hours, a gel phase appeared

when the sample was left unstirred. The solvents were removed under vacuum and the dark orange residue was dried overnight. The solid residue was then taken back in $CDCl_3$ for ^1H NMR analysis

The spectrum displays NH shifts typical of hydrogen bonding and the disappearance of peaks from the protecting group. The drastic broadening of the peaks confirms the formation of a supramolecular polymer.

HRMS (ESI+): m/z calcd. for $C_{174}H_{288}F_{24}N_{16}O_{26}P_4$: 754.5421 $[M-4PF_6]^{4+}$, found: 754.5430.

*Bis-Me-UPy[c2]daisy chains (**6**^{Cont})*

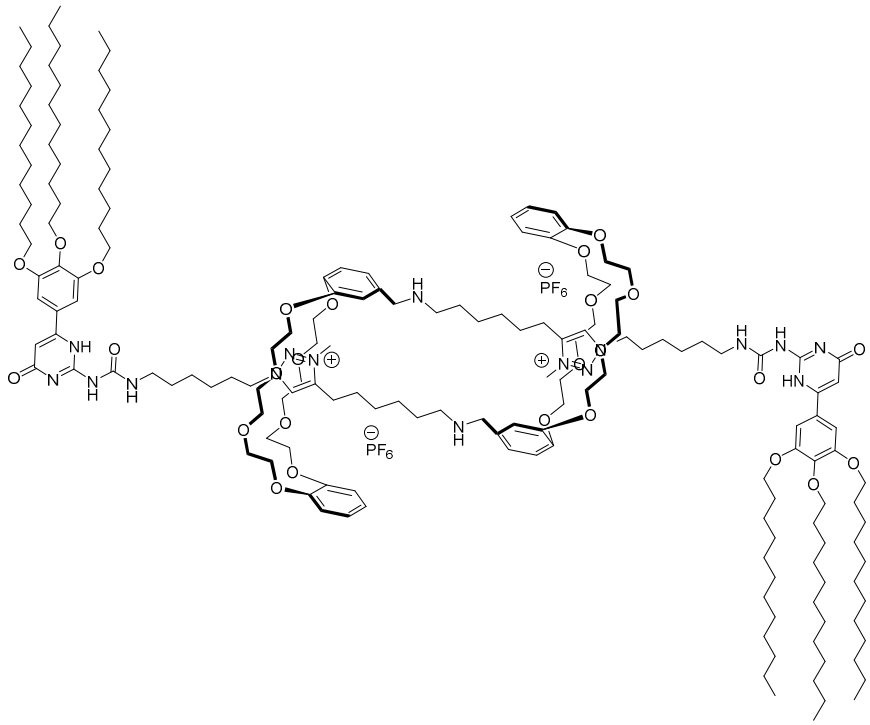

6^{Cont}

Protected compound **5**^{Cont} (50 mg, 15 µmol) was dissolved in dry toluene (250 µL) in a vial and degassed with using argon. The vial was tightly closed and irradiated under stirring using a 150W Xenon-Mercury lamp with a 320-375 nm filter. After six hours, the sample remained in the liquid state when left unstirred. The solvents were removed under vacuum and the dark orange residue was dried overnight. The solid residue was then taken back in $CDCl_3$ for ^1H NMR analysis

The spectrum displays very weak NH shifts typical of hydrogen bonding and the disappearance of peaks from the protecting group. The drastic broadening of the peaks confirms the formation of a supramolecular polymer.

HRMS (ESI+): m/z calcd. for $C_{174}H_{286}F_{12}N_{16}O_{26}P_2$: 1508.0769 $[M-2PF_6]^{2+}$, found: 1508.0671.

*1,4-bis((trimethylsilyl)ethynyl)benzene (**47**)*

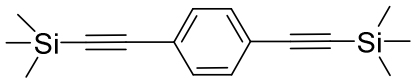

47

1,4-dibromobenzene (1.0 g, 4.24 mmol), trimethylsilylacetylene (1.32 mL, 9.33 mmol), bis(triphenylphosphine)palladium(II) dichloride (325 mg, 0.42 mmol), copper iodide (400 mg, 2.1 mmol), triphenylphosphine (980 mg, 3.74 mmol) and triethylamine (5 mL) were dissolved in tetrahydrofuran (20 mL) under argon. The solution was degassed using freeze-thaw cycles before being stirred at 80°C overnight. The solvent was removed and the residue purified by column chromatography (SiO_2, cyclohexane/CH_2Cl_2 95/5) to yield compound **47** (1.06 g, 92%) as a white solid.

R_f = 0.25 (cyclohexane).

^{1}H NMR ($CDCl_3$, 400 MHz, 25°C): δ = 7.38 (s, 4H), 0.25 (s, 18H).

^{13}C NMR ($CDCl_3$, 100 MHz, 25°C): δ = 131.9, 123.3, 104.7, 96.5, 0.1.

ESI-MS: m/z calcd. for $C_{16}H_{22}Si_2$: 271.13 $[M+H]^+$, found: 271.15.

*1,4-diethynylbenzene (**48**)*

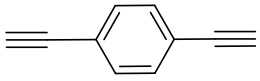

48

To a solution of 1,4-bis((trimethylsilyl)ethynyl)benzene **47** (1.0 g, 3.76 mmol) in a 1:1 mixture of dichloromethane and methanol (25 mL), potassium carbonate (5.19 g, 37.6 mmol) was added and the reaction mixture was stirred overnight at room temperature. The reaction mixture was

diluted with dichloromethane (25 mL) and then washed with water (3 × 30 mL). The organic phase was dried on sodium sulfate and the solvents evaporated to yield bis-alkyne **48** (471 mg, quantitative) as a white solid, which turned slowly to brown and should be stored in the refrigerator.

^{1}H NMR ($CDCl_3$, 400 MHz, 25°C): δ = 7.44 (s, 4H), 3.17 (s, 2H).

^{13}C NMR ($CDCl_3$, 100 MHz, 25°C): δ = 132.2, 122.7, 83.2, 79.2.

ESI-MS: m/z calcd. for $C_{10}H_6$: 127.05 $[M+H]^+$, found: 127.11.

*((4-bromo-2,5-bis((2-hexyldecyl)oxy)phenyl)ethynyl)trimethylsilane (**49**)*

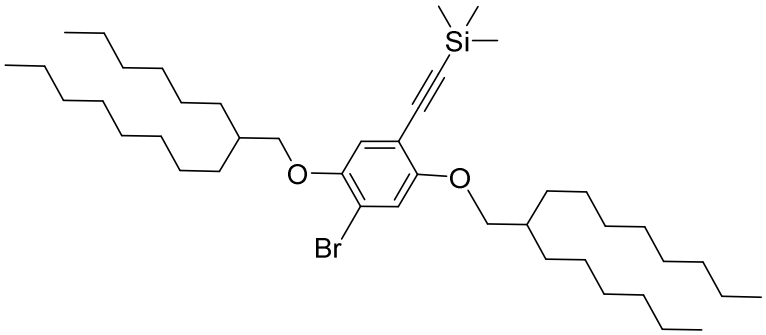

49

To an oven dried Schlenk were added 4-dibromo-2,5-bis((2-hexyldecyl)oxy)benzene **24** (4.9 g, 6.38 mmol), trimethylsilylacetylene (1.24 mL, 8.93 mmol), triphenylphosphine (335 mg, 1.28 mmol) in a 1:1 mixture of triethylamine and tetrahydrofuran (34 mL). The solution was degassed using freeze-thaw cycles and bis(triphenylphosphine)palladium(II) dichloride (269 mg, 0.38 mmol), copper iodide (243 mg, 1.28 mmol) were added. The solution was degassed using freeze-thaw cycles again and the reaction mixture was heated overnight at 40 °C. The reaction was quenched with a saturated solution of ammonium chloride (20 mL) and extracted with dichloromethane (30 mL). The organic phase was washed with a solution of saturated ammonium chloride (20 mL), water (20 mL) and dried over sodium sulfate. After removal of the solvent, the product was treated with pentane and filtered. Evaporation of the solvent under vacuum followed by purification by column chromatography (SiO_2, cyclohexane/CH_2Cl_2 95/5) afforded compound **49** (4.1 g, 88%) as a light yellow oil.

R_f = 0.3 (cyclohexane).

^{1}H NMR ($CDCl_3$, 400 MHz, 25°C): δ = 7.03 (s, 1H), 6.92 (s, 1H), 3.82 (d, *J* = 5.5 Hz, 4H), 1.81-1.74 (m, 2H), 1.54-1.19 (m, 48H), 0.92-0.83 (m, 12H), 0.25 (s, 9H).

^{13}C NMR ($CDCl_3$, 100 MHz, 25°C): δ = 155.0, 149.5, 117.7, 117.5, 113.7, 112.3, 100.8, 99.1, 77.2, 72.9, 72.2, 38.3, 38.1, 32.1, 32.1, 32.0, 32.0, 31.5, 31.4, 31.4, 30.2, 30.2, 29.9, 29.8, 29.8, 29.7, 29.5, 29.5, 27.0, 27.0, 27.0, 26.9, 22.8, 14.3, 0.1.

*1,4-bis((2,5-bis((2-hexyldecyl)oxy)-4-((trimethylsilyl)ethynyl)phenyl)ethynyl)benzene (**50**)*

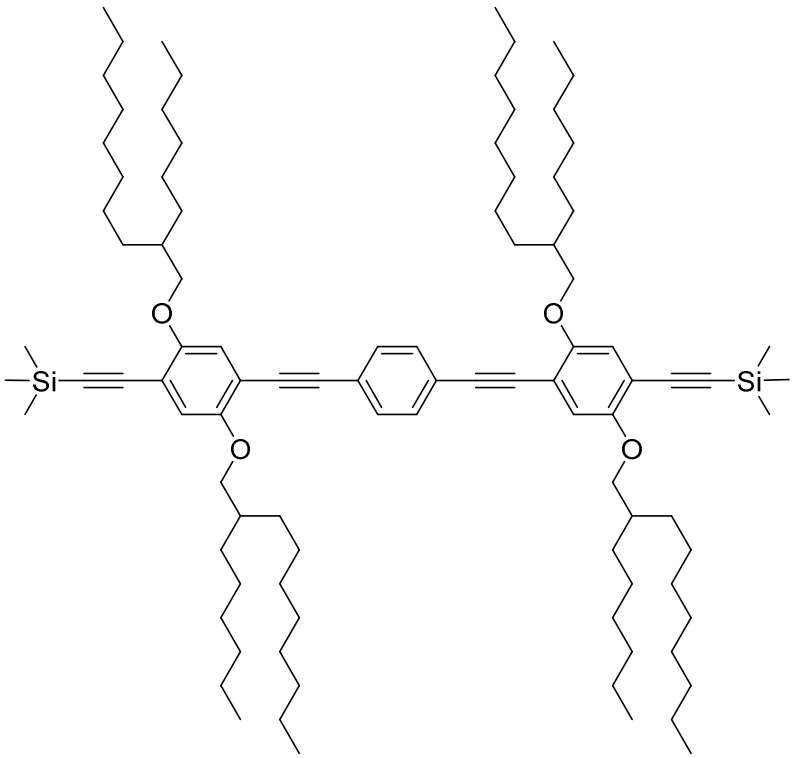

50

To an oven-dried Schlenk were added compound **49** (1.2 g, 1.65 mmol), 1,4-diethynylbenzene **48** (95 mg, 0.75 mmol), triphenylphosphine (316 mg, 1.2 mmol), triethylamine (15 mL) and dry tetrahydrofuran (7 mL) and the solution was degassed using freeze-thaw cycles. Bis(triphenylphosphine)palladium(II) dichloride (53 mg, 75 μmol) and copper iodide (129 mg, 0.67 mmol) were added and the solution was degassed using freeze-thaw cycles again. The reaction mixture was stirred at 80 °C overnight. After cooling down to room temperature, the reaction mixture was quenched with a saturated solution of ammonium chloride (20 mL) and extracted with diethyl ether (40 mL). The organic phase was washed with a saturated solution

of ammonium chloride (20 mL), water (20 mL) and dried over sodium sulfate. After removing the solvent, the product was treated with pentane and filtered. Evaporation of the filtrate and further purification by column chromatography (SiO_2, cyclohexane/CH_2Cl_2 90/10 → 85/15) provide compound **50** (811 mg, 75%) as a light yellow oil, which solidifies in few days.

R_f = 0.1 (cyclohexane/CH_2Cl_2 90/10).

^{1}H NMR ($CDCl_3$, 400 MHz, 25°C): δ = 7.47 (s, 4H), 6.93 (s, 4H), 3.86 (d, *J* = 6.0 Hz, 8H), 1.83-1.78 (m, 4H), 1.60-1.16 (m, 96H), 0.89-0.85 (m, 24H), 0.26 (s, 18H).

^{13}C NMR ($CDCl_3$, 100 MHz, 25°C): δ = 154.5, 153.8, 131.5, 123.4, 117.1, 116.4, 114.0, 113.8, 101.3, 100.2, 94.7, 88.1, 77.2, 72.4, 72.0, 38.3, 38.3, 32.1, 32.0, 31.6, 31.4, 30.3, 30.2, 29.9, 29.9, 29.8, 29.8, 29.5, 27.1, 27.0, 27.0, 22.8, 14.3, 0.2.

Anal. calcd for $C_{96}H_{158}O_4Si_2$: C 80.49, H 11.12, Si 3.92; found: C 80.37, H 11.44, Si 3.73.

*1,4-bis((4-ethynyl-2,5-bis((2-hexyldecyl)oxy)phenyl)ethynyl)benzene (**51**)*

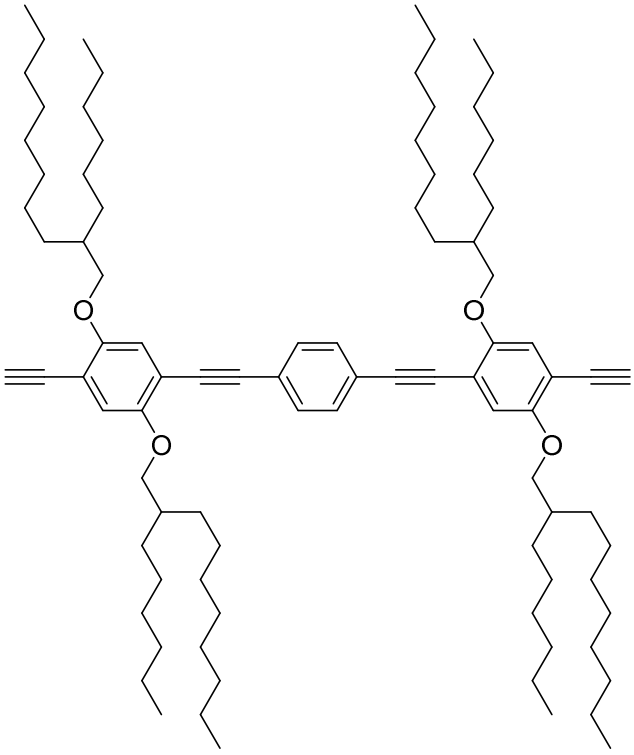

51

To a solution of compound **50** (329 mg, 0.23 mmol) in a 1:1 mixture of dichloromethane and methanol (16 mL), potassium carbonate (317 mg, 2.3 mmol) was added and the mixture was

stirred overnight at room temperature. The reaction mixture was then washed with water (3 × 20 mL), dried over sodium sulfate. Removal of the solvent afforded compound **51** (288 mg, 97%) as a red viscous oil.

^{1}H NMR ($CDCl_3$, 400 MHz, 25°C): δ = 7.48 (s, 4H), 6.98 (s, 2H), 6.97 (s, 2H), 3.87 (d, *J* = 5.7 Hz, 8H), 3.32 (s, 2H), 1.83-1.78 (m, 4H), 1.62-1.15 (m, 96H), 0.89-0.85 (m, 24H).

^{13}C NMR ($CDCl_3$, 100 MHz, 25°C): δ = 154.4, 153.7, 131.4, 123.3, 117.4, 116.8, 114.3, 112.9, 94.6, 87.8, 82.3, 80.0, 77.2, 72.6, 72.4, 38.2, 38.0, 31.9, 31.9, 31.9, 31.8, 31.5, 31.5, 31.4, 30.1, 30.0, 29.7, 29.7, 29.6, 29.4, 26.9, 26.9, 26.8, 26.8, 22.7, 14.1, 14.1.

Anal. calcd for $C_{90}H_{142}O_4$: C 83.92, H 11.11, found: C 83.6, H 11.37.

*Bis-benzyl acetate linker (**52**)*

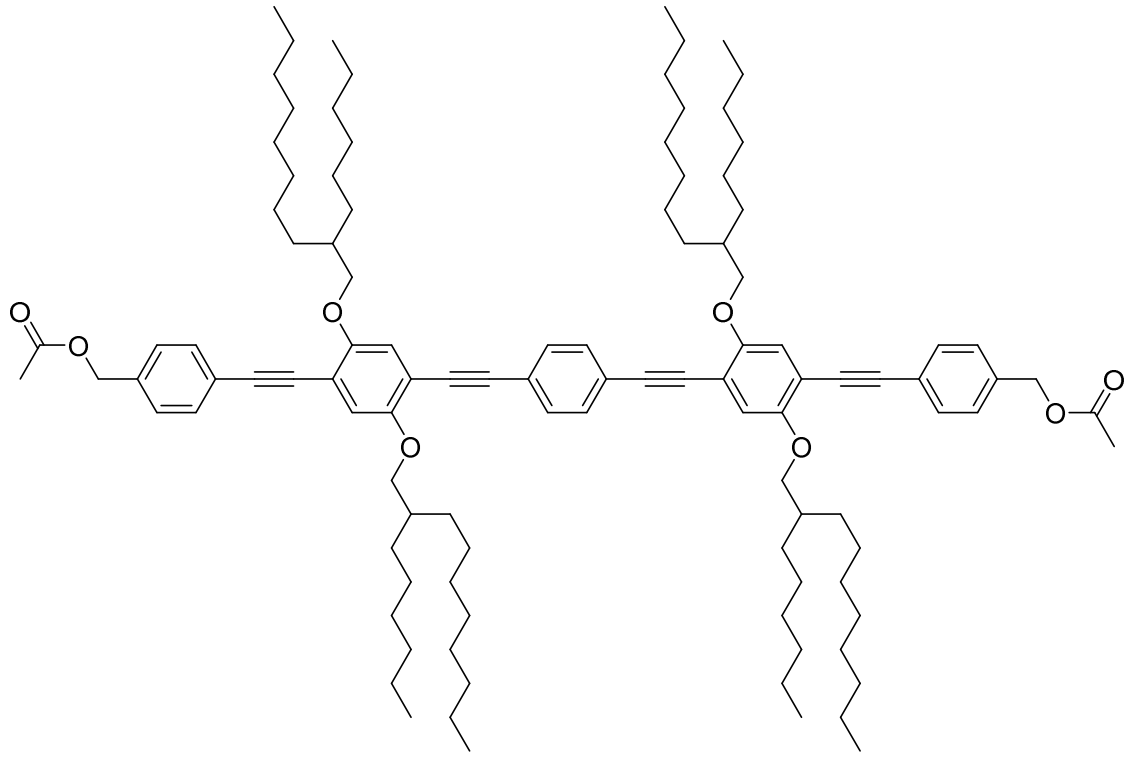

52

Compound **51** (600 mg, 0.47 mmol) and 4-bromobenzyl acetate **13** (32 mg, 1.4 mmol) were dissolved in a 1:1 mixture of dry triethylamine/tetrahydrofuran in an oven dried schlenk tube. After two freeze-thaw cycles, tetrakis(triphenylphosphine)palladium(0) (54 mg, 47 μmol) were added and the schlenk was degased one more time. The solution was then heated up to 75°C for 36 hours. Then the solvents were evaporated and the residue further purified by column

chromatography (SiO_2, cyclohexane/EtOAc 1/0 → 90/10) to yield product **52** (550 mg, 75%) as a bright yellow solid.

R_f = 0.15 (cyclohexane/EtOAc 10/1).

^{1}H NMR ($CDCl_3$, 400 MHz, 25°C): δ = 7.53 (d, *J* = 7.8 Hz, 4H), 7.49 (s, 4H), 7.35 (d, *J* = 7.8 Hz, 4H), 7.01 (s, 2H), 7.00 (s, 2H), 4.73 (s, 4H), 3.90 (d, *J* = 5.7 Hz, 8H), 2.12 (s, 6H), 1.92-1.88 (m, 4H), 1.62-1.15 (m, 96H), 0.89-0.86 (m, 24H).

^{13}C NMR ($CDCl_3$, 100 MHz, 25°C): δ = 170.8, 153.9, 135.9，131.7, 131.4，128.0, 123.5, 123.3, 116.6, 113.9, 113.8, 94.6, 94.5, 88.0, 86.5, 72.4, 65.9, 38.2, 31.9, 31.9, 31.8, 30.1, 29.8, 29.6, 29.4, 26.9, 26.9, 22.7, 21.0, 14.1, 14.1, 14.1.

*Bis-benzyl azide linker (**53**)*

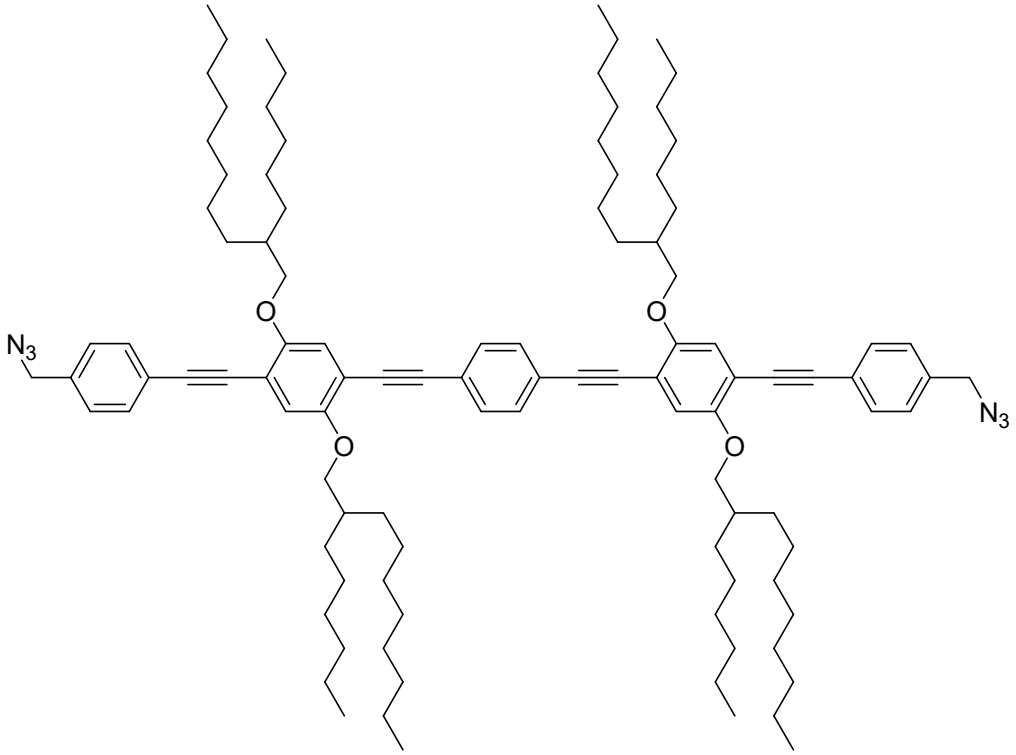

53

A solution of compound **52** (350 mg, 0.22 mmol) in a 9:1 mixture of dichloromethane/methanol (10 mL) was treated with potassium carbonate (305 mg, 2.2 mmol) and the solution was stirred at room temperature overnight. The solvent was then removed in vacuo, and the resulting mixture was dissolved with a mixture of dichloromethane (20 mL) and water (20 mL), and the

aqueous phase was extracted with dichloromethane (3 × 20 mL). The organic phases were combined, dried over sodium sulfate, and evaporated in vacuo to give the resulting bis-benzyl alcohol, which was pure enough to be used as such in the next step.

A solution of the crude bis-benzyl alcohol in dichloromethane (10 mL) was cooled down to 0°C and triethylamine (190 µL, 1.32 mmol) and methanesulfonyl chloride (110 µL, 1.32 mmol) were added. The reaction mixture was then stirred overnight at room temperature. The organic phase was then extracted with water (10 mL) and a saturated solution of ammonium chloride (10 mL), dried over sodium sulfate and concentrated in vacuo to provide the mesylated derivative, which was pure enough to be used as such in the next step.

A solution of this crude mesylate in a 1:1 mixture of dimethylformamide and tetrahydrofuran (0.9 mL) was treated with sodium azide (172 mg, 2.65 mmol) and heated up overnight to 50°C. After cooling down to room temperature, the reaction mixture was diluted with dichloromethane (10 mL). The organic phase was then extracted with water (10 mL) and a saturated solution of ammonium chloride (10 mL), dried over sodium sulfate and concentrated in vacuo. Further purification by column chromatography (SiO_2, cyclohexane/CH_2Cl_2 9/1) provided compound **53** (199 mg, 58% over 3 steps) as a yellow oil, which solidifies over time.

R_f = 0.1 (cyclohexane/CH_2Cl_2 9/1).

^{1}H NMR ($CDCl_3$, 400 MHz, 25°C): δ = 7.55 (d, *J* = 8.2 Hz, 4H), 7.50 (s, 4H), 7.30 (d, *J* = 8.4 Hz, 4H), 7.01 (s, 2H), 7.00 (s, 2H), 4.37 (s, 4H), 3.92 (d, *J* = 5.8 Hz, 8H), 1.90-1.80 (m, 4H), 1.64-1.14 (m, 96H), 0.91-0.81 (m, 24H).

^{13}C NMR (100 MHz, $CDCl_3$, 25°C): δ = 153.9, 135.4, 132.0, 131.4, 128.1, 123.6, 123.3, 116.6, 113.9, 113.8, 94.6，94.3, 88.0, 86.8, 72.4, 38.2, 31.9, 31.9, 31.5, 30.1, 29.8, 29.7, 29.6, 29.4, 26.9, 22.7, 14.1, 14.1.

MALDI-TOF: m/z calcd. for $C_{102}H_{154}N_6O_4$: 1549.188 $[M]^+$, found: 1549.135.

*Covalent polymer(**54**)*

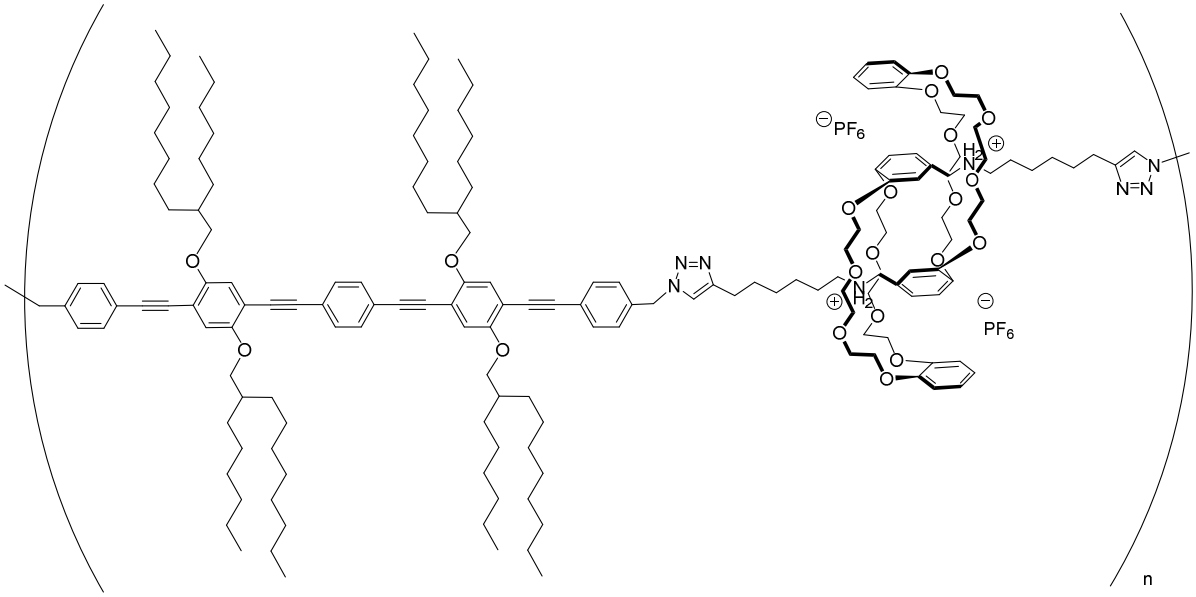

54

Compound **53** (143.0 mg, 92 µmol) and pseudo-rotaxane **12** (137.6 mg, 92 µmol) were dissolved in dry dichloromethane (5 mL) and tetrakis(acetonitrile)copper(I) hexafluorophosphate (68.8 mg, 185 µmol) and 2,6-lutidine (60 µL, 185 µmol) were added to the solution. The mixture was stirred for five minutes at room temperature and for two hours at 35 °C under microwave irradiation (50W). The solvents were removed under vacuum and the poorly soluble light yellow residue gently washed with cold dichloromethane (10 mL) and diethylether.(10 mL) Then a 4:1 mixture of dichloromethane/acetonitrile (5 mL) and an aqueous solution of ethylenediaminetetraacetic acid at pH 9 (5 mL) were added to the flask and the solution was stirred for two hours. The organic phase was separated and vigorously stirred with a saturated ammonium hexafluorophosphate aqueous solution (5 mL) for 1 hour. The organic phase was separated and the aqueous phase extracted with dichloromethane (2 x 5 mL). The combined organic phases were washed with water (2 x 10 mL), and dried over sodium sulfate. The solvents were evaporated to yield polymer **54** (235 mg, 85%) as a bright yellow film. ^{1}H NMR spectrum in a 4:1 $CDCl_3/CD_3CN$ mixture shows broadening of the signal characteristic of a polymer and no traces of the starting materials.

Methylated Covalent Polymer (7^{Ext})

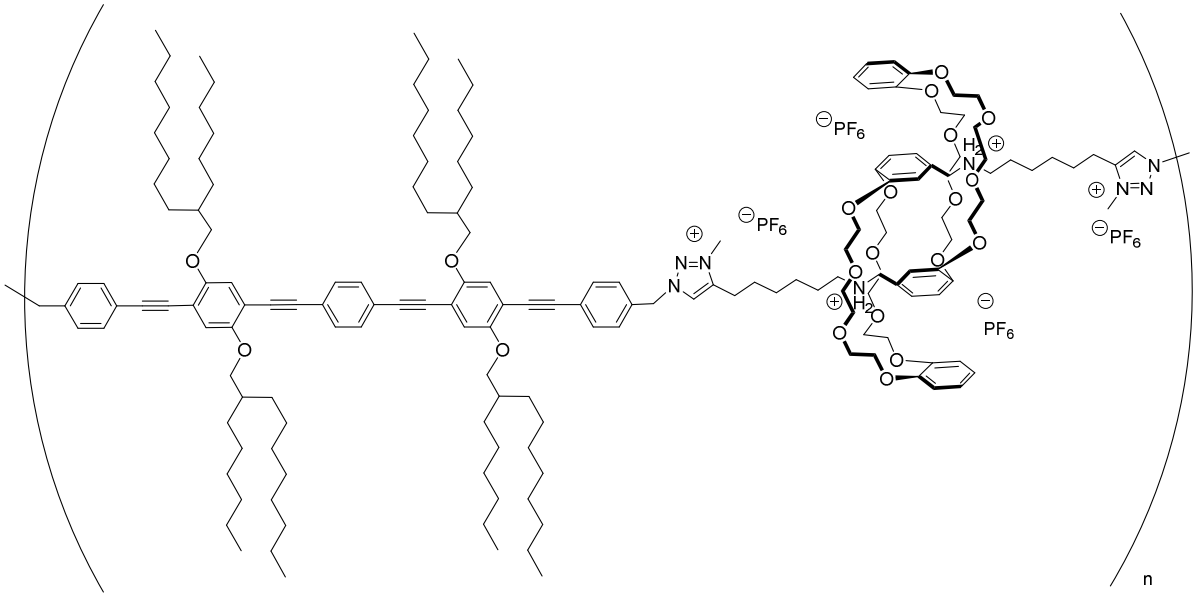

7^{Ext}

Polymer **54** (100 mg, 33 µmol) was dissolved in a 1:1 mixture of chloroform/methyl iodide (5 mL). The reaction mixture was stirred for 4 days at room temperature Solvents were evaporated and the solid was taken back in a 4:1 mixture of dichloromethane/acetonitrile (5 mL). This solution was stirred with a saturated ammonium hexafluorophosphate aqueous solution (5 mL) for 1 hour. The organic phase was separated and the aqueous phase extracted with dichloromethane (3 x 5 mL). The combined organic phases were dried over sodium sulfate and evaporated to yield methylated polymer **7^{Ext}** (109 mg, 100%) as a bright yellow film

*Methylated Covalent Polymer (**7**^{Cont})*

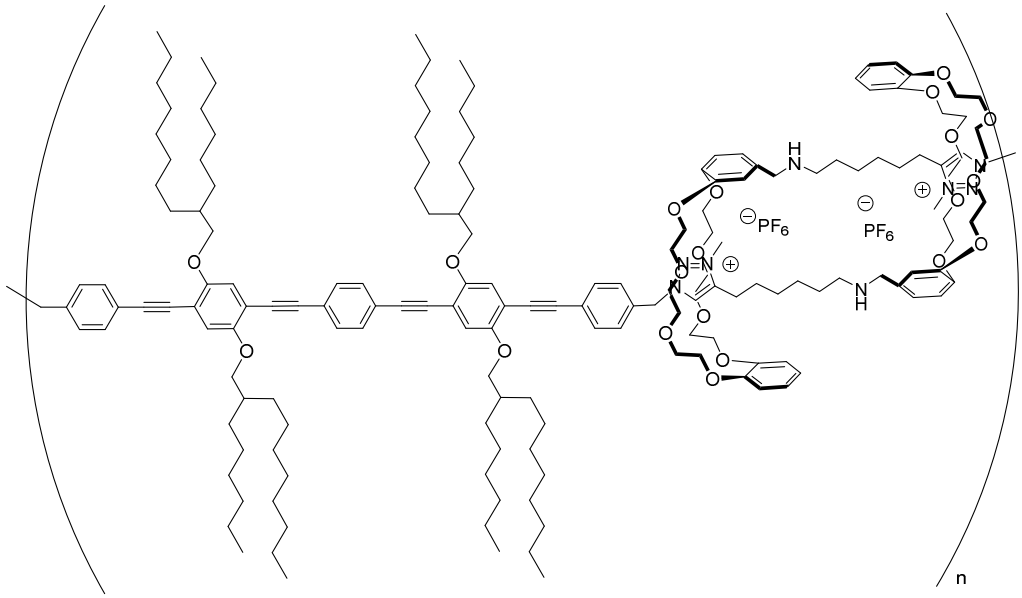

7^{Cont}

Polymer **7**^{Ext} (50 mg, 17 µmol) was dissolved in chloroform (5mL) and washed with a 1M sodium hydroxide aqueous solution (5 mL). The organic phase was separated, and the aqueous phase was extracted with chloroform (2 x 5 mL). The combined organic phases were washed with water (10 mL) and dried over sodium sulfate. The solvent was evaporated to yield contracted polymer **7**^{Cont} (49 mg, 100%) as a bright yellow film. ^{1}H NMR of the polymer shows the shift of the triazole proton from 8.07 to 8.93, confirming complexation from the crown-ether rings.

*2,2'-(((((1,4-phenylenebis(oxy))bis(ethane-2,1-diyl))bis(oxy))bis(ethane-2,1-diyl))bis(oxy))bis(ethan-1-ol) (**55**)*

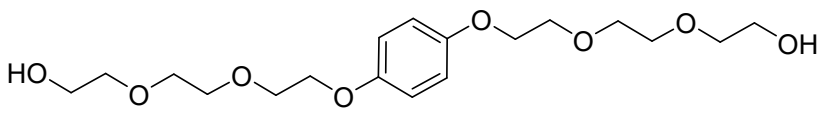

55

Hydroquinone (2.0 g, 18.2 mmol) was dissolved in dry dimethylformamide (75 mL) and potassium carbonate (10.0 g, 72.4 mmol) and lithium bromide (79 mg, 9.1 mmol) were added under argon at room temperature. Then, 2-[2-(2-chloroethoxy)ethoxy]ethanol (5.8 mL, 40

mmol) in dry dimethylformamide (25 mL) was added dropwise and the reaction was stirred at 80°C for three days under argon. The crude mixture was filtered and the solvent was removed. The residue was dissolved in chloroform (100 mL) and the organic phase was washed with water (100 mL), 10% sodium hydroxyde (100 mL), 10% hydrochloric acid (100 mL), water (2x 100 mL) and brine (50 mL), and dried over sodium sulfate. The first aqueous solution was extracted with chloroform (3 x 50 mL) and the organic layer was then washed with 10% sodium hydroxide (100 mL), 10% hydrochloric acid (100 mL), water (2 x 100 mL) and brine (50 mL), dried over sodium sulfate. Both crude fractions were purified by column chromatography (SiO_2, EtOAc/MeOH 1/0 → 90/10) to yield compound **55** (2.2 g, 33 %) as a yellow oil.

^{1}H NMR ($CDCl_3$, 400 MHz, 25°C): δ = 6.64 (s, 4H), 4.07 (t, *J* = 4.9 Hz, 4H), 3.83 (t, *J* = 4.9 Hz, 4H), 3.73-3.67 (m, 12H), 3.60 (t, *J* = 4.5 Hz, 4H), 2.50 (brs, 2H).

^{13}C NMR ($CDCl_3$, 100 MHz, 25°C): δ = 153.2, 115.7, 72.6, 70.9, 70.5, 70.0, 68.2, 61.9.

ESI-MS: m/z calcd. for $C_{18}H_{30}O_8$: 375.20 $[M+H]^+$, found: 375.41.

*1,4-bis(2-(2-(2-azidoethoxy)ethoxy)ethoxy)benzene (**52**)*

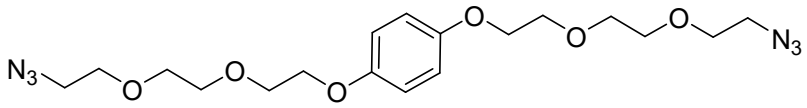

56

Compound **55** (2.23 g, 5.96 mmol) was dissolved in dry tetrahydrofuran (139 mL) and then methanesulfonyl chloride (1.4 mL, 18.1 mmol) and triethylamine (2.8 mL, 20.1 mmol) were added. The reaction mixture was stirred at room temperature under argon for 5 hours. The solvent was removed and the crude product was redissolved in dichloromethane (100 mL). The organic phase was washed with water (3 x 100 mL) and 5% sodium bicarbonate (3 x 100 mL), dried over sodium sulfate to yield the bis-mesylate compound as a pale brown solid, which was pure enough to be used as such in the next step.

This crude residue was dissolved in dry dimethylformamide (300 mL) and sodium azide (7.0 g, 107 mmol) was added. The reaction mixture was stirred at 50°C under argon overnight. The reaction mixture was diluted with diethyl ether (300 mL), washed with water (3x 300 mL) and dried over sodium sulfate. After filtration and removal of the solvent compound **56**(1.5 g, 66 % over two steps) was obtained as a yellow oil.

^{1}H NMR ($CDCl_3$, 400 MHz, 25°C): δ = 6.84 (s, 4H), 4.07 (t, *J* = 4.9 Hz, 4H), 3.83 (t, *J* = 4.9 Hz, 4H), 3.74-3.72 (m, 4H), 3.69-3.66 (m, 8H) 3.38 (t, *J* = 5.1 Hz, 4H).

^{13}C NMR ($CDCl_3$, 100 MHz, 25°C): δ = 153.3, 115.7, 71.0, 70.9, 70.2, 70.1, 68.2, 50.8.

HRMS (ESI+): m/z calcd. for $C_{18}H_{28}N_6O_6$: 425.2149 $[M+H]^+$, found: 425.2145.

*2,2',2''-(((((benzene-1,3,5-triyltris(oxy))tris(ethane-2,1-diyl))tris(oxy))tris(ethane-2,1-diyl))tris(oxy))tris(ethan-1-ol) (**57**)*

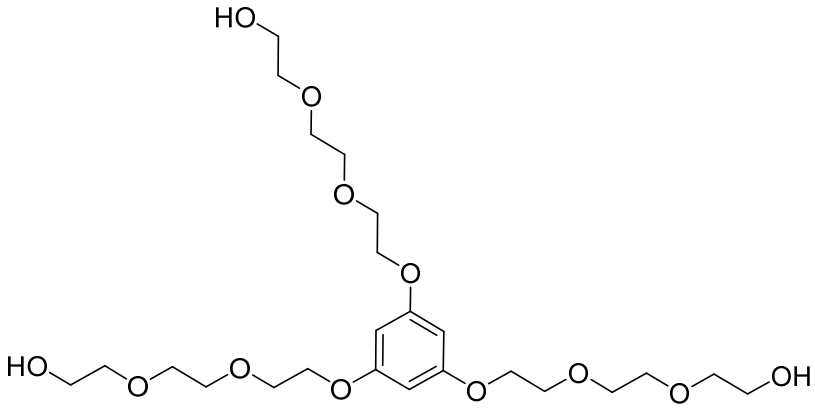

57

1,3,5-trihydroxybenzene dihydrate (2.0 g, 12.3 mmol) was suspended under argon in dry toluene (50 mL) and heated at reflux overnight using a Dean-Stark apparatus to remove water. After evaporation of the solvent, the crude product was dissolved in dry dimethylformamide (90 mL), and potassium carbonate (10.2 g, 74 mmol) and lithium bromide (803 mg, 9.25 mmol) were added. Then 2-[2-(2-chloroethoxy)ethoxy]ethanol (5.9 mL, 40.7 mmol) in dry dimethylformamide (30 mL) was added dropwise and the reaction mixture was heated at 80°C under argon for 4 days. The crude mixture was filtered and the solvent was removed. The residue was dissolved in chloroform (130 mL) and washed with water (130 mL). The aqueous layer was then washed with chloroform (3 x 100 mL) and the combined organic layers were then washed with a saturated solution of sodium bicarbonate (3 x 75 mL) and brine (50 mL), and then dried over sodium sulfate. The organic phase was purified by column chromatography (SiO_2, EtOAc/MeOH 95/5 → 90/10) to yield compound **57** (606 mg, 9 %) as a colorless oil.

^{1}H NMR ($CDCl_3$, 400 MHz, 25°C): δ = 6.08 (s, 3H), 4.03 (t, *J* = 4.8 Hz, 6H), 3.78 (t, *J* = 4.8 Hz, 6H), 3.68-3.62 (m, 18H), 3.55 (t, *J* = 4.6 Hz, 6H), 2.91 (brs 3H).

^{13}C NMR ($CDCl_3$, 100 MHz, 25°C): δ = 160.5, 94.6, 72.6, 70.8, 70.4, 69.7, 67.4, 61.7.

ESI-MS: m/z calcd. for $C_{24}H_{42}O_{12}$: 598.29 $[M+H]^+$, found: 598.46.

*1,3,5-tris(2-(2-(2-azidoethoxy)ethoxy)ethoxy)benzene (**58**)*

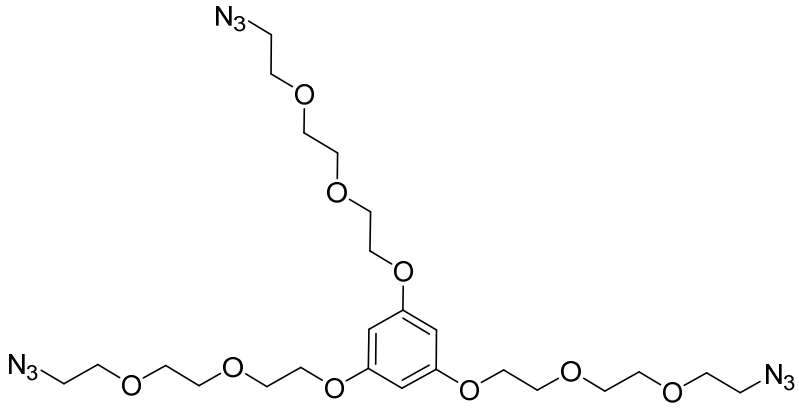

58

Compound **57** (196 mg, 0.38 mmol) was dissolved in dry tetrahydrofuran (10 mL) and methanesulfonyl chloride (140 µL, 1.81 mmol) and triethylamine (270 µL, 1.94 mmol) were added. The reaction mixture was stirred at room temperature under argon for 5 hours. The solvent was removed and the crude residue was taken back in dichloromethane (15 mL). The organic phase was washed with water (3 x 15 mL) and 5% sodium bicarbonate (3 x 15 mL) and dried over sodium sulfate. Evaporation of the solvent yielded the bis mesylate compound which was pure enough to be used as such in the next step.

This crude residue was dissolved in dry dimethylformamide (30 mL) and sodium azide (731 mg, 11.3 mmol) was added. The reaction mixture was stirred at 50°C under argon overnight. The reaction mixture was diluted with diethyl ether (50 mL), washed with water (3 x 50 mL) and dried over sodium sulfate. After filtration and removal of the solvent compound **58** (180 mg, 80 %) was obtained as a yellow oil.

^{1}H NMR ($CDCl_3$, 400 MHz, 25°C): δ = 6.11 (s, 3H), 4.07 (t, *J* = 4.8 Hz, 6H), 3.83 (t, *J* = 4.8 Hz, 6H), 3.74-3.71 (m, 6H), 3.69-3.67 (m, 12H), 3.38 (t, *J* = 5.1 Hz, 6H).

^{13}C NMR ($CDCl_3$, 100 MHz, 25°C): δ = 160.7, 94.6, 70.9, 70.9, 70.2, 69.9, 67.6, 50.8.

HRMS (ESI+): m/z calcd. for $C_{24}H_{39}N_9O_9$: 598.2949 $[M+H]^+$, found: 598.2937.

Synthesis of 8^{GelxM}

Under argon,a solution of compound **12** (25 mg, 17.1 µmol), compound **56** (X_1 eq., X_2 mg, X_3 mmol), compound **58** (Y_1 eq., Y_2 mg, Y_3 mmol) and Tetrakis(acetonitrile)copper(I) hexafluorophosphate (15.9 mg, 42.7 µmol) in dry dichloromethane (200 µL) was prepared. The solution was homogenized, and then 1,6-lutidine (1.5 µL, 12.9 µmol) was added. The solution was homogenized again using a 500 µL pipette and poured into a metallic mould, wrapped into aluminium foil and heated at 40°C in a sand bath for 30 min. The mould was cooled to room temperature and opened to recover a plastic-like material which swell into a gel upon addition of solvent. The gel was immersed first in DCM to remove unreacted material, then in a basic solution of EDTA, a NH_4PF_6 sat. solution, and water. The clean gel was then kept in dry acetonitrile.

$\mathbf{8}^{Gel1}$: X1=0.33, X2=2.39, X3=0.005638; Y1=0.44, Y2=4.49, Y3=0.007517.

$\mathbf{8}^{Gel2}$: X1=0.5, X2=3.63, X3=0.008542; Y1=0.33, Y2=3.37, Y3=0.005638.

$\mathbf{8}^{Gel3}$: X1=0.66, X2=4.79, X3=0.01128; Y1=0.22, Y2=2.25, Y3=0.003758.

The methylated version of the different gels $\mathbf{8}^{Gel1M}$, $\mathbf{8}^{Gel2M}$ and $\mathbf{8}^{Gel3M}$ were obtained by immersing the corresponding gels in a 1:1 solution of acetonitrile/methyl iodide for 4 days. The gel was then immersed acetonitrile, a NH_4PF_6 sat. solution, and water. The gels stored in dry in acetonitrile.

*2,6-dimethoxy-2,7-dimethyl-indane-1-one (**55**)*

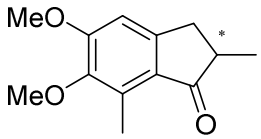

55

Polyphosphoric acid (35 mL) was mechanically stirred and heated at 70°C before methacrylic acid (13 mL, 152.5 mmol) and 2,3-dimethoxytoluene (12 mL, 80.7 mmol) were added. After 3 hours of stirring at 70°C, the mixture was poured onto a mixture of water and crushed ice and vigorously stirred overnight. The solution was extracted with ethyl acetate (4 x 50 mL). The organic phases were washed with saturated sodium bicarbonate (30 mL), water (30 mL) and

brine (30 mL). The solution was dried over sodium sulfate and concentrated. The resulting solid was recrystallized in heptane to yield compound **55** (11.3 g, 64 %) as brown crystals.
^{1}H NMR ($CDCl_3$, 400 MHz, 25°C): δ = 6.74 (s, 1H), 3.92 (s, 3H), 3.76 (s, 3H), 3.27-3.22 (m, 1H), 2.66-2.60 (m, 2H), 2.56 (s, 3H), 1.26 (d, *J* = 7.2 Hz, 3H).

^{13}C NMR ($CDCl_3$, 100 MHz, 25°C): δ = 208.9, 158.1, 151.8, 146.9, 132.1, 127.3, 105.9, 60.4, 55.8, 42.6, 34.5, 16.6, 10.6.

HRMS (ESI+): m/z calcd. for $C_{13}H_{16}O_3$: 227.1254 $[M+Li]^+$, found 227.1249.

*5,6-dihydroxy-2,7-dimethyl-indane-1-one (**56**)*

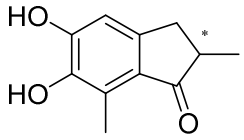

56

To a solution of compound **55** (8.9 g, 40.4 mmol) in dichloromethane (35 mL) cooled down to 0°C was added dropwise 1 M boron tribromide in dichloromethane (92 mL, 92.1 mmol) was added dropwise. The solution was stirred overnight at room temperature and methanol (150 mL) was added dropwise at 0°C. The solution was concentrated under vacuum and methanol was added (150 mL). This operation was repeated three times and the solvents finally evaporated under vacuum to yield the crude bis-phenol **56** (7.46 g, 97%) as a grey powder, which was pure enough to be used as such in the next step.
^{1}H NMR (CD_3OD, 400 MHz, 25°C): δ = 6.69 (s, 1H), 3.19-3.17 (m, 1H), 2.62-2.50 (m, 2H), 2.47 (s, 3H), 1.20 (d, *J* = 7.2 Hz, 3H).

^{13}C NMR (CD_3OD, 100 MHz, 25°C): δ = 212.1, 153.7, 150.1, 144.2, 126.9, 125.3, 109.7, 43.9, 34.9, 17.1, 10.6.

HRMS (ESI+): m/z calcd. for $C_{11}H_{12}O_3$: 199.0941 $[M+Li]^+$, found 199.0944.

*Ethyl 2-({6-[(1-ethoxy-1-oxopropan-2-yl)oxy]-2,7-dimethyl-1-oxo-2,3-dihydro-1H-inden-5-yl}oxy)propanoate (**57**)*

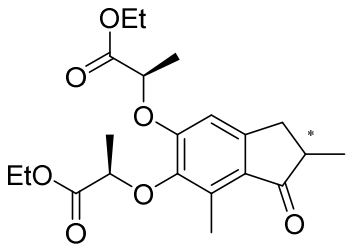

57

To a solution of compound **56** (7.46 g, 97.5 mmol), triphenylphosphine (25.5 g, 97.4 mmol) and ethyl lactate (11.2 mL, 97.5 mmol) in tetrahydrofuran (200 mL) cooled down to 0°C, was added dropwise diisopropyl azodicarboxylate (19.3 mL, 97.4 mmol). The solution was allowed to warm to room temperature and was stirred overnight. The solvents were removed and the crude residue was purified by column chromatography (SiO_2, cyclohexane/EtOAc 9/1) to yield compound **57** (10.2 g, 62%) as a yellow oil.

R_f = 0.4 (cyclohexane/EtOAc 3/1).

^{1}H NMR ($(CD_3)_2CO$, 400 MHz, 25°C): δ = 6.80 (s, 1H), 5.09 (q, *J* = 6.8 Hz, 1H), 4.98 (q, *J* = 6.8 Hz, 1H), 4.18-4.09 (m, 4H), 3.27-3.19 (m, 1H), 2.60-2.58 (m, 1H), 2.56 (s, 3H), 2.55-2.50 (m, 1H), 1.66 (d, *J* = 6.8 Hz, 3H), 1.58 (d, *J* = 6.8 Hz, 3H), 1.24 (t, *J* = 6.8 Hz, 3H), 1.21 (t, *J* = 6.8 Hz, 3H), 1.18 (d, *J* = 7.2 Hz, 3H).

^{13}C NMR ($(CD_3)_2CO$, 100 MHz, 25°C): δ = 208.5, 172.8, 171.8, 156.0, 152.0, 146.0, 132.9, 128.5, 108.3, 77.6, 73.3, 62.1, 61.4, 43.4, 35.0, 22.4, 19.3, 18.7, 16.8, 14.6, 11.7.

HRMS (ESI+): m/z calcd. for $C_{21}H_{28}O_7$: 399.1990 $[M+Li]^+$, found 399.1990.

*Ethyl 2-({6-[(1-ethoxy-1-oxopropan-2-yl)oxy]-2,7-dimethyl-1-sulfanylidene-2,3-dihydro-1H-inden-5-yl}oxy)propanoate (**58**)*

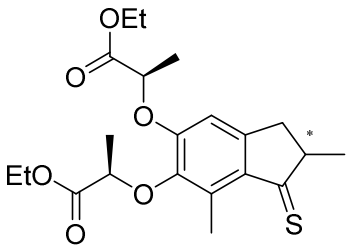

58

Compound **57** (800 mg, 2.0 mmol) and phosphorus pentasulfide (680 mg, 3.0 mmol) were heated in toluene (5 mL) at 80 ˚C for 1 hour. The mixture was then passed through a pad of silica and eluted with ethyl acetate until the eluent was colorless. After evaporation of the solvent, compound **58** (750 mg, 89% yield) was recovered as a purple oil. This compound was directly used in the next step.

^{1}H NMR ($CDCl_3$, 400 MHz, 25°C): δ = 6.61 (s, 1H), 4.88 (q, *J* = 6.8 Hz, 1H), 4.82 (q, *J* = 6.8 Hz, 1H), 4.26-4.18 (m, 4H), 3.33-3.26 (m, 1H), 3.00-2.96 (m, 1H), 2.77 (s, 3H), 2.71-2.66 (m, 1H), 1.69 (d, *J* = 6.8 Hz, 3H), 1.62 (d, *J* = 6.8 Hz, 3H), 1.39 (d, *J* = 7.2 Hz, 3H), 1.25 (t, *J* = 6.8 Hz, 6H).

^{13}C NMR ($CDCl_3$, 100 MHz, 25°C): δ = 248.7, 172.1, 171.0, 154.6, 152.8, 145.2, 138.1, 135.1, 106.1, 77.2, 72.6, 60.9, 55.5, 43.4, 38.9, 21.6, 21.5, 18.6, 18.2, 14.0, 13.8.

ESI-MS: m/z calcd. for $C_{21}H_{28}O_6S$: 409.17 $[M+H]^+$, found 409.28.

*2-[(2-hydroxyphenyl) disulfanyl] phenol (**60**)*

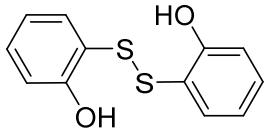

60

2-mercaptophenol (18 mL, 174.0 mmol) was suspended in water (110 mL) and a solution of iodine (19.2 g, 75.7 mmol) in methanol (270 mL) was added dropwise until the brown color persisted. The solution was then diluted with ethyl acetate (300 mL) and water (200 mL). The aqueous layer was extracted with ethyl acetate (2 x 200 mL). The combined organic phases were washed with a saturated sodium thiosulfate solution (200 mL), brine (200 mL), and then dried over sodium sulfate. Evaporation of the solvent under vacuum yielded compound **60** (21.4 g, 99%) as a colorless oil.

^{1}H NMR ($CDCl_3$, 400 MHz, 25°C): δ = 7.35 (dt, *J* = 7.6, 1.6 Hz, 2H), 7.22 (dd, *J* = 8.0, 1.6 Hz, 2H), 7.00 (dd, *J* = 8.4, 1.2 Hz, 2H), 6.83 (dt, *J* = 7.6, 1.2 Hz, 2H), 6.22 (s, 2H).

^{13}C NMR ($CDCl_3$, 100 MHz, 25°C): δ = 156.9, 136.2, 133.3, 121.1, 120.0, 115.8.

*1-methoxy-2-[(2-methoxyphenyl) disulfanyl]benzene (**61**)*

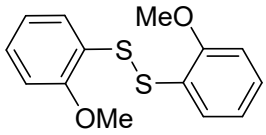

61

Compound **60** (21.4 g, 85.3 mmol) was diluted in acetone (210 mL) along with potassium carbonate (35.4 g, 256 mmol). Methyl iodide (15.9 mL, 256 mmol) was added and the solution was stirred at room temperature overnight. The mixture was filtered and diluted with dichloromethane (400 mL). The solution was washed with water (2 x 300 mL), dried over sodium sulfate and evaporated under vacuum to yield compound **61** (22.9 g, 99%) as a white compound.

^{1}H NMR ($CDCl_3$, 400 MHz, 25°C): δ = 7.53 (dd, *J* = 7.6, 1.2 Hz, 2H), 7.19 (t, *J* = 7.6 Hz, 2H), 6.93-6.89 (m, 2H), 6.85 (d, *J* = 8.4 Hz, 2H), 3.90 (s, 6H).

^{13}C NMR ($CDCl_3$, 100 MHz, 25°C): δ = 156.5, 127.7, 127.5, 124.5, 121.3, 110.4, 55.8.

ESI-MS: m/z calcd. for $C_{14}H_{14}O_2S_2$: 279.05 $[M+H]^+$, found: 279.15.

*N,N-diethyl 3-hydroxyl benzamide (**62**)*

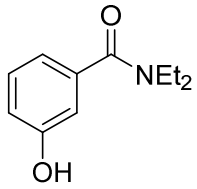

62

To a solution of 3-hydroxybenzoic acid (20.0 g, 145 mmol) in thionyl chloride (137 mL) was added 3 drops of dimethylformamide under argon. The mixture was stirred at 70°C for one hour and then cooled down to room temperature. The solvent was removed by azeotropic distillation using toluene. The residue was taken back into dry dichloromethane (85 mL) and cooled down to 0°C. Diethylamine (54 mL, 522 mmol) was added dropwise and the solution was stirred at 0°C for one hour. After removal of the solvent, the residue was taken back in water (200 mL) and the pH was adjusted to 3 using 1 M hydrochloric acid. The solution was extracted with ethyl acetate (3 x 150 mL). The organic phase was dried over sodium sulfate, evaporated under vacuum, and dissolved in the minimal amount of dichloromethane. This solution was added to

a flask containing stirred ethyl acetate cooled down to 0°C. The formation of a white precipitate was observed. The solid was recovered by filtration to yield compound **62** (27.4 g, 98%) as a white powder.

^{1}H NMR ($CDCl_3$, 400 MHz, 25°C): δ = 8.64 (brs, 1H), 7.13 (t, *J* = 8.0 Hz, 1H), 6.85-6.84 (m, 1H), 6.77- 6.75 (m, 2H), 3.53 (brs, 2H), 3.24 (brs, 2H), 1.23 (brs, 3H), 1.07 (brs, 3H).

^{13}C NMR ($CDCl_3$, 100 MHz, 25°C): δ = 172.14, 157.08, 137.08, 129.42, 117.09, 116.92, 114.02, 43.54, 39.54, 14.06, 12.77.

ESI-MS: m/z calcd. for $C_{11}H_{15}NO_2$: 194.12 $[M+H]^+$, found: 193.98.

*N,N-diethyl-3-methoxybenzamide (**63**)*

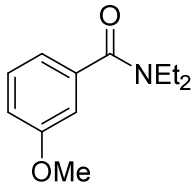

63

Compound **62** (27.4 g, 141.8 mmol) and potassium carbonate (39.2 g, 284.0 mmol) were suspended in acetone (230 mL). Methyl iodide (17.7 mL, 284.0 mmol) was added and the solution was stirred overnight at room temperature. The solvent was evaporated and the residue was taken back in ethyl acetate (500 mL), water (500 mL) and extracted with ethyl acetate (2 x 300 mL). The combined organic phases were dried on sodium sulfate, and the solvent evaporated to yield compound **63** (26.2 g, 89%) as a white solid.

^{1}H NMR ($CDCl_3$, 400 MHz, 25°C): δ = 7.29 (dd, *J* = 8.0 Hz, 1H), 6.94-6.90 (m, 3H), 3.82 (s, 3H), 3.54 (brs, 2H), 3.26 (brs, 2H), 1.24 (brs, 3H), 1.12 (brs, 3H).

^{13}C NMR ($CDCl_3$, 100 MHz, 25°C): δ = 170.8, 159.4, 138.4, 129.4, 118.2, 114.8, 111.5, 55.1, 43.1, 39.0, 14.1, 12.7.

ESI-MS: m/z calcd. for $C_{12}H_{17}NO_2$: 208.13 $[M+H]^+$, found: 208.19

*N,N-diethyl-3-methoxy-2-[(2-methoxyphenyl)sulfanyl]benzamide (**64**)*

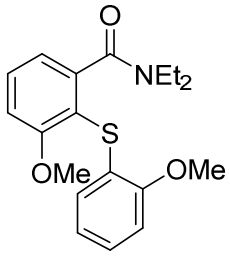

64

To a solution of dry tetrahydrofuran (350 mL) under argon were added tetramethylethylenediamine (3.60 mL, 23.9 mmol) and 1.4M *sec*-butyllithium in hexane (17.1 mL, 23.9 mmol) at -78°C. After 30 minutes of stirring, a solution of compound **63** (4.5 g, 21.7 mmol) in tetrahydrofuran (75 mL) was added dropwise. The solution was stirred for an hour. Then the disulfide **61** (11.0 g, 39.5 mmol) was added. The solution was stirred and allowed to slowly come back to room temperature overnight. The mixture was then diluted with diethylether (400 mL) and washed with 1 M sodium hydroxide (200 mL). The organic layer was concentrated and the residue was purified by column chromatography (SiO_2, EtOAc/cyclohexane 1:6) to yield compound **64** (3 g, 40%) as a white solid.

R_f = 0.2 (cyclohexane/EtOAc 2/1).

^{1}H NMR ($CDCl_3$, 400 MHz, 25°C): δ = 7.43 (dd, *J* = 8.0 Hz, 1H), 7.06-7.02 (m, 1H), 6.95-6.93 (m, 2H), 6.78 (d, *J* = 7.6 Hz, 1H), 6.75-6.67 (m, 2H), 3.87 (s, 3H), 3.74 (s, 3H), 3.73-3.64 (m, 1H), 3.39-3.30 (m, 1H), 3.15-3.06 (m, 1H), 3.04-2.95 (m, 1H), 1.18 (t, *J* = 6.8 Hz, 3H), 0.98 (t, *J* = 7.2 Hz, 3H).

^{13}C NMR ($CDCl_3$, 100 MHz, 25 °C): δ = 168.6, 160.5, 155.6, 145.2, 131.1, 127.0, 125.8, 125.4, 120.9, 118.7, 116.1, 111.2, 110.2, 56.1, 55.7, 42.6, 38.5, 13.8, 12.4.

HRMS (ESI+): m/z calcd. for $C_{19}H_{23}NO_3S$: 352.1554 $[M+Li]^+$, found 352.1553.

*4,5-dimethoxy-9H-thioxanthen-9-one (**65**)*

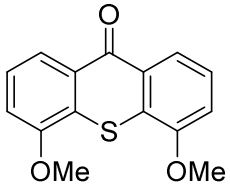

65

To a solution of compound **64** (4.3 g, 12.5 mmol) in tetrahydrofuran (87 mL) was a added freshly prepared 0.56 M solution of lithium diisopropylamine in tetrahydrofuran (39 mL, 62.3 mmol) dropwise at 0°C. The mixture was allowed to come back to room temperature and was stirred for one hour. The solution was diluted with saturated ammonium chloride (150 mL) and extracted with diethylether (3 x 150 mL). The combined organic phases were dried on sodium sulfate and evaporated under vacuum to yield compound **65** (3.34 g, 99%) as a bright yellow solid.

^{1}H NMR ($CDCl_3$, 400 MHz, 25°C): δ = 8.25 (dd, *J* = 8.0, 0.8 Hz, 2H), 7.45 (dd, *J* = 8.0 Hz, 2H), 7.13 (dd, *J* = 8.0, 0.8 Hz, 2H), 4.06 (s, 6H).

^{13}C NMR ($CDCl_3$, 100 MHz, 25°C): δ = 180.2, 154.9, 130.0, 127.7, 126.0, 121.5, 112.1, 56.4.

HRMS (ESI+): m/z calcd. for $C_{15}H_{12}O_3S$: 279.0662 $[M+Li]^+$, found 279.0664.

*4,5-bis[(tert-butyldimethylsilyl)oxy]-9H-thioxanthen-9-one (**66**)*

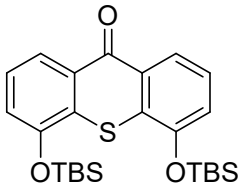

66

To a solution of compound **65** (4.0 g, 14.7 mmol) in dichloromethane (90 mL) cooled down to 0°C was added 1M boron tribromide in dichloromethane (58.9 mL, 58.9 mmol) dropwise. The solution was stirred overnight at room temperature and methanol (150 mL) was added dropwise at 0°C. The solution was concentrated under vacuum and methanol was added (150 mL). This operation was repeated three times and solvents were finally evaporated under vacuum to yield the crude bis-phenol, which was pure enough to be used as such in the next step.

The bis-phenol and imidazole (3.4 g, 50 mmol) were dissolved in tetrahydrofuran (90 mL) and cooled down to 0°C. *Tert*-butyldimethylsilyl chloride (7.5 g, 50 mmol) was added in one portion and the solution was stirred at room temperature for 4 hours. The mixture was filtered and the solid washed with tetrahydrofuran (200 mL). The solvent was evaporated and the residue purified by column chromatography (SiO_2, cyclohexane) to yield compound **66** (5.6 g, 80%) as a greenish solid.

R_f = 0.7 (cyclohexane/EtOAc 6/1).

^{1}H NMR ($CDCl_3$, 400 MHz, 25°C): δ = 8.25 (dd, *J* = 8.0, 1.2 Hz, 2H), 7.35 (dd, *J* = 8.0 Hz, 2H), 7.10 (dd, *J* = 8.0, 1.4 Hz, 2H), 1.11 (s, 18H), 0.35 (s, 12H).

^{13}C NMR ($CDCl_3$, 100 MHz, 25°C): δ = 180.6, 151.3, 130.60, 130.4, 125.7, 122.0, 119.7, 25.9, 18.5, -4.1.

HRMS (ESI+): m/z calcd. for $C_{25}H_{36}O_3SSi_2$: 479.2079 $[M+Li]^+$, found: 479.2071.

*{4,5-bis[(tert-butyldimethylsilyl)oxy]-9H-thioxanthen-9-ylidene}hydrazine (**67**)*

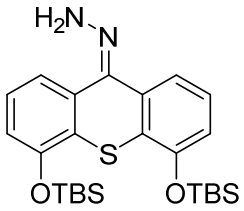

67

To a solution of compound **66** (750 mg, 1.6 mmol) in tetrahydrofuran (10 mL) was added phosphorus pentasulfide (1.0 g, 4.8 mmol) and the mixture was heated to 65 ˚C for 1 hour. Then the suspension was filtered through a short silica plug and the residue was washed with dichloromethane until the eluent was colorless. The solvent was evaporated to provide corresponding thioketone (775 mg, quant.) as an orange solid. This crude product was used directly in the next step without any further purification.

^{1}H NMR ($CDCl_3$, 400 MHz, 25°C): δ = 8.68 (d, *J* = 8.0 Hz, 2H), 7.30 (dd, *J* = 8.0 Hz, 2H), 7.09 (d, *J* = 8.0 Hz,2H), 1.09 (s, 18H), 0.28 (s, 12H).

^{13}C NMR (100 MHz, $CDCl_3$, 25°C): δ = 211.3, 151.3, 138.7, 126.2, 126.1, 125.8, 118.6, 25.4, 18.4, -4.1.

ESI-MS: m/z calcd. for $C_{25}H_{36}O_2S_2Si_2$: 489.18 $[M+H]^+$, found 489.27.

To the previously prepared intermediate (775 mg, 1.6 mmol) suspended in absolute ethanol (17 mL) was added hydrazine monohydrate (1.33 mL) dropwise and the mixture was stirred at 80 ˚C for 1 hour. The solvent were evaporated and the crude residue was purified by flash column chromatography (SiO_2, toluene → toluene/EtOAc 100/1) affording hydrazine **67** (500 mg, 65%) as a colorless solid.

^{1}H NMR ($CDCl_3$, 400 MHz, 25°C): δ = 7.65 (dd, *J* = 8.0, 1.2 Hz, 1H), 7.44 (dd, *J* = 8.0, 1.0 Hz, 1H), 7.21 (dd,*J* = 8.0 Hz, 1H), 7.17 (dd, *J* = 8.0 Hz, 1H), 6.84 (dd, *J* = 8.0, 1.0 Hz, 1H), 6.79 (dd, *J* = 8.0, 1.2 Hz, 1H), 1.09 (s, 9H), 1.07 (s, 9H), 0.32 (s, 6H), 0.28 (s, 6H).

^{13}C NMR ($CDCl_3$, 100 MHz, 25°C): δ = 152.5, 150.7, 142.0, 135.2, 127.6, 126.6, 126.6, 125.2, 124.1, 120.5, 118.7, 117.7, 116.7, 25.9, 25.8, 18.4, -4.1.

ESI-MS: m/z calcd. for $C_{25}H_{38}N_2O_2SSi_2$: 487.23 $[M+H]^+$, found 487.31

*Episulfide (**68**)*

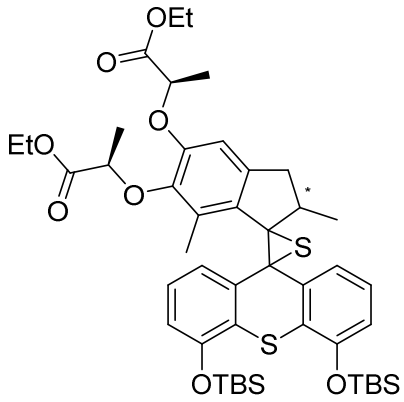

68

To a solution of freshly prepared hydrazone **67** (500 mg, 1.0 mmol) in dry tetrahydrofuran (5 mL) under argon was added sodium sulfate (750 mg, 5.1 mmol) and manganese dioxide (433 mg, 5.0 mmol) at 0 ˚C. The mixture was protected from light with aluminum foil and stirred at 0 ˚C for 50 min. Then, the solution was filtered under argon *via* a cannula and the solid residue was washed with additional dry tetrahydrofuran (3 x 5 mL). To the filtrate was added a solution of freshly prepared compound **58** (406 mg, 1.0 mmol) in dry tetrahydrofuran (5 mL) at 0˚C dropwise. The resulting mixture was stirred at room temperature overnight. The solvent was evaporated and the crude residue was purified by flash column chromatography (SiO_2, toluene → toluene/EtOAc 1000/1 → 200/1) to yield episulfide **68** (636 mg, 74%; 230 mg of each isomer, 176 mg of the mixture containing both isomers) as an orange viscous oil.

For *R,R,R*-isomer: R_f = 0.7 (toluene/EtOAc 6/1);

^{1}H NMR ($CDCl_3$, 400 MHz, 25°C): δ = 7.39 (dd, *J* = 8.0, 0.8 Hz, 1H), 7.24 (dd, *J* = 7.6, 1.2 Hz, 1H), 7.10 (dd, *J* = 8.0 Hz, 1H), 7.01 (dd, *J* = 8.0 Hz, 1H), 6.73 (dd, *J* = 8.0, 1.2 Hz, 1H), 6.60 (dd, *J* = 8.0, 1.2 Hz, 1H), 6.35 (s, 1H), 4.61 (q, *J* = 6.8 Hz, 1H), 4.22-4.15 (m, 5H), 3.22-

3.17 (m, 1H), 2.16 (s, 3H), 2.07 (d, *J* = 14.8 Hz, 1H), 1.52 (d, *J* = 6.8 Hz, 3H), 1.42 (d, *J* = 6.8 Hz, 3H), 1.35-1.32 (m, 1H), 1.31 (t, *J* = 6.8 Hz, 3H), 1.23 (t, *J* = 7.2 Hz, 3H), 1.05 (s, 9H), 0.98 (s, 9H), 0.92 (d, *J* = 6.8 Hz, 3H), 0.26 (s, 3H), 0.24 (s, 3H), 0.09 (s, 3H), -0.07(s, 3H).

^{13}C NMR ($CDCl_3$, 100 MHz, 25°C): δ = 172.5, 171.9, 151.6, 151.5, 149.7, 144.7, 140.3, 139.9, 136.1, 131.6, 128.9, 127.9, 127.8, 126.2, 125.5, 123.5, 121.7, 117.5, 116.9, 108.9, 77.5, 77.2, 73.2, 71.6, 61.9, 60.9, 60.6, 41.1, 37.7, 25.9, 25.8, 21.1, 18.9, 18.4, 18.3, 18.2, 14.2, 14.1, 12.4, -3.9, -4.2, -4.3, -4.7.

ESI-MS: m/z calcd. for $C_{46}H_{64}O_8S_2Si_2$: 865.37 $[M+H]^+$, found 865.46.

For *R,R,S*-isomer: R_f = 0.65 (toluene/EtOAc 6/1);

^{1}H NMR ($CDCl_3$, 400 MHz, 25°C): δ = 7.38 (dd, *J* = 8.0, 1.2 Hz, 1H), 7.24 (dd, *J* = 8.0, 1.2 Hz, 1H), 7.09 (dd, *J* = 8.0 Hz, 1H), 7.00 (dd, *J* = 8.0 Hz, 1H), 6.73 (dd, *J* = 8.0, 1.2 Hz, 1H), 6.59 (dd, *J* = 8.0, 1.2 Hz, 1H), 6.26 (s, 1H), 4.59 (q, *J* = 6.8 Hz, 2H), 4.22-4.12 (m, 4H), 3.23-3.18 (m, 1H), 2.13 (s, 3H), 2.04 (d, *J* = 14.8 Hz, 1H), 1.52 (d, *J* = 6.8 Hz, 3H), 1.35-1.32 (m, 1H), 1.28 (d, *J* = 6.8 Hz, 3H), 1.24 (t, *J* = 6.8 Hz, 3H), 1.18 (t, *J* = 7.2 Hz, 3H), 1.06 (s, 9H), 0.95 (s, 9H), 0.92 (d, *J* = 7.2 Hz, 3H), 0.26 (s, 3H), 0.24 (s, 3H), 0.07 (s, 3H), -0.09 (s, 3H).

^{13}C NMR ($CDCl_3$, 100 MHz, 25°C): δ = 172.7, 171.9, 151.5, 151.4, 149.1, 143.8, 140.0, 139.7, 136.1, 131.5, 128.8, 127.9 (2C), 126.2, 125.5, 123.6, 121.7, 117.5, 116.9, 107.8, 77.2, 76.5, 72.5, 71.4, 61.7, 61.1, 60.6, 40.9, 37.6, 25.9, 25.8, 21.1, 18.6, 18.4, 18.3, 18.2, 14.1, 14.0, 12.4, -4.0, -4.2, -4.3, -4.8.

HRMS (ESI+): m/z calcd. for $C_{46}H_{65}O_8S_2Si_2$: 871.3739 $[M+Li]^+$, found 871.3738.

*Motor (**69**)*

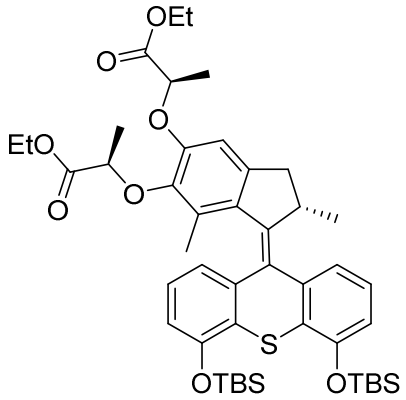

69

Compound **68** (480 mg, 0.6 mmol) was dissolved in toluene (10 mL) along with triphenylphosphine (727 mg, 2.8 mmol). The mixture was stirred at reflux overnight before it was concentrated and further purified by flash column chromatography (SiO_2, toluene/EtOAc 1/0 → 50/1) to yield the motor **69** (434 mg, 94 %) as colorless solid.

^{1}H NMR ($CDCl_3$, 400 MHz, 25°C): δ = 7.29 (d, *J* = 7.2 Hz, 1H), 7.13 (dd, *J* = 8.0 Hz, 1H), 6.86 (dd, *J* = 8.0 Hz, 1H), 6.69 (dd, *J* = 8.0, 1.2 Hz, 1H), 6.64 (dd, *J* = 7.6, 1.2 Hz, 1H), 6.63 (dd, *J* = 7.6, 1.2 Hz, 1H), 6.54 (s, 1H), 4.78-4.72 (m, 2H), 4.27-4.09 (m, 5H), 3.38-3.31 (m, 1H), 2.32 (d, *J* = 15.2 Hz, 1H), 1.61 (d, *J* = 6.8 Hz, 3H), 1.44 (d, *J* = 6.8 Hz, 3H), 1.22 (t, *J* = 7.2 Hz, 3H), 1.21 (t, *J* = 7.2 Hz, 3H), 1.21 (s, 3H), 1.09 (s, 9H), 1.08 (s, 9H), 0.62 (d, *J* = 6.8 Hz, 3H), 0.29 (s, 3H), 0.27 (s, 6H), 0.25 (s, 3H).

^{13}C NMR ($CDCl_3$, 100 MHz, 25°C): δ = 172.4, 172.0, 152.7, 152.2, 149.6, 145.5, 144.4, 142.0, 141.8, 138.3, 133.4, 130.9, 128.1, 127.7, 127.1, 126.4, 126.1, 121.0, 120.2, 116.3, 115.5, 108.1, 76.9, 73.0, 61.2, 60.6, 39.4, 38.0, 25.9 (6C), 18.9, 18.5, 18.4 (3C), 14.4, 14.1, 14.0, -3.9, -4.0, -4.3, -4.4.

HRMS (ESI+): m/z calcd. for $C_{46}H_{64}O_8SSi_2$: 839.4016 $[M+Li]^+$, found 839.4006.

*Bis-OH Motor (**70**)*

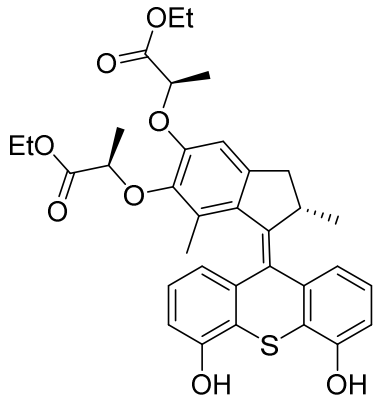

70

Compound **69** (210 mg, 0.25 mmol) was dissolved in tetrahydrofuran (5 mL) and cooled down to 0°C before 1M tetrabutylammonium fluoride in tetrahydrofuran (0.56 mL) was added dropwise. The mixture was stirred for 5 min before a saturated solution of ammonium chloride (10 mL) was added and the mixture was extracted with dichloromethane (3 × 20 mL). The combined organic layers were dried over sodium sulfate and concentrated in vacuum. The

residue was purified by flash column chromatography (SiO_2, CH_2Cl_2/MeOH 1/0 → 10/1) to give compound **70** (150 mg, 98 %) as a pale green solid.

^{1}H NMR (CD_3OD, 400 MHz, 25°C): δ = 7.24 (d, *J* = 7.2 Hz, 1H), 7.15 (dd, *J* = 8.0 Hz, 1H), 6.86 (dd, *J* = 8.0 Hz, 1H), 6.72 (dd, *J* = 8.0, 1.2 Hz, 1H), 6.66 (dd, *J* = 8.0, 1.0 Hz, 1H), 6.64 (s, 1H), 6.64 (dd, *J* = 7.6, 0.8 Hz, 1H), 4.86 (q, *J* = 6.8 Hz, 1H), 4.78 (q, *J* = 6.8 Hz, 1H), 4.22-4.09 (m, 5H), 3.40-3.35 (m, 1H), 2.35 (d, *J* = 14.8 Hz, 1H), 1.57 (d, *J* = 6.8 Hz, 3H), 1.38 (d, *J* = 6.8 Hz, 3H), 1.23 (t, *J* = 6.8 Hz, 3H), 1.20 (t, *J* = 6.8 Hz, 3H), 1.20 (s, 3H), 0.62 (d, *J* = 6.4 Hz, 3H).

^{13}C NMR (CD_3OD, 100 MHz, 25°C): δ = 174.2, 173.5, 155.7, 155.2, 151.1, 146.5, 145.5, 143.8, 143.5, 140.2, 134.7, 131.9, 130.2, 127.9, 127.8, 124.0, 123.3, 120.5, 120.0, 113.2, 113.1, 109.4, 77.9, 74.1, 62.4, 62.0, 40.4, 39.3, 19.3, 18.9, 18.7, 15.0, 14.5, 14.4.

HRMS (ESI+): calcd. for $C_{34}H_{36}O_8S$: 611.2286 $[M+Li]^+$, found 611.2284.

*Bis-alkyne motor (**72**)*

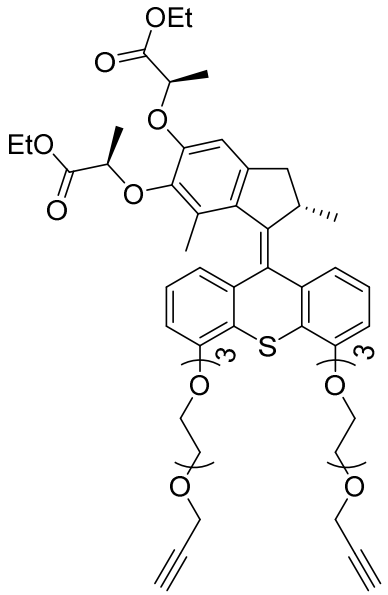

72

Compound **70** (80 mg, 0.13 mmol) and potassium carbonate (59 mg, 0.43 mmol) were dissolved in dimethyl formamide (6 mL) along with 2-{2-[2-(prop-2-yn-1-yloxy)ethoxy]ethoxy}ethyl 4-methylbenzene-1-sulfonate **71** (136 mg, 0.4 mmol). The mixture was stirred at 45 ˚C for 48 hours under argon. Then the mixture was diluted with water (10 mL) and extracted with

dichloromethane (3 × 20 mL). The combined organic phases were dried over sodium sulfate, the solvents removed and the residue purified by flash column chromatography (SiO_2, cyclohexane/EtOAc 5/1 → 1/1) to give compound **72** (101 mg, 81%) as a yellowish solid.

^{1}H NMR ($CDCl_3$, 400 MHz, 25°C): δ = 7.32 (d, *J* = 7.6 Hz, 1H), 7.21 (dd, *J* = 8.0 Hz, 1H), 6.93 (dd, *J* = 8.0 Hz, 1H), 6.76 (d, *J* = 7.6 Hz, 1H), 6.69 (dd, *J* = 8.0, 1.0 Hz, 1H), 6.64 (dd, *J* = 7.6, 1.2 Hz, 1H), 6.54 (s, 1H), 4.79 (q, *J* = 6.8 Hz, 1H), 4.76 (q, *J* = 6.8 Hz, 1H), 4.31-4.08 (m, 13H), 3.98-3.93 (m, 4H), 3.85-3.82 (m, 4H), 3.72-3.67 (m, 12H), 3.37-3.32 (m, 1H), 2.42 (t, *J* = 2.4 Hz, 1H), 2.41 (t, *J* = 2.4 Hz, 1H), 2.32 (d, *J* = 14.8 Hz, 1H), 1.61 (d, *J* = 6.8 Hz, 3H), 1.46 (d, *J* = 6.8 Hz, 3H), 1.22 (t, *J* = 7.2 Hz, 3H), 1.20 (s, 3H), 1.19 (t, *J* = 7.2 Hz, 3H), 0.62 (d, *J* = 6.8 Hz, 3H).

^{13}C NMR ($CDCl_3$, 100 MHz, 25°C): δ = 172.5, 172.0, 155.8, 155.3, 149.6, 145.9, 144.4, 141.9, 141.7, 138.2, 133.4, 131.0, 127.6, 126.7, 126.4, 124.9, 124.6, 120.9, 120.3, 109.5, 109.0, 108.0, 79.7, 77.2, 76.8, 74.5, 72.9, 71.1, 70.8, 70.4, 69.7, 69.6, 69.1, 68.8, 61.2, 60.7, 58.4, 39.5, 38.1, 18.9, 18.6, 18.4, 14.5, 14.1, 14.0.

HRMS (ESI+): calcd. for $C_{52}H_{64}O_{14}S$: 951.4172 $[M+Li]^+$, found 951.4147.

*Bis-alkyne-bis-acid Motor (**73**)*

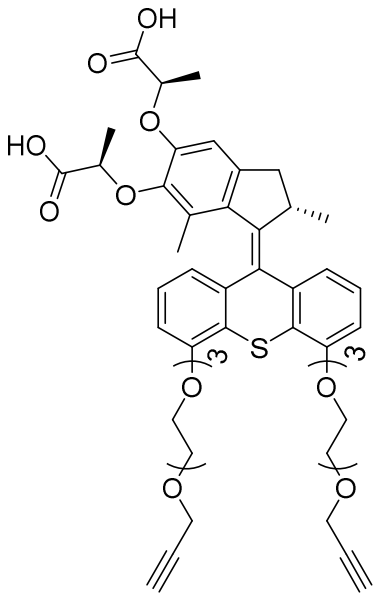

73

Compound **72** (90.0 mg, 8 μmol) was dissolved in a 1:1 mixture of tetrahydrofuran/methanol (0.5 mL) and then sodium hydroxide (4.5 mg, 0.11 mmol) in water (0.25 mL water) was added.

The mixture was stirred at room temperature for 3 h and then diluted with 0.2 M hydrochloric acid (5 mL) at 0 ˚C. The mixture was then washed with dichloromethane (3 × 10 mL). The combined organic phases were dried over sodium sulfate, the solvent evaporated to afford compound **73** (69.0 mg, 82 %) as a slightly yellow solid, which was pure enough to be used as such in the next step.

^{1}H NMR (CD_3OD, 400 MHz, 25°C): δ = 7.37 (d, *J* = 7.6 Hz, 1H), 7.27 (dd, *J* = 8.0 Hz, 1H), 6.98 (dd, *J* = 8.0 Hz, 1H), 6.87 (d, *J* = 7.6 Hz, 1H), 6.81 (d, *J* = 7.6 Hz, 1H), 6.67 (s, 1H), 6.60 (dd, *J* = 8.0, 1.2 Hz, 1H), 4.81 (q, *J* = 7.2 Hz, 1H), 4.62 (q, *J* = 6.8 Hz, 1H), 4.30-4.10 (m, 9H), 3.92-3.89 (m, 4H), 3.78-3.77 (m, 4H), 3.66-3.60 (m, 12H), 3.40-3.35 (m, 1H), 2.80 (t, *J* = 2.4 Hz, 1H), 2.79 (t, *J* = 2.4 Hz, 1H), 2.36 (d, *J* = 15.2 Hz, 1H), 1.60 (d, *J* = 6.8 Hz, 3H), 1.38 (d, *J* = 6.8 Hz, 3H), 1.17 (s, 3H), 0.60 (d, *J* = 6.8 Hz, 3H).

^{13}C NMR (CD_3OD, 100 MHz, 25°C): δ = 176.1, 175.5, 157.4, 156.8, 151.5, 147.2, 145.5, 143.8, 143.2, 139.5, 134.5, 131.9, 129.3, 128.0 (2C), 126.4, 125.6, 122.0, 121.3, 110.8, 110.6, 109.5, 80.7, 78.4, 76.0, 74.3, 73.7, 72.1, 71.7, 71.6, 71.4, 70.9, 70.8, 70.2, 70.1, 62.3, 59.1, 40.4, 39.3, 19.3, 19.1, 18.8, 15.2.

HRMS (ESI+): calcd. for $C_{48}H_{56}O_{14}S$: 895.3546 $[M+Li]^+$, found 895.3542.

*Tetra-alkyne Motor (**M-9**)*

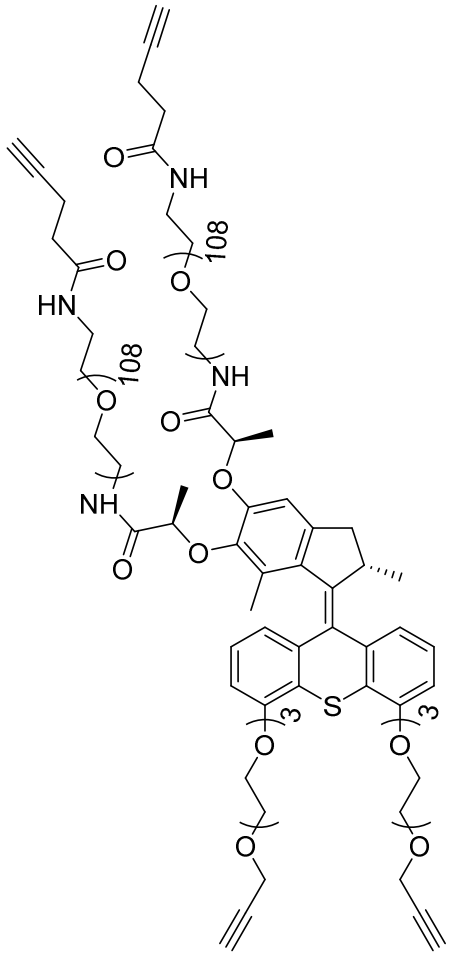

M-9

To a solution of *bis*-acid **73** (41.0 mg, 50 µmol) in dry dichloromethane (3 mL) was added hydroxybenzotriazole (16.4 mg, 0.11 mmol) and 1-ethyl-3-(3-dimethylaminopropyl)carbodiimide hydrochloride (66.8 mg, 0.35 mmol) at room temperature. After stirring for 30 min, alkyne-PEG_{5000}-NH_2 (473.0 mg, 0.1 mmol) along with dichloromethane (3 mL) were added and the mixture was stirred at room temperature overnight. The solvent was removed under vacuum and the residue was purified by reversed phase column chromatography (C_{18} Merck, methanol/water 3/7 → 8/2) yielding compound **M-9** (310 mg, 62 %) as a white powder.

^{1}H NMR (CD_3OD, 400 MHz, 25°C): δ = 7.41 (d, J = 7.8 Hz, 1H), 7.32 (t, J = 8.0 Hz, 1H), 7.05 (t, J = 8.0 Hz, 1H), 6.95 (d, J = 8.0 Hz, 1H), 6.90 (d, J = 8.0 Hz, 1H), 6.75 (s, 1H), 6.65 (d, J = 7.7 Hz, 1H), 4.73 (q, J = 6.8 Hz, 1H), 4.43 (q, J = 6.8 Hz, 1H), 4.36–4.30 (m, 2H), 4.28–4.19 (m, 3H), 4.18–4.14 (m, 4H), 3.99–3.93 (m, 4H), 3.86–3.78 (m, 12H), 3.75–3.52 (m, 864H), 3.49–3.42 (m, 8H), 3.37 (t, J = 5.5 Hz, 6H), 2.86 (t, J = 2.3 Hz, 1H), 2.85 (t, J = 2.3 Hz, 1H),

2.50–2.44 (m, 4H), 2.43–2.38 (m, 4H), 2.30 (t, *J* = 2.6 Hz, 2H), 1.54 (d, *J* = 6.6 Hz, 3H), 1.30 (d, *J* = 6.9 Hz, 3H), 1.18 (s, 3H), 0.63 (d, *J* = 6.8 Hz, 3H).

*Bis-azide Motor (**75**)*

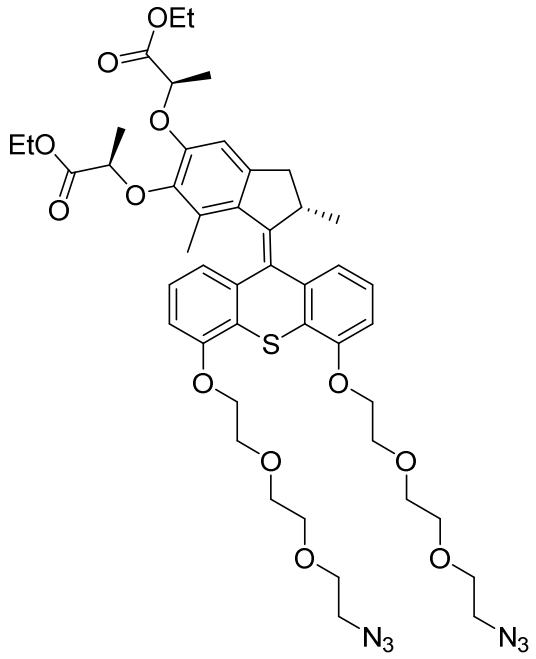

75

Compound **70** (15.9 mg, 26 µmol) was dissolved in dimethylformamide (1.6 mL) along with potassium carbonate (10.9 mg, 79 µmol) and 2-(2-(2-azidoethoxy)ethoxy)ethyl 4-methylbenzenesulfonate **74** (26.0 mg, 79 µmol). The reaction was stirred under argon at 45°C for 36 hours. The mixture was diluted with dichloromethane (5 mL) and water (5 mL), and extracted with dichloromethane (3 x 5 mL). The organic phase was dried over sodium sulfate, filtered, and evaporated under vacuum. The residue was purified over column chromatography (SiO_2, cyclohexane/EtOAc 2/1 → 1/1) to yield compound **75** (21 mg, 87%) as a sticky yellow solid.

^{1}H NMR ($CDCl_3$, 400 MHz, 25°C): δ = 7.32 (d, *J* = 7.6 Hz, 1H), 7.21 (dd, *J* = 8.0 Hz, 1H), 6.94 (dd, *J* =8.0 Hz, 1H), 6.76 (d, *J* = 7.6 Hz, 1H), 6.69 (dd, *J* = 8.0, 1.0 Hz, 1H), 6.64 (dd, *J* = 7.6, 1.2 Hz, 1H), 6.54 (s, 1H), 4.83-4.72 (m, 2H), 4.34-4.06 (m, 10H), 4.00-3.93 (m, 4H), 3.87-3.82 (m, 4H), 3.76-3.66 (m, 8H), 3.38 (brt, *J* = 4.9 Hz, 3H), 3.37-3.32 (m, 1H), 2.33 (d, *J* = 14.8 Hz, 1H), 1.63 (d, *J* = 7.8 Hz, 3H), 1.47 (d, *J* = 7.8 Hz, 3H), 1.22 (t, *J* = 7.1 Hz, 3H), 1.20 (s, 3H), 1.19 (t, *J* = 7.1 Hz, 3H), 0.62 (d, *J* = 6.8 Hz, 3H).

^{13}C NMR ($CDCl_3$, 100 MHz, 25°C): δ = 172.6, 172.1, 155.9, 155.4, 149.7, 146.0, 144.5, 142.0, 141.9, 138.4, 13.4, 131.1, 127.7, 126.9, 126.5, 125.0, 124.7, 121.0, 120.4, 109.6, 109.1, 108.1, 73.0, 71.3, 70.9, 70.2, 69.8, 68.9, 61.3, 60.8, 50.8, 39.6, 38.2, 27.0, 19.1, 18.7, 18.5, 14.6, 14.2.

HRMS (ESI+): m/z calcd. for $C_{46}H_{58}N_6O_{12}S$: 917.375 $[M]^+$, found: 917.375.

*Bis-azide-bis-acid Motor (**76**)*

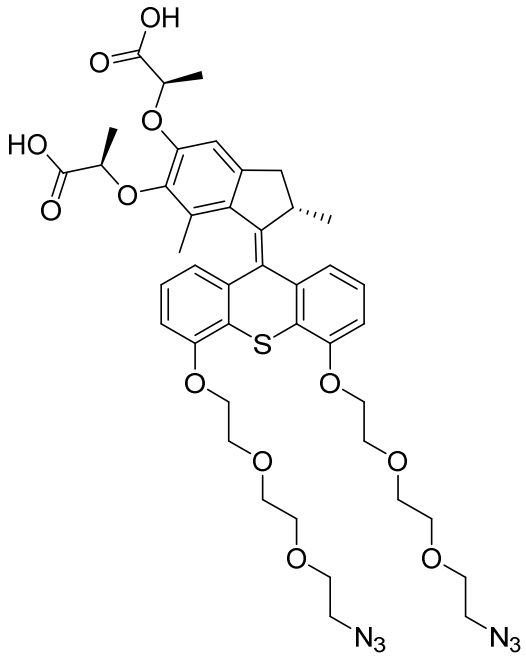

76

Compound **75** (20.5 mg, 22 µmol) was dissolved in a 1:1:1 mixture of tetrahydrofuran/methanol/water (1 mL) along with sodium hydroxide (4.5 mg, 0.11 mmol) and stirred overnight at 40°C. The reaction was quenched using a 2 M hydrochloric acid solution (1 mL). The reaction mixture was extracted with dichloromethane (5 x 10 mL), the organic phase was dried over sodium sulfate, filtered, and evaporated under vacuum to yield compound **76** (18.6 mg, 97 %) as a pale-green solid. The crude compound was used without further purification in the next synthetic step.

^{1}H NMR ($CDCl_3$, 400 MHz, 25°C): 7.34 (d, *J* = 7.8 Hz, 1H), 7.23 (dd, *J* = 8.0 Hz, 1H), 6.96 (dd, *J* =8.0 Hz, 1H), 6.78 (d, *J* = 7.7 Hz, 1H), 6.72 (dd, *J* = 7.5, 1.0 Hz, 1H), 6.69 (s, 1H), 6.65 (dd, *J* = 7.5, 1.0 Hz, 1H), 4.89-4.78 (m, 1H), 4.44-4.34 (m, 1H), 4.34-4.25 (m, 2H), 4.25-4.08 (m, 3H), 4.03-3.90 (m, 4H), 3.89-3.79 (m, 4H), 3.78-3.67 (m, 8H), 3.63 (s, 1H), 3.38 (t, *J* = 5.5

Hz, 3H), 3.35-3.30 (m, 1H), 2.39 (d, *J* = 15.8 Hz, 1H), 1.65 (d, *J* = 7.0 Hz, 3H), 1.43 (d, *J* = 7.0 Hz, 3H), 1.25 (s, 3H), 0.64 (d, *J* = 6.7 Hz, 3H).

^{13}C NMR ($CDCl_3$, 100 MHz, 25°C): δ = 175.5, 175.3, 156.2, 155.5, 145.5, 145.4, 143.2, 141.5, 137.9, 131.1, 130.9, 128.7, 126.8, 126.7, 125.2, 124.5, 121.0, 120.3, 110.5, 109.8, 109.4, 71.3 (2C), 71.0, 70.9, 70.2 (2C), 69.9, 69.1, 68.9, 50.9 (2C), 39.7, 38.2, 32.1, 29.8, 22.8, 19.0, 18.5, 18.2, 15.2, 14.3.

HRMS (ESI+): m/z calcd. for $C_{42}H_{50}N_6O_{12}S$: 885.311 $[M+Na]^+$, found: 885.312.

*Tetra-azide Motor (**M-10**)*

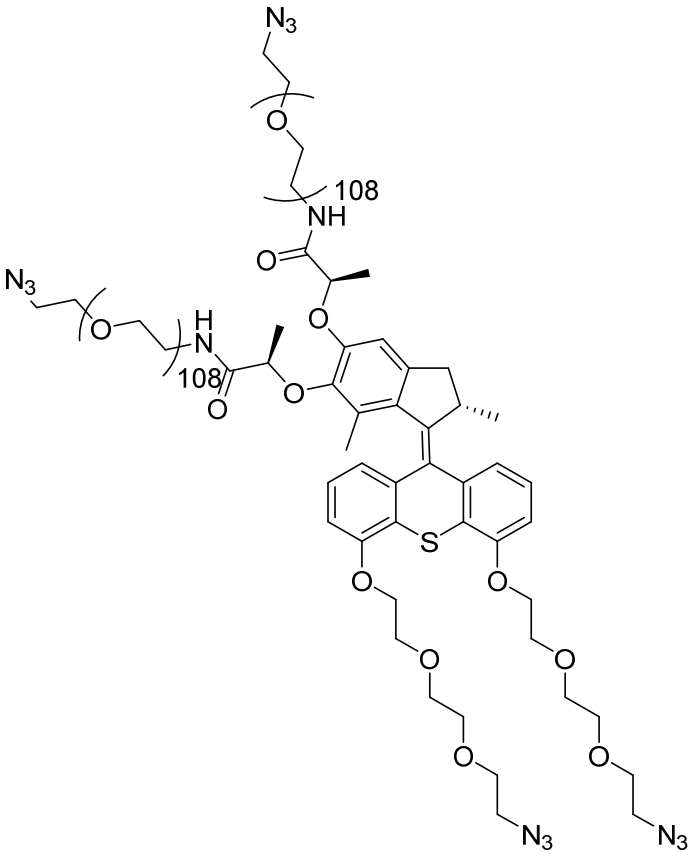

M-10

To a solution of bis-acid **76** (17.0 mg, 20 μmol) in dichloromethane (1.5 mL) were added 1-ethyl-3-(3-dimethylaminopropyl)carbodiimide hydrochloride (28.4 mg, 0.15 mmol) and hydroxybenzotriazole (6.9 mg, 0.45 mmol) under argon. After stirring for 20 minutes at room temperature, N_3-PEG_{5000}-NH_2 (191.2 mg, 40 μmol) was added. The mixture was stirred overnight at room temperature. After evaporation of the solvent, the crude residue was purified

via reverse-phase column chromatography (C_{18}, methanol/water 3/7 → 7/3) to yield compound **M-10** (75.0 mg, 39%) as a white solid.

^{1}H NMR ($CDCl_3$, 400 MHz, 25°C): δ = 7.08 (d, *J* = 7.8 Hz, 1H), 6.99 (t, *J* = 8.0 Hz, 1H), 6.72 (t, *J* =8.0 Hz, 1H), 6.61 (d, *J* = 7.7 Hz, 1H), 6.56 (dd, *J* = 7.5, 1.0 Hz, 1H), 6.43 (s, 1H), 6.32 (dd, *J* = 7.5, 1.0 Hz, 1H), 4.40 (q, *J* = 6.8 Hz, 1H), 4.21 (br, 2H), 4.10 (q, *J* = 6.8 Hz, 1H), 4.04–3.84 (m, 8H), 3.70–3.60 (m, 4H), 3.54–3.46 (m, 12H), 3.42–3.16 (m, 864H), 3.15–3.11 (m, 4H), 3.07–3.01 (m, 4H), 2.10 (d, *J* = 15.8 Hz, 1H), 1.22 (d, *J* = 7.0 Hz, 3H), 0.98 (d, *J* = 7.0 Hz, 3H), 0.85 (s, 3H), 0.30 (d, *J* = 6.7 Hz, 3H).

*Synthesis of **Gel 50***

A solution of copper bromide (1.5 mg, 1.0×10^{-2} mmol) and *N*,*N*,*N*′,*N*′,*N*″-pentamethyldiethylenetriamine (PMDETA) (2 μL, 1.0×10^{-2} mmol) in dimethylformamide (40 μL) was added to a mixture of compounds **M-9** (10.7 mg, 1×10^{-3} mmol) and **R-11** (1.7 mg, 1×10^{-3} mmol) in dimethylformamide (160 μL) and homogenized before being pipetted into a 458 micron thick mold and heated to 80 °C for 30 min. The device was then allowed to cool for 1 h and produced a blue gel (**Gel 50**) that was washed by immersion in saturated aq. EDTA solution, water and acetonitrile to yield a clear, colorless gel (1.9 × 1.9 × 0.05 cm). The reaction could also be performed in a vial equipped with a stirring bar.

*Synthesis of **Gel 25***

A solution of copper bromide (0.9 mg, 6.4×10^{-3} mmol) and PMDETA (1.3 μL, 6.4×10^{-3} mmol) in dimethylformamide (25 μL) was added to a mixture of compounds **M-9** (6.7 mg, 6.4×10^{-4} mmol), **R-11** (0.5 mg, 3.2×10^{-4} mmol) and **M-10** (3.4 mg, 3.2×10^{-4} mmol) in dimethylformamide (100 μL) and homogenized before being pipetted into a 458 micron thick mold and heated to 80 °C for 30 min. The device was then allowed to cool for 1 h and produced a blue gel (**Gel 25**) that was washed by immersion in saturated aq. EDTA solution, water and acetonitrile to yield a clear, colorless gel (1.5 × 1.9 × 0.05 cm). The reaction could also be performed in a vial equipped with a stirring bar.

*Synthesis of **Gel 12***

A solution of copper bromide (0.9 mg, 6.4×10^{-3} mmol) and PMDETA (1.3 µL, 6.4×10^{-3} mmol) in DMF (40 µL) was added to a mixture of compounds **M-9** (6.7 mg, 6.4×10^{-4} mmol), **R-11** (0.26 mg, 1.6×10^{-4} mmol) and **M-10** (5.0 mg, 4.8×10^{-4} mmol) in dimethylformamide (160 µL) and homogenized before being pipetted into a 458 micron thick mold and heated to 80 °C for 30 min. The device was then allowed to cool for 1 h and produced a blue gel (**Gel 12**) that was washed by immersion in saturated aq. EDTA solution, water and acetonitrile to yield a clear, colorless gel (1.5 × 1.9 × 0.05 cm). The reaction could also be performed in a vial equipped with a stirring bar.

*Synthesis of **Gel 5***

A solution of copper bromide (0.9 mg, 6.4×10^{-3} mmol) and PMDETA (1.3 µL, 6.4×10^{-3} mmol) in DMF (40 µL) was added to a mixture of compounds **M-9** (6.7 mg, 6.4×10^{-4} mmol), **R-11** (0.1 mg, 6.4×10^{-5} mmol) and **M-10** (6.0 mg, 5.7×10^{-4} mmol) in dimethylformamide (160 µL) and homogenized before being pipetted into a 458 micron thick mold and heated to 80 °C for 30 min. The device was then allowed to cool for 1 h and produced a blue gel (**Gel 5**) that was washed by immersion in saturated aq. EDTA solution, water and acetonitrile to yield a clear, colorless gel (1.5 × 1.9 × 0.05 cm). The reaction could also be performed in a vial equipped with a stirring bar.

*Synthesis of **Gel 0***

A solution of copper bromide (0.9 mg, 6.4×10^{-3} mmol) and PMDETA (1.3 µL, 6.4×10^{-3} mmol) in DMF (40 µL) was added to a mixture of compounds **M-9** (6.7 mg, 6.4×10^{-4} mmol) and **M-10** (6.7 mg, 6.4×10^{-4} mmol) in DMF (160 µL) and homogenized before being pipetted into a 458 micron thick mold and heated to 80 °C for 30 min. The device was then allowed to cool for 1 h and produced a blue gel (**Gel 0**) that was washed by immersion in saturated aq. EDTA solution, water and acetonitrile to yield a clear, colorless gel (1.5 × 1.9 × 0.05 cm). The reaction could also be performed in a vial equipped with a stirring bar.

Annexes

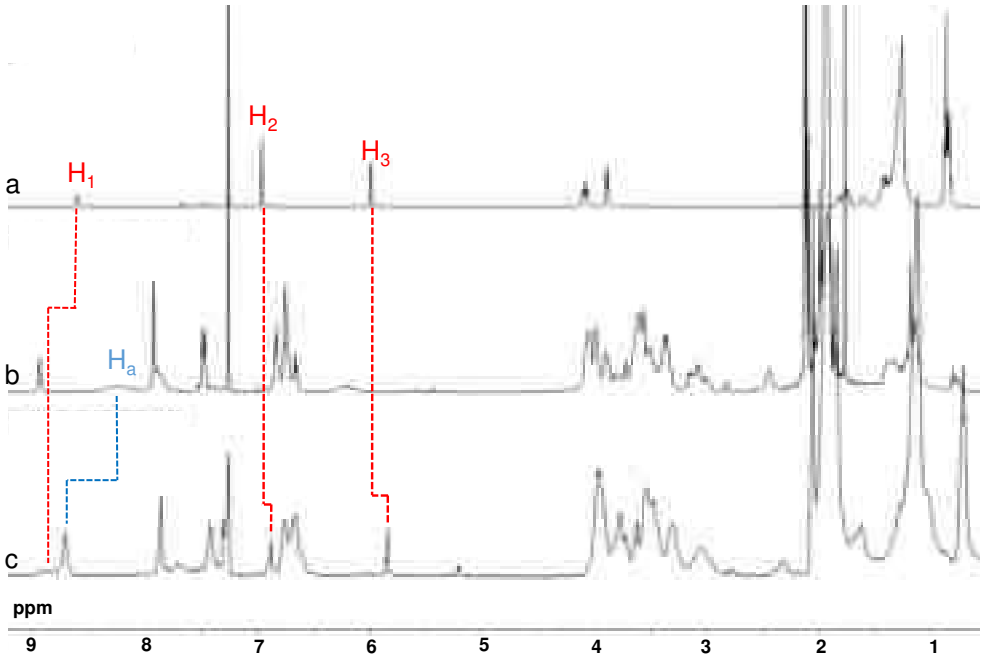

Figure A 1 | ^{1}H NMR in a 4:1 mixture of $CDCl_3/CD_3CN$ of a) $\mathbf{2}^{Cont}$, b) **3**, c) the 1:1 $\mathbf{2}^{Cont}$:**3** supramolecular polymer at 1 mM.

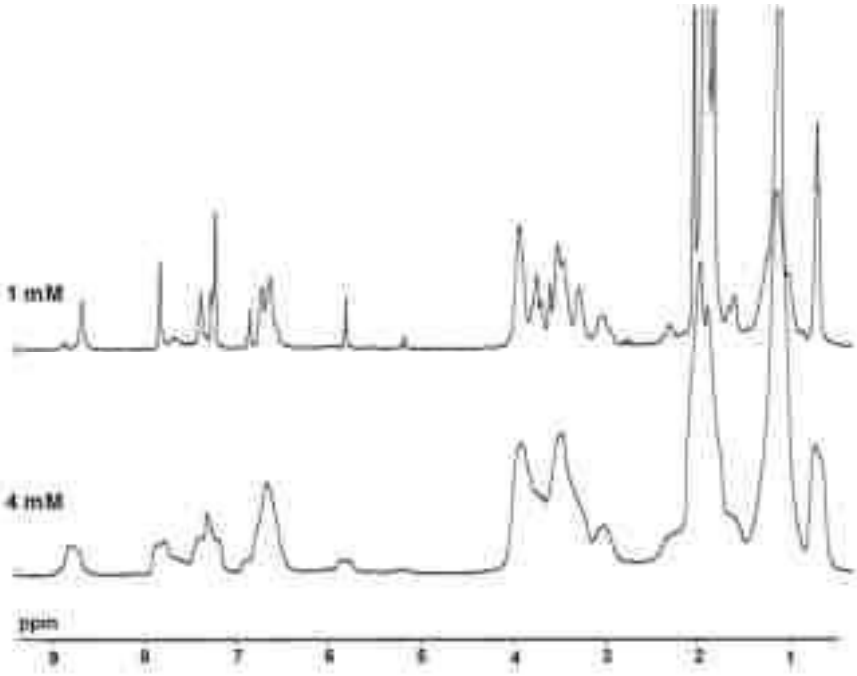

Figure A 2 | Concentration dependent ^{1}H NMR spectrum of the 1:1 $\mathbf{2}^{Cont}$:**3** contracted supramolecular polymer in a 4:1 mixture of $CDCl_3/CD_3CN$.

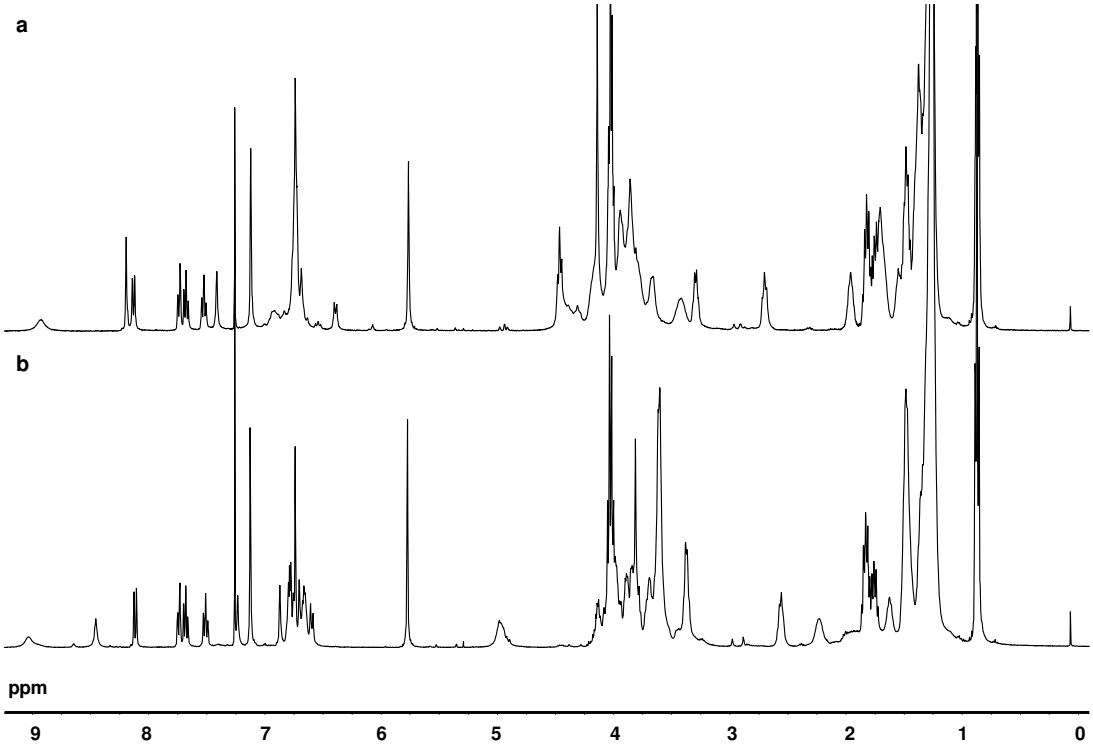

Figure A 3 | ^{1}H NMR spectra of a) compound $\mathbf{5}^{\mathbf{Ext}}$ at 5 mM in $CDCl_3$ and b) $\mathbf{5}^{\mathbf{Cont}}$ at 2 mM in $CDCl_3$.

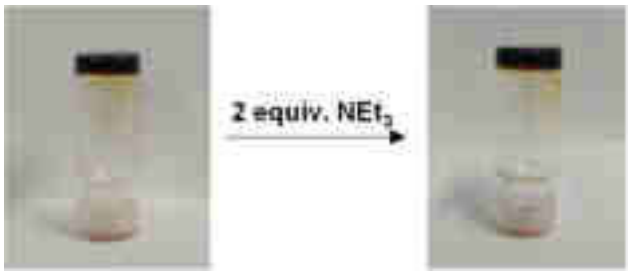

Figure A 4 | Behavior of 18 wt. % gel of $\mathbf{46}^{\mathbf{Ext\text{-}G}}$ in toluene upon addition of two equivalent of triethylamine.

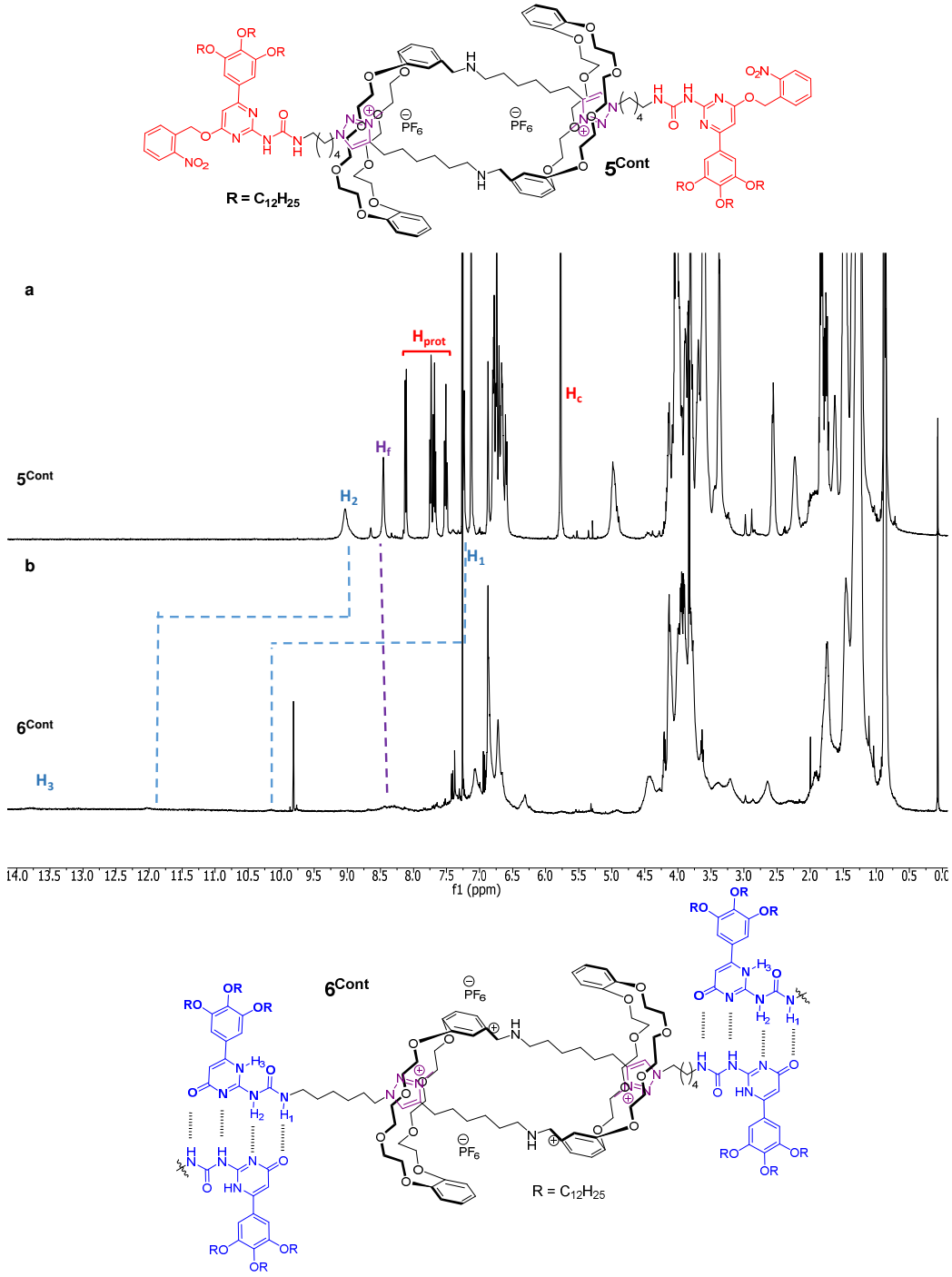

Figure A 5 | ^{1}H NMR in $CDCl_3$ of a 5 mM solution of a) $\mathbf{5}^{Cont}$ and b) $\mathbf{6}^{Cont}$ after 6 hours of irradiation.

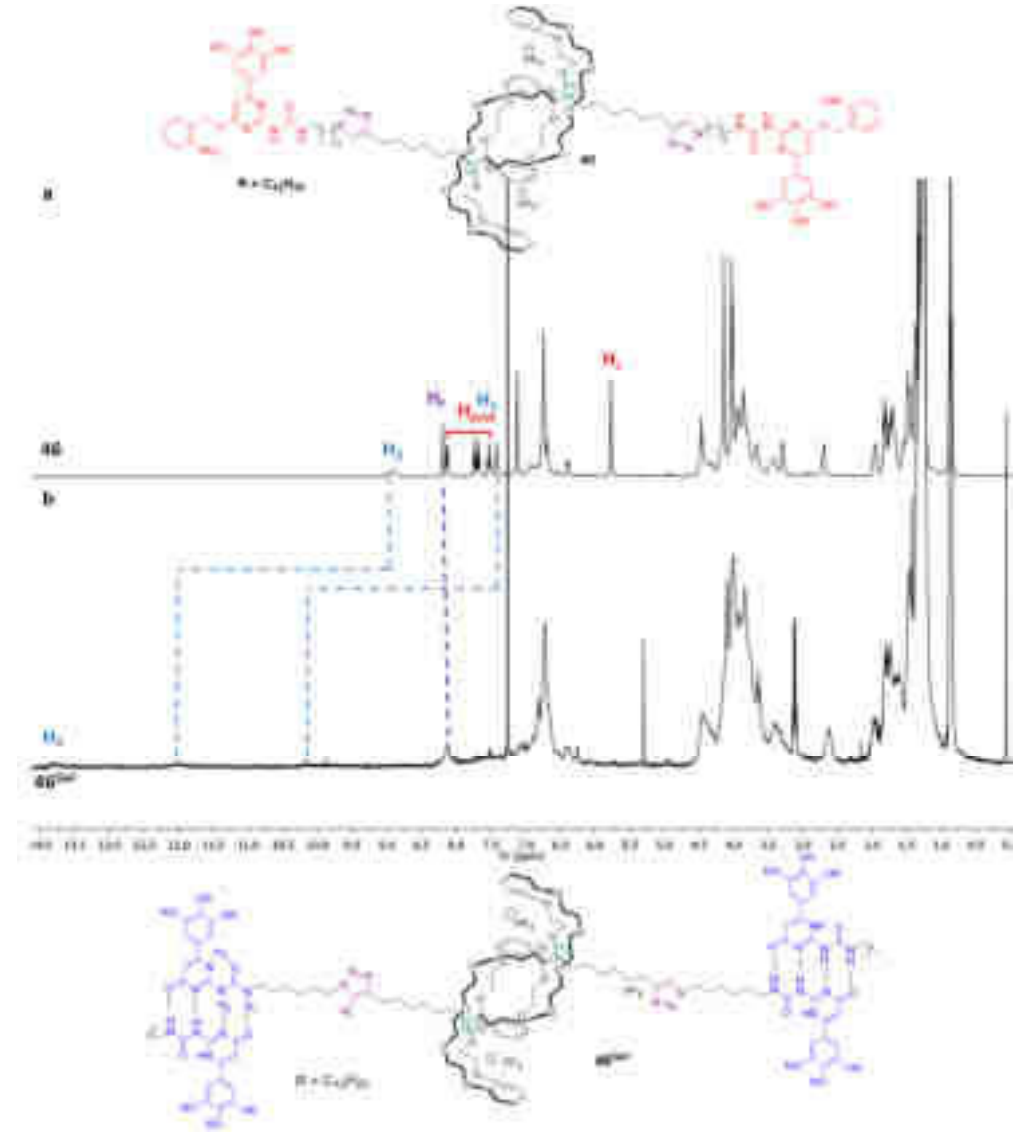

Figure A 6 | ^{1}H NMR in $CDCl_3$ of a 5 mM solution of a) **46** and b) **46^{gel}** after 6 hours of irradiation

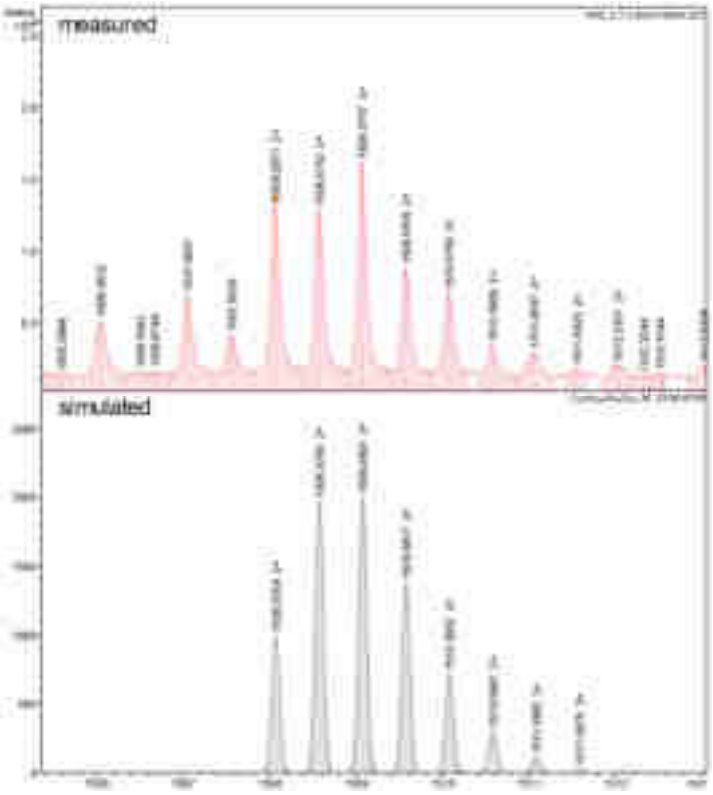

Figure A 7 | Measured and simulated partial HRMS (ESI+) spectrum of **6^{Cont}**.

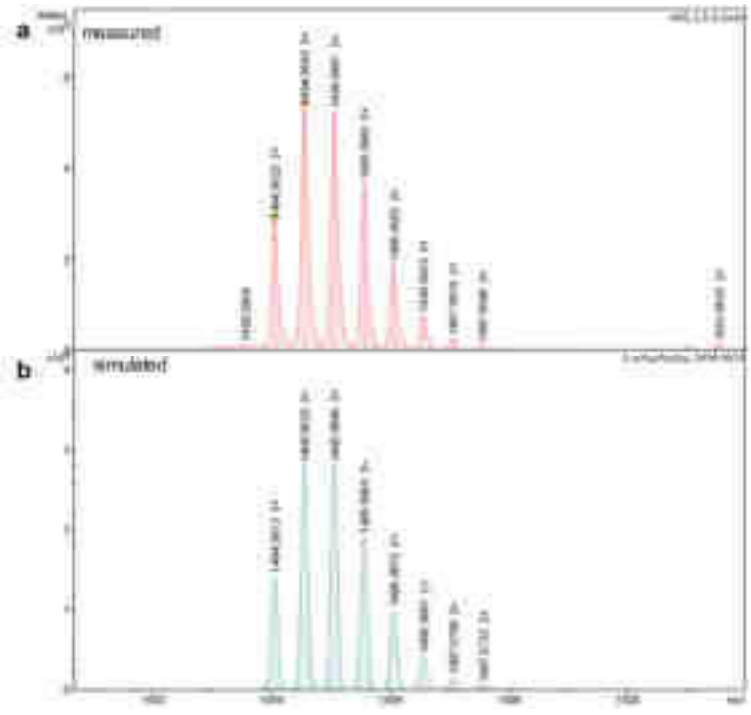

Figure A 8 | Measured and simulated partial HRMS (ESI+) spectrum of **46^{Ext}**.

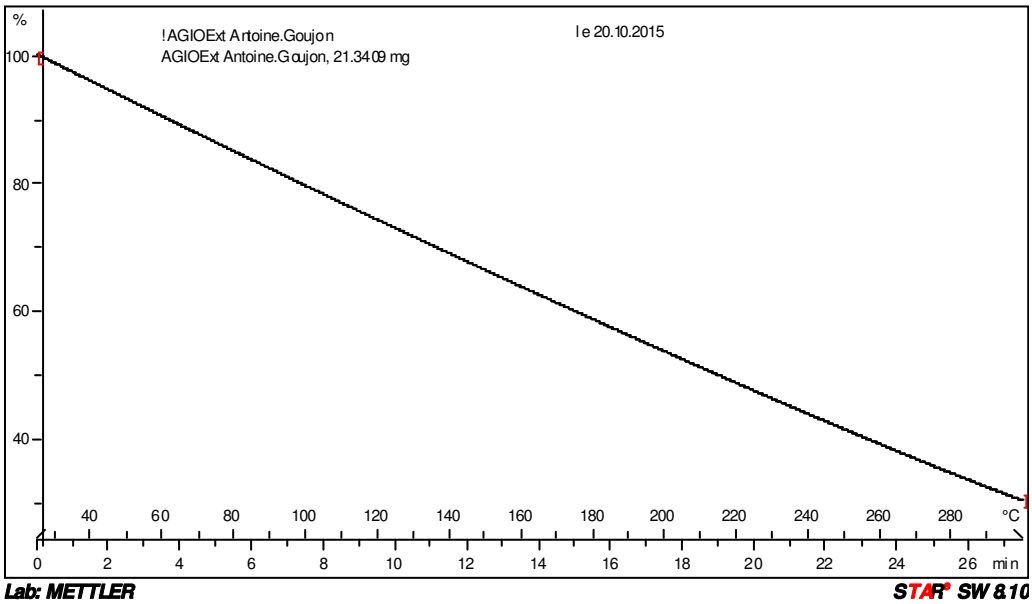

Figure A 9 | Thermogravimetric analysis (TGA) performed on **6**$^{\text{Ext-G}}$ as a gel in toluene.

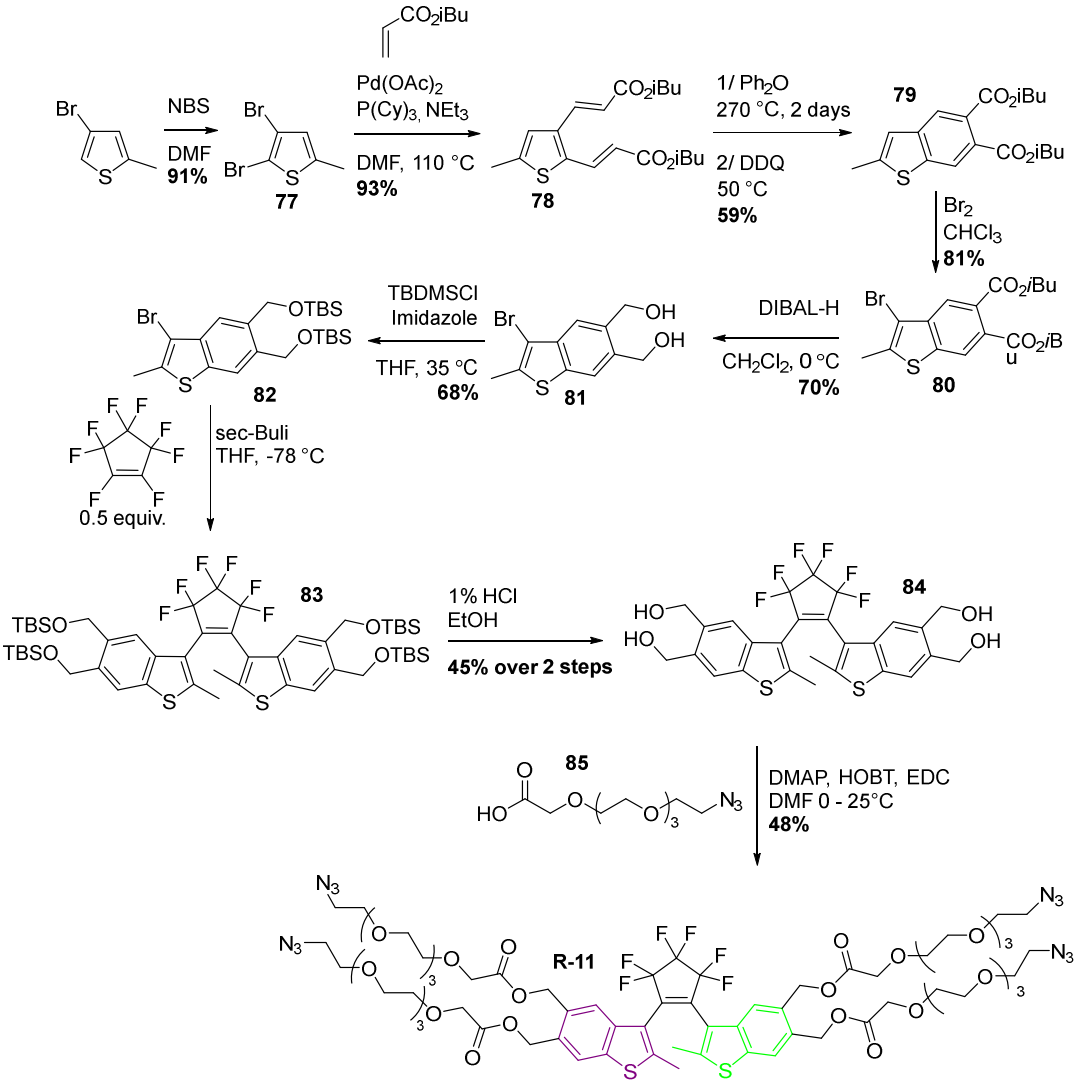

Figure A 10 | Synthesis of the modulating unit **R-11**.

Antoine Goujon

Macroscopic Amplification of Nanoscopic Motions Induced by Molecular Machines

Résumé

Ces vingt dernières années, le domaine du design et de la synthèse de machines moléculaires complexes a fait d'énormes progrès, souvent inspiré par la beauté de la machinerie présente dans les systèmes vivants. Cependant, l'amplifications des mouvements d'un grand nombre de machines moléculaires à des échelles de tailles largement supérieures à leurs dimensions restent un défi théorique et expérimental ambitieux et ardu. Ce travail décrit comment l'organisation de machines et moteurs moléculaires dans des réseaux polymères supramoléculaires ou covalents permet de synthétiser des matériaux dans lesquels leurs mouvements individuels nanométriques sont amplifiés jusqu'à l'échelle macroscopique. Les trois premiers chapitres décrivent l'utilisation d'une architecture de type [c2]daisy chains, une molécule capable d'effectuer des contraction/extensions similaires aux mouvements des sarcomères présents dans les muscles, dans des réseaux polymères supramoléculaires et covalents. Leur introduction dans des polymères supramoléculaires à liaisons hydrogène basées sur le motif de reconnaissance uracil:2,6-diacetylaminopyridine associé à des interactions latérales tel que les interactions π résulta en la formation de fibre supramoléculaires contractiles dont la taille et la morphologie a pu être commuté entre deux états étendus et contractés. L'incorporation de motifs uréidopyrimidinone comme connecteur supramoléculaire en revanche donna accès à des gels supramoléculaires, évoluant vers un état liquide lors de la contraction des chaines polymères. Finalement, l'inclusion de daisy chains dans un réseau polymère 3D a donné accès à un gel chimique. Ce matériau a pu être contracté et étendu à l'échelle macroscopique grâce à l'action combinée des machines moléculaires le constituant. Le quatrième chapitre est dédié à l'amélioration d'un gel contractile basé sur l'utilisation de moteurs moléculaires rotatif comme nœud de réticulation d'un réseau polymère. Une unité modulatrice, capable d'être commuté entre un état "ouvert" et "fermé", a été introduite dans le réseau aux côtés du moteur. Le modulateur dans son état "fermé" permet aux moteurs moléculaires de contracter efficacement le réseau, tandis que dans son état ouvert il permet aux chaines de se dérouler alors que le moteur ne tourne pas, ce qui provoque l'extension du réseau qui retourne à sa taille initiale. En résumé, le travail décrit dans ce manuscrit illustre que des machines moléculaires soigneusement conçue peuvent être introduites dans des réseaux polymères, fournissant des matériaux dont les propriétés macroscopiques sont affectées par les mouvements nanoscopiques de ses constituants. Ces résultats fournissent des pistes et une base fondamentale pour l'élaboration d'une nouvelle classe de matériaux contractiles basés sur des machines moléculaires.

Mots clés : machines moléculaires, polymères, polymères supramoléculaires, systèmes hors-équilibres, chimie organique, chimie supramoléculaire.

Abstract

The last twenty years have seen tremendous progresses in the design and synthesis of complex molecular machines, often inspired by the beauty of the machinery found in biological systems. However, amplification of the molecular machines motion over several orders of magnitude above their typical length scale is still an ambitious challenge. This work describes how self-organization of molecular machines or motors allows for the synthesis of materials translating the motions of their components into a macroscopic response. The three first chapters describe the use of a [c2]daisy chains architecture, a molecule able to perform contraction/extension motions similarly to the sarcomere units of muscles, into systems such as supramolecular polymers and covalent networks. Their inclusion into hydrogen bonding supramolecular polymers based on the uracil:2,6-diacetylaminopyridine recognition motifs combined with lateral interactions such as π-stacking provided micrometric muscle-like fibers contracting and extending upon deprotonation and protonation. The incorporation of ureidopyrimidone moieties as supramolecular connectors yielded highly organized gels, which evolved to a liquid state upon contraction of the polymer chains. Finally, covalent poly[c2]daisy chains were synthesized and investigated, notably the formation of a 3D network swelling into a gel. This material could contract and extend at the macroscopic scale upon contraction and extension of the molecular machines used as monomers. Finally, a fourth chapter is dedicated to the improvement of contractile chemical gels made by using a molecular motor as reticulating nodes. A modulating unit, able to be switched between a "closed" and an "opened" state, was introduced into the polymer network along with the motor. The locked structure in the "closed" state allowed contraction of the gel upon rotation of the molecular motors, while the "opened" state allowed unwinding of the entangled polymer chains and extension of the gel when the motor is off. Overall, the work presented in this manuscript demonstrates that carefully designed molecular machines can be incorporated into large supramolecular or covalent assemblies, providing materials which collective motions alter their macroscopic properties. These results provide valuable insights for the elaboration of a new class of muscle-like materials based on molecular machines.

Keywords : molecular machines, polymer, supramolecular polymer, out-of-equilibrium system, organic chemistry, supramolecular chemistry